Michael Meßner

A Fast Multipole Galerkin Boundary Element Method for the Transient Heat Equation

Monographic Series TU Graz

Computation in Engineering and Science

Series Editors

G. Brenn	Institute of Fluid Mechanics and Heat Transfer
G. A. Holzapfel	Institute of Biomechanics
W. von der Linden	Institute of Theoretical and Computational Physics
M. Schanz	Institute of Applied Mechanics
O. Steinbach	Institute of Computational Mathematics

Monographic Series TU Graz

Computation in Engineering and Science Volume 23

Michael Meßner

A Fast Multipole Galerkin Boundary Element Method for the Transient Heat Equation

---

This work is based on the dissertation *"A Fast Multipole Galerkin Boundary Element Method for the Transient Heat Equation"*, presented by Michael Meßner at Graz University of Technology, Institute of Applied Mechanics in December 2013.
Supervisor: M. Schanz (Graz University of Technology)
Reviewer: J. Tausch (Southern Methodist University, Dallas,Tex.)

© 2014 Verlag der Technischen Universität Graz

Cover photo	Vier-Spezies-Rechenmaschine by courtesy of the Gottfried Wilhelm Leibniz Bibliothek – Niedersächsische Landesbibliothek Hannover
Layout	Wolfgang Karl, TU Graz / Universitätsbibliothek Christina Fraueneder, TU Graz / Büro des Rektorates
Printed	by TU Graz / Büroservice

Verlag der Technischen Universität Graz

www.ub.tugraz.at/Verlag

Print:

ISBN: 978-3-85125-350-4

E-Book:

ISBN: 978-3-85125-351-1

DOI: 10.3217/978-3-85125-350-4

Dieses Werk ist lizenziert unter einer Creative Commons Namensnennung 3.0 Österreich Lizenz.

http://creativecommons.org/licenses/by-nc-nd/3.0/at/

Acknowledgment

The author is gratefully indebted to the *Marshallplan–Jubiläumsstiftung* for the financial support and to *Southern Methodist University*, especially to Prof. Tausch, for the hospitality during the visiting scholar position from January until May 2013.

Notation

We use C to denote positive constants within proofs, whose value may change within a chain of estimates. This convention is motivated by the fact that we do not want to determine the exact value of such constants, but only state their existence. Apart from that we stick to the following notation, unless explicitly defined otherwise within the context.

In order to avoid this list to become overly extensive, we allow the combination of sub- and superscripts or accents from the list below.

General

a	scalar
$\mathbf{a}$	vector
a	coefficient vector
$\mathbf{A}$	matrix
A	coefficient matrix
$\mathfrak{A}$	index set

Material Parameters

λ	heat conduction coefficient $[\mathrm{W}/^{\circ}\mathrm{Cm}]$
ϱ	density $[\mathrm{kg}/\mathrm{m}^3]$
c_p	specific heat capacity $[\mathrm{Wsec}/^{\circ}\mathrm{Ckg}]$
α	heat diffusion coefficient $[\mathrm{m}^2/\mathrm{sec}]$
κ	heat transfer coefficient $[\mathrm{W}/^{\circ}\mathrm{Cm}^2]$
κ^*	scaled heat transfer coefficient $[\mathrm{m}/\mathrm{sec}]$

Geometric/Temporal Quantities

Ω	spatial domain $\subset \mathbb{R}^3$
Γ	piecewise Lipschitz boundary of Ω
Υ	time interval $(0,T)$
$t,\ \tau$	temporal points in Υ
$\tilde{\mathbf{x}},\ \tilde{\mathbf{y}}$	spatial points in Ω

$\mathbf{x}$, $\mathbf{y}$	spatial points on Γ
$\hat{\mathbf{x}}$, $\hat{\mathbf{y}}$	spatial points in reference coordinates
$\phi_i(t)$	discontinuous temporal test and trial function
$\varphi_j(\mathbf{x})$	discontinuous spatial test and trial function
$\psi_k(\mathbf{x})$	continuous spatial test and trial function
c_{ϕ_i}, $\mathbf{c}_{\varphi_j}$, $\mathbf{c}_{\psi_k}$	center of ϕ_i, φ_j, ψ_k

Function Spaces

$H^{r,s}(\mathbb{R}^3 \times \mathbb{R})$	anisotropic Sobolev space $L_2(\mathbb{R}; H^r(\mathbb{R}^3)) \cap H^s(\mathbb{R}; L_2(\mathbb{R}^3))$
$H^{r,s}(\Gamma \times \Upsilon)$	restriction of $H^{r,s}(\mathbb{R}^3 \times \mathbb{R})$ (cf. Appendix A)
$\widetilde{H}^{r,s}(\Gamma_i \times \Upsilon)$	restriction of $H^{r,s}(\Gamma \times \Upsilon)$ (cf. Appendix A)
$T_{h_t}^{d_t}(\Upsilon)$	pw. polynomial ansatz space on Υ $d_t := d_{d_t}$ or $d_t := c_{d_t}$
$X_{h_x}^{d_x}(\Gamma)$	pw. polynomial ansatz space on Γ with $d_x := d_{d_x}$ or $d_x := c_{d_x}$
$S_{h_x,h_t}^{d_x,d_t}(\Gamma \times \Upsilon)$	piecewise polynomial tensor product space $X_{h_x}^{d_x}(\Gamma) \otimes T_{h_t}^{d_t}(\Upsilon)$

Functions and Operators

$G(\mathbf{r},d)$	heat kernel with $\mathbf{r} := \mathbf{x} - \mathbf{y} \in \mathbb{R}^3$ and $0 < d := t - \tau \in \mathbb{R}$
$G^{(-i)}(\mathbf{r},d)$	i^{th} temporal anti-derivative of the heat kernel
$u(\mathbf{x},t)$	(surface)temperature $[^\circ\mathrm{C}]$
$\mathbf{q}(\mathbf{x},t)$	heat flux $[\mathrm{W}/\mathrm{m}^2]$
$q(\mathbf{x},t)$	surface heat flux $[\mathrm{W}/\mathrm{m}^2]$
$q^*(\mathbf{x},t)$	scaled surface heat flux $[^\circ\mathrm{Cm}/\mathrm{sec}]$
$u_h(\mathbf{x},t)$	discrete (surface) temperature
$q_h(\mathbf{x},t)$	discrete surface heat flux
$g_G(\mathbf{x},t)$	given boundary data, $G \in \{D,N,R\}$
$g_G^*(\mathbf{x},t)$	scaled given boundary data, $G \in \{N,R\}$
$\bar{g}_G(\mathbf{x},t)$	perturbed given boundary data, $G \in \{D,N,R\}$
$\tilde{g}_D(\mathbf{x},t)$	extended given Dirichlet data
$\mathcal{I}$	identity
$\mathcal{V}$	single layer operator
$\mathcal{K}$	double layer operator
$\mathcal{K}'$	adjoint double layer operator
$\mathcal{D}$	hyper-singular operator
$\mathcal{S}$	symmetric Steklov-Poincaré operator
$\bar{\mathcal{S}}$	approximation of the symmetric Steklov-Poincaré operator
$\mathcal{Q}_{h_x}^{d_x}$	$L_2(\Gamma) \to X_{h_x}^{d_x}(\Gamma)$ projection

$\mathcal{Q}_{h_t}^{d_t}$	$L_2(\Upsilon) \to T_{h_t}^{d_t}(\Upsilon)$ projection
$\mathcal{Q}_{h_x}^{d_x}\mathcal{Q}_{h_t}^{d_t}$	$L_2(\Gamma\times\Upsilon) \to S_{h_x,h_t}^{d_x,d_t}(\Gamma\times\Upsilon)$ projection

FMM (cFMM, FGT, pFMM) Symbols

ℓ_t, L_t	temporal cluster level / leaf cluster level
ℓ_x, L_x	spatial cluster level / leaf cluster level
h_t^i	temporal cluster half length, $i \in \{0,\dots,L_t\}$
h_x^i	spatial cluster half length, $i \in \{0,\dots,L_x\}$
$\bar{h}_x^i$	extended spatial cluster half length, $i \in \{0,\dots,L_x\}$
$I_m^{\ell_t}$	temporal cluster
$X_u^{\ell_x}$	spatial cluster
$\Phi_{I_m^{\ell_t}}$	mapping $I_m^{\ell_t} \to [-1,1]$
$\Phi_{X_u^{\ell_x}}$	mapping $X_u^{\ell_x} \to [-1,1]^3$
$L_i(t)$	i^{th} Lagrange polynomial
$T_k(x)$	k^{th} Chebyshev polynomial
n_t	number of time steps per temporal leaf cluster
n_x	number of elements per spatial leaf cluster
$\mathcal{I}_p^d$	d variate Lagrange interpolation operator of order p
$\mathfrak{S}(\mathcal{I}_p^d)$	index set of all interpolation nodes in $\mathcal{I}_p^d$
$\mathfrak{P}(I_m^{\ell_t})$	index set $\{k : \phi_k(t) \subset I_m^{\ell_t}\}$
$\mathfrak{C}(I_m^{\ell_t})$	index set $\{k : I_k^{\ell_t+1} \subset I_m^{\ell_t}\}$
$\mathcal{S}_q^d$	d variate truncated Chebyshev expansion operator of order q
$\mathfrak{S}(\mathcal{S}_q^d)$	index set of expansion coefficients in $\mathcal{S}_q^d$
$\mathfrak{P}(X_u^{\ell_x})$	index set $\{k : \varphi_k(\mathbf{x})/\psi_k(\mathbf{x})$ with $\mathbf{c}_{\varphi_k}/\mathbf{c}_{\psi_k} \in X_u^{\ell_x}\}$
$\mathfrak{C}(X_u^{\ell_x})$	index set of child clusters $\{k : X_k^{\ell_x+1} \subset X_u^{\ell_x}\}$
$\mathfrak{N}(X_u^{\ell_x})$	index set of neighbor clusters $\{k : \bar{X}_k^{\ell_x} \cap \bar{X}_u^{\ell_x} \neq \emptyset\}$
$\mathfrak{n}_x$	number of interacting spatial clusters in each spatial direction
$\mathfrak{I}(X_u^{\ell_x})$	index set $\{k : X_k^{\ell_x}$ interacting with $X_u^{\ell_x}\}$
$\mathcal{V}_B$	boundary integral operator with spatial cutoff
$\check{\mathcal{V}}$	cFMM, FGT, pFMM approximated boundary integral operator
$E_g^{\pm}$	quadrature error of Gauss-Legendre rule of order g
L_x°	spatial levels above L_x for the FGT's in the nearfield
$V_d^{\pm}$	time integrated single layer kernel for $d \geq 1$
μ, M	dyadic splitting parameters
$V_{0,m}^{+}$, $V_{1,m}^{-}$	dyadic splitting of V_0^{+} respectively V_1^{-}
$V_{0,M}^{+}$, $V_{1,M}^{-}$	localized singular part of V_0^{+} respectively V_1^{-}
$\dot{\mathcal{V}}_B$	boundary integral operator with accelerated nearfield

Abstract

Transient heat transfer plays a major role in many physical and chemical processes, which implies the need for efficient numerical simulation tools in a wide range of engineering fields, such as mechanical, chemical and process engineering. Our aim is to develop a stable, robust, and efficient boundary element algorithm to solve problems arising from applications in those disciplines. It is a well known fact that uniqueness, solvability, and quasi-optimality of space-time Galerkin boundary element methods follows from the boundedness and ellipticity of the thermal single layer- and hyper-singular operator. To handle the arising dense matrix problems we accelerate our solver via the parabolic fast multipole method and thus obtain almost optimal complexity in the number of unknowns. Since the heat kernel is smooth for positive time and exponentially decaying in space, we approximate the kernel by a multivariate Lagrange-Chebyshev interpolation for well separated space-time clusters, which enables an efficient evaluation of their contributions to the thermal layer potentials. Finally, we investigate some benchmark problems to show that the error, induced by the fast multipole method, can be controlled and does not destroy the convergence rates of the Galerkin scheme. Furthermore, we simulate some problems from industrial applications to show the suitability of the proposed method for large scale problems.

Zusammenfassung

Die instationäre Wärmeleitung spielt eine wichtige Rolle in vielen physikalischen und chemischen Prozessen, was die Notwendigkeit von effizienten numerischen Methoden zur Folge hat. Unser Ziel ist es daher einen stabilen, robusten und effizienten Randelemente Algorithmus zu entwickeln. Es ist hinlänglich bekannt, dass die eindeutige Lösbarkeit und Stabilität sowie die quasi-Optimalität von Galerkin Randelemente Methoden aus der Beschränktheit und Elliptizität des Einfachschicht- und Hypersinglären Operators folgt. Um die resultierenden voll besetzten Matrizen effizient behandeln zu können, beschleunigen wir unsere Randelemente Formulierung mittels der parabolischen Fast Multipole Methode, welche einen beinahe optimalen Algorithmus in der Anzahl der Unbekannten ermöglicht. Da die Kernfunktion für positive Zeit glatt und im Raum exponentiell abklingend ist, verwenden wir eine Raum-Zeit Entwicklung in Chebysev und Lagrange Polynomen für hinreichend getrennte Raum-Zeit Cluster um den Einfluss der Vergangenheit effizient zu berechnen. An einigen Referenz Beispielen werden wir zeigen, dass die parabolische Fast Multipole Method das theoretischen Konvergenzverhalten der Galerkin Methode nicht zerstört. Ausserdem werden wir noch Industrie Anwendungen modellieren um die Eignung der Methode für die Simulation industrieller Probleme zu zeigen.

CONTENTS

1 INTRODUCTION

1.1 Overview

The physical problem of transient heat transport and storage in solid media, coined by the term heat conduction, has caught the interest of the scientific society from the early 18^{th} century on. It were people like Gabriel Daniel Fahrenheit ($1686-1736$) with the invention of the *mercury thermometer*, Joseph Black ($1728-1799$) with the observation of *specific heat*, Pierre Simon Laplace ($1749-1827$) with its experimental determination, and many more, who lead to Jean Baptiste Joseph Fourier's ($1768-1830$) masterpiece *Théorie de la Propagation de la Chaleur dans les Solids* [35], submitted to the French Academy in 1807. However, due to lack of approval by his colleagues this paper never got published and it was not until 1822, when Fourier decided to put in print *Théorie Analytique de la Chaleur* [35] by himself that his theory became accessible to a broader audience. Soon, this latter contribution got widely accepted by the scientific community, even more so as analogies to other fields were recognized. Among others, some of the fields inspired by Fourier's theory were *chemistry* with molecular diffusion, *electrodynamics* although there the analogy was misleading, *probability theory* with random walks, and stochastic differential equations. While each of these individual fields offers its fascination, we refer the reader for a more profound survey to [35] and steer our attention towards the heat equation and its application behind the original intention.

Already Fourier himself offered a powerful way of solving initial boundary value problems of the heat equation. Following the approach of his predecessors Daniel Bernoulli ($1700-1782$), Jean D'Alembert ($1717-1783$), and Leonhard Euler ($1707-1783$) he applied the method of separation of variables yielding solutions in form of trigonometric series [35]. However, it was not until the second half of the 20^{th} century when the integral equation approach from classical potential [25] theory was extended to the heat equation [29, 40], which proved to be a powerful tool for showing existence and uniqueness of solutions to the heat equation in terms of layer potentials. While in general a closed form solution for neither of these approaches can be found, they still provide the basics for approximation schemes to solve heat conduction problems in more general settings. In this context one should mention finite difference- and finite element methods, which are PDE based approximation techniques. Of course these techniques are not limited to the heat equation, nonetheless we would like to refer the reader to [13, 16] for some groundbreaking developments made in the context of the heat equation and [52] for the apparently first application of the FEM to heat conduction problems. While these PDE based methods are

domain based as well, the second category of approximations schemes is boundary based and may be summarized by the term boundary integral equation (BIE) methods with the corresponding counterparts being Nyström- and boundary element methods (BEM) – in the same way as a Finite Difference scheme replaces derivatives by finite difference quotients instead of taking the variational approach, a Nyström method replaces the integrals by quadrature rules. It appears that the former method was first applied to the heat equation in [48] while the latter seems to have a longer history appearing first with a detour via an inverse Laplace transformation [41], before being directly applied in time domain with a space-time Galerkin discretization [11, 37], and finally with a convolution quadrature method (CQM) based approach [31]. For a more complete review we refer to [12].

Besides the distinction between PDE (or domain) and BIE (or boundary) based approaches these two categories of solvers feature other opposing properties as well. The most evident probably being that the resulting linear system in the former case turns out to be sparsely, while in the latter case it is densely populated. Even though the reduction to the boundary leads to $N_\Gamma = \mathcal{O}(h_\Gamma^{-2})$ instead of $N_\Omega = \mathcal{O}(h_\Omega^{-3})$ in the case of a domain based method, where N_Ω/N_Γ are the numbers of degrees of freedom and h_Ω/h_Γ the discretization parameters. The quadratic complexity of solving for a dense system matrix destroys this advantage due to $\mathcal{O}(N_\Gamma^2) = \mathcal{O}(h_\Gamma^{-4})$ instead of $\mathcal{O}(N_\Omega) = \mathcal{O}(h_\Omega^{-3})$ for a sparsely populated system. At first sight this drawback seems to completely rule out BIE based methods for large scale problems, however, there are fast algorithms available [20, 27, 47, 49] to reduce the cost to almost $\mathcal{O}(N_\Gamma) = \mathcal{O}(h_\Gamma^{-2})$ and thus gain competitiveness again. This observation serves as a motivation to improve upon such approaches for the efficient solution of heat conduction problems.

Most industrial processes are strongly linked to and driven by heat transfer. Therefore, it is a crucial task for the design engineer to be able to accurately and efficiently perform thermal simulations, e.g., the simulation of press hardening tools within the thermo-mechanical simulation of the press hardening process [3, 32, 39, 42]. The conceptual idea of this process is to heat the raw metal sheet above crystallization temperature, bring it into the final shape and cool it down at a high, predefined rate. This can be achieved by an arbitrarily complicated grid of cooling channels penetrating the press hardening tool. With the aid of some agent flowing through these channels, such a layout allows to withdraw energy from the hot metal sheet. Roughly speaking, the influence of elastic/plastic stresses onto the thermal behavior of such tools can be neglected and, therefore, the thermal simulation can be isolated from the thermo-mechanical simulation. The design engineer knows the cooling rate leading to the desired crystal structure, which allows him to compute the energy to be withdrawn by the tools. This information can be translated into a set of mixed boundary conditions for homogeneous initial boundary value problems, which we solve with fast boundary element methods for two major reasons. First, the geometry of press hardening tools is extremely complicated and, therefore, a reduction of the problem to the boundary leads to a significantly reduced meshing effort. Second, since only the surface temperature distribution of the press hardening tool is required for the

coupled thermo-mechanical simulation of the press hardening process afterwards, a direct boundary element method seems a rather natural approach.

1.2 State of the Art

Boundary integral equations related to the heat equation have been studied in [4, 8, 11, 37, 40]. For classically used second kind integral equations, e.g., a double layer potential approach for the Dirichlet problem and a single layer potential ansatz for the Neumann problem, the compactness of these integral operators on smooth domains provided by Pogorzelski et al. [40] guarantees well posedness of the problem and the analysis of numerical methods. However, in the case of non smooth domains and first kind integral equations the situation is more complicated. Brown [8] gave some first results on Lipschitz domains before almost contemporaneously Arnold and Noon [4] and Costabel [11] showed the boundedness and coercivity of the thermal single layer operator. Furthermore, Costabel [11] showed the coercivity of the hyper-singular operator and the boundedness of all thermal boundary integral operators in the appropriate anisotropic Sobolev space setting on Lipschitz domains. With these results the analysis follows the well known pattern of the elliptic theory, i.e., the Lemma of Lax Milgram guarantees uniqueness and solvability of corresponding operator equations and their Galerkin variational formulation. Using conforming finite-dimensional subspaces of the natural energy spaces, uniqueness and solvability translates directly to the discrete system, where Cea's Lemma provides quasi-optimality. Using the approximation property of the finite-dimensional ansatz spaces, the regularity of the boundary integral operators, and assuming certain regularity of the discretization one can derive explicit error estimates in various norms around the energy norm. However, despite the beauty of this theory, the problem with the high computational complexity has yet to be solved.

The first attempt to solve heat conduction problems by thermal layer potential representations in almost optimal complexity was presented by Greengard and Strain [20]. However, their method is limited to bounded domains, where they split the temporal range of the heat kernel into a local (recent) and history (distant) part. For the history part they use a Fourier series expansion with periodic boundary conditions, which converges exponentially due to the smoothness of the heat kernel with sufficient temporal separation. For the local part, on the other hand, a representation via the method of images is used. In this case the short temporal range results in a sharply peaked heat kernel where Taylor expansion is very well suited. One year later, the same authors presented the fast Gauss transform (FGT) [21], which can be used to efficiently represent the solution of pure initial value problems of the heat equation via an initial potential in form of a Gauss transform (the heat kernel with a fixed variance is a Gaussian). Their approach is based on a hierarchical subdivision of the computational domain and expansion of the Gaussian kernel into a Hermite series around the center of source boxes. Such an expansion allows to efficiently evaluate the

collective influence of all sources contained in that box onto a collection of target points located in some target box. Later on Strain [45] extended this idea to two-dimensional free-space heat conduction by interpreting the representation of the initial value solution by an initial potential as an evolution equation and thus finding the solution by repeated application of the FGT. Duhamel's principle is used to find solutions of inhomogeneous problems and an analogy between the forcing term and surface densities in the thermal layer potential representation of initial boundary value problems is used to sketch the solution of heat conduction problems in domains with boundaries. Unfortunately this paper only presents some preliminary results and refers to forthcoming papers that seem to never have appeared. In an attempt to overcome the limitations of the earlier presented spectral approach Greengard and Lin [17] presented a spectral approximation of the free-space heat kernel, where the difficulties of dealing with the approximation of the now continuous spectrum are elaborated. Instead of sampling a finite number of Fourier modes a finite range of the Fourier integral needs to be approximated, which is done via dyadic splitting and a composite quadrature rule. Note that this makes an application of the fast Fourier transform (FFT) impossible and requires some nonuniform FFT instead. From there it appears that it took a few years until Li and Greengard [27] incorporated this approach into a method for the evaluation of thermal layer potentials. They propose to combine the spectral approximation of the free-space heat kernel for the history part with a full product integration scheme for the evaluation of the local part to overcome the *geometrically induced stiffness* proper to asymptotic expansions and partial product integration schemes [27] and fed the readers hope with the presentation of some numerical examples in a future paper. To the authors knowledge this has been the last contribution in the field of spectral methods, while in the meantime Tausch [47] introduced the parabolic fast multipole method (pFMM). A Lagrange interpolation of the heat kernel in time together with a hierarchical clustering and incorporation of causality leads to a causal FMM structure in time. What remains is a family of Gauss transforms, which are efficiently evaluated by means of the FGT concept based on a Chebyshev expansion of the time interpolated heat kernel and a spatial clustering. Thus, using the causal fast multipole method (cFMM) structure in time to collect spatial contributions via an adapted FGT scheme in space according to some space-time admissibility condition dictated by the time scaling of the heat kernel one ends up with the pFMM. The asymptotic smoothness of the heat kernel in time and the exponential decay in space together with the exponential convergence of the Chebyshev-Lagrange expansion guarantees an application of the pFMM accelerated farfield or smooth part of the thermal layer potential in almost optimal time. Furthermore, the nearfield or singular part of the potential can be evaluated directly in optimal complexity because the exponential decay in space allows a truncation of distant potential contributions.

Advantages of a pFMM accelerated space-time Galerkin BEM We opted for a Galerkin approach, because it can deal with Lipschitz domains compared to the higher regularity requirements by product integration and Nyström methods. Moreover, due to the

complications encountered with the spectral approximation of the free-space heat kernel, we resort to the parabolic fast multipole method based on a hierarchical space-time clustering and a Lagrange-Chebyshev expansion of the heat kernel. Finally, we would like to remark that such an approach seems to rule out the combination of the CQM in combination with a fast algorithm in space, because the Laplace transform destroys the Gaussian structure of the heat kernel. As a consequence of which the spatial variables of the heat kernel do not separate into individual directions leading to a higher computational cost.

1.3 Outline

Chapter 2 is concerned with a derivation of the heat equation and related initial boundary value problems. We also derive related boundary integral equations and use them to present boundary integral formulations of initial boundary value problems and their Galerkin variational formulations.

In Chapter 3, we introduce a rather standard space-time discretization on which we define finite-dimensional tensor product ansatz and test spaces. With these ingredients, we define Galerkin boundary element methods for the approximate solution of the previously defined initial boundary value problems related to the heat equation. Additionally, we provide some error estimates, which guarantee optimal convergence of these methods.

Boundary element methods lead to dense system matrices, which imply $\mathcal{O}(N_x^2 N_t^2)$ work in the number of spatial N_x and temporal unknowns N_t in terms of storage and computation. Therefore, we devote Chapter 4 to reduce both storage and work to almost $\mathcal{O}(N_x N_t)$. We pursue a variant of the fast multipole method, which is based on the idea that one can cluster degrees of freedom and efficiently evaluate their influence on each other in a hierarchic way.

Finally, in Chapter 5 we test our method on some benchmark problems to check whether the stated goal, namely a stable and robust algorithm with optimal complexity in the number of unknowns, has been achieved. Furthermore, we use our fast method to solve industrial applications involving heat diffusion, which would not be solvable without the fast algorithm.

2 HEAT TRANSFER

2.1 Heat Diffusion

In this thesis, we deal with the solution of initial boundary value problems related to the heat equation in open domains $\Omega \subset \mathbb{R}^3$ with a piecewise Lipschitz boundary Γ. We are interested in the solution throughout a time interval $\Upsilon := (0,T)$ with $\mathbb{R} \ni T > 0$ and assume once and for all that Ω does not change over time. Furthermore, we restrict ourselves to problems with homogeneous, isotropic, and density persistent material behavior.

2.1.1 Heat Equation

The heat equation describes heat diffusion through solids and static fluids or gases [5, 24]. It is derived from Fourier's law and conservation of energy. The former is obtained from phenomenological observations and links the heat flux $\mathbf{q}[\mathrm{W/m^2}]$ to the negative gradient of the temperature $u[^\circ\mathrm{C}]$ via the thermal conduction coefficient $\lambda\,[\mathrm{W/^\circ Cm}]$

$$\mathbf{q}(\tilde{\mathbf{x}},t) = -\lambda \nabla_{\tilde{\mathbf{x}}} u(\tilde{\mathbf{x}},t) \qquad (\tilde{\mathbf{x}},t) \in \Omega \times \Upsilon\,. \tag{2.1}$$

Observe that the homogeneous and isotropic material behavior leads to a constant thermal conduction coefficient. Furthermore, conservation of energy is required by the first law of thermodynamics, which states that the rate of internal energy change $\partial U/\partial t := \partial_t U[\mathrm{W}]$ must balance the heat flux $Q[\mathrm{W}]$ through the boundary Γ and the internal energy generation $P[\mathrm{W}]$ at all times

$$\partial_t U(t) = Q(t) + P(t) \qquad t \in \Upsilon\,. \tag{2.2}$$

Due to the assumption of homogeneous and density persistent material behavior we have a constant density $\varrho[\mathrm{kg/m^3}]$ and a constant specific heat capacity $c_p[\mathrm{Wsec/^\circ Ckg}]$, hence the rate of internal energy change is given by

$$\partial_t U(t) := \int_\Omega \varrho c_p \partial_t u(\tilde{\mathbf{x}},t)\mathrm{d}\tilde{\mathbf{x}} \qquad t \in \Upsilon\,. \tag{2.3}$$

An application of the Divergence Theorem to the heat flux through the boundary Γ together with Fourier's law (2.1) yields

$$Q(t) := -\int_\Gamma \mathbf{n}_{\mathbf{x}}{}^\top \mathbf{q}(\mathbf{x},t)\mathrm{d}s_{\mathbf{x}} = -\int_\Omega \nabla_{\tilde{\mathbf{x}}}^\top \mathbf{q}(\tilde{\mathbf{x}},t)\mathrm{d}\tilde{\mathbf{x}} = \int_\Omega \lambda \Delta u(\tilde{\mathbf{x}},t)\mathrm{d}\tilde{\mathbf{x}} \qquad t \in \Upsilon\,, \tag{2.4}$$

where $\mathbf{n}_\mathbf{x}$ denotes the outer unit normal vector at $\mathbf{x} \in \Gamma$ and the minus sign guarantees a positive outward heat flux. The internal energy generation is given by the volume integral over the energy density function $f[\mathrm{W/m^3}]$

$$P(t) := \int_\Omega f(\tilde{\mathbf{x}},t)\mathrm{d}\tilde{\mathbf{x}} \qquad t \in \Upsilon \tag{2.5}$$

and, finally, (2.2) with (2.3), (2.4) and (2.5) leads to the heat equation

$$\varrho c_p \partial_t u(\tilde{\mathbf{x}},t) = \lambda \Delta u(\tilde{\mathbf{x}},t) + f(\tilde{\mathbf{x}},t) \qquad (\tilde{\mathbf{x}},t) \in \Omega \times \Upsilon\,. \tag{2.6}$$

2.1.2 Initial Boundary Value Problems

In order to give a proper statement of heat diffusion problems in form of initial boundary value problems, we need to supplement the heat equation (2.6) with a combination of initial- and boundary values. Therefore, we prescribe an initial condition throughout the entire domain

$$u(\tilde{\mathbf{x}},0) = u_0(\tilde{\mathbf{x}}) \qquad \tilde{\mathbf{x}} \in \Omega$$

and boundary conditions on some subsets of the space-time cylinder's lateral boundary. To this end we split the boundary into disjoint parts $\Gamma_D, \Gamma_N, \Gamma_R$ such that $\Gamma_D \cap \Gamma_N = \Gamma_D \cap \Gamma_R = \Gamma_N \cap \Gamma_R = \emptyset$ and $\overline{\Gamma}_D \cup \overline{\Gamma}_N \cup \overline{\Gamma}_R = \Gamma$. Imposing a temperature field $u[^\circ\mathrm{C}]$ is classically referred to as Dirichlet boundary condition

$$u(\mathbf{x},t) = g_D(\mathbf{x},t) \qquad (\mathbf{x},t) \in \Gamma_D \times \Upsilon\,,$$

whereas prescribing a surface heat flux $q[\mathrm{W/m^2}]$ is called a Neumann boundary condition

$$q(\mathbf{x},t) := \lambda \partial_{n_\mathbf{x}} u(\mathbf{x},t) = g_N(\mathbf{x},t) \qquad (\mathbf{x},t) \in \Gamma_N \times \Upsilon\,,$$

where $\partial_{n_\mathbf{x}} := \mathbf{n}_\mathbf{x}{}^\top \nabla_\mathbf{x}$. Observe that this definition guarantees a positive outward surface heat flux in agreement with (2.4). Finally, a linear combination of Dirichlet and Neumann boundary conditions is denoted by a Robin type or convective boundary condition with the heat transfer coefficient $\kappa[\mathrm{W/^\circ Cm^2}]$

$$q(\mathbf{x},t) + \kappa(\mathbf{x},t)u(\mathbf{x},t) = g_R(\mathbf{x},t) \qquad (\mathbf{x},t) \in \Gamma_R \times \Upsilon\,.$$

Remark 2.1. *The latter type of boundary condition is the most physical one for heat transfer problems, where it is referred to as Newton's law of cooling*

$$q(\mathbf{x},t) = -\kappa(\mathbf{x},t)\,(u(\mathbf{x},t) - u_\infty(\mathbf{x},t)) \qquad (\mathbf{x},t) \in \Gamma_R \times \Upsilon\,.$$

It states that the surface heat flux $q(\mathbf{x},t)$ is proportional to the temperature difference between the surface of the domain and the surrounding environment $u(\mathbf{x},t) - u_\infty(\mathbf{x},t)$ with the proportionality factor being the heat transfer coefficient κ. In general $\kappa = \kappa(\mathbf{x},t,u(\mathbf{x},t))$, however, for our purpose $\kappa = \kappa(\mathbf{x},t)$ with $0 \le \kappa(\mathbf{x},t) \le \kappa_0 \in \mathbb{R}$ will be sufficient.

For the remainder of this work we assume a vanishing energy density function $f(\tilde{\mathbf{x}},t) \equiv 0$ and vanishing initial conditions $u(\tilde{\mathbf{x}},0) \equiv 0$. Thus we may state a homogeneous initial boundary value problem of the homogeneous heat equation involving all three types of boundary condition by

$$\alpha \Delta u(\tilde{\mathbf{x}},t) = \partial_t u(\tilde{\mathbf{x}},t) \qquad (\tilde{\mathbf{x}},t) \in \Omega \times \Upsilon\,, \tag{2.7a}$$

$$u(\tilde{\mathbf{x}},0) = 0 \qquad \tilde{\mathbf{x}} \quad \in \Omega\,, \tag{2.7b}$$

$$u(\mathbf{x},t) = g_D(\mathbf{x},t) \qquad (\mathbf{x},t) \in \Gamma_D \times \Upsilon\,, \tag{2.7c}$$

$$\lambda \partial_{n_\mathbf{x}} u(\mathbf{x},t) = g_N(\mathbf{x},t) \qquad (\mathbf{x},t) \in \Gamma_N \times \Upsilon\,, \tag{2.7d}$$

$$\lambda \partial_{n_\mathbf{x}} u(\mathbf{x},t) + \kappa(\mathbf{x},t) u(\mathbf{x},t) = g_R(\mathbf{x},t) \qquad (\mathbf{x},t) \in \Gamma_R \times \Upsilon\,, \tag{2.7e}$$

with the heat diffusion coefficient $\alpha[\mathrm{m}^2/\mathrm{sec}] = \lambda / \varrho c_p$. Eliminating appropriate boundary parts $\Gamma_i \subset \Gamma$ with $i \in \{D,N,R\}$ one obtains homogeneous initial boundary value problems of different type, which we will reformulate in terms of boundary integral equations in Section 2.4.

2.2 Boundary Integral Equations of the Heat Equation

2.2.1 Representation Formula

We know that the solution of the homogeneous heat equation with homogeneous initial conditions is given by the representation formula [11, Theorem 2.20]

$$u(\tilde{\mathbf{x}},t) = \int_0^t \int_\Gamma G(\tilde{\mathbf{x}}-\mathbf{y},t-\tau) \frac{q(\mathbf{y},\tau)}{\varrho c_p} \mathrm{d}s_\mathbf{y} \mathrm{d}\tau - \int_0^t \int_\Gamma \alpha \partial_{n_\mathbf{y}} G(\tilde{\mathbf{x}}-\mathbf{y},t-\tau) u(\mathbf{y},\tau) \mathrm{d}s_\mathbf{y} \mathrm{d}\tau$$
$$(\tilde{\mathbf{x}},t) \in \Omega \times \Upsilon\,, \tag{2.8}$$

provided that the Dirichlet- and Neumann trace of the solution are known and the heat equation's fundamental solution [40] is given by

$$G(\mathbf{x}-\mathbf{y},t-\tau) = \begin{cases} (4\pi\alpha(t-\tau))^{-\frac{3}{2}} \exp\left(-\frac{|\mathbf{x}-\mathbf{y}|^2}{4\alpha(t-\tau)}\right) & \mathbf{x}-\mathbf{y} \in \mathbb{R}^3,\ t-\tau \geq 0 \\ 0 & \mathbf{x}-\mathbf{y} \in \mathbb{R}^3,\ t-\tau < 0 \end{cases}. \tag{2.9}$$

Observe that in the classical terminology the first expression on the left hand side of (2.8) is called the single layer potential and the second term the double layer potential.

It is a well known fact that one way of solving homogeneous initial boundary value problems of the homogeneous heat equation (2.7a) – (2.7e) via the representation formula (2.8) boils down to compute the complete set of Dirichlet- and Neumann traces. This is achieved

by taking the Dirichlet- and Neumann traces of the representation formula (2.8) leading to the first- and second boundary integral equation, respectively. Then one can use this set of equations, incorporate appropriate boundary conditions and solve for the yet unknown trace data, which together with the representation formula (2.8) defines the solution of the respective initial boundary value problem. Such a strategy is commonly referred to as direct boundary integral approach.

Remark 2.2. *While we focus on the direct approach, mentioned above, there are other possible techniques based on the observation that both potentials in* (2.8) *satisfy the homogeneous heat equation with homogeneous initial conditions. Thus one can find solutions of related initial boundary value problems by solving a single- or double layer ansatz for unknown densities $q(\mathbf{x},t)$ or $u(\mathbf{x},t)$, which satisfy the boundary data. The related potentials are then solutions $u(\tilde{\mathbf{x}},t)$ of the initial boundary value problems. Such strategies are called indirect boundary integral approaches.*

2.2.2 Boundary Integral Equations

As mentioned before, we take the Dirichlet trace of the representation formula (2.8), i.e., $\Omega \ni \tilde{\mathbf{x}} \to \mathbf{x} \in \Gamma$, to obtain the first boundary integral equation

$$\mathcal{V}q^*(\mathbf{x},\tau) - (\mathcal{J}+\mathcal{K})\,u(\mathbf{x},t) = 0 \tag{2.10}$$

and the thermal single- and double layer operator

$$\mathcal{V}q^*(\mathbf{x},t) := \int_0^t \int_\Gamma G(\mathbf{x}-\mathbf{y},t-\tau)q^*(\mathbf{y},\tau)\mathrm{d}s_\mathbf{y}\mathrm{d}\tau\,, \tag{2.11}$$

$$\mathcal{K}u(\mathbf{x},t) := \int_0^t \int_\Gamma \alpha\partial_{n_\mathbf{y}} G(\mathbf{x}-\mathbf{y},t-\tau)u(\mathbf{y},\tau)\mathrm{d}s_\mathbf{y}\mathrm{d}\tau\,, \tag{2.12}$$

where for notation's sake we have introduced the scaled heat flux (cf. (2.4) and (2.8))

$$q^*(\mathbf{y},\tau) := \frac{q(\mathbf{y},\tau)}{\varrho c_p} = -\mathbf{n}_\mathbf{y}^\top \frac{\mathbf{q}(\mathbf{y},\tau)}{\varrho c_p} = \alpha\partial_{n_\mathbf{y}} u(\mathbf{y},\tau)\,. \tag{2.13}$$

Observe that $\mathcal{J}(\mathbf{x}) = \pm\mathcal{I}(\mathbf{x})/2$ almost everywhere on Γ, with the plus sign applying for the interior and the minus sign for the exterior problem. Next, in order to obtain a symmetric representation, we take the scaled Neumann trace of the representation formula (2.8), i.e., α times the gradient with $\tilde{\mathbf{x}} \ni \Omega \to \mathbf{x} \in \Gamma$ in the inner product with the outer normal vector $\mathbf{n}_\mathbf{x}$, which yields the second boundary integral equation

$$\left(-\mathcal{J}+\mathcal{K}'\right) q^*(\mathbf{x},t) + \mathcal{D}u(\mathbf{x},t) = 0\,, \tag{2.14}$$

with the adjoint double layer- and the hyper-singular operator

$$\mathcal{K}'q^*(\mathbf{x},t) := \int_0^t \int_\Gamma \alpha\partial_{n_\mathbf{x}} G(\mathbf{x}-\mathbf{y},t-\tau)q^*(\mathbf{y},\tau)\mathrm{d}s_\mathbf{y}\mathrm{d}\tau\,, \tag{2.15}$$

$$\mathcal{D}u(\mathbf{x},t) := -\alpha\partial_{n_\mathbf{x}} \int_0^t \int_\Gamma \alpha\partial_{n_\mathbf{y}} G(\mathbf{x}-\mathbf{y},t-\tau)u(\mathbf{y},\tau)\mathrm{d}s_\mathbf{y}\mathrm{d}\tau\,. \tag{2.16}$$

2.3 Properties of Boundary Integral Operators

Even though the heat equation is the prototypical parabolic partial differential equation, it turns out that the related boundary integral operators have similar properties as in the elliptic case. However, the setting is slightly different [11, 37]. The correct function spaces are not the rather well known classical Sobolev spaces $H^r(\Gamma)$ [2, 28] but their anisotropic counterparts $H^{r,s}(\Gamma\times\Upsilon)$ [28, 29]. Since it is not the aim of this thesis to elaborate their theory in full detail, we only provide a short exposition of some basic concepts in Appendix A, where we report just enough details to understand the basic properties of thermal boundary integral operators (remainder of this section), Galerkin variational formulations of boundary integral formulations of initial boundary value problems (Section 2.4), and error estimates for their approximate solutions (Section 3.2).

2.3.1 The Calderon Projector in the Energy Norm

The Calderon projector [11] of the heat equation $\mathcal{C} : H^{\frac{1}{2},\frac{1}{4}}(\Gamma\times\Upsilon)\times H^{-\frac{1}{2},-\frac{1}{4}}(\Gamma\times\Upsilon) \to H^{\frac{1}{2},\frac{1}{4}}(\Gamma\times\Upsilon)\times H^{-\frac{1}{2},-\frac{1}{4}}(\Gamma\times\Upsilon)$ for the interior problem is defined by the boundary integral equations (2.10) and (2.14)

$$\mathcal{C}\begin{pmatrix} u \\ q^* \end{pmatrix} := \begin{pmatrix} \frac{\mathcal{I}}{2}-\mathcal{K} & \mathcal{V} \\ \mathcal{D} & \frac{\mathcal{I}}{2}+\mathcal{K}' \end{pmatrix}\begin{pmatrix} u \\ q^* \end{pmatrix} = \begin{pmatrix} u \\ q^* \end{pmatrix}.$$

Subtracting the identity and interchanging its columns we get the operator $\mathcal{A} : H^{-\frac{1}{2},-\frac{1}{4}}(\Gamma\times\Upsilon)\times H^{\frac{1}{2},\frac{1}{4}}(\Gamma\times\Upsilon) \to H^{\frac{1}{2},\frac{1}{4}}(\Gamma\times\Upsilon)\times H^{-\frac{1}{2},-\frac{1}{4}}(\Gamma\times\Upsilon)$

$$\mathcal{A} := \begin{pmatrix} \mathcal{V} & -\mathcal{K} \\ \mathcal{K}' & \mathcal{D} \end{pmatrix}.$$

Theorem 2.1. *$\mathcal{A}$ is bounded and $H^{-\frac{1}{2},-\frac{1}{4}}(\Gamma\times\Upsilon)\times H^{\frac{1}{2},\frac{1}{4}}(\Gamma\times\Upsilon)$ elliptic [11, Theorem 3.11], which implies the boundedness of all boundary integral operators, the $H^{-\frac{1}{2},-\frac{1}{4}}(\Gamma\times\Upsilon)$ ellipticity of the single layer operator [4, 37] [11, Corollary 3.13] and the $H^{\frac{1}{2},\frac{1}{4}}(\Gamma\times\Upsilon)$ ellipticity of the hyper-singular operator [11, Corollary 3.13].*

Corollary 2.1. *The symmetric Steklov-Poincaré operator* $\mathcal{S} := \mathcal{D} + (\frac{\mathcal{T}}{2} + \mathcal{K}')\mathcal{V}^{-1}(\frac{\mathcal{T}}{2} + \mathcal{K})$ *is bounded and* $H^{\frac{1}{2},\frac{1}{4}}(\Gamma \times \Upsilon)$ *elliptic.*

Proof. We have

$$\mathcal{S}u = \left(\tfrac{\mathcal{T}}{2} + \mathcal{K}'\right) q^* + \mathcal{D}u$$

with

$$\mathcal{V}q^* - \left(\tfrac{\mathcal{T}}{2} + \mathcal{K}\right) u = 0$$

and

$$\langle \mathcal{S}u, u\rangle_{\Gamma\times\Upsilon} = \left\langle \begin{pmatrix} 0 \\ \mathcal{S}u \end{pmatrix}, \begin{pmatrix} q^* \\ u \end{pmatrix} \right\rangle_{\Gamma\times\Upsilon} = \left\langle \mathcal{A} \begin{pmatrix} q^* \\ u \end{pmatrix}, \begin{pmatrix} q^* \\ u \end{pmatrix} \right\rangle_{\Gamma\times\Upsilon},$$

thus the ellipticity and boundedness follows from Theorem 2.1. □

Remark 2.3. *For* $r,s > 0$ *the spaces* $\widetilde{H}^{r,s}(\Gamma_i \times \Upsilon)$ *with* $\Gamma_i \subset \Gamma$ *and* $i \in \{D,N,R\}$ *defined in Appendix A are subspaces of* $H^{r,s}(\Gamma \times \Upsilon)$*. Thus the boundedness and* $\widetilde{H}^{r,s}(\Gamma_i \times \Upsilon)$ *ellipticity of the Steklov-Poincaré operator follows directly.*

2.3.2 Mapping Properties of Boundary Integral Operators

Theorem 2.2. *On Lipschitz boundaries* Γ *and for* $s \in \left(-\frac{1}{2}, \frac{1}{2}\right)$ *the boundary integral operators of the heat equation*

$$\begin{aligned}
\mathcal{V} &: H^{-\frac{1}{2}+s,(-\frac{1}{2}+s)/2}(\Gamma \times \Upsilon) \to H^{\frac{1}{2}+s,(\frac{1}{2}+s)/2}(\Gamma \times \Upsilon)\,, \\
\pm\tfrac{\mathcal{T}}{2} + \mathcal{K} &: H^{\frac{1}{2}+s,(\frac{1}{2}+s)/2}(\Gamma \times \Upsilon) \to H^{\frac{1}{2}+s,(\frac{1}{2}+s)/2}(\Gamma \times \Upsilon)\,, \\
\pm\tfrac{\mathcal{T}}{2} + \mathcal{K}' &: H^{-\frac{1}{2}+s,(-\frac{1}{2}+s)/2}(\Gamma \times \Upsilon) \to H^{-\frac{1}{2}+s,(-\frac{1}{2}+s)/2}(\Gamma \times \Upsilon)\,, \\
\mathcal{D} &: H^{\frac{1}{2}+s,(\frac{1}{2}+s)/2}(\Gamma \times \Upsilon) \to H^{-\frac{1}{2}+s,(-\frac{1}{2}+s)/2}(\Gamma \times \Upsilon)
\end{aligned}$$

are isomorphisms [11, Theorem 4.8 and 4.16].

2.4 Galerkin Variational Boundary Integral Formulations

Now, we are in the position to provide boundary integral formulations of homogeneous initial boundary value problems related to the homogeneous heat equation, i.e., (2.7a) through (2.7e). As mentioned before, we limit ourselves to direct formulations based on the Calderon projector and its restrictions in Section 2.3.1.

Remark 2.4. *Observe that due to the scaling of the heat flux* (2.13) *and the definition of the boundary integral equations* (2.10) *and* (2.14) *it is convenient to rewrite the Neumann boundary condition* (2.7d)

$$q^*(\mathbf{x},t) = g_N^* \qquad (\mathbf{x},t) \in \Gamma_N \times \Upsilon$$

and the Robin boundary condition (2.7e)

$$q^*(\mathbf{x},t) + \kappa^*(\mathbf{x},t)u(\mathbf{x},t) = g_R^* \qquad (\mathbf{x},t) \in \Gamma_R \times \Upsilon$$

with $(\cdot)^* := (\cdot)/\varrho c_p$. *Furthermore, due to* $\varrho c_p = const.$ *and Remark 2.1 we still have* $0 \leq \kappa^*(\mathbf{x},t) \leq \kappa_0^* \in \mathbb{R}$.

2.4.1 Initial Dirichlet Boundary Value Problem

Using the first boundary integral equation (2.10) we state the initial Dirichlet boundary value problem, i.e., (2.7a), (2.7b), (2.7c) with given $g_D \in H^{\frac{1}{2},\frac{1}{4}}(\Gamma \times \Upsilon)$ and $\Gamma := \Gamma_D$ and Remark 2.4

$$\mathcal{V}q^*(\mathbf{x},t) = \left(\tfrac{\mathcal{I}}{2} + \mathcal{K}\right) g_D(\mathbf{x},t) \qquad (\mathbf{x},t) \in \Gamma \times \Upsilon\,,$$

which in $H^{-\frac{1}{2},-\frac{1}{4}}(\Gamma \times \Upsilon)$ is equivalent to find $q^* \in H^{-\frac{1}{2},-\frac{1}{4}}(\Gamma \times \Upsilon)$ such that

$$\langle \mathcal{V}q^*, w\rangle_{\Gamma\times\Upsilon} = \left\langle \left(\tfrac{\mathcal{I}}{2} + \mathcal{K}\right) g_D, w\right\rangle_{\Gamma\times\Upsilon} \qquad \forall w \in H^{-\frac{1}{2},-\frac{1}{4}}(\Gamma \times \Upsilon)\,. \tag{2.17}$$

Uniqueness of the solution follows from the boundedness and $H^{-\frac{1}{2},-\frac{1}{4}}(\Gamma \times \Upsilon)$ ellipticity of the single layer operator provided by Theorem 2.1.

2.4.2 Initial Neumann Boundary Value Problem

We use the second boundary integral equation (2.14) to give a boundary integral formulation of the initial Neumann boundary value problem, i.e., (2.7a), (2.7b), (2.7d) with given $g_N^* \in H^{-\frac{1}{2},-\frac{1}{4}}(\Gamma \times \Upsilon)$ (cf. Remark 2.4) and $\Gamma := \Gamma_N$

$$\mathcal{D}u(\mathbf{x},t) = \left(\tfrac{\mathcal{I}}{2} - \mathcal{K}'\right) g_N^* \qquad (\mathbf{x},t) \in \Gamma \times \Upsilon\,,$$

which in $H^{\frac{1}{2},\frac{1}{4}}(\Gamma \times \Upsilon)$ is equivalent to find $u \in H^{\frac{1}{2},\frac{1}{4}}(\Gamma \times \Upsilon)$ such that

$$\langle \mathcal{D}u, v\rangle_{\Gamma\times\Upsilon} = \left\langle \left(\tfrac{\mathcal{I}}{2} - \mathcal{K}'\right) g_N^*, v\right\rangle_{\Gamma\times\Upsilon} \qquad \forall v \in H^{\frac{1}{2},\frac{1}{4}}(\Gamma \times \Upsilon)\,. \tag{2.18}$$

Uniqueness of the solution follows from the boundedness and $H^{\frac{1}{2},\frac{1}{4}}(\Gamma \times \Upsilon)$ ellipticity of the hyper-singular operator ensured by Theorem 2.1.

2.4.3 Initial Robin Boundary Value Problem

Similar to [44, page 181] we use the symmetric representation of the Steklov-Poincaré operator in Corollary 2.1 as a Dirichlet to Neumann map and state a boundary integral formulation for the homogeneous initial Robin boundary value problem, i.e., (2.7a), (2.7b), (2.7e) with given $g_R^* \in H^{-\frac{1}{2},-\frac{1}{4}}(\Gamma \times \Upsilon)$, $0 \leq \kappa^* \leq \kappa_0^* \in \mathbb{R}$ (cf. Remark 2.4) and $\Gamma := \Gamma_R$

$$(\mathcal{S} + \kappa^*)\, u(\mathbf{x},t) = g_R^*(\mathbf{x},t) \qquad (\mathbf{x},t) \in (\Gamma \times \Upsilon)\,.$$

In $H^{\frac{1}{2},\frac{1}{4}}(\Gamma \times \Upsilon)$ this is equivalent to find $u \in H^{\frac{1}{2},\frac{1}{4}}(\Gamma \times \Upsilon)$ such that

$$\langle (\mathcal{S} + \kappa^*)\, u, v \rangle_{\Gamma \times \Upsilon} = \langle g_R^*, v \rangle_{\Gamma \times \Upsilon} \qquad \forall v \in H^{\frac{1}{2},\frac{1}{4}}(\Gamma \times \Upsilon)\,. \tag{2.19}$$

Uniqueness of the solution follows from the $H^{\frac{1}{2},\frac{1}{4}}(\Gamma \times \Upsilon)$ boundedness and ellipticity of the Steklov-Poincareé operator given in Corollary 2.1 and the properties of the scalded heat transfer coefficient κ^*.

2.4.4 Mixed Initial Boundary Value Problems

In what follows now we present a boundary integral formulation similar to [44, page 180] for a mixed initial boundary value problem, i.e., (2.7a), (2.7b), (2.7c), (2.7d) and (2.7e) with $\Gamma := \overline{\Gamma}_D \cup \overline{\Gamma}_N \cup \overline{\Gamma}_R$ and $0 \leq \kappa^* \leq \kappa_0^* \in \mathbb{R}$ (cf. Remark 2.4). For this purpose we define

$$g_{NR}^*(\mathbf{x},t) := \begin{cases} g_N^*(\mathbf{x},t) & (\mathbf{x},t) \in \Gamma_N \times \Upsilon \\ g_R^*(\mathbf{x},t) & (\mathbf{x},t) \in \Gamma_R \times \Upsilon \end{cases}, \qquad \kappa_{NR}^*(\mathbf{x},t) := \begin{cases} 0 & (\mathbf{x},t) \in \Gamma_N \times \Upsilon \\ \kappa^*(\mathbf{x},t) & (\mathbf{x},t) \in \Gamma_R \times \Upsilon \end{cases},$$

$\Gamma_{NR} := \Gamma_N \cup \Gamma_R + \overline{\Gamma}_N \cap \overline{\Gamma}_R$ and assume an arbitrary but fixed extension of the given Dirichlet data

$$u(\mathbf{x},t) = \tilde{g}_D(\mathbf{x},t) + \tilde{u}(\mathbf{x},t) \qquad (\mathbf{x},t) \in \Gamma \times \Upsilon\,,$$

such that $H^{\frac{1}{2},\frac{1}{4}}(\Gamma \times \Upsilon) \ni \tilde{g}_D(\mathbf{x},t) = g_D(\mathbf{x},t)$ for $(\mathbf{x},t) \in \Gamma_D \times \Upsilon$ and $\tilde{u} \in \widetilde{H}^{\frac{1}{2},\frac{1}{4}}(\Gamma_{NR} \times \Upsilon)$. We choose a boundary integral formulation based on the symmetric Steklov-Poincaré operator defined in Corollary 2.1 as a Dirichlet to Neumann map

$$(\mathcal{S} + \kappa_{NR}^*)\, \tilde{u}(\mathbf{x},t) = g_{NR}^*(\mathbf{x},t) - (\mathcal{S} + \kappa_{NR}^*)\, \tilde{g}_D(\mathbf{x},t) \qquad (\mathbf{x},t) \in \Gamma_{NR} \times \Upsilon\,,$$

which in $\widetilde{H}^{\frac{1}{2},\frac{1}{4}}(\Gamma_{NR} \times \Upsilon)$ is equivalent to find $\tilde{u} \in \widetilde{H}^{\frac{1}{2},\frac{1}{4}}(\Gamma_{NR} \times \Upsilon)$ such that

$$\langle (\mathcal{S} + \kappa_{NR}^*)\, \tilde{u}, v \rangle_{\Gamma_{NR} \times \Upsilon} = \langle g_{NR}^* - (\mathcal{S} + \kappa_{NR}^*)\, \tilde{g}_D, v \rangle_{\Gamma_{NR} \times \Upsilon} \qquad \forall v \in \widetilde{H}^{\frac{1}{2},\frac{1}{4}}(\Gamma_{NR} \times \Upsilon)\,. \tag{2.20}$$

Uniqueness of the solution follows from the $\widetilde{H}^{\frac{1}{2},\frac{1}{4}}(\Gamma_{NR} \times \Upsilon)$ boundedness and ellipticity of the Steklov-Poincaré operator provided by Corollary 2.1, Remark 2.3 and the properties of the scaled heat transfer coefficient κ_{NR}^*.

Remark 2.5. *Assume the absence of some boundary parts $\Gamma_i \subset \Gamma$ with $i \in \{D,N,R\}$ in the exposition of Section 2.4.4, then we obtain the following initial boundary value problems:*

- $\Gamma_R := \emptyset$ *initial Dirichlet-Neumann boundary value problem.*
- $\Gamma_N := \emptyset$ *initial Dirichlet-Robin boundary value problem.*
- $\Gamma_D := \emptyset$ *initial Neumann-Robin boundary value problem.*

3 SPACE-TIME GALERKIN BOUNDARY ELEMENT METHODS

Due to the properties of the boundary integral operators presented in Section 2.3, a space-time Galerkin discretization with conforming subspaces is straight forward [6, 7, 44, 46] and inherits the unique solvability of the continuous Galerkin variational formulations of Section 2.4. Furthermore, these properties allow us to derive error estimates in close analogy to the elliptic theory [43, 44].

3.1 Space-Time Discretization

3.1.1 Space-Time Triangulation

All of the Galerkin variational forms stated in Section 2.4 are discretized by using piecewise polynomial space-time tensor product spaces defined on a triangulation of the computational domain $\Gamma \times \Upsilon$.

Spatial triangulation We only work with flat triangular boundary elements and, therefore, restrict our exposition explicitly to that case. For this purpose we assume an interpolation approximation of the piecewise Lipschitz boundary Γ by Q open, triangular, and linear elements χ_q such that

$$\Gamma \approx \bigcup_{q=0}^{Q-1} \overline{\chi}_q \tag{3.1}$$

with $\chi_i \cap \chi_j = \emptyset$ for $i \neq j$. If $\overline{\chi}_i$ and $\overline{\chi}_j$ share one common edge or point, they are said to be neighboring elements. For such a triangulation we introduce local parametrizations, which consist of mappings $\Theta_q(\hat{\mathbf{x}}) : \hat{\chi} \to \chi_q$ between the reference element $\hat{\chi} \subset \mathbb{R}^2$ in parameter domain and a physical element $\chi_q \subset \mathbb{R}^3$ such that

$$\Gamma \approx \bigcup_{q=0}^{Q-1} \Theta_q(\overline{\hat{\chi}}) \, .$$

Observe that each boundary element χ_q is uniquely defined by its vertices $\{\mathbf{x}_q^j\}_{j=1}^3 \subset \Gamma$ and linear interpolation between. The reference element on the other hand is defined by

$$\hat{\chi} := \{\hat{x}_1, \hat{x}_2 : 0 < \hat{x}_1 < 1, 0 < \hat{x}_2 < \hat{x}_1\}$$

with vertices $\{\hat{\mathbf{x}}^j\}_{j=1}^3$. Hence together with a set of linear functions $\{\eta_j : \hat{\chi} \to [0,1]\}_{j=1}^3$ with

$$\eta_j(\hat{\mathbf{x}}) = \begin{cases} 1 & \hat{\mathbf{x}} = \hat{\mathbf{x}}^k \quad k = j \\ 0 & \hat{\mathbf{x}} = \hat{\mathbf{x}}^k \quad k \neq j \end{cases}$$

we can then define the above mentioned mappings by

$$\Theta_q(\hat{\mathbf{x}}) = \sum_{j=1}^{3} \eta_j(\hat{\mathbf{x}}) \mathbf{x}_q^j \, .$$

Finally, in order to provide error bounds of the Galerkin boundary element methods afterwards, we assume the boundary triangulation to be globally quasi-uniform, i.e., there is a constant $C > 0$ independent of Q such that

$$\min_{\chi \in \{\chi_q\}_{q=0}^{Q-1}} (\operatorname{diam}(\chi)) \leq C \max_{\chi \in \{\chi_q\}_{q=0}^{Q-1}} (\operatorname{diam}(\chi)) \, .$$

Temporal triangulation Contrary to the more general assumptions on the spatial aspects of the computational domain, time is one-dimensional, linear, and directional. Therefore, we restrict ourselves to an equidistant partition of the time interval Υ with continuously indexed time steps $\nu_p = (ph_t, (p+1)h_t)$ of step size h_t

$$\overline{\Upsilon} = \bigcup_{p=0}^{P-1} \overline{\nu}_p \, . \tag{3.2}$$

With the definition of the reference element $\hat{\nu} := (0,1)$ and the mappings $\theta_p : \hat{\nu} \to \nu_p$

$$\theta_p(\hat{t}) = (p + \hat{t})h_t \, ,$$

this leads to the local parametrization of the time interval

$$\overline{\Upsilon} = \bigcup_{p=0}^{P-1} \theta_p(\overline{\hat{\nu}}) \, .$$

3.1.2 Tensor Product Test- and Trial Spaces

On these triangulations, i.e., (3.1) and (3.2), we define piecewise polynomial ansatz spaces of polynomial degree d_x in space and d_t in time. The spatial ansatz space can either consist of globally continuous c_{d_x} or discontinuous d_{d_x} functions (cf. [26, 33])

$$\begin{aligned} X_{h_x}^{c_{d_x}}(\Gamma) &:= \operatorname{span}\{\psi_\ell(\mathbf{x})\}_{\ell=0}^{N_x-1} \, , \\ X_{h_x}^{d_{d_x}}(\Gamma) &:= \operatorname{span}\{\varphi_\ell(\mathbf{x})\}_{\ell=0}^{N_x-1} \, . \end{aligned} \tag{3.3}$$

In principle, the same idea also works for the temporal ansatz space, however, in order not to destroy the Töplitz structure of the system [37], we restrict ourselves to globally discontinuous test and trial spaces. Nevertheless, for consistency sake we have chosen the same notation as in the spatial case, hence

$$T_{h_t}^{d_{d_t}}(\Upsilon) := \operatorname{span}\{\phi_j(t)\}_{j=0}^{N_t-1} . \tag{3.4}$$

Finally, we use (3.3) and (3.4) to construct piecewise polynomial space-time tensor product spaces

$$S_{h_x,h_t}^{c_{d_x},d_{d_t}}(\Gamma\times\Upsilon) := X_{h_x}^{c_{d_x}}(\Gamma)\otimes T_{h_t}^{d_{d_t}}(\Upsilon) ,$$
$$S_{h_x,h_t}^{d_{d_x},d_{d_t}}(\Gamma\times\Upsilon) := X_{h_x}^{d_{d_x}}(\Gamma)\otimes T_{h_t}^{d_{d_t}}(\Upsilon)$$

for the discretization of all Galerkin discretized thermal layer potentials in Section 2.4.

3.1.3 Galerkin Discretization of Thermal Layer Potentials

The Galerkin variational forms of the thermal single-, double-, and adjoint double layer operators appearing in Section 2.4 are defined as the weakly singular bilinear forms listed below

$$\langle \mathcal{V}q^*, w\rangle_{\Gamma\times\Upsilon} = \int_{t=0}^{T}\int_{\Gamma} w(\mathbf{x},t)\int_{\tau=0}^{t}\int_{\Gamma} G(\mathbf{x}-\mathbf{y},t-\tau)q^*(\mathbf{y},\tau)\,\mathrm{d}s_{\mathbf{y}}\mathrm{d}\tau\,\mathrm{d}s_{\mathbf{x}}\mathrm{d}t , \tag{3.5}$$

$$\langle \mathcal{K}u, w\rangle_{\Gamma\times\Upsilon} = \int_{t=0}^{T}\int_{\Gamma} w(\mathbf{x},t)\int_{\tau=0}^{t}\int_{\Gamma} \alpha\frac{\partial}{\partial n_{\mathbf{y}}}G(\mathbf{x}-\mathbf{y},t-\tau)u(\mathbf{y},\tau)\,\mathrm{d}s_{\mathbf{y}}\mathrm{d}\tau\,\mathrm{d}s_{\mathbf{x}}\mathrm{d}t , \tag{3.6}$$

$$\langle \mathcal{K}'q^*, v\rangle_{\Gamma\times\Upsilon} = \int_{t=0}^{T}\int_{\Gamma} v(\mathbf{x},t)\int_{\tau=0}^{t}\int_{\Gamma} \alpha\frac{\partial}{\partial n_{\mathbf{x}}}G(\mathbf{x}-\mathbf{y},t-\tau)q^*(\mathbf{y},\tau)\,\mathrm{d}s_{\mathbf{y}}\mathrm{d}\tau\,\mathrm{d}s_{\mathbf{x}}\mathrm{d}t , \tag{3.7}$$

while for the hyper-singular operator we need to perform integration by parts to obtain the following weakly singular representation

$$\begin{aligned}\langle \mathcal{D}u, v\rangle_{\Gamma\times\Upsilon} = &\int_{t=0}^{T}\int_{\Gamma} \mathbf{curl}_{\mathbf{x}}^{\top} v(\mathbf{x},t)\int_{\tau=0}^{t}\int_{\Gamma} \alpha^2 G(\mathbf{x}-\mathbf{y},t-\tau)\mathbf{curl}_{\mathbf{y}}u(\mathbf{y},\tau)\,\mathrm{d}s_{\mathbf{y}}\mathrm{d}\tau\,\mathrm{d}s_{\mathbf{x}}\mathrm{d}t\\ &-\int_{t=0}^{T}\int_{\Gamma} \mathbf{n}_{\mathbf{x}}{}^{\top} v(\mathbf{x},t)\int_{\tau=0}^{t}\int_{\Gamma} \alpha^2\frac{\partial}{\partial\tau}G(\mathbf{x}-\mathbf{y},t-\tau)\mathbf{n}_{\mathbf{y}}u(\mathbf{y},\tau)\,\mathrm{d}s_{\mathbf{y}}\mathrm{d}\tau\,\mathrm{d}s_{\mathbf{x}}\mathrm{d}t\end{aligned} \tag{3.8}$$

with $\mathbf{curl}_{\mathbf{x}} := \mathbf{n}_{\mathbf{x}}\times\nabla_{\mathbf{x}}$. This result is due to some unpublished notes of G. Of, which follow along the lines of [44, Theorem 6.17] but can already be found in [11, Theorem 6.1].

We observe that piecewise constant ansatz functions in time are an appropriate choice for the Galerkin discretization of all boundary integral operators in Theorem 2.2 since $T_{h_t}^{d_0}(\Upsilon)$ is a conforming subspace of $H^s(\mathbb{R})$ with $s < 1/2$. Therefore, and due to the fact that all Galerkin variational forms (3.5), (3.6), (3.7) and (3.8) are defined in a weakly singular sense, the space-time discretization for all of them looks the same as long as we use conforming spatial subspaces as well. Hence, we will exemplary perform the discretization for the single layer operator (3.5), which is defined in a weakly singular sense. Thus we exchange the order of integration and end up with

$$\begin{aligned}
\langle \mathcal{V} q^*, v\rangle_{\Gamma\times\Upsilon} &\approx \langle \mathcal{V} q_h^*, \varphi_k\phi_i\rangle_{\Gamma\times\Upsilon} \qquad \forall k,i \\
&= \int_{t=0}^{T}\int_{\Gamma} \varphi_k(\mathbf{x})\phi_i(t) \int_{\tau=0}^{t}\int_{\Gamma} G(\mathbf{x}-\mathbf{y},t-\tau) \sum_{j=0}^{i}\sum_{\ell=0}^{N_x-1} \varphi_\ell(\mathbf{y})\phi_j(\tau)(q_\ell^*)_j \,\mathrm{d}s_{\mathbf{y}}\mathrm{d}\tau\,\mathrm{d}s_{\mathbf{x}}\mathrm{d}t \\
&= \sum_{j=0}^{i}{}'\sum_{\ell=0}^{N_x-1} \int_{\mathrm{supp}(\varphi_k)} \varphi_k(\mathbf{x}) \int_{\mathrm{supp}(\varphi_\ell)} \varphi_\ell(\mathbf{y}) \int_{t=ih_t}^{(i+1)h_t}\int_{\tau=jh_t}^{(j+1)h_t} G(\mathbf{x}-\mathbf{y},t-\tau)\,\mathrm{d}\tau\mathrm{d}t\,\mathrm{d}s_{\mathbf{y}}\mathrm{d}s_{\mathbf{x}}(q_\ell^*)_j \\
&= \sum_{j=0}^{i}{}'\sum_{\ell=0}^{N_x-1} \int_{\mathrm{supp}(\varphi_k)} \varphi_k(\mathbf{x}) \int_{\mathrm{supp}(\varphi_\ell)} \varphi_\ell(\mathbf{y}) V_{ij}(\mathbf{x}-\mathbf{y})\,\mathrm{d}s_{\mathbf{y}}\mathrm{d}s_{\mathbf{x}}(q_\ell^*)_j\,,
\end{aligned}$$

where we use $\sum'$ to point out the special case where $j = i$, in which the upper limit of the inner time integral is changed to

$$V_{ii}(\mathbf{x}-\mathbf{y}) = \int_{t=ih_t}^{(i+1)h_t}\int_{\tau=ih_t}^{t} G(\mathbf{x}-\mathbf{y},t-\tau)\,\mathrm{d}\tau\mathrm{d}t\,.$$

Due to the translational invariance of the kernel $G(\mathbf{x}-\mathbf{y},t-\tau)$ and the equidistant time discretization, the time integrated kernel $V_{ij}(\mathbf{x}-\mathbf{y})$ does not depend on the absolute value of the indices i and j but only on their difference $d := i-j$. Hence, with this observation and causality we end up with a lower triangular Töplitz structure

$$\left(\sum_{j=0}^{i}{}'\mathbf{V}_{ij}\mathbf{q}_j^*\right)_{i=0}^{N_t-1} = \left(\sum_{d=0}^{i}{}'\mathbf{V}_d\mathbf{q}_{i-d}^*\right)_{i=0}^{N_t-1} = \begin{pmatrix} \mathbf{V}_0 & 0 & \dots & 0 \\ \mathbf{V}_1 & \ddots & \ddots & \vdots \\ \vdots & \ddots & \ddots & 0 \\ \mathbf{V}_{N_t-1} & \dots & \mathbf{V}_1 & \mathbf{V}_0 \end{pmatrix} \begin{pmatrix} \mathbf{q}_0^* \\ \mathbf{q}_1^* \\ \vdots \\ \mathbf{q}_{N_t-1}^* \end{pmatrix},$$

where we have replaced the spatial sum by matrix notation. It is easily seen that solving for such an operator

$$\sum_{d=0}^{i}{}'\mathbf{V}_d\mathbf{q}_{i-d}^* = \mathbf{f}_i \qquad \forall i = 0,\dots N_t-1$$

can be done explicitly in each time step

$$\mathbf{q}_i^* = (\mathbf{V}_0)^{-1} \left(\mathbf{f}_i - \sum_{d=1}^{i} \mathbf{V}_d \mathbf{q}_{i-d}^* \right) .$$

However, it involves the convolution over the complete history on the right hand side, which is computationally very expensive. How to deal with this problem effectively is the main topic of this thesis and elaborated in Chapter 4.

3.1.4 Computation of Matrix Entries

Since all Galerkin bilinear forms (3.5) through (3.8) are defined in a weakly singular form, we can exchange the order of integration. Then the previously defined tensor product trial and test spaces allow us to perform spatial and temporal integration completely independent from each other. Since we limit ourselves to equidistant time discretization, it is rather straightforward to perform time integration analytically. For the single layer operator this has been done in [37] and is extended to the remaining operators here.

Analytic integration in time. Introducing local time variables $t = (i+\hat{t})h_t$ and $\tau = (j+\hat{\tau})h_t$ with $\hat{t}, \hat{\tau} \in (-1,1)$ we obtain

$$V_d(\mathbf{r}) = \begin{cases} \sqrt{\frac{h_t}{\alpha^3}} \int_0^1 \int_0^{\hat{t}} G\left(\frac{\mathbf{r}}{\sqrt{\alpha h_t}}, d+\hat{t}-\hat{\tau}\right) \mathrm{d}\hat{\tau}\mathrm{d}\hat{t} & d = 0 \\ \sqrt{\frac{h_t}{\alpha^3}} \int_0^1 \int_0^1 G\left(\frac{\mathbf{r}}{\sqrt{\alpha h_t}}, d+\hat{t}-\hat{\tau}\right) \mathrm{d}\hat{\tau}\mathrm{d}\hat{t} & d \geq 1 \end{cases} , \tag{3.9}$$

which results in

$$V_d(\mathbf{r}) = \sqrt{\frac{h_t}{\alpha^3}} \left[G^{(-2)}\left(\frac{\mathbf{r}}{\sqrt{\alpha h_t}}, d+1\right) - 2G^{(-2)}\left(\frac{\mathbf{r}}{\sqrt{\alpha h_t}}, d\right) + G^{(-2)}\left(\frac{\mathbf{r}}{\sqrt{\alpha h_t}}, d-1\right) \right] \tag{3.10}$$

with

$$G^{(-2)}(\boldsymbol{r}, \mathfrak{d}) = \begin{cases} 0 & \mathfrak{d} \leq 0 \\ \frac{\sqrt{\mathfrak{d}}}{4\pi} \left[\operatorname{erfc}\left(\frac{|\boldsymbol{r}|}{\sqrt{4\mathfrak{d}}}\right) \left(\frac{|\boldsymbol{r}|}{\sqrt{4\mathfrak{d}}} + \frac{\sqrt{\mathfrak{d}}}{|\boldsymbol{r}|}\right) - \exp\left(-\frac{|\boldsymbol{r}|^2}{4\mathfrak{d}}\right) \left(\frac{1}{\sqrt{\pi}}\right) \right] & \mathfrak{d} > 0 \end{cases} .$$

Since all the integrals in (3.5) through (3.8) are weakly singular as already mentioned

before, we obtain the kernels for the double- and the adjoint double layer potential by

$$\begin{aligned}
K_d(\mathbf{r}) &= \alpha \frac{\partial}{\partial \mathbf{n_y}} V_d(\mathbf{r}) = \alpha \mathbf{n_y}^\top \nabla_{\mathbf{y}} V_d(\mathbf{r}) \\
&= \mathbf{n_y}^\top \sqrt{\tfrac{h_t}{\alpha}} \Big[\nabla_{\mathbf{y}} G^{(-2)} \left(\tfrac{\mathbf{r}}{\sqrt{\alpha h_t}}, d+1 \right) - 2 \nabla_{\mathbf{y}} G^{(-2)} \left(\tfrac{\mathbf{r}}{\sqrt{\alpha h_t}}, d \right) \\
&\qquad + \nabla_{\mathbf{y}} G^{(-2)} \left(\tfrac{\mathbf{r}}{\sqrt{\alpha h_t}}, d-1 \right) \Big], \\
K'_d(\mathbf{r}) &= \alpha \frac{\partial}{\partial \mathbf{n_x}} V_d(\mathbf{r}) = \alpha \mathbf{n_x}^\top \nabla_{\mathbf{x}} V_d(\mathbf{r}) = -\alpha \mathbf{n_x}^\top \nabla_{\mathbf{y}} V_d(\mathbf{r}) \\
&= -\mathbf{n_x}^\top \sqrt{\tfrac{h_t}{\alpha}} \Big[\nabla_{\mathbf{y}} G^{(-2)} \left(\tfrac{\mathbf{r}}{\sqrt{\alpha h_t}}, d+1 \right) - 2 \nabla_{\mathbf{y}} G^{(-2)} \left(\tfrac{\mathbf{r}}{\sqrt{\alpha h_t}}, d \right) \\
&\qquad + \nabla_{\mathbf{y}} G^{(-2)} \left(\tfrac{\mathbf{r}}{\sqrt{\alpha h_t}}, d-1 \right) \Big]
\end{aligned}$$

with

$$\nabla_{\mathbf{y}} G^{(-2)}(\boldsymbol{r}, \mathfrak{d}) = \begin{cases} 0 & \mathfrak{d} \leq 0 \\ -\frac{\boldsymbol{r}\sqrt{\mathfrak{d}}}{4\pi|\boldsymbol{r}|^2} \left[\operatorname{erfc}\left(\frac{|\boldsymbol{r}|}{\sqrt{4\mathfrak{d}}} \right) \left(\frac{|\boldsymbol{r}|}{\sqrt{4\mathfrak{d}}} - \frac{\sqrt{\mathfrak{d}}}{|\boldsymbol{r}|} \right) - \exp\left(-\frac{|\boldsymbol{r}|^2}{4\mathfrak{d}} \right) \left(\frac{1}{\sqrt{\pi}} \right) \right] & \mathfrak{d} > 0 \end{cases}.$$

Finally, we still have to perform the time integration for the hyper-singular operator. For the first part of (3.8) we can recycle $V_d(\mathbf{r})$ while the time integrated kernel for the second part is given by

$$\begin{aligned}
D_d(\mathbf{r}) = \sqrt{\alpha h_t} \Big[& \left(\tfrac{\partial}{\partial \tau} G \right)^{(-2)} \left(\tfrac{\mathbf{r}}{\sqrt{\alpha h_t}}, d+1 \right) - 2 \left(\tfrac{\partial}{\partial \tau} G \right)^{(-2)} \left(\tfrac{\mathbf{r}}{\sqrt{\alpha h_t}}, d \right) \\
& + \left(\tfrac{\partial}{\partial \tau} G \right)^{(-2)} \left(\tfrac{\mathbf{r}}{\sqrt{\alpha h_t}}, d-1 \right) \Big]
\end{aligned} \tag{3.11}$$

with

$$\left(\tfrac{\partial}{\partial \tau} G \right)^{(-2)} (\boldsymbol{r}, \mathfrak{d}) = \begin{cases} 0 & \mathfrak{d} \leq 0 \\ -\frac{1}{4\pi|\boldsymbol{r}|} \operatorname{erfc}\left(\frac{|\boldsymbol{r}|}{\sqrt{4\mathfrak{d}}} \right) & \mathfrak{d} > 0 \end{cases}.$$

Numerical integration in space. The spatial integration for general unstructured domains can in general not be performed analytically, hence we resort to numerical schemes. For $d > 1$ the time integrated kernels (3.10) – (3.11) are $C^\infty(\mathbb{R}^3)$, thus we use standard

Gauss quadrature. However, for $d \in \{0,1\}$ they behave like

$$\begin{aligned}
\lim_{\mathbf{r}\to\mathbf{0}} V_0(\mathbf{r}) &= \mathscr{O}\left(\tfrac{1}{|\mathbf{r}|}\right), & \lim_{\mathbf{r}\to\mathbf{0}} V_1(\mathbf{r}) &= \mathscr{O}(|\mathbf{r}|), \\
\lim_{\mathbf{r}\to\mathbf{0}} K_0(\mathbf{r}) &= \mathscr{O}\left(\tfrac{\mathbf{n_y}^\top \mathbf{r}}{|\mathbf{r}|^3}\right), & \lim_{\mathbf{r}\to\mathbf{0}} K_1(\mathbf{r}) &= \mathscr{O}\left(\tfrac{\mathbf{n_y}^\top \mathbf{r}}{|\mathbf{r}|}\right), \\
\lim_{\mathbf{r}\to\mathbf{0}} K_0'(\mathbf{r}) &= \mathscr{O}\left(\tfrac{\mathbf{n_x}^\top \mathbf{r}}{|\mathbf{r}|^3}\right), & \lim_{\mathbf{r}\to\mathbf{0}} K_1'(\mathbf{r}) &= \mathscr{O}\left(\tfrac{\mathbf{n_x}^\top \mathbf{r}}{|\mathbf{r}|}\right), \\
\lim_{\mathbf{r}\to\mathbf{0}} D_0(\mathbf{r}) &= \mathscr{O}\left(\tfrac{1}{|\mathbf{r}|}\right), & \lim_{\mathbf{r}\to\mathbf{0}} D_1(\mathbf{r}) &= \mathscr{O}(|\mathbf{r}|),
\end{aligned}$$

therefore we use the formulas of Erichsen and Sauter [15].

3.2 Error Estimates for Galerkin Boundary Element Methods

In this section, we provide error estimates for boundary element formulations based on the Galerkin variational formulations given in Section 2.4. In the following, we recall the approximation properties of piecewise polynomial tensor product spaces $S^{d_x,d_t}_{h_x,h_t}(\Gamma\times\Upsilon) \subset H^{p,q}(\Gamma\times\Upsilon)$, where $d_t = d_{d_t}$ and d_x can either mean c_{d_x} or d_{d_x} according to (3.3) if not specified any further.

Theorem 3.1. *[11, Proposition 5.3] Assume $0 \le r \le d_x+1$, $0 \le s \le d_t+1$ and $p \le r$, $q \le s$ with $pq \ge 0$. Moreover, let $\mathcal{Q}^{d_x}_{h_x}\mathcal{Q}^{d_t}_{h_t} : L_2(\Gamma\times\Upsilon) \to S^{d_x,d_t}_{h_x,h_t}(\Gamma\times\Upsilon)$ be the $L_2(\Gamma\times\Upsilon)$ projection*

$$\langle u - \mathcal{Q}^{d_x}_{h_x}\mathcal{Q}^{d_t}_{h_t} u, v_h\rangle_{L_2(\Gamma\times\Upsilon)} = 0 \qquad \forall v_h \in S^{d_x,d_t}_{h_x,h_t}(\Gamma\times\Upsilon),$$

then we have for all $u \in H^{r,s}(\Gamma\times\Upsilon)$

$$\inf_{v\in S^{d_x,d_t}_{h_x,h_t}(\Gamma\times\Upsilon)} \|u-v\|_{H^{p,q}(\Gamma\times\Upsilon)} \le \|u - \mathcal{Q}^{d_x}_{h_x}\mathcal{Q}^{d_t}_{h_t} u\|_{H^{p,q}(\Gamma\times\Upsilon)} \le C(h_x^a + h_t^b)\|u\|_{H^{r,s}(\Gamma\times\Upsilon)}$$

with

$$a = \min\left\{r-p, r-\frac{qr}{s}\right\} \qquad \text{and} \qquad b = \min\left\{s-q, s-\frac{ps}{r}\right\}.$$

We always have $q = p/2$ in this paper, hence the most meaningful choice for s and r is $s = r/2$, which leads to the full convergence rates in space and time of $a = r-p$ and $b = s-q$, respectively. Due to $b = a/2$ it is obvious that choosing $h_t = \mathscr{O}(h_x^2)$ leads to the optimal combined convergence rate.

Corollary 3.1. *Assume $|p| \le d_x+1$ and $|q| \le d_t+1$ and $pq \ge 0$ then the $L_2(\Gamma\times\Upsilon)$ projection $\mathcal{Q}^{d_x}_{h_x}\mathcal{Q}^{d_t}_{h_t} : L_2(\Gamma\times\Upsilon) \to S^{d_x,d_t}_{h_x,h_t}(\Gamma\times\Upsilon)$ satisfies the stability condition*

$$\|\mathcal{Q}^{d_x}_{h_x}\mathcal{Q}^{d_t}_{h_t} u\|_{H^{p,q}(\Gamma\times\Upsilon)} \le C\|u\|_{H^{p,q}(\Gamma\times\Upsilon)}. \tag{3.12}$$

Proof. The triangle inequality yields

$$\|\mathcal{Q}_{h_x}^{d_x}\mathcal{Q}_{h_t}^{d_t}u\|_{H^{p,q}(\Gamma\times\Upsilon)} \leq \|u\|_{H^{p,q}(\Gamma\times\Upsilon)} + \|\mathcal{Q}_{h_x}^{d_x}\mathcal{Q}_{h_t}^{d_t}u - u\|_{H^{p,q}(\Gamma\times\Upsilon)}$$

thus with Theorem 3.1, $r = p$, and $s = q$ we get the assertion for $0 \leq p \leq d_x + 1$ and $0 \leq q \leq d_t + 1$

$$\|\mathcal{Q}_{h_x}^{d_x}\mathcal{Q}_{h_t}^{d_t}u\|_{H^{p,q}(\Gamma\times\Upsilon)} \leq (1+C)\|u\|_{H^{p,q}(\Gamma\times\Upsilon)} \,.$$

By duality we have

$$\begin{aligned}
\|\mathcal{Q}_{h_x}^{d_x}\mathcal{Q}_{h_t}^{d_t}u\|_{H^{-p,-q}(\Gamma\times\Upsilon)} &\leq \sup_{0\neq v\in H^{p,q}(\Gamma\times\Upsilon)} \frac{\left\langle \mathcal{Q}_{h_x}^{d_x}\mathcal{Q}_{h_t}^{d_t}u, v\right\rangle_{\Gamma\times\Upsilon}}{\|v\|_{H^{p,q}(\Gamma\times\Upsilon)}} \\
&= \sup_{0\neq v\in H^{p,q}(\Gamma\times\Upsilon)} \frac{\left\langle u, \mathcal{Q}_{h_x}^{d_x}\mathcal{Q}_{h_t}^{d_t}v\right\rangle_{\Gamma\times\Upsilon}}{\|v\|_{H^{p,q}(\Gamma\times\Upsilon)}} \\
&\leq (1+C)\|u\|_{H^{-p,-q}(\Gamma\times\Upsilon)} \,,
\end{aligned}$$

which concludes the proof. □

Theorem 3.1 is useful for error estimates in the energy norm, however, it is more practical to work with the L_2 error. In order to provide such estimates in the case of the energy space being a negative indexed Sobolev space, we need the following inverse inequality.

Theorem 3.2. *[37, Lemma 7.4] Assume a globally quasi-uniform triangulation. Then for $0 \leq p \leq d_x$ and $0 \leq q \leq d_t$ there is a constant C independent of $S_{h_x,h_t}^{d_x,d_t}(\Gamma\times\Upsilon)$ such that*

$$\|u\|_{L_2(\Gamma\times\Upsilon)} \leq C(h_x^{-p} + h_t^{-q})\|u\|_{H^{-p,-q}(\Gamma\times\Upsilon)} \qquad \forall u \in S_{h_x,h_t}^{d_x,d_t}(\Gamma\times\Upsilon) \,.$$

Whenever the energy space is a Sobolev space of positive order we will use a duality argument called Aubin-Nitsche trick [44] to estimate the L_2 error.

Note that in the following we fix the spaces $S_{h_x,h_t}^{d_{d_x},d_{d_t}}(\Gamma\times\Upsilon)$, respectively $S_{h_x,h_t}^{c_{d_x},d_{d_t}}(\Gamma\times\Upsilon)$ by choosing a suitable $d_x \in \{0,1\}$ and setting $d_t = 0$. The latter is due to the restriction to a piecewise constant time discretization in Section 3.1.

3.2.1 Initial Dirichlet Boundary Value Problem

If we solve (2.17) for the approximate solution, i.e., find $q_h^* \in S_{h_x,h_t}^{d_1,d_0}(\Gamma\times\Upsilon)$ such that

$$\langle \mathcal{V}q_h^*, v_h\rangle_{\Gamma\times\Upsilon} = \left\langle \left(\tfrac{\mathcal{I}}{2} + \mathcal{K}\right) g_D, v_h\right\rangle_{\Gamma\times\Upsilon} \qquad \forall v_h \in S_{h_x,h_t}^{d_1,d_0}(\Gamma\times\Upsilon) \,, \tag{3.13}$$

all assumptions of Cea's Lemma are satisfied due to the $H^{-\frac{1}{2},-\frac{1}{4}}(\Gamma\times\Upsilon)$ ellipticity and boundedness of $\mathcal{V}$. Therefore, we have uniqueness of the approximate Galerkin solution $q_h^* \in S_{h_x,h_t}^{d_1,d_0}(\Gamma\times\Upsilon)$ and for $q^* \in H_{pw}^{2,1}(\Gamma\times\Upsilon)$ Theorem 3.1 gives an upper bound for the error in the energy norm

$$\|q^* - q_h^*\|_{H^{-\frac{1}{2},-\frac{1}{4}}(\Gamma\times\Upsilon)} \leq C(h_x^{\frac{5}{2}} + h_t^{\frac{5}{4}})\|q^*\|_{H_{pw}^{2,1}(\Gamma\times\Upsilon)} \,. \tag{3.14}$$

In order to derive a more practical estimate in the L_2 norm [37, Theorem 7.6], we use the triangle inequality, Theorem 3.2 and the triangle inequality again

$$\begin{aligned}
\|q^* - q_h^*\|_{L_2(\Gamma\times\Upsilon)} &\leq \|q^* - \mathcal{Q}_{h_x}^{d_1}\mathcal{Q}_{h_t}^{d_0}q^*\|_{L_2(\Gamma\times\Upsilon)} + \|\mathcal{Q}_{h_x}^{d_1}\mathcal{Q}_{h_t}^{d_0}q^* - q_h^*\|_{L_2(\Gamma\times\Upsilon)} \\
&\leq \|q^* - \mathcal{Q}_{h_x}^{d_1}\mathcal{Q}_{h_t}^{d_0}q^*\|_{L_2(\Gamma\times\Upsilon)} \\
&\qquad + C(h_x^{-\frac{1}{2}} + h_t^{-\frac{1}{4}})\|\mathcal{Q}_{h_x}^{d_1}\mathcal{Q}_{h_t}^{d_0}q^* - q_h^*\|_{H^{-\frac{1}{2},-\frac{1}{4}}(\Gamma\times\Upsilon)} \\
&\leq \|q^* - \mathcal{Q}_{h_x}^{d_1}\mathcal{Q}_{h_t}^{d_0}q^*\|_{L_2(\Gamma\times\Upsilon)} \\
&\qquad + C(h_x^{-\frac{1}{2}} + h_t^{-\frac{1}{4}})\Big(\|q^* - \mathcal{Q}_{h_x}^{d_1}\mathcal{Q}_{h_t}^{d_0}q^*\|_{H^{-\frac{1}{2},-\frac{1}{4}}(\Gamma\times\Upsilon)} \\
&\qquad\qquad + \|q^* - q_h^*\|_{H^{-\frac{1}{2},-\frac{1}{4}}(\Gamma\times\Upsilon)}\Big) \,.
\end{aligned}$$

With Theorem 3.1 for the first two terms and (3.14) for the last term we get

$$\|q^* - q_h^*\|_{L_2(\Gamma\times\Upsilon)} \leq \mathscr{C}(h_x,h_t)(h_x^2 + h_t)\|q^*\|_{H_{pw}^{2,1}(\Gamma\times\Upsilon)} \,, \tag{3.15}$$

where

$$\mathscr{C}(h_x,h_t) \leq C\max\left[\left(\frac{h_x^2}{h_t}\right)^{\frac{1}{4}}, \left(\frac{h_x^2}{h_t}\right)^{-\frac{1}{4}}\right] . \tag{3.16}$$

However, in our numerical examples we always approximate the right hand side by the L_2 projection $\bar{g}_D = \mathcal{Q}_{h_x}^{c_1}\mathcal{Q}_{h_t}^{d_0}g_D \in S_{h_x,h_t}^{c_1,d_0}(\Gamma\times\Upsilon)$ of the given Dirichlet data g_D^* and, therefore, end up with a perturbed Galerkin variational formulation, i.e., find $\bar{q}_h^* \in S_{h_x,h_t}^{d_1,d_0}(\Gamma\times\Upsilon)$ such that

$$\langle \mathcal{V}\bar{q}_h^*, v_h\rangle_{\Gamma\times\Upsilon} = \left\langle \left(\tfrac{\mathcal{I}}{2} + \mathcal{K}\right)\bar{g}_D, v_h\right\rangle_{\Gamma\times\Upsilon} \qquad \forall v_h \in S_{h_x,h_t}^{d_1,d_0}(\Gamma\times\Upsilon) \,, \tag{3.17}$$

which is why we may not be able to verify (3.15) but observe a different behavior.

Lemma 3.1. *Let $q^* \in H_{pw}^{2,1}(\Gamma\times\Upsilon)$ be the solution of the variational form* (2.17)*. Then the solution $\bar{q}_h^* \in S_{h_x,h_t}^{d_1,d_0}(\Gamma\times\Upsilon)$ of the perturbed variational formulation* (3.17) *with $g_D \in H^{2,1}(\Gamma\times\Upsilon)$ and $\bar{g}_D = \mathcal{Q}_{h_x}^{c_1}\mathcal{Q}_{h_t}^{d_0}g_D \in S_{h_x,h_t}^{c_1,d_0}(\Gamma\times\Upsilon)$ satisfies*

$$\|q^* - \bar{q}_h^*\|_{L_2(\Gamma\times\Upsilon)} \leq \mathscr{C}(h_x,h_t)\left((h_x^2 + h_t)\|q^*\|_{H_{pw}^{2,1}(\Gamma\times\Upsilon)} + (h_x + h_t^{\frac{1}{2}})\|g_D\|_{H^{2,1}(\Gamma\times\Upsilon)}\right)$$

with $\mathscr{C}(h_x,h_t)$ given in (3.16)*.*

Proof. We use the triangle inequality and Theorem 3.2 to estimate

$$\begin{aligned}\|q^* - \bar{q}_h^*\|_{L_2(\Gamma\times\Upsilon)} &\leq \|q^* - q_h^*\|_{L_2(\Gamma\times\Upsilon)} + \|q_h^* - \bar{q}_h^*\|_{L_2(\Gamma\times\Upsilon)} \\ &\leq \|q^* - q_h^*\|_{L_2(\Gamma\times\Upsilon)} + C(h_x^{-\frac{1}{2}} + h_t^{-\frac{1}{4}})\|q_h^* - \bar{q}_h^*\|_{H^{-\frac{1}{2},-\frac{1}{4}}(\Gamma\times\Upsilon)} .\end{aligned} \tag{3.18}$$

As an intermediate result obtained by subtracting (3.17) from (3.13)

$$\langle \mathcal{V}(q_h^* - \bar{q}_h^*), v_h\rangle_{\Gamma\times\Upsilon} = \left\langle \left(\tfrac{\mathcal{I}}{2} + \mathcal{K}\right)(g_D - \bar{g}_D), v_h\right\rangle_{\Gamma\times\Upsilon} = \langle \mathcal{K}(g_D - \bar{g}_D), v_h\rangle_{\Gamma\times\Upsilon} \qquad \forall v_h \in S_{h_x,h_t}^{d_1,d_0}(\Gamma\times\Upsilon)$$

we can bound the second term in (3.18) due to the boundedness of the double layer operator by the approximation error of the Dirichlet data

$$\begin{aligned}\|q_h^* - \bar{q}_h^*\|^2_{H^{-\frac{1}{2},-\frac{1}{4}}(\Gamma\times\Upsilon)} &\leq C\,\langle \mathcal{V}(q_h^* - \bar{q}_h^*), (q_h^* - \bar{q}_h^*)\rangle_{\Gamma\times\Upsilon} \\ &= C\,\langle \mathcal{K}(g_D - \bar{g}_D), (q_h^* - \bar{q}_h^*)\rangle_{\Gamma\times\Upsilon} \\ &\leq C\|g_D - \bar{g}_D\|_{H^{\frac{1}{2},\frac{1}{4}}(\Gamma\times\Upsilon)}\|q_h^* - \bar{q}_h^*\|_{H^{-\frac{1}{2},-\frac{1}{4}}(\Gamma\times\Upsilon)} .\end{aligned}$$

Thus with (3.15), Theorem 3.1, and (3.16) we get the assertion. □

Remark 3.1. *Observe that in this case there is no point in using linear spatial approximation of the solution, since the error is dominated by the approximation of the given Dirichlet data. Expanding the terms of the estimate it is obvious that one can achieve the same order of convergence by using* $\bar{q}_h^* \in S_{h_x,h_t}^{d_0,d_0}(\Gamma\times\Upsilon)$ *instead of* $\bar{q}_h^* \in S_{h_x,h_t}^{d_1,d_0}(\Gamma\times\Upsilon)$*. The only way to remedy this situation would be to approximate the right hand side by piecewise quadratic functions in space.*

3.2.2 Initial Neumann Boundary Value Problem

We solve (2.18) for the approximate solution, i.e., find $u_h \in S_{h_x,h_t}^{c_1,d_0}(\Gamma\times\Upsilon)$ such that

$$\langle \mathcal{D}u_h, w_h\rangle_{\Gamma\times\Upsilon} = \left\langle \left(\tfrac{\mathcal{I}}{2} - \mathcal{K}'\right) g_N^*, w_h\right\rangle_{\Gamma\times\Upsilon} \qquad \forall w_h \in S_{h_x,h_t}^{c_1,d_0}(\Gamma\times\Upsilon) . \tag{3.19}$$

Since $\mathcal{D} : H^{\frac{1}{2},\frac{1}{4}}(\Gamma\times\Upsilon) \to H^{-\frac{1}{2},-\frac{1}{4}}(\Gamma\times\Upsilon)$ is bounded, $H^{\frac{1}{2},\frac{1}{4}}(\Gamma\times\Upsilon)$ elliptic and we have chosen a conforming discretization $u_h \in S_{h_x,h_t}^{c_1,d_0}(\Gamma\times\Upsilon) \subset H^{\frac{1}{2},\frac{1}{4}}(\Gamma\times\Upsilon)$ we get uniqueness and quasi-optimality of the approximate solution. Assuming $u \in H^{2,1}(\Gamma\times\Upsilon)$ Theorem 3.1 gives the following bound

$$\|u - u_h\|_{H^{\frac{1}{2},\frac{1}{4}}(\Gamma\times\Upsilon)} \leq C(h_x^{\frac{3}{2}} + h_t^{\frac{3}{4}})\|u\|_{H^{2,1}(\Gamma\times\Upsilon)} . \tag{3.20}$$

Again, it is more practical to work with an L_2 error estimate. However, instead of the inverse inequality we have to use a duality argument commonly referred to as Aubin-Nitsche trick. Observe that in all our numerical examples we work with the L_2 projection $\bar{g}_N^* = \mathcal{Q}_{h_x}^{d_0}\mathcal{Q}_{h_t}^{d_0} g_N^* \in S_{h_x,h_t}^{d_0,d_0}(\Gamma\times\Upsilon)$ of the given Neumann data g_N^* and, hence, are solving the perturbed problem, i.e., find $\bar{u}_h \in S_{h_x,h_t}^{c_1,d_0}(\Gamma\times\Upsilon)$ such that

$$\langle \mathcal{D}\bar{u}_h, w_h\rangle_{\Gamma\times\Upsilon} = \left\langle \left(\tfrac{\mathcal{I}}{2} - \mathcal{K}'\right)\bar{g}_N^*, w_h\right\rangle_{\Gamma\times\Upsilon} \qquad \forall w_h \in S_{h_x,h_t}^{c_1,d_0}(\Gamma\times\Upsilon)\,. \tag{3.21}$$

Lemma 3.2. *[44, Theorem 12.10] Assume that $\mathcal{D} : H^{1,\frac{1}{2}}(\Gamma\times\Upsilon) \to L_2(\Gamma\times\Upsilon)$ is bounded and bijective and, moreover $\mathcal{K}' : H^{-s,-\frac{s}{2}}(\Gamma\times\Upsilon) \to H^{-s,-\frac{s}{2}}(\Gamma\times\Upsilon)$ is bounded for $s\in[0,1]$. Let $u \in H^{2,1}(\Gamma\times\Upsilon)$ be the unique solution of* (2.18) *and $\bar{u}_h \in S_{h_x,h_t}^{c_1,d_0}(\Gamma\times\Upsilon)$ the unique solution of* (3.21) *with $g_N^* \in H_{pw}^{1,\frac{1}{2}}(\Gamma\times\Upsilon)$ and $\bar{g}_N^* = \mathcal{Q}_{h_x}^{d_0}\mathcal{Q}_{h_t}^{d_0} g_N^* \in S_{h_x,h_t}^{d_0,d_0}(\Gamma\times\Upsilon)$, then we have*

$$\|u-\bar{u}_h\|_{L_2(\Gamma\times\Upsilon)} \le C(h_x^2+h_t)\left(\|u\|_{H^{2,1}(\Gamma\times\Upsilon)} + \|g_N^*\|_{H_{pw}^{1,\frac{1}{2}}(\Gamma\times\Upsilon)}\right).$$

Proof. By duality we have

$$\|u-\bar{u}_h\|_{L_2(\Gamma\times\Upsilon)} = \sup_{0\neq w\in L_2(\Gamma\times\Upsilon)} \frac{\langle u-\bar{u}_h, w\rangle_{\Gamma\times\Upsilon}}{\|w\|_{L_2(\Gamma\times\Upsilon)}}\,.$$

Since we assumed $\mathcal{D}$ to be an isomorphism from $H^{1,\frac{1}{2}}(\Gamma\times\Upsilon) \to L_2(\Gamma\times\Upsilon)$ there this is a unique $v \in H^{1,\frac{1}{2}}(\Gamma\times\Upsilon)$ such that

$$\begin{aligned}\|u-\bar{u}_h\|_{L_2(\Gamma\times\Upsilon)} &= \sup_{0\neq v\in H^{1,\frac{1}{2}}(\Gamma\times\Upsilon)} \frac{\langle u-\bar{u}_h, \mathcal{D}v\rangle_{\Gamma\times\Upsilon}}{\|\mathcal{D}v\|_{L_2(\Gamma\times\Upsilon)}} \\ &= \sup_{0\neq v\in H^{1,\frac{1}{2}}(\Gamma\times\Upsilon)} \frac{\langle \mathcal{D}(u-\bar{u}_h), v\rangle_{\Gamma\times\Upsilon}}{\|\mathcal{D}v\|_{L_2(\Gamma\times\Upsilon)}}\,.\end{aligned}$$

Subtracting (3.21) from (2.18) we have

$$\langle \mathcal{D}(u-\bar{u}_h), w_h\rangle_{\Gamma\times\Upsilon} = \left\langle \left(\tfrac{\mathcal{I}}{2} - \mathcal{K}'\right)(g_N^* - \bar{g}_N^*), w_h\right\rangle_{\Gamma\times\Upsilon} \qquad \forall w_h \in S_{h_x,h_t}^{c_1,d_0}(\Gamma\times\Upsilon) \tag{3.22}$$

and with the triangle inequality we get

$$\begin{aligned}\|u-\bar{u}_h\|_{L_2(\Gamma\times\Upsilon)} \le &\sup_{0\neq v\in H^{1,\frac{1}{2}}(\Gamma\times\Upsilon)} \frac{\left\langle \mathcal{D}(u-\bar{u}_h), v - \mathcal{Q}_{h_x}^{c_1}\mathcal{Q}_{h_t}^{d_0} v\right\rangle_{\Gamma\times\Upsilon}}{\|\mathcal{D}v\|_{L_2(\Gamma\times\Upsilon)}} \\ &+ \sup_{0\neq v\in H^{1,\frac{1}{2}}(\Gamma\times\Upsilon)} \frac{\left\langle \left(\tfrac{\mathcal{I}}{2} - \mathcal{K}'\right)(g_N^* - \bar{g}_N^*), \mathcal{Q}_{h_x}^{c_1}\mathcal{Q}_{h_t}^{d_0} v\right\rangle_{\Gamma\times\Upsilon}}{\|\mathcal{D}v\|_{L_2(\Gamma\times\Upsilon)}}\,.\end{aligned} \tag{3.23}$$

Due to the boundedness and bijectivity of the hyper-singular operator and Theorem 3.1 we can bound the first of (3.23) term by

$$\begin{aligned}\sup_{0\neq v\in H^{1,\frac{1}{2}}(\Gamma\times\Upsilon)} \frac{\left\langle \mathcal{D}(u-\bar{u}_h), v-\mathcal{Q}^{c_1}_{h_x}\mathcal{Q}^{d_0}_{h_t}v\right\rangle_{\Gamma\times\Upsilon}}{\|\mathcal{D}v\|_{L_2(\Gamma\times\Upsilon)}} &\leq C\|u-\bar{u}_h\|_{H^{\frac{1}{2},\frac{1}{4}}(\Gamma\times\Upsilon)}\\ &\quad\times \sup_{0\neq v\in H^{1,\frac{1}{2}}(\Gamma\times\Upsilon)} \frac{\|v-\mathcal{Q}^{c_1}_{h_x}\mathcal{Q}^{d_0}_{h_t}v\|_{H^{\frac{1}{2},\frac{1}{4}}(\Gamma\times\Upsilon)}}{\|v\|_{H^{1,\frac{1}{2}}(\Gamma\times\Upsilon)}}\\ &\leq C(h_x^{\frac{1}{2}}+h_t^{\frac{1}{4}})\Big(\|u-u_h\|_{H^{\frac{1}{2},\frac{1}{4}}(\Gamma\times\Upsilon)}\\ &\qquad +\|u_h-\bar{u}_h\|_{H^{\frac{1}{2},\frac{1}{4}}(\Gamma\times\Upsilon)}\Big),\end{aligned}$$

where the first term is bounded by (3.20), while for the second term we use the ellipticity of the hyper-singular operator, the Galerkin orthogonality (3.22), the boundedness of the adjoint double layer operator, Theorem 3.1, and Young's inequality

$$\begin{aligned}\|u_h-\bar{u}_h\|^2_{H^{\frac{1}{2},\frac{1}{4}}(\Gamma\times\Upsilon)} &\leq C\,\langle \mathcal{D}(u_h-\bar{u}_h),(u_h-\bar{u}_h)\rangle_{\Gamma\times\Upsilon}\\ &= C\left\langle (\tfrac{\mathcal{I}}{2}+\mathcal{K}')(\bar{g}_N-g_N),(u_h-\bar{u}_h)\right\rangle_{\Gamma\times\Upsilon}\\ &\leq C\|\bar{g}_N-g_N\|_{H^{-\frac{1}{2},-\frac{1}{4}}(\Gamma\times\Upsilon)}\|u_h-\bar{u}_h\|_{H^{\frac{1}{2},\frac{1}{4}}(\Gamma\times\Upsilon)}\\ &\leq C(h_x^{\frac{3}{2}}+h_t^{\frac{3}{4}})\|g_N\|_{H^{1,\frac{1}{2}}_{pw}(\Gamma\times\Upsilon)}\|u_h-\bar{u}_h\|_{H^{\frac{1}{2},\frac{1}{4}}(\Gamma\times\Upsilon)}.\end{aligned}$$

For the second term of (3.23) we use the boundedness of the adjoint double layer potential, the boundedness of the hyper-singular operator, Theorem 3.1, and Corollary 3.1

$$\begin{aligned}\sup_{0\neq v\in H^{1,\frac{1}{2}}(\Gamma\times\Upsilon)} \frac{\left\langle \left(\frac{\mathcal{I}}{2}-\mathcal{K}'\right)(g_N^*-\bar{g}_N^*),\mathcal{Q}^{c_1}_{h_x}\mathcal{Q}^{d_0}_{h_t}v\right\rangle_{\Gamma\times\Upsilon}}{\|\mathcal{D}v\|_{L_2(\Gamma\times\Upsilon)}} &\leq \|\left(\tfrac{\mathcal{I}}{2}-\mathcal{K}'\right)(g_N^*-\bar{g}_N^*)\|_{H^{-1,-\frac{1}{2}}(\Gamma\times\Upsilon)}\\ &\quad\times \sup_{0\neq v\in H^{1,\frac{1}{2}}(\Gamma\times\Upsilon)} \frac{\|\mathcal{Q}^{c_1}_{h_x}\mathcal{Q}^{d_0}_{h_t}v\|_{H^{1,\frac{1}{2}}(\Gamma\times\Upsilon)}}{\|\mathcal{D}v\|_{L_2(\Gamma\times\Upsilon)}}\\ &\leq C(h_x^2+h_t)\|\bar{g}_N^*\|_{H^{1,\frac{1}{2}}_{pw}(\Gamma\times\Upsilon)}.\end{aligned}$$

□

3.2.3 Initial Robin Boundary Value Problem

If we solve (2.19) for the approximate solution, i.e., find $u_h \in S^{c_1,d_0}_{h_x,h_t}(\Gamma\times\Upsilon)$ such that

$$\langle(\mathcal{S}+\kappa^*)\,u_h, v_h\rangle_{\Gamma\times\Upsilon} = \langle g_R^*, v_h\rangle_{\Gamma\times\Upsilon} \qquad \forall v_h \in S^{c_1,d_0}_{h_x,h_t}(\Gamma\times\Upsilon)\,, \tag{3.24}$$

Cea's Lemma is satisfied due to the $H^{\frac{1}{2},\frac{1}{4}}(\Gamma\times\Upsilon)$ boundedness and ellipticity of $(\mathcal{S}+\kappa^*)$ provided by Section 2.4.3. Thus, assuming $u \in H^{2,1}(\Gamma\times\Upsilon)$ Theorem 3.1 gives an upper bound for the error in the energy norm

$$\|u-u_h\|_{H^{\frac{1}{2},\frac{1}{4}}(\Gamma\times\Upsilon)} \leq C(h_x^{\frac{3}{2}}+h_t^{\frac{3}{4}})\|u\|_{H^{2,1}(\Gamma\times\Upsilon)}\,. \tag{3.25}$$

However, due to the inverse single layer operator, we can not directly realize the Steklov Poincaré operator. Therefore, we proceed as in [44, page 284] by solving the variational Dirichlet problem first , i.e., find $q_h^* \in S^{d_0,d_0}_{h_x,h_t}(\Gamma\times\Upsilon)$ such that

$$\langle \mathcal{V} q_h^*, w_h\rangle_{\Gamma\times\Upsilon} = \left\langle \left(\tfrac{\mathcal{I}}{2}+\mathcal{K}\right) u, w_h\right\rangle_{\Gamma\times\Upsilon} \qquad \forall w_h \in S^{d_0,d_0}_{h_x,h_t}(\Gamma\times\Upsilon)\,, \tag{3.26}$$

which leads to the following approximation of the Steklov-Poincaré operator

$$\bar{\mathcal{S}}u = \left(\tfrac{\mathcal{I}}{2}+\mathcal{K}'\right) q_h^* + \mathcal{D}u \tag{3.27}$$

and the perturbed variational problem, namely find $\bar{u}_h \in S^{c_1,d_0}_{h_x,h_t}(\Gamma\times\Upsilon)$ such that

$$\left\langle \left(\bar{\mathcal{S}}+\kappa^*\right)\bar{u}_h, v_h\right\rangle_{\Gamma\times\Upsilon} = \langle \bar{g}_R^*, v_h\rangle_{\Gamma\times\Upsilon} \qquad \forall v_h \in S^{c_1,d_0}_{h_x,h_t}(\Gamma\times\Upsilon)\,, \tag{3.28}$$

where we consider a perturbed right hand side $\bar{g}_R^* := \mathcal{Q}^{d_0}_{h_x}\mathcal{Q}^{d_0}_{h_t} g_R^* \in S^{d_0,d_0}_{h_x,h_t}(\Gamma\times\Upsilon)$ as well.

Lemma 3.3. *[44, Lemma 12.11] The approximated Steklov-Poincaré operator in* (3.27) $\bar{\mathcal{S}} : H^{\frac{1}{2},\frac{1}{4}}(\Gamma\times\Upsilon) \to H^{-\frac{1}{2},-\frac{1}{4}}(\Gamma\times\Upsilon)$ *is bounded*

$$\|\bar{\mathcal{S}}u\|_{H^{-\frac{1}{2},-\frac{1}{4}}(\Gamma\times\Upsilon)} \leq C\|u\|_{H^{\frac{1}{2},\frac{1}{4}}(\Gamma\times\Upsilon)}$$

and $H^{\frac{1}{2},\frac{1}{4}}(\Gamma\times\Upsilon)$ *elliptic*

$$\langle\bar{\mathcal{S}}u, u\rangle_{\Gamma\times\Upsilon} \geq C\|u\|^2_{H^{\frac{1}{2},\frac{1}{4}}(\Gamma\times\Upsilon)} \qquad \forall u \in H^{\frac{1}{2},\frac{1}{4}}(\Gamma\times\Upsilon)\,.$$

Further, for $s \in (1/2,1]$ *assuming that* $\mathcal{K}' : H^{-s,-\frac{s}{2}}(\Gamma\times\Upsilon) \to H^{-s,-\frac{s}{2}}(\Gamma\times\Upsilon)$ *is bounded,* $\mathcal{V} : H^{-1+s,\frac{-1+s}{2}}(\Gamma\times\Upsilon) \to H^{s,\frac{s}{2}}(\Gamma\times\Upsilon)$ *is bounded and bijective, and* $\mathcal{S}u \in H^{1,\frac{1}{2}}_{pw}(\Gamma\times\Upsilon)$, *the approximate Steklov-Poincaré operator satisfies*

$$\|(\mathcal{S}-\bar{\mathcal{S}})u\|_{H^{-s,-\frac{s}{2}}(\Gamma\times\Upsilon)} \leq C\left(h_x^{s+1}+h_t^{\frac{s+1}{2}}\right)\|\mathcal{S}u\|_{H^{1,\frac{1}{2}}_{pw}(\Gamma\times\Upsilon)}\,.$$

Proof. For the solution $q_h^* \in S_{h_x,h_t}^{d_0,d_0}(\Gamma\times\Upsilon)$ of the variational problem (3.26) we have due to the ellipticity of the single layer operator and the boundedness of the double layer operator provided by Theorem 2.1

$$\|q_h^*\|_{H^{-\frac{1}{2},-\frac{1}{4}}(\Gamma\times\Upsilon)} \leq C\|u\|_{H^{\frac{1}{2},\frac{1}{4}}(\Gamma\times\Upsilon)} .$$

Thus the boundedness of the approximate Steklov-Poincaré operator follows with the triangle inequality, the boundedness of the hyper-singular operator and the adjoint operator given in Theorem 2.1

$$\begin{aligned}\|\bar{\mathcal{S}}u\|_{H^{-\frac{1}{2},-\frac{1}{4}}(\Gamma\times\Upsilon)} &= \|\mathcal{D}u + \left(\tfrac{\mathcal{I}}{2}+\mathcal{K}'\right) q_h^*\|_{H^{-\frac{1}{2},-\frac{1}{4}}(\Gamma\times\Upsilon)} \\ &\leq C\left(\|u\|_{H^{\frac{1}{2},\frac{1}{4}}(\Gamma\times\Upsilon)} + \|q_h^*\|_{H^{-\frac{1}{2},-\frac{1}{4}}(\Gamma\times\Upsilon)}\right) \\ &\leq C\|u\|_{H^{\frac{1}{2},\frac{1}{4}}(\Gamma\times\Upsilon)} .\end{aligned}$$

The ellipticity follows from the ellipticity of the hyper-singular operator and the single layer operator guaranteed by Theorem 2.1

$$\begin{aligned}\left\langle \bar{\mathcal{S}}u, u\right\rangle_{\Gamma\times\Upsilon} &= \langle \mathcal{D}u, u\rangle_{\Gamma\times\Upsilon} + \left\langle \left(\tfrac{\mathcal{I}}{2}+\mathcal{K}'\right) q_h^*, u\right\rangle_{\Gamma\times\Upsilon} \\ &= \langle \mathcal{D}u, u\rangle_{\Gamma\times\Upsilon} + \left\langle q_h^*, \left(\tfrac{\mathcal{I}}{2}+\mathcal{K}\right) u\right\rangle_{\Gamma\times\Upsilon} \\ &= \langle \mathcal{D}u, u\rangle_{\Gamma\times\Upsilon} + \langle q_h^*, \mathcal{V}q_h^*\rangle_{\Gamma\times\Upsilon} \geq C\|u\|^2_{H^{\frac{1}{2},\frac{1}{4}}(\Gamma\times\Upsilon)} .\end{aligned}$$

Taking the difference between the exact and approximated Steklov-Poincaré operator, i.e., Corollary 2.1 with $\mathcal{V}^{-1}(\frac{\mathcal{I}}{2}+\mathcal{K})u := q$ and (3.27) with the unique solution q_h^* of (3.26), the boundedness of the adjoint double layer operator, and Cea's Lemma together with Theorem 3.1 yields

$$\begin{aligned}\|\left(\mathcal{S}-\bar{\mathcal{S}}\right)u\|_{H^{-\frac{1}{2},-\frac{1}{4}}(\Gamma\times\Upsilon)} &= \|\left(\tfrac{\mathcal{I}}{2}+\mathcal{K}'\right)(q^*-q_h^*)\|_{H^{-\frac{1}{2},-\frac{1}{4}}(\Gamma\times\Upsilon)} \\ &\leq C\|q^*-q_h^*\|_{H^{-\frac{1}{2},-\frac{1}{4}}(\Gamma\times\Upsilon)} \\ &\leq C\left(h_x^{\frac{3}{2}}+h_t^{\frac{3}{4}}\right)\|\mathcal{S}u\|_{H^{1,\frac{1}{2}}_{pw}(\Gamma\times\Upsilon)} .\end{aligned} \tag{3.29}$$

With the aid of an Aubin-Nitsche duality argument for (3.26) this result can be extended. We use the bijectivity and boundedness of $\mathcal{V}: H^{-1+s,\frac{-1+s}{2}}(\Gamma\times\Upsilon) \to H^{s,\frac{s}{2}}(\Gamma\times\Upsilon)$ and the boundedness of $\mathcal{K}': H^{-s,-\frac{s}{2}}(\Gamma\times\Upsilon) \to H^{-s,-\frac{s}{2}}(\Gamma\times\Upsilon)$ for $s\in(1/2,1]$. Furthermore, in order to conclude the proof, we use the Galerkin orthogonality of (3.26), Theorem 3.1,

estimate (3.29), and Young's inequality

$$\begin{aligned}
\| \left(\mathcal{S}-\bar{\mathcal{S}}\right) u\|_{H^{-s,-\frac{s}{2}}(\Gamma\times\Upsilon)} &\leq C\|q^*-q_h^*\|_{H^{-s,-\frac{s}{2}}(\Gamma\times\Upsilon)} \\
&= C \sup_{0\neq v\in H^{s,\frac{s}{2}}(\Gamma\times\Upsilon)} \frac{\left\langle q^*-q_h^*, v\right\rangle_{\Gamma\times\Upsilon}}{\|v\|_{H^{s,\frac{s}{2}}(\Gamma\times\Upsilon)}} \\
&= C \sup_{0\neq w\in H^{s-1,\frac{s-1}{2}}(\Gamma\times\Upsilon)} \frac{\left\langle \mathcal{V}(q^*-q_h^*), w-\mathcal{Q}_{h_x}^{d_1}\mathcal{Q}_{h_t}^{d_0} w\right\rangle_{\Gamma\times\Upsilon}}{\|\mathcal{V}w\|_{H^{s,\frac{s}{2}}(\Gamma\times\Upsilon)}} \\
&\leq C\left(h_x^{\frac{2s-1}{2}}+h_t^{\frac{2s-1}{4}}\right)\|q^*-q_h^*\|_{H^{-\frac{1}{2},-\frac{1}{4}}(\Gamma\times\Upsilon)} \\
&\leq C\left(h_x^{s+1}+h_t^{\frac{s+1}{2}}\right)\|\mathcal{S}u\|_{H_{pw}^{1,\frac{1}{2}}(\Gamma\times\Upsilon)} .
\end{aligned}$$

□

In order to derive an error estimate for the solution $\bar{u}_h \in S_{h_x,h_t}^{c_1,d_0}(\Gamma\times\Upsilon)$ of (3.28), we subtract (3.28) from (3.24) to obtain the Galerkin orthogonality

$$\left\langle \left(\mathcal{S}+\kappa^*\right) u_h - \left(\bar{\mathcal{S}}+\kappa^*\right)\bar{u}_h, v_h\right\rangle_{\Gamma\times\Upsilon} = \left\langle g_R-\bar{g}_R^*, v_h\right\rangle_{\Gamma\times\Upsilon} \qquad \forall v_h\in S_{h_x,h_t}^{c_1,d_0}(\Gamma\times\Upsilon) ,$$

which we use together with the $H^{\frac{1}{2},\frac{1}{4}}(\Gamma\times\Upsilon)$ ellipticity of $(\bar{\mathcal{S}}+\kappa^*)$ to estimate

$$\begin{aligned}
\|u_h-\bar{u}_h\|^2_{H^{\frac{1}{2},\frac{1}{4}}(\Gamma\times\Upsilon)} &\leq C\left\langle \left(\bar{\mathcal{S}}+\kappa^*\right)(u_h-\bar{u}_h), u_h-\bar{u}_h\right\rangle_{\Gamma\times\Upsilon} \\
&= C\left\langle (\bar{\mathcal{S}}-\mathcal{S})u_h+(g_R-\bar{g}_R^*), u_h-\bar{u}_h\right\rangle_{\Gamma\times\Upsilon} \\
&\leq C\|(\bar{\mathcal{S}}-\mathcal{S})u_h+(g_R-\bar{g}_R^*)\|_{H^{-\frac{1}{2},-\frac{1}{4}}(\Gamma\times\Upsilon)}\|u_h-\bar{u}_h\|_{H^{\frac{1}{2},\frac{1}{4}}(\Gamma\times\Upsilon)} .
\end{aligned}$$

With the triangle inequality, the boundedness of the operators $\mathcal{S}$ and $\bar{\mathcal{S}}$, and Lemma 3.3 we obtain

$$\begin{aligned}
\|u_h-\bar{u}_h\|_{H^{\frac{1}{2},\frac{1}{4}}(\Gamma\times\Upsilon)} &\leq C\|(\bar{\mathcal{S}}-\mathcal{S})u_h\|_{H^{-\frac{1}{2},-\frac{1}{4}}(\Gamma\times\Upsilon)} + \|g_R^*\|_{H_{pw}^{1,\frac{1}{2}}(\Gamma\times\Upsilon)} \\
&\leq C\Big(\|(\bar{\mathcal{S}}-\mathcal{S})u\|_{H^{-\frac{1}{2},-\frac{1}{4}}(\Gamma\times\Upsilon)} \\
&\qquad + \|(\bar{\mathcal{S}}-\mathcal{S})(u_h-u)\|_{H^{-\frac{1}{2},-\frac{1}{4}}(\Gamma\times\Upsilon)} + \|g_R^*\|_{H_{pw}^{1,\frac{1}{2}}(\Gamma\times\Upsilon)}\Big) \\
&\leq C\left(h_x^{\frac{3}{2}}+h_t^{\frac{3}{4}}\right)\left(\|\mathcal{S}u\|_{H_{pw}^{1,\frac{1}{2}}(\Gamma\times\Upsilon)} + \|u\|_{H^{2,1}(\Gamma\times\Upsilon)} + \|g_R^*\|_{H_{pw}^{1,\frac{1}{2}}(\Gamma\times\Upsilon)}\right)
\end{aligned}$$

and together with (3.25) we can bound the error for the solution of (3.28) by

$$\begin{aligned}\|u-\bar{u}_h\|_{H^{\frac{1}{2},\frac{1}{4}}(\Gamma\times\Upsilon)} &\leq \|u-u_h\|_{H^{\frac{1}{2},\frac{1}{4}}(\Gamma\times\Upsilon)} + \|u_h-\bar{u}_h\|_{H^{\frac{1}{2},\frac{1}{4}}(\Gamma\times\Upsilon)} \\ &\leq C\left(h_x^{\frac{3}{2}}+h_t^{\frac{3}{4}}\right)\left(\|u\|_{H^{2,1}(\Gamma\times\Upsilon)} + \|\mathcal{S}u\|_{H^{1,\frac{1}{2}}_{pw}(\Gamma\times\Upsilon)} + \|g_R^*\|_{H^{1,\frac{1}{2}}_{pw}(\Gamma\times\Upsilon)}\right).\end{aligned} \tag{3.30}$$

Again, for practical reasons it is more convenient to work with the L_2 error. Thanks to the help of G. Of and O. Steinbach we provide such an estimate for the solution $\bar{u}_h \in S^{c_1,d_0}_{h_x,h_t}(\Gamma\times\Upsilon)$ of the perturbed problem (3.28) in a similar manner to Lemma 3.2.

Lemma 3.4. *Assume that $\mathcal{S}: H^{1,\frac{1}{2}}(\Gamma\times\Upsilon)\to L_2(\Gamma\times\Upsilon)$ is bounded and bijective, $0\leq\kappa^*\leq\kappa_0^*\in\mathbb{R}$, the assumptions on $\bar{\mathcal{S}}$ in Lemma 3.3 are met. Further, assume that $u\in H^{2,1}(\Gamma\times\Upsilon)$ is the unique solution of* (2.19) *with $g_R^*\in H^{1,\frac{1}{2}}_{pw}(\Gamma\times\Upsilon)$, then the unique solution $\bar{u}_h\in S^{c_1,d_0}_{h_x,h_t}(\Gamma\times\Upsilon)$ of* (3.28) *with $\bar{g}_R^* := \mathcal{Q}^{d_0}_{h_x}\mathcal{Q}^{d_0}_{h_t}g_R^*\in S^{d_0d_0}_{h_x,h_t}(\Gamma\times\Upsilon)$ satisfies*

$$\|u-\bar{u}_h\|_{L_2(\Gamma\times\Upsilon)} \leq C(h_x^2+h_t)\left(\|u\|_{H^{2,1}(\Gamma\times\Upsilon)} + \|\mathcal{S}u\|_{H^{1,\frac{1}{2}}_{pw}(\Gamma\times\Upsilon)} + \|g_R^*\|_{H^{1,\frac{1}{2}}_{pw}(\Gamma\times\Upsilon)}\right).$$

Proof. Similar to the proof of Lemma 3.2 we have by duality

$$\|u-\bar{u}_h\|_{L_2(\Gamma\times\Upsilon)} = \sup_{0\neq w\in L_2(\Gamma\times\Upsilon)} \frac{\langle u-\bar{u}_h, w\rangle_{\Gamma\times\Upsilon}}{\|w\|_{L_2(\Gamma\times\Upsilon)}}$$

and there this is a unique $v\in H^{1,\frac{1}{2}}(\Gamma\times\Upsilon)$ such that

$$\|u-\bar{u}_h\|_{L_2(\Gamma\times\Upsilon)} = \sup_{0\neq v\in H^{1,\frac{1}{2}}(\Gamma\times\Upsilon)} \frac{\langle (u-\bar{u}_h), (\mathcal{S}+\kappa^*)\,v\rangle_{\Gamma\times\Upsilon}}{\|(\mathcal{S}+\kappa^*)v\|_{L_2(\Gamma\times\Upsilon)}}.$$

Subtracting (3.28) from (2.19), we have the Galerkin orthogonality

$$\left\langle (\mathcal{S}+\kappa^*)\,u - \left(\bar{\mathcal{S}}+\kappa^*\right)\bar{u}_h, v_h\right\rangle_{\Gamma\times\Upsilon} = \left\langle (\mathcal{I}-\mathcal{Q}^{d_0}_{h_x}\mathcal{Q}^{d_0}_{h_t})\,\kappa^*, v_h\right\rangle_{\Gamma\times\Upsilon} \qquad \forall v_h\in S^{c_1,d_0}_{h_x,h_t}(\Gamma\times\Upsilon),$$

which leads to

$$\begin{aligned}\|u-\bar{u}_h\|_{L_2(\Gamma\times\Upsilon)} \leq \sup_{0\neq v\in H^{1,\frac{1}{2}}(\Gamma\times\Upsilon)} \Bigg(&\frac{\left\langle (\mathcal{S}+\kappa^*)\,(u-\bar{u}_h), v-\mathcal{Q}^{c_1}_{h_x}\mathcal{Q}^{d_0}_{h_t}v\right\rangle_{\Gamma\times\Upsilon}}{\|\,(\mathcal{S}+\kappa^*)\,v\|_{L_2(\Gamma\times\Upsilon)}} \\ &+ \frac{\left\langle (\bar{\mathcal{S}}-\mathcal{S})\bar{u}_h, \mathcal{Q}^{c_1}_{h_x}\mathcal{Q}^{d_0}_{h_t}v\right\rangle_{\Gamma\times\Upsilon}}{\|\,(\mathcal{S}+\kappa^*)\,v\|_{L_2(\Gamma\times\Upsilon)}} + \frac{\left\langle (\mathcal{I}-\mathcal{Q}^{d_0}_{h_x}\mathcal{Q}^{d_0}_{h_t})g_R^*, \mathcal{Q}^{c_1}_{h_x}\mathcal{Q}^{d_0}_{h_t}\right\rangle_{\Gamma\times\Upsilon}}{\|\,(\mathcal{S}+\kappa^*)\,v\|_{L_2(\Gamma\times\Upsilon)}}\Bigg)\end{aligned}$$

and

$$\|u-\bar{u}_h\|_{L_2(\Gamma\times\Upsilon)} \leq \sup_{0\neq v\in H^{1,\frac{1}{2}}(\Gamma\times\Upsilon)} \left(\frac{\left\langle (\mathcal{S}+\kappa^*)(u-\bar{u}_h), v-\mathcal{Q}_{h_x}^{c_1}\mathcal{Q}_{h_t}^{d_0}v\right\rangle_{\Gamma\times\Upsilon}}{\|(\mathcal{S}+\kappa^*)v\|_{L_2(\Gamma\times\Upsilon)}} + \frac{\left\langle (\bar{\mathcal{S}}-\mathcal{S})(u-\bar{u}_h), \mathcal{Q}_{h_x}^{c_1}\mathcal{Q}_{h_t}^{d_0}v\right\rangle_{\Gamma\times\Upsilon}}{\|(\mathcal{S}+\kappa^*)v\|_{L_2(\Gamma\times\Upsilon)}} + \frac{\left\langle (\bar{\mathcal{S}}-\mathcal{S})u, \mathcal{Q}_{h_x}^{c_1}\mathcal{Q}_{h_t}^{d_0}v\right\rangle_{\Gamma\times\Upsilon}}{\|(\mathcal{S}+\kappa^*)v\|_{L_2(\Gamma\times\Upsilon)}} + \frac{\left\langle (\mathcal{I}-\mathcal{Q}_{h_x}^{d_0}\mathcal{Q}_{h_t}^{d_0})g_R^*, \mathcal{Q}_{h_x}^{c_1}\mathcal{Q}_{h_t}^{d_0}v\right\rangle_{\Gamma\times\Upsilon}}{\|(\mathcal{S}+\kappa^*)v\|_{L_2(\Gamma\times\Upsilon)}} \right).$$

Due to the boundedness and bijectivity of the Steklov-Poincaré operator provided by Corollary 2.1, Corollary 3.1, and Theorem 3.1 we can control the first term with the help of (3.30) and Young's inequality

$$\begin{aligned}\frac{\left\langle (\mathcal{S}+\kappa^*)(u-\bar{u}_h), v-\mathcal{Q}_{h_x}^{c_1}\mathcal{Q}_{h_t}^{d_0}v\right\rangle_{\Gamma\times\Upsilon}}{(\|\mathcal{S}+\kappa^*)v\|_{L_2(\Gamma\times\Upsilon)}} &\leq \|(\mathcal{S}+\kappa^*)(u-\bar{u}_h)\|_{H^{-\frac{1}{2},-\frac{1}{4}}(\Gamma\times\Upsilon)} \\ &\quad\times \frac{\|v-\mathcal{Q}_{h_x}^{c_1}\mathcal{Q}_{h_t}^{d_0}v\|_{H^{\frac{1}{2},\frac{1}{4}}(\Gamma\times\Upsilon)}}{\|(\mathcal{S}+\kappa^*)v\|_{L_2(\Gamma\times\Upsilon)}} \\ &\leq C(h_x^{\frac{1}{2}}+h_t^{\frac{1}{4}})\|u-\bar{u}_h\|_{H^{\frac{1}{2},\frac{1}{4}}(\Gamma\times\Upsilon)} \\ &\leq C(h_x^2+h_t)\left(\|u\|_{H^{2,1}(\Gamma\times\Upsilon)}+\|\mathcal{S}u\|_{H_{pw}^{1,\frac{1}{2}}(\Gamma\times\Upsilon)}\right).\end{aligned}$$

For the second term we use the boundedness and bijectivity of the Steklov-Poincaré operator, Lemma 3.3, estimate (3.30), and Young's inequality

$$\begin{aligned}\frac{\left\langle (\bar{\mathcal{S}}-\mathcal{S})(u-\bar{u}_h), \mathcal{Q}_{h_x}^{c_1}\mathcal{Q}_{h_t}^{d_0}v\right\rangle_{\Gamma\times\Upsilon}}{\|(\mathcal{S}+\kappa^*)v\|_{L_2(\Gamma\times\Upsilon)}} &\leq \frac{\|u-\bar{u}_h\|_{H^{\frac{1}{2},\frac{1}{4}}(\Gamma\times\Upsilon)}\|(\bar{\mathcal{S}}-\mathcal{S})\mathcal{Q}_{h_x}^{c_1}\mathcal{Q}_{h_t}^{d_0}v\|_{H^{-\frac{1}{2},-\frac{1}{4}}(\Gamma\times\Upsilon)}}{\|(\mathcal{S}+\kappa^*)v\|_{L_2(\Gamma\times\Upsilon)}} \\ &\leq C(h_x^{\frac{1}{2}}+h_t^{\frac{1}{4}})\|u-\bar{u}_h\|_{H^{\frac{1}{2},\frac{1}{4}}(\Gamma\times\Upsilon)} \\ &\leq C(h_x^2+h_t)\left(\|u\|_{H^{2,1}(\Gamma\times\Upsilon)}+\|\mathcal{S}u\|_{H_{pw}^{1,\frac{1}{2}}(\Gamma\times\Upsilon)}\right).\end{aligned}$$

With Corollary 3.1, the boundedness of the Steklov-Poincaré operator, and Lemma 3.3 we

can bound the third term

$$\begin{aligned}\frac{\left\langle(\bar{\mathcal{S}}-\mathcal{S})u,\mathcal{Q}_{h_x}^{c_1}\mathcal{Q}_{h_t}^{d_0}v\right\rangle_{\Gamma\times\Upsilon}}{\|(\mathcal{S}+\kappa^*)v\|_{L_2(\Gamma\times\Upsilon)}}&\leq\frac{\|(\bar{\mathcal{S}}-\mathcal{S})u\|_{H^{-1,-\frac{1}{2}}(\Gamma\times\Upsilon)}\|\mathcal{Q}_{h_x}^{c_1}\mathcal{Q}_{h_t}^{d_0}v\|_{H^{1,\frac{1}{2}}(\Gamma\times\Upsilon)}}{\|(\mathcal{S}+\kappa^*)v\|_{L_2(\Gamma\times\Upsilon)}}\\&\leq C\|(\bar{\mathcal{S}}-\mathcal{S})u\|_{H^{-1,-\frac{1}{2}}(\Gamma\times\Upsilon)}\\&\leq C(h_x^2+h_t)\|\mathcal{S}u\|_{H^{1,\frac{1}{2}}_{pw}(\Gamma\times\Upsilon)}\end{aligned}$$

and finally, with $g_R^*\in H^{1,\frac{1}{2}}_{pw}(\Gamma\times\Upsilon)$, Corollary 3.1, the boundedness of the Steklov-Poincaré operator, and Theorem 3.1 we conclude the proof by estimating the forth term

$$\begin{aligned}\frac{\left\langle(\mathcal{I}-\mathcal{Q}_{h_x}^{d_0}\mathcal{Q}_{h_t}^{d_0})g_R^*,\mathcal{Q}_{h_x}^{c_1}\mathcal{Q}_{h_t}^{d_0}v\right\rangle_{\Gamma\times\Upsilon}}{\|(\mathcal{S}+\kappa^*)v\|_{L_2(\Gamma\times\Upsilon)}}&\leq\frac{\|(\mathcal{I}-\mathcal{Q}_{h_x}^{d_0}\mathcal{Q}_{h_t}^{d_0})g_R^*\|_{H^{-1,-\frac{1}{2}}(\Gamma\times\Upsilon)}\|\mathcal{Q}_{h_x}^{c_1}\mathcal{Q}_{h_t}^{d_0}v\|_{H^{1,\frac{1}{2}}(\Gamma\times\Upsilon)}}{\|(\mathcal{S}+\kappa^*)v\|_{L_2(\Gamma\times\Upsilon)}}\\&\leq C(h_x^2+h_t)\|g_R^*\|_{H^{1,\frac{1}{2}}_{pw}(\Gamma\times\Upsilon)}\,.\end{aligned}$$

□

3.2.4 Mixed Initial Boundary Value Problems

We solve the variational form (2.20) with $\Gamma_{NR}:=\Gamma_N\cup\Gamma_R+\overline{\Gamma}_N\cap\overline{\Gamma}_R$ for the approximate solution, i.e., find $\tilde{u}_h\in S^{c_1,d_0}_{h_x,h_t}(\Gamma_{NR}\times\Upsilon):=S^{c_1,d_0}_{h_x,h_t}(\Gamma\times\Upsilon)\cap\widetilde{H}^{\frac{1}{2},\frac{1}{4}}(\Gamma_{NR}\times\Upsilon)$ such that

$$\langle(\mathcal{S}+\kappa^*_{NR})\,\tilde{u}_h,v_h\rangle_{\Gamma_{NR}\times\Upsilon}=\langle g^*_{NR}-(\mathcal{S}+\kappa^*_{NR})\,\tilde{g}_D,v_h\rangle_{\Gamma_{NR}\times\Upsilon}\qquad\forall v_h\in S^{c_1,d_0}_{h_x,h_t}(\Gamma_{NR}\times\Upsilon)\,. \tag{3.31}$$

Uniqueness and solvability of the continuous problem (2.20) directly translate to the discrete problem (3.31), since we are working with conforming finite-dimensional subspaces. Furthermore, Cea's Lemma guarantees quasi-optimality and assuming $\tilde{u}\in\widetilde{H}^{2,1}(\Gamma_{NR}\times\Upsilon)$ Theorem 3.1 provides the estimate

$$\|\tilde{u}-\tilde{u}_h\|_{\widetilde{H}^{\frac{1}{2},\frac{1}{4}}(\Gamma_{NR}\times\Upsilon)}\leq C(h_x^{\frac{3}{2}}+h_t^{\frac{3}{4}})\|\tilde{u}\|_{\widetilde{H}^{2,1}(\Gamma_{NR}\times\Upsilon)}\,.$$

However, we work with an approximation of the Steklov-Poincaré operator (3.27) and an approximation of $\bar{g}^*_{NR}=\mathcal{Q}_{h_x}^{d_0}\mathcal{Q}_{h_t}^{d_0}g^*_{NR}\in S^{d_0,d_0}_{h_x,h_t}(\Gamma_{NR}\times\Upsilon)$ and $\bar{\tilde{g}}_D=\mathcal{Q}_{h_x}^{c_1}\mathcal{Q}_{h_t}^{d_0}\tilde{g}_D\in S^{c_1,d_0}_{h_x,h_t}(\Gamma\times\Upsilon)$. Thus we solve the perturbed problem, namely find $\bar{\tilde{u}}_h\in S^{c_1,d_0}_{h_x,h_t}(\Gamma_{NR}\times\Upsilon)$ such that

$$\left\langle\left(\bar{\mathcal{S}}+\kappa^*_{NR}\right)\bar{\tilde{u}}_h,v_h\right\rangle_{\Gamma\times\Upsilon}=\left\langle\bar{g}^*_{NR}-\left(\bar{\mathcal{S}}+\kappa^*_{NR}\right)\bar{\tilde{g}}_D,v_h\right\rangle_{\Gamma\times\Upsilon}\qquad\forall v_h\in S^{c_1,d_0}_{h_x,h_t}(\Gamma_{NR}\times\Upsilon)\,. \tag{3.32}$$

Lemma 3.5. *Assume that* $\mathcal{S} : H^{1,\frac{1}{2}}(\Gamma\times\Upsilon) \to L_2(\Gamma\times\Upsilon)$ *is bounded and bijective and* $0 \le \kappa^* \le \kappa_0^* \in \mathbb{R}$. *Further, suppose that the assumptions on* $\bar{\mathcal{S}}$ *in Lemma 3.3 are met. If* $\tilde{u} \in \widetilde{H}^{2,1}(\Gamma_{NR}\times\Upsilon)$ *is the unique solution of* (2.20) *with* $g^*_{NR} \in H^{1,\frac{1}{2}}_{pw}(\Gamma_{NR}\times\Upsilon)$ *and* $\tilde{g}_D \in H^{2,1}(\Gamma\times\Upsilon)$, *then the unique solution* $\bar{\tilde{u}}_h \in S^{c_1,d_0}_{h_x,h_t}(\Gamma\times\Upsilon)\cap\widetilde{H}^{\frac{1}{2},\frac{1}{4}}(\Gamma_{NR}\times\Upsilon)$ *of* (3.32) *with* $\bar{g}^*_{NR} := \mathcal{Q}^{d_0}_{h_x}\mathcal{Q}^{d_0}_{h_t} g^*_{NR} \in S^{d_0,d_0}_{h_x,h_t}(\Gamma_{NR}\times\Upsilon)$ *and* $\bar{\tilde{g}}_D := \mathcal{Q}^{c_1}_{h_x}\mathcal{Q}^{d_0}_{h_t}\tilde{g}_D \in S^{c_1,d_0}_{h_x,h_t}(\Gamma\times\Upsilon)$ *satisfies*

$$\begin{aligned}\|\tilde{u}-\bar{\tilde{u}}_h\|_{L_2(\Gamma_{NR}\times\Upsilon)} \le C(h_x^2+h_t)\Bigg(&\|\tilde{u}\|_{\widetilde{H}^{2,1}(\Gamma_{NR}\times\Upsilon)} + \|\mathcal{S}\tilde{u}\|_{H^{1,\frac{1}{2}}_{pw}(\Gamma_{NR}\times\Upsilon)}\\ &+\|g^*_{NR}\|_{H^{1,\frac{1}{2}}_{pw}(\Gamma_{NR}\times\Upsilon)} + \|\mathcal{S}\tilde{g}_D\|_{H^{1,\frac{1}{2}}_{pw}(\Gamma\times\Upsilon)} + \|\tilde{g}_D\|_{H^{2,1}(\Gamma\times\Upsilon)}\Bigg).\end{aligned}$$

Proof. Due to $\widetilde{H}^{\frac{1}{2},\frac{1}{4}}(\Gamma_{NR}\times\Upsilon) \subset H^{\frac{1}{2},\frac{1}{4}}(\Gamma\times\Upsilon)$ Lemma 3.4 applies almost directly, except for an application of $\bar{\mathcal{S}}$ in the right hand side and an approximation of the extended Dirichlet data. These perturbations lead to additional terms in the Galerkin orthogonality of Lemma 3.4's proof resulting in the last two terms of the estimate. □

Remark 3.2. *Due to the definition of the boundary element space* $S^{c_1,d_0}_{h_x,h_t}(\Gamma_{NR}\times\Upsilon) := S^{c_1,d_0}_{h_x,h_t}(\Gamma\times\Upsilon)\cap\widetilde{H}^{\frac{1}{2},\frac{1}{4}}(\Gamma_{NR}\times\Upsilon)$ *with* $\Gamma_{NR} := \Gamma_N\cup\Gamma_R + \overline{\Gamma}_N\cap\overline{\Gamma}_R$ *it is clear that the elimination of a boundary part* Γ_i *with* $i\in\{D,N,R\}$ *of the continuous problem in Section 2.4.4 carries directly over to the discrete problem.*

Example 3.1. *We have chosen* $\Omega = (-0.5,0.5)^3 \subset \mathbb{R}^3$, $\Upsilon = (0,0.5)$, *and* $g_D(\mathbf{x},t) = G(\mathbf{x}-\mathbf{x}_0,t)$ *with* $\mathbf{x}_0 = (1.5,1.5,1.5)^\top$ *and* $\alpha = 1$ *to solve the initial Dirichlet boundary value problem* (3.17) *for* $\bar{q}_h^* \in S_{h_x,h_t}^{d_0,d_0}(\Gamma\times\Upsilon)$ *instead of* $\bar{q}_h^* \in S_{h_x,h_t}^{d_1,d_0}(\Gamma\times\Upsilon)$ *(cf. Remark 3.1), which serves as a verification of Lemma 3.1. In Table 3.1 and Figure 3.1 we observe the predicted* $\mathcal{O}(\sqrt{h_t})$ *convergence for* $h_t = \mathcal{O}(h_x^2)$. *However, we also observe that* $h_t = \mathcal{O}(h_x^2)$ *is not the optimal refinement scheme for* $\bar{q}_h^* \in S_{h_x,h_t}^{d_0,d_0}(\Gamma\times\Upsilon)$, *as the envelope over all curves shows faster possible convergence for* $h_t = \mathcal{O}(h_x^a)$ *with* $a < 2$. *Furthermore, for a either purely temporal or purely spatial refinement we observe a much better behavior than the bound of Lemma 3.1 predicts. Namely, the error is bounded from below rather than showing the asymptotic growth of Lemma 3.1. Finally, since the finest discretization already requires* 3.5 GB *of memory, takes* 4270 sec *of computation time, and the method scales like* $\mathcal{O}(N_x^2 N_t^2)$ *another refinement level is out of reach.*

$N_t \backslash N_x$	*24*	*96*	*384*	*1,536*
2	$5.60\ 10^{-1}$	$3.84\ 10^{-1}$	$3.25\ 10^{-1}$	$3.09\ 10^{-1}$
8	$5.04\ 10^{-1}$	$2.59\ 10^{-1}$	$1.47\ 10^{-1}$	$1.02\ 10^{-1}$
32	$4.98\ 10^{-1}$	$2.46\ 10^{-1}$	$1.23\ 10^{-1}$	$6.33\ 10^{-2}$
128	$4.97\ 10^{-1}$	$2.46\ 10^{-1}$	$1.21\ 10^{-1}$	$6.02\ 10^{-2}$

Table 3.1: $\|q^* - \bar{q}_h^*\|_{L_2(\Gamma\times\Upsilon)} / \|q^*\|_{L_2(\Gamma\times\Upsilon)}$ for $N_t \backslash N_x$.

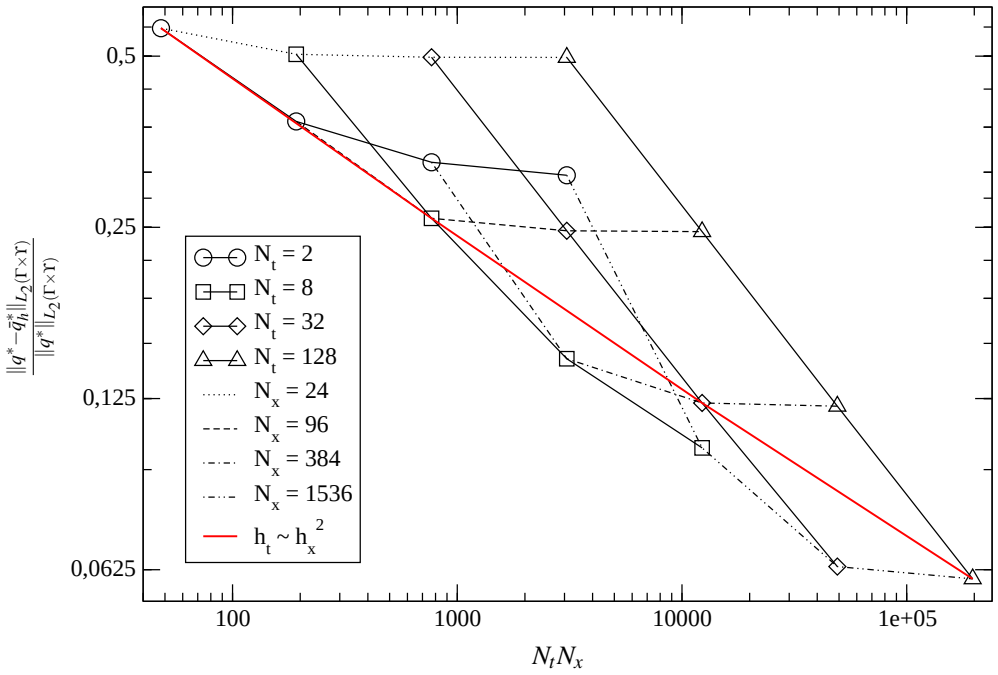

Figure 3.1: Relative Neumann $L_2(\Gamma\times\Upsilon)$ error for various space-time discretizations.

Example 3.2. *We have chosen* $\Omega = (-0.5,0.5)^3 \subset \mathbb{R}^3$, $\Upsilon = (0,0.5)$, *and* $g_N^*(\mathbf{x},t) = \alpha\partial_{\mathbf{n}_\mathbf{x}} G(\mathbf{x}-\mathbf{x}_0,t)$ *with* $\mathbf{x}_0 = (1.5,1.5,1.5)^\top$ *and* $\alpha = 1$ *to solve the initial Neumann boundary value problem* (3.21) *for* $\bar{u}_h \in S^{c_1,d_0}_{h_x,h_t}(\Gamma\times\Upsilon)$, *which serves as a verification of Lemma 3.2. In Table 3.2 and Figure 3.2 we clearly observe the predicted* $\mathcal{O}(h_t)$ *convergence for* $h_t = \mathcal{O}(h_x^2)$. *Since this behavior coincides with the envelope over all curves in Figure 3.2 it is clear that this refinement scheme is optimal in the total number of unknowns* N_xN_t. *Additionally, when looking at the far ends of either the spatial or temporal discretization, one can observe the respective optimal orders of convergence of the opposite discretization, i.e.,* $\mathcal{O}(h_t)$ *and* $\mathcal{O}(h_x^2)$. *Finally, since the finest discretization level requires* 1.8 GB *of memory, takes* 6510 sec *of computation time, and the method has quadratic complexity a further refinement level did not fit into our machine.*

$N_t\backslash N_x$	*14*	*50*	*194*	*770*
2	$4.54\ 10^{-1}$	$3.98\ 10^{-1}$	$3.95\ 10^{-1}$	$3.96\ 10^{-1}$
8	$2.71\ 10^{-1}$	$1.16\ 10^{-1}$	$9.51\ 10^{-2}$	$9.38\ 10^{-2}$
32	$2.59\ 10^{-1}$	$7.25\ 10^{-2}$	$2.76\ 10^{-2}$	$2.22\ 10^{-2}$
128	$2.58\ 10^{-1}$	$6.93\ 10^{-2}$	$1.76\ 10^{-2}$	$6.69\ 10^{-3}$

Table 3.2: $\|u-\bar{u}_h\|_{L_2(\Gamma\times\Upsilon)}/\|u\|_{L_2(\Gamma\times\Upsilon)}$ for $N_t\backslash N_x$.

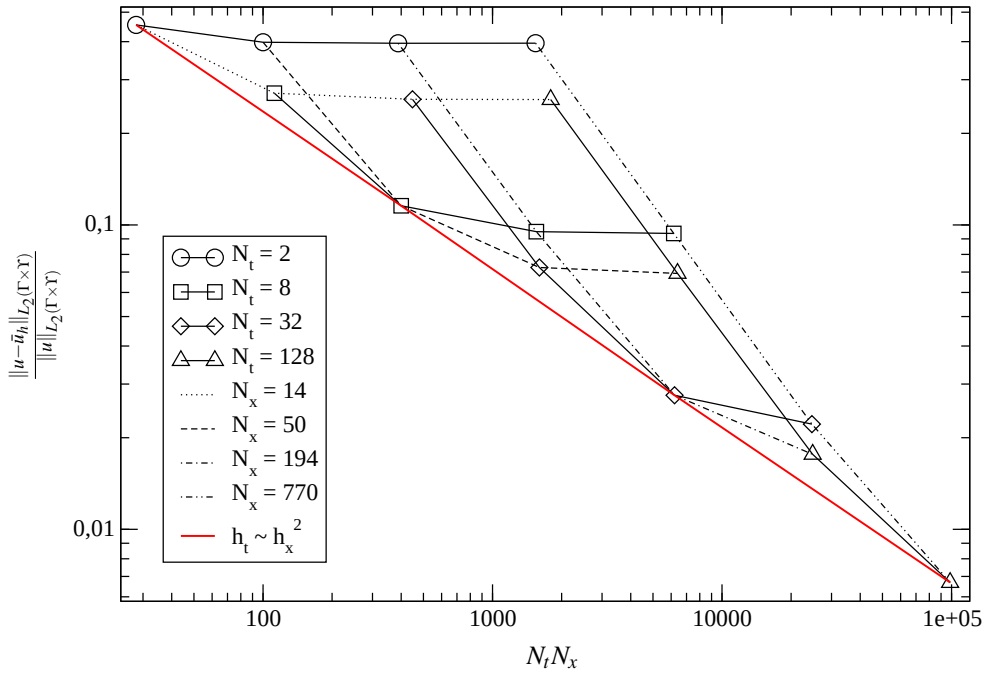

Figure 3.2: Relative Dirichlet $L_2(\Gamma\times\Upsilon)$ error for various space-time discretizations.

Example 3.3. *We have chosen* $\Omega = (-0.5,0.5)^3 \subset \mathbb{R}^3$, $\Upsilon = (0,0.5)$, *and* $g_R^*\mathbf{x},t) = \alpha\partial_{\mathbf{n}_\mathbf{x}} G(\mathbf{x}-\mathbf{x}_0,t) + \kappa^*(\mathbf{x})G(\mathbf{x}-\mathbf{x}_0,t)$ *with* $\mathbf{x}_0 = (1.5,1.5,1.5)^\top$ *and* $\alpha,\kappa^* = 1$ *to solve the initial Robin boundary value problem* (3.28) *for* $\bar{u}_h \in S^{c_1,d_0}_{h_x,h_t}(\Gamma\times\Upsilon)$. *In Table 3.3 and Figure 3.3 we clearly observe the predicted* $\mathcal{O}(h_t)$ *convergence for* $h_t = \mathcal{O}(h_x^2)$ *of Lemma 3.4. Since the slope of this behavior coincides with the envelope over all curves in Figure 3.3 it is clear that this refinement scheme is again optimal. Moreover, looking at the corner values of Table 3.3 we can observe the respective optimal orders of convergence of both, the spatial and temporal ansatz space. Finally, since the finest discretization level requires* 5.4 GB *of memory, takes* 8060 sec *of computation time, and the method has* $\mathcal{O}(N_x^2 N_t^2)$ *complexity we are not able to solve further refinement levels. Observe that this initial boundary value problem is based on an approximation of the Steklov-Poincaré operator, which requires the solution of a Dirichlet boundary value problem in each iteration and thus the higher cost compared to the previous two examples.*

$N_t \backslash N_x$	*14*	*50*	*194*	*770*
2	$3.26\ 10^{-1}$	$3.17\ 10^{-1}$	$3.17\ 10^{-1}$	$3.17\ 10^{-1}$
8	$1.23\ 10^{-1}$	$8.84\ 10^{-2}$	$8.54\ 10^{-2}$	$8.52\ 10^{-2}$
32	$9.24\ 10^{-2}$	$3.20\ 10^{-2}$	$2.19\ 10^{-2}$	$2.11\ 10^{-2}$
128	$9.04\ 10^{-2}$	$2.47\ 10^{-2}$	$8.16\ 10^{-3}$	$5.46\ 10^{-3}$

Table 3.3: $\|u-\bar{u}_h\|_{L_2(\Gamma\times\Upsilon)}/\|u\|_{L_2(\Gamma\times\Upsilon)}$ for $N_t\backslash N_x$.

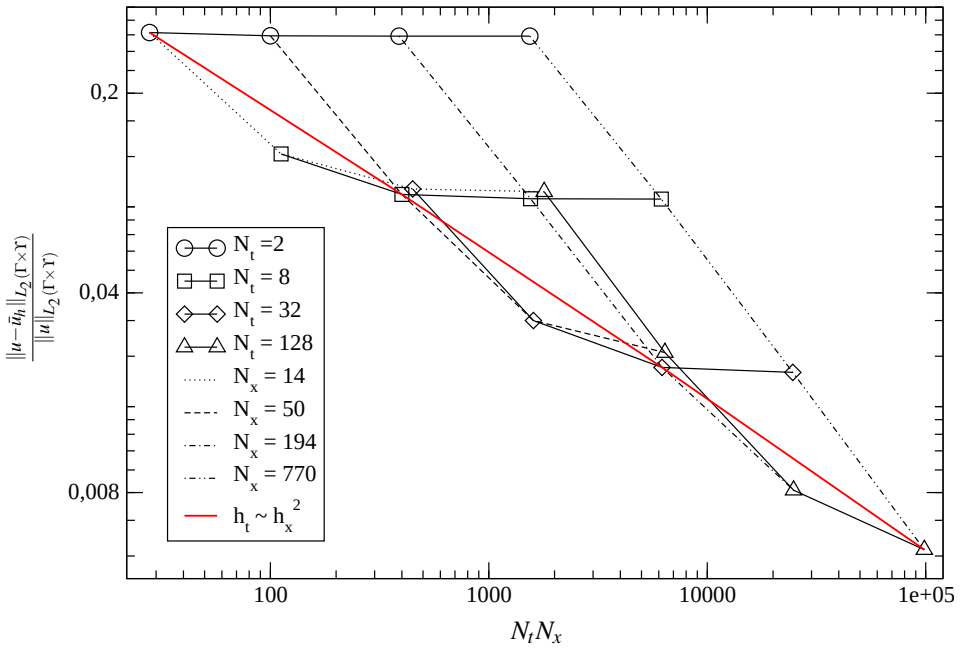

Figure 3.3: Relative Dirichlet $L_2(\Gamma\times\Upsilon)$ error for various space-time discretizations.

Example 3.4. *We have chosen* $\Omega = (-0.5,0.5)^3$ *with* $\Gamma_N = (-0.5,0.5)\times 0.5\times(-0.5,0.5)$, $\Gamma_D = (-0.5,0.5)\times -0.5\times(-0.5,0.5)$, *and* $\overline{\Gamma}_R = \Gamma\setminus(\overline{\Gamma}_N\cup\overline{\Gamma}_D)$ *and* $\Upsilon = (0,0.5)$. *On this partition of the boundary we define* $g_D(\mathbf{x},t) = G(\mathbf{x}-\mathbf{x}_0,t)$, $g_N^*(\mathbf{x},t) = \alpha\partial_{\mathbf{n_x}}G(\mathbf{x}-\mathbf{x}_0,t)$, *and* $g_R^*(\mathbf{x},t) = \alpha\partial_{\mathbf{n_x}}G(\mathbf{x}-\mathbf{x}_0,t)+\kappa^*G(\mathbf{x}-\mathbf{x}_0,t)$ *with* $\mathbf{x}_0 = (1.5,1.5,1.5)^\top$ *and* $\alpha,\kappa^* = 1$ *to solve* (3.32) *for* $\tilde{\bar{u}}_h \in S^{c_1,d_0}_{h_x,h_t}(\Gamma_{NR}\times\Upsilon) := S^{c_1,d_0}_{h_x,h_t}(\Gamma\times\Upsilon)\cap\widetilde{H}^{\frac{1}{2},\frac{1}{4}}(\Gamma_{NR}\times\Upsilon)$. *In Table 3.4 and Figure 3.4 we clearly observe the predicted* $\mathcal{O}(h_t)$ *convergence for* $h_t = \mathcal{O}(h_x^2)$ *of* $\bar{u}_h = \tilde{\bar{g}}_D + \tilde{\bar{u}}_h \in S^{c_1,d_0}_{h_x,h_t}(\Gamma\times\Upsilon)$ *in Lemma 3.5. Again, since the finest discretization level requires* 4.1 GB *of memory, takes* 6890 sec *of computation time, hence due to the quadratic complexity of the method further refinement levels have to be omitted. Observe that this mixed initial boundary value problem computationally less expensive then the initial Robin boundary value problem, since the Dirichlet and the Neumann boundary condition are less expensive than the Robin boundary condition.*

$N_t\backslash N_x$	*14*	*50*	*194*	*770*
2	$3.22\ 10^{-1}$	$3.14\ 10^{-1}$	$3.14\ 10^{-1}$	$3.13\ 10^{-1}$
8	$1.22\ 10^{-1}$	$8.81\ 10^{-2}$	$8.51\ 10^{-2}$	$8.48\ 10^{-2}$
32	$9.16\ 10^{-2}$	$3.20\ 10^{-2}$	$2.19\ 10^{-2}$	$2.11\ 10^{-2}$
128	$8.95\ 10^{-2}$	$2.47\ 10^{-2}$	$8.15\ 10^{-3}$	$5.45\ 10^{-3}$

Table 3.4: $\|u-\bar{u}_h\|_{L_2(\Gamma\times\Upsilon)}/\|u\|_{L_2(\Gamma\times\Upsilon)}$ for $N_t\backslash N_x$.

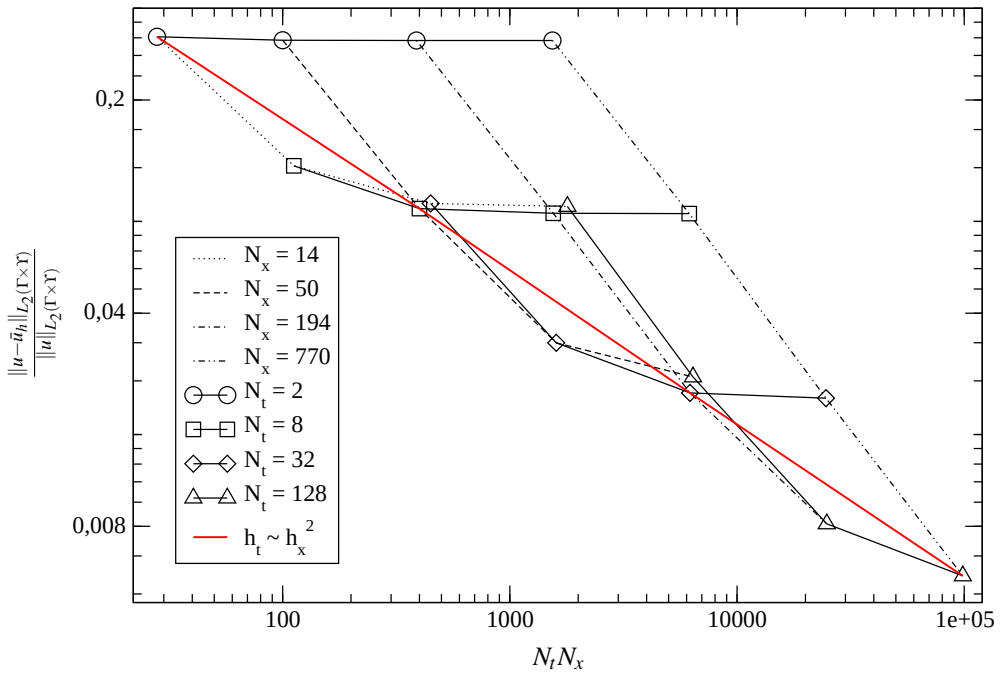

Figure 3.4: Relative Dirichlet $L_2(\Gamma\times\Upsilon)$ error for various space-time discretizations.

4 THE PARABOLIC FAST MULTIPOLE METHOD

The fast multipole method (FMM) [18] has originally been developed to solve many body problems in two-dimensional potential field theory. Its name stems from the multipole expansion of an electrostatic point charge in the original paper [18]. Ever since the algorithm has been extended to higher dimensions, further improved by using different expansions and applied to different physical problems [10, 19, 36]. Even though the panel clustering method [23] has appeared almost contemporaneously to the original FMM publication, we follow the common misuse of terminology. It has become customary to refer to efficient evaluation schemes for point-point interactions, based on a hierarchical clustering of the computational domain and separation of variables for well separated clusters through some kind of kernel expansion, as FMM algorithms. In this context, Galerkin boundary element methods may be conceived as weighted and integrated point-point interactions problems. The basic idea of such algorithms is to collect the influence of sources in clusters and evaluate their collective influence on all admissible target clusters, i.e., clusters where the expansion converges. This way the otherwise $\mathcal{O}(N^2)$ cost for the evaluation of the point-point interaction problem is reduced to $\mathcal{O}(N)$ with N being the number of unknowns. Such methods have seen quite some success in the elliptic [22, 30, 38] and lately also in the parabolic case [34, 47, 49].

Obviously, the FMM concept is kernel dependent, thus we need to investigate the heat kernel in more detail. Its asymptotic smoothness for $t-\tau>0$ and exponential decay in space (see Figure 4.1a and 4.1b, respectively) kind of already defines the required adaption of the FMM algorithm. One may perceive it as a combination of a one-dimensional causal FMM [49] (cFMM) in time with a fast Gauss transform [21] (FGT) applied to the spatial variable. Based on this observation we will first explain these two algorithms by themselves, before joining them together to the parabolic FMM [47] (pFMM) algorithm.

Since it is of major importance for the remainder of this chapter, we would like to emphasize at this point that the spatial variable of the heat kernel naturally separates due to basic properties of the exponential function

$$G(\mathbf{r},\delta)=\prod_{i=1}^{3}\frac{1}{(4\pi\alpha\delta)^{\frac{1}{2}}}\exp\left(-\frac{|r_i|^2}{4\alpha\delta}\right)=\prod_{i=1}^{3}G(r_i,\delta)\,. \tag{4.1}$$

Hence, for the most part it is sufficient to look at properties of the one-dimensional heat kernel with the multi-dimensional case following from this Gaussian structure. As a matter of fact, the spatial dimension of the algorithm is not limited to three space dimensions, however, since we only deal with three-dimensional heat diffusion problems we develop

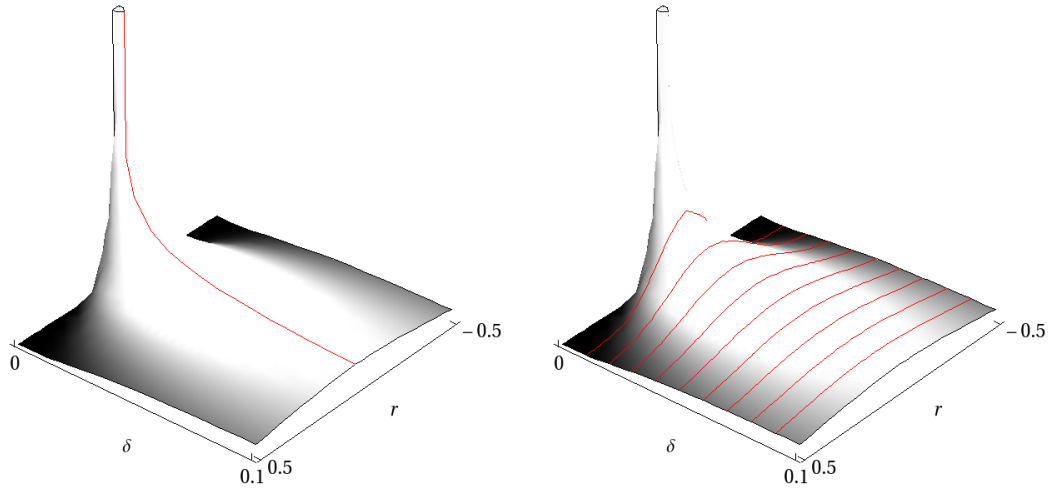

(a) The heat kernel is asymptotically smooth in time – see curve at $r = 0$.

(b) For fixed time variables the heat kernel is a Gaussian in space – see set of curves.

Figure 4.1: One-dimensional heat kernel $G(r,\delta)$ for $(r,\delta) \in (-0.5,0.5) \times (0,0.1)$.

the algorithm for that special case. Observe that $\alpha \neq 1$ corresponds to a time scaling (2.7a), therefore we set $\alpha \equiv 1$ for the remainder of this chapter. Another important property of the heat kernel is the space-time scaling property

$$G(\mathbf{r},\delta) = \delta^{-\frac{3}{2}} G\left(\frac{\mathbf{r}}{\sqrt{\delta}}, 1\right), \tag{4.2}$$

which tells us that the heat kernel gets more and more peaked in space the smaller the variance (see Figure 4.1).

In the remainder of this chapter we proceed as follows: We introduce a hierarchical space-time clustering in Section 4.1 and recall some basics from multivariate approximation theory in Section 4.2. In Section 4.3, we construct space independent thermal layer potentials and evaluate them via the cFMM, in Section 4.4 we present an efficient realization of thermal layer potentials with fixed time variable through the FGT and in Section 4.5 we combine the ideas of Section 4.3 and Section 4.4 to efficiently solve Galerkin space-time discretized boundary integral equations of the heat equation via the pFMM. Sections 4.2 through 4.5 are a presentation of [47, 49, 50] from the authors perspective with an adaption to the Galerkin method where necessary. Finally, due to the temporal nearfield being so expensive, whenever the space-time scaling is not optimal, we present some more recent results [34] in Section 4.6 to improve the spatial evaluation of the temporal nearfield.

4.1 Space-Time Clustering

In this section, we introduce a hierarchical clustering of the computational domain as the first basic ingredient for any FMM algorithm. We distinguish between the temporal and spatial cluster tree due to the different structure of the temporal and spatial dimension of the space-time cylinder $\Gamma \times \Upsilon$, respectively. While the spatial discretization is rather unstructured, the temporal discretization has a very simple nature that we seek to conserve.

4.1.1 Temporal Cluster-Tree

We want the temporal cluster tree to inherit the uniformity of time discretization (3.2). Since time is a one-dimensional and ordered manifold in $\mathbb{R}$, there are no empty temporal clusters, which allows a simple cluster structure without geometric sorting (see Figure 4.2).

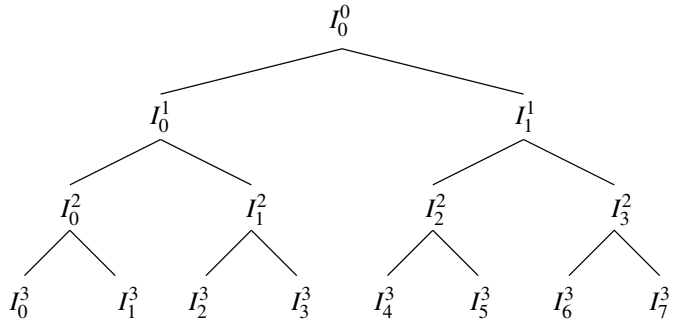

Figure 4.2: Completely uniform temporal binary tree.

Definition 4.1. *We define the temporal root cluster to coincide with the time interval of interest $I_0^0 := \Upsilon = [0,T]$ with center $c^{I_0^0} = T/2$ and cluster half length $h_t^0 = T/2$. Further, we choose a leaf level L_t and split all clusters $I_k^{\ell_t}$ recursively into two equal sized children*

$$\mathfrak{C}(I_k^{\ell_t}) = \{I_{2k+i}^{\ell_t+1}\}_{i=0}^{1} \qquad \forall \ell_t = 0,\dots L_t - 1 \quad \textit{and} \quad \forall k = 0,\dots 2^{\ell_t} - 1\,.$$

This way we end up with 2^{ℓ_t} uniform clusters with interval half length $h_t^{\ell_t} = T/2^{\ell_t+1}$ in each level. In particular, we have 2^{L_t} temporal leaf clusters which we split into n_t uniform time steps of step size $h_t = 2h_t^{L_t}/n_t$. Thus we define the panel list

$$\mathfrak{P}(I_k^{\ell_t}) = \bigcup_{i=0}^{n_t-1} \{2^{L_t-\ell_t}k + i\} \qquad \forall \ell_t = 0,\dots L_t - 1 \quad \textit{and} \quad \forall k = 0,\dots 2^{\ell_t} - 1$$

containing the indices of all time steps belonging to a temporal cluster $I_k^{\ell_t}$.

4.1.2 Spatial Cluster-Tree

The spatial component of the computational domain is more involved than the temporal one for the following reason. We are dealing with a polyhedral triangulation of an arbitrary Lipschitz domain's boundary Γ , i.e., a two-dimensional Lipschitz manifold embedded in three-dimensional space. We can not expect the spatial clustering to be uniform like in time, since there will be empty clusters, i.e., clusters not intersecting with Γ (see Figure 4.3 and 4.4). Nevertheless, we restrict ourselves to a very simple structure only, namely a regular, axis parallel and thus tensorial cluster-tree. This choice facilitates an FMM algorithm, whose translation operators inherit the tensor structure of the heat kernel (4.1) – a feature that in general would not be possible with more sophisticated clustering strategies.

Definition 4.2. *We define the root cluster X_0^0 to be the cubic bounding box with half-side length*

$$h_x^0 = \frac{\|\tilde{\mathbf{x}} - \check{\mathbf{x}}\|_\infty}{2}\,, \qquad \tilde{\mathbf{x}}, \check{\mathbf{x}} \in \Gamma$$

and center

$$c_i^{X_0^0} = \max_{\tilde{\mathbf{x}}, \check{\mathbf{x}} \in \Gamma} \frac{|\tilde{x}_i + \check{x}_i|}{2}\,, \qquad i \in \{1,2,3\}\,.$$

Further, we recursively split all $X_k^{\ell_x}$ into eight equal sized child cubes

$$\mathfrak{C}(X_k^{\ell_x}) = \{X_{8k+i}^{\ell_x+1}\}_{i=0}^{7} \qquad \forall \ell_x = 0, \dots L_x - 1 \quad \textit{and} \quad \forall k = 0, \dots 8^{\ell_x} - 1$$

with half-side length $h_x^{\ell_x+1} = h_x^0 / 2^{\ell_x+1}$. Throughout this process, test and trial functions φ_j with center of mass $\mathbf{c}^{\varphi_j}$ are assigned to the panel list $\mathfrak{P}(X_k^{\ell_x})$ of one and only one cluster $X_k^{\ell_x}$ in each level

$$\mathfrak{P}(X_k^{\ell_x}) = \{j : \mathbf{c}^{\varphi_j} \in X_k^{\ell_x}\}\,.$$

We drop all $X_k^{\ell_x}$ with $\mathfrak{P}(X_k^{\ell_x}) = \emptyset$ while we collect all nonempty clusters per level in a cluster list

$$\mathfrak{X}(\ell_x) = \{k : \mathfrak{P}(X_k^{\ell_x}) \neq \emptyset\}$$

and stop at level $\ell_x = L_x$ once $N_x = n_x \dim(\mathfrak{X}(\ell_x))$ with a pre-specified n_x is reached.

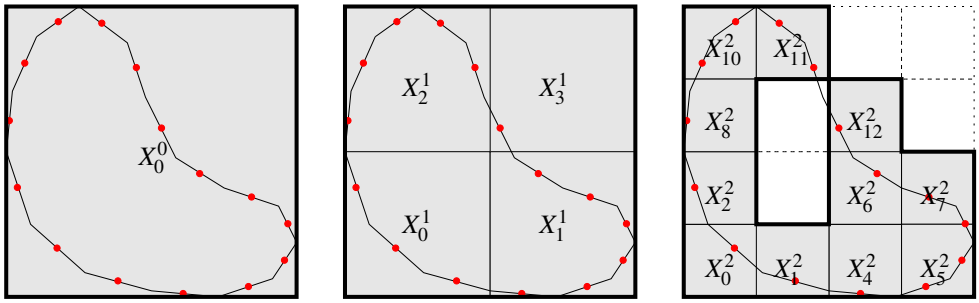

Figure 4.3: Cross-section through spatial cluster structure (• are $\mathbf{c}^{\varphi_j}$).

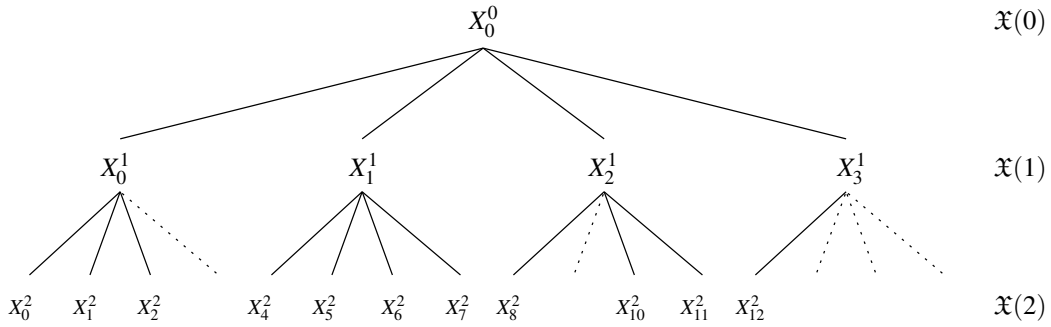

Figure 4.4: Spatial cluster-tree corresponding to Figure 4.3.

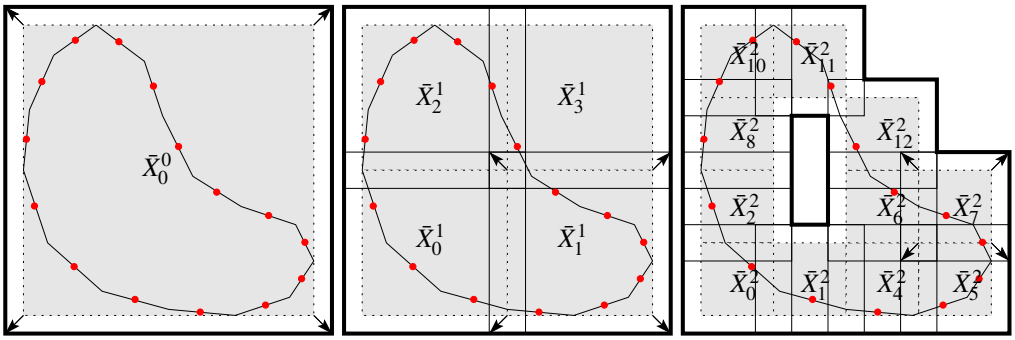

Figure 4.5: Spatial cluster extension as described in Definition 4.3.

Since we work with Galerkin discretized boundary integral operators, we need to evaluate their bilinear forms (3.5), (3.6), (3.7), and (3.8) cluster-wise over the support of test and trial functions. Therefore, the spatial cluster tree must contain the entire support of all test and trial functions. Observe that Definition 4.2 does not ensure that (see Figure 4.3, where the boundary is not completely contained in the union of all leaf clusters), thus we define an extension of all clusters as follows.

Definition 4.3. *Find the maximal bounding box of all test or trial functions assigned to each leaf cluster*

$$\bar{h}_x^{L_x} = \max_k \left(\max_{\mathbf{x} \in \bigcup_{j \in \mathfrak{P}(X_k^{L_x})} supp(\varphi_j)} \|\mathbf{c}^{X_k^{L_x}} - \mathbf{x}\|_\infty \right)$$

and uniformly extend all clusters $X_k^{\ell_x} \to \bar{X}_k^{\ell_x}$ in all levels $\ell_x = 0, \dots L_x$ by

$$\bar{h}_x^{\ell_x} = h_x^{\ell_x} + \left(\bar{h}_x^{L_x} - h_x^{L_x}\right) .$$

Observe that after the extension described in Definition 4.3 $\bigcup \bar{X}_k^{\ell_x}$ covers the entire computational domain Γ (see Figure 4.5) while this was not ensured by $\bigcup X_k^{\ell_x}$ (see Figure 4.3).

4.2 Multivariate Lagrange Interpolation and Chebyshev Expansion

The second major ingredient required by any FMM is a separation of variables through an appropriate kernel expansion. Thus we recall the basics from Lagrange interpolation and Chebyshev expansion theory, which we need for the kernel expansions later on. Throughout this section we make use of the linear transformation $\Phi : [-1,1] \to [a,b]$ defined by

$$\Phi(\hat{z}) = \frac{a+b}{2} + \frac{b-a}{2}\hat{z} .$$

In the multi-dimensional case it is understood that $\Phi : [-1,1]^d \to [\mathbf{a},\mathbf{b}]$ is equivalent to $\{\Phi : [-1,1] \to [a_i,b_i]\}_{i=1}^d$ with $[\mathbf{a},\mathbf{b}] = [a_1,b_1] \times [\dots] \times [a_d,b_d]$. Furthermore, due to Definitions 4.1 through 4.3 we always have $b_1 - a_1 = \cdots = b_d - a_d$ and thus write $(b-a)$ instead of $(b_i - a_i)$. Finally, to clarify the notation, for α a d-dimensional multi-index, e.g., $\alpha = (\alpha_1, \dots, \alpha_d)$ we have $|\alpha| = \alpha_1 + \cdots + \alpha_d$, $\alpha! = \alpha_1! \dots \alpha_d!$ and $\alpha^n = (\alpha_1^n, \dots, \alpha_d^n)$.

4.2.1 Lagrange Interpolation

Let us assume a continuous function $f : [a,b] \to \mathbb{R}$ and write its interpolation on the nodes $\{\omega_i^p\}_{i=0}^p \in [-1,1]$

$$\mathcal{J}_p f(t) = \sum_{i=0}^{p} f\left(\Phi(\omega_i^p)\right) L_i\left(\Phi^{-1}(t)\right) \tag{4.3}$$

in terms of the Lagrange polynomials

$$L_i(\hat{t}) = \prod_{k \neq i} \frac{\hat{t} - \omega_k^p}{\omega_i^p - \omega_k^p} , \qquad \hat{t} \in [-1,1] .$$

If we choose the roots of the $(p+1)^{st}$ Chebyshev polynomial as interpolation nodes

$$\omega_i^p = \cos\left(\frac{\pi}{2}\frac{2i+1}{p+1}\right) ,$$

then the interpolation error is bounded by

$$|(\mathcal{I}-\mathcal{J}_p)f(t)| \leq \frac{\|D_t^{(p+1)}f(t)\|_\infty}{(p+1)!}\left(\frac{b-a}{4}\right)^{p+1} . \tag{4.4}$$

Multivariate interpolation The interpolation of $f:[\mathbf{a},\mathbf{b}]\to\mathbb{R}$ on a tensor grid of interpolation nodes $\{\omega_\alpha^p\}_{\alpha=0}^p = \{\{\omega_{\alpha_1}^p\}_{\alpha_1=0}^p \times\cdots\times\{\omega_{\alpha_d}^p\}_{\alpha_d=0}^p\} \in [-1,1]^d$

$$\mathcal{J}_p^d f(\mathbf{t}) = \sum_{\alpha=0}^{p} f\left(\Phi(\omega_\alpha^p)\right) L_\alpha\left(\Phi^{-1}(\mathbf{t})\right) \tag{4.5}$$

induces an error bounded by [22, Lemma 3]

$$|(\mathcal{I}-\mathcal{J}_p^d)f(\mathbf{t})| \leq \sum_{\|\alpha\|_\infty=1} \frac{\|D_{\mathbf{t}}^{\alpha(p+1)}f(\mathbf{t})\|_\infty}{(\alpha(p+1))!}\left(\frac{b-a}{4}\right)^{|\alpha|(p+1)} . \tag{4.6}$$

4.2.2 Chebyshev Expansion

Let us assume an analytic function $f:[a,b]\to\mathbb{R}$, then we may write its expansion

$$\mathcal{S}_\infty f(x) = \sum_{i=0}^{\infty} f_i T_i\left(\Phi^{-1}(x)\right) \tag{4.7}$$

with the Chebyshev polynomials of the first kind

$$T_i(\hat{x}) = \cos\left(i\arccos(\hat{x})\right) , \qquad \hat{x}\in[-1,1] .$$

Due to their $L_w^2[-1,1]$ orthogonality with respect to the weight function $w(\hat{x}) = 1/\sqrt{1-\hat{x}^2}$

$$\int_{-1}^{1} T_m(\hat{x})T_n(\hat{x})w(\hat{x})\mathrm{d}\hat{x} = \frac{\pi}{\gamma_n}\delta_{mn} \quad \text{with} \quad \gamma_n = \begin{cases} 1 & n=0 \\ 2 & n\geq 1 \end{cases} \tag{4.8}$$

it is easily verified that the coefficients f_i in (4.7) are given by

$$f_i = \frac{\gamma_i}{\pi}\int_{-1}^{1} f\left(\Phi(\hat{x})\right) T_i(\hat{x})w(\hat{x})\mathrm{d}\hat{x} . \tag{4.9}$$

After expanding the function $f(x)$ itself in a Chebyshev series, we are interested in the expansion of its derivative

$$\mathcal{S}_\infty \frac{\partial}{\partial x} f(x) = \frac{\partial}{\partial x} \mathcal{S}_\infty f(x) = \frac{\partial}{\partial x} \sum_{i=0}^{\infty} f_i T_i \left(\Phi^{-1}(x)\right) = \sum_{i=0}^{\infty} f_i \frac{\partial}{\partial x} T_i \left(\Phi^{-1}(x)\right) \,, \tag{4.10}$$

what turns out to be a rather straightforward task, because we do not have to change the expansion coefficients (4.9). We simply shift the derivative over to the Chebyshev polynomials and replace them by their derivatives, which are given in terms of the Chebyshev polynomials of the second kind

$$\frac{\partial}{\partial \hat{x}} T_i(\hat{x}) = i U_{i-1}(\hat{x}) \quad \text{with} \quad U_{i-1}(\hat{x}) = \frac{\sin(i \arccos(\hat{x}))}{\sqrt{1-\hat{x}^2}} \,, \tag{4.11}$$

thus we may write

$$\mathcal{S}_\infty \frac{\partial}{\partial x} f(x) = \sum_{i=0}^{\infty} f_i \, i U_{i-1} \left(\Phi^{-1}(x)\right) \frac{\partial}{\partial x} \Phi^{-1}(x) \,. \tag{4.12}$$

Multivariate expansion The expansion of $f : [\mathbf{a}, \mathbf{b}] \to \mathbb{R}$ is given by

$$\mathcal{S}_\infty^d f(\mathbf{x}) = \sum_{\alpha=0}^{\infty} c_\alpha T_\alpha \left(\Phi^{-1}(\mathbf{x})\right)$$

with the coefficients

$$c_\alpha = \frac{\gamma_\alpha}{\pi^d} \int\limits_{[-1,1]^d} f\left(\Phi(\hat{\mathbf{x}})\right) T_\alpha(\hat{\mathbf{x}}) w_\alpha(\hat{\mathbf{x}}) \mathrm{d}\hat{\mathbf{x}} \,.$$

In the same manner as for the derivative (4.10) in the one-dimensional case we introduce the Chebyshev expansion of the gradient

$$\mathcal{S}_\infty^d \nabla_{\mathbf{x}} f(\mathbf{x}) = \nabla_{\mathbf{x}} \mathcal{S}_\infty^d f(\mathbf{x}) = \nabla_{\mathbf{x}} \sum_{\alpha=0}^{\infty} c_\alpha T_\alpha \left(\Phi^{-1}(\mathbf{x})\right) = \sum_{\alpha=0}^{\infty} c_\alpha \nabla_{\mathbf{x}} T_\alpha \left(\Phi^{-1}(\mathbf{x})\right) \tag{4.13}$$

with

$$\nabla_{\mathbf{x}} T_\alpha \left(\Phi^{-1}(\mathbf{x})\right) = \begin{pmatrix} \alpha_1 U_{\alpha_1 - 1}(x_1) & T_{\alpha_2}(x_2) & \dots & T_{\alpha_d}(x_d) \\ T_{\alpha_1}(x_1) & \alpha_2 U_{\alpha_2 - 1}(x_2) & \dots & T_{\alpha_d}(x_d) \\ \vdots & \vdots & \ddots & \vdots \\ T_{\alpha_1}(x_1) & T_{\alpha_2}(x_2) & \dots & \alpha_d U_{\alpha_d - 1}(x_d) \end{pmatrix} \frac{1}{\det\left(\mathbf{J}_\Phi(\mathbf{x})\right)} \,. \tag{4.14}$$

Remark 4.1. *Assume that we truncate* (4.7) *after* $q+1$ *terms and compute the coefficients in* (4.9) *by replacing the integral with a* q^{th} *order Gauss-Chebyshev quadrature rule*

$$\mathcal{S}_q f(x) = \sum_{i=0}^{q} f_i T_i\left(\Phi^{-1}(x)\right) \quad \textit{and} \quad f_i \approx \frac{\gamma_i}{q+1} \sum_{k=0}^{q} T_i(\omega_k^q) f\left(\Phi(\omega_k^q)\right) \ ,$$

then we obtain $\mathcal{S}_q f = \mathcal{J}_q f$.

Remark 4.1 shows us how to convert a truncated Chebyshev expansion into a Lagrange interpolation formula. The extension of this idea to the multi-dimensional case would give us an estimate of the truncation error with coefficients in a hyper-cubic region. However, this is not optimal because the tensor product space spanned by the Lagrange polynomials does not span the full polynomial space of the hyper-cube's dimension. As we will see in Section 4.4.1, we can find a better truncation criterion with coefficients in a hyper-simplicial region by estimating the specific truncation error of the heat kernel itself.

Remark 4.2. *Observe that* $\mathcal{S}_\infty$ *is a* $L_w^2[-1,1]$ *orthogonal projector with*

$$\sum_{i=0}^{\infty} |f_i|^2 \leq \|S_\infty f(\Phi(\hat{x}))\|^2_{L_w[-1,1]} \leq \|f(\Phi(\hat{x}))\|^2_{L_w[-1,1]} \ ,$$

which translates to the truncated expansion and the multi-dimensional case as well.

4.3 Purely Time Dependent Thermal Layer Potentials

In the case of a purely time dependent density $q^*(\mathbf{y},\tau) := q^*(\tau)$ on a sphere one can perform the spatial integration in the thermal layer potentials analytically. We chose this special case as a starting point for the derivation of the pFMM, because it isolates the temporal aspect of the algorithm, the cFMM. For simplicity we choose a unit-sphere with boundary Γ_S (and $\alpha \equiv 1$, as mentioned at the beginning of this chapter) in which case the single layer potential due to the density $q^*(\tau)$ becomes

$$\begin{aligned}
\mathcal{V}q^*(t) &= \int_0^t \int_{\Gamma_S} \frac{1}{(4\pi(t-\tau))^{\frac{3}{2}}} \exp\left(-\frac{|\mathbf{x}-\mathbf{y}|^2}{4(t-\tau)}\right) \mathrm{d}s_{\mathbf{y}} q^*(\tau)\mathrm{d}\tau \\
&= \int_0^t \frac{1}{\sqrt{4\pi(t-\tau)}} \left[1 - \exp\left(-\frac{1}{(t-\tau)}\right)\right] q^*(\tau)\mathrm{d}\tau \\
&:= \int_0^t V(t-\tau) q^*(\tau)\mathrm{d}\tau
\end{aligned} \tag{4.15}$$

Turning this problem around we assume $f(t) = f(\mathbf{x},t) \in H^{\frac{1}{2},\frac{1}{4}}(\Gamma_S \times \Upsilon)$ to be given and solve for the density $q^*(\tau) = q^*(\mathbf{y},\tau) \in H^{-\frac{1}{2},-\frac{1}{4}}(\Gamma_S \times \Upsilon)$ such that

$$\langle \mathcal{V} q^*, w \rangle_{\Gamma_S \times \Upsilon} = \langle f, w \rangle_{\Gamma_S \times \Upsilon} \qquad \forall w \in H^{-\frac{1}{2},-\frac{1}{4}}(\Gamma_S \times \Upsilon) \, . \tag{4.16}$$

In the remainder of this section we dedicate ourselves to solve the Galerkin discretized version of (4.16). Since the solution is constant in space, it turns out that the spatial integration can be performed analytically once again and the Galerkin discretized integral equation according to Section 3.1.1 reduces to finding $q_h^* \in T_{h_t}^{d_0}(\Upsilon)$ such that

$$\langle \mathcal{V} q_h^*, w_h \rangle_{\Upsilon} = \langle f, w_h \rangle_{\Upsilon} \qquad \forall w_h \in T_{h_t}^{d_0}(\Upsilon) \, , \tag{4.17}$$

which eventually leads to the linear system

$$\mathsf{V}\,\mathsf{q}^* = \mathsf{f}$$

with $\mathsf{f}_i := \langle f, \phi_i \rangle$ and $\mathsf{V}_{ij} := \langle \mathcal{V}\phi_j, \phi_i \rangle$ given in Appendix B.1 and $i \in \{0,\dots,N_t\}$. Observe that this matrix has lower triangular Töplitz structure due to causality of the integral operator $\mathcal{V}$. Clearly, the computation of the right hand side involves $\mathscr{O}(N_t)$ operations, whereas solving the linear system has $\mathscr{O}(N_t^2)$ complexity even if done by forward substitution. Therefore, we apply the cFMM algorithm, which allows us to reduce this prohibitively large amount of work to almost optimal complexity.

Remark 4.3. *Observe that the results of Section 3.2.1 still hold for the solution of* (4.17)*, however, due to the vanishing spatial error (constant spatial solution lies in any piecewise polynomial ansatz space) estimate* (3.14) *simplifies to*

$$\|q^* - q_h^*\|_{H^{-\frac{1}{2},-\frac{1}{4}}(\Gamma_S \times \Upsilon)} \leq C h_t^{\frac{5}{4}} \|q^*\|_{H^{2,1}_{pw}(\Gamma_S \times \Upsilon)}$$

and estimate (3.15) *to*

$$\|q^* - q_h^*\|_{L_2(\Gamma_S \times \Upsilon)} \leq C h_t \|q^*\|_{H^{2,1}_{pw}(\Gamma_S \times \Upsilon)} \, .$$

4.3.1 Lagrange Interpolation of the Time Dependent Kernel

Based on the hierarchical clustering of Υ as described in Section 4.1.1 we interpolate the time dependent kernel in (4.16) with $t \in I_m^{\ell_t} \subset \Upsilon$ and $\tau \in I_n^{\ell_t} \subset \Upsilon$. For this purpose we introduce local variables $\hat{t}, \hat{\tau} \in [-1,1]$

$$t = \Phi_{I_m^{\ell_t}}(\hat{t}) = c_{I_m^{\ell_t}} + h_t^{\ell_t} \hat{t} \quad \text{and} \quad \tau = \Phi_{I_n^{\ell_t}}(\hat{\tau}) = c_{I_n^{\ell_t}} + h_t^{\ell_t} \hat{\tau}$$

and end up with

$$V(t-\tau) = V\left(\Phi_{I_m^{\ell_t}}(\hat{t}) - \Phi_{I_n^{\ell_t}}(\hat{\tau}) \right) = V\left((d_{mn}^{\ell_t} + \hat{t} - \hat{\tau}) h_t^{\ell_t} \right) \, ,$$

where $d_{mn}^{\ell_t} = (c_{I_m^{\ell_t}} - c_{I_n^{\ell_t}})/h_t^{\ell_t}$.

Lemma 4.1. *Let $t \in I_m^{\ell_t}$ and $\tau \in I_n^{\ell_t}$, then the interpolation error of the kernel in* (4.16) *by a bivariate interpolation ($\mathcal{J}_p^2 = \mathcal{J}_{p,t} \circ \mathcal{J}_{p,\tau} \equiv \mathcal{J}_{p,\tau} \circ \mathcal{J}_{p,t}$) as described in Section 4.2.1*

$$\mathcal{J}_p^2 V(t-\tau) = \sum_{a,b=0}^{p} V\left(\Phi_{I_m^{\ell_t}}(\omega_a^p) - \Phi_{I_n^{\ell_t}}(\omega_b^p)\right) L_a\left(\Phi_{I_m^{\ell_t}}^{-1}(t)\right) L_b\left(\Phi_{I_n^{\ell_t}}^{-1}(\tau)\right)$$

for two well separated clusters

$$d_{mn}^{\ell_t} - 2 > 1 \tag{4.18}$$

is bounded by

$$|(\mathcal{I} - \mathcal{J}_p^2) V(t-\tau)| \leq C\left((d_{mn}^{\ell_t} - 2) h_t^{\ell_t}\right)^{-\frac{1}{2}} \left(\frac{1}{d_{mn}^{\ell_t} - 2}\right)^{p+1} .$$

Proof. In order to prove the given bound using estimate (4.6) we need to show that the kernel in (4.15) is asymptotically smooth. With $V(t-\tau) := V_1(t-\tau) + V_2(t-\tau)$ and

$$V_1(t-\tau) := \frac{1}{\sqrt{4\pi(t-\tau)}} ,$$
$$V_2(t-\tau) := \frac{-1}{\sqrt{4\pi(t-\tau)}} \exp\left(-\frac{1}{t-\tau}\right)$$

it is easily seen that $V_1(t-\tau)$ fulfills

$$\left|\frac{D_t^i D_\tau^j V_1(t-\tau)}{(i+j)!}\right| \leq \frac{C}{|t-\tau|^{i+j+\frac{1}{2}}} .$$

However, for $V_2(t-\tau)$ such a relation is less obvious. For this purpose we define $\delta := t - \tau$ and use Cauchy's integral formula to estimate

$$\frac{V_2^{(n)}(\delta)}{n!} = \frac{(-1)^n}{2\pi\imath} \int_\gamma \frac{1}{\sqrt{4\pi\zeta}} \exp\left(-\frac{1}{\zeta}\right) \frac{1}{(\delta-\zeta)^{n+1}} \mathrm{d}\zeta .$$

We choose the contour γ to be a circle with positive radius $a < \delta$ centered at δ

$$\gamma = \{\zeta : |\delta - \zeta| = a\} .$$

For this choice we obtain the estimates

$$|\delta - \zeta| = a , \quad \mathfrak{Re}\left(\tfrac{1}{\zeta}\right) \geq 0 , \quad \text{and} \quad |\zeta| \geq \delta - a ,$$

which lead to

$$\left|\frac{V_2^{(n)}(\delta)}{n!}\right| \leq (4\pi(\delta - a))^{-\frac{1}{2}} a^{-n}$$

and maximize $(\delta-a)^{-\frac{1}{2}}a^{-n}$ for the optimal radius $a=2n\delta/(2n+1)$, which results in

$$\left|\frac{D_t^i D_\tau^j V_2(t-\tau)}{(i+j)!}\right| \leq \frac{C(i+j)^{\frac{1}{2}}}{|t-\tau|^{i+j+\frac{1}{2}}}\,.$$

Thus we may state the asymptotic smoothness condition for the kernel in (4.16) as

$$\frac{|D_t^i D_\tau^j V(t-\tau)|}{(i+j)!} \leq \frac{C(i+j)^{\frac{1}{2}}}{|t-\tau|^{i+j+\frac{1}{2}}}\,. \tag{4.19}$$

Hence, from estimate (4.6), the well separation condition (4.18), Definition 4.1, and condition (4.19) the assertion follows immediately

$$\begin{aligned}
|(\mathcal{I}-\mathcal{J}_p^2)V(t-\tau)| &\leq \sum_{\|\alpha\|_\infty=1} \frac{\|D_t^{\alpha_1(p+1)} D_\tau^{\alpha_2(p+1)} V(t-\tau)\|_\infty}{(\alpha(p+1))!} \left(\frac{h_t^{\ell_t}}{2}\right)^{|\alpha|(p+1)} \\
&\leq \sum_{\|\alpha\|_\infty=1} \frac{C(|\alpha|\,(p+1))^{\frac{1}{2}}}{\left|(d_{mn}^{\ell_t}-2)h_t^{\ell_t}\right|^{|\alpha|(p+1)+\frac{1}{2}}} \left(\frac{h_t^{\ell_t}}{2}\right)^{|\alpha|(p+1)} \\
&\leq C\left((d_{mn}^{\ell_t}-2)h_t^{\ell_t}\right)^{-\frac{1}{2}} \sum_{\|\alpha\|_\infty=1} \frac{(|\alpha|\,(p+1))^{\frac{1}{2}}}{2^{|\alpha|(p+1)}} \left(\frac{1}{d_{mn}^{\ell_t}-2}\right)^{|\alpha|(p+1)} \\
&\leq C\left((d_{mn}^{\ell_t}-2)h_t^{\ell_t}\right)^{-\frac{1}{2}} \left(\frac{1}{d_{mn}^{\ell_t}-2}\right)^{p+1}\,.
\end{aligned}$$

□

4.3.2 Temporal Multi-Level Structure

We establish a temporal multilevel structure similar to a classic one-dimensional multilevel FMM. However, we additionally incorporate the causality of the Volterra type integral operator in time by only regarding clusters from the past within the neighbor and interaction lists.

Definition 4.4. *From Definition 4.1, Lemma 4.1, and causality of the kernel it follows that each cluster has the following neighbor list*

$$\mathfrak{N}(I_m^{\ell_t}) = \begin{cases} \{m\} & m=0 \\ \{m-1,m\} & m>0 \end{cases},$$

which are all clusters of the same level sharing at least one point. The interaction list

$$\mathfrak{I}(I_m^{\ell_t}) = \bigcup_{k\in\mathfrak{N}\left(I_{\lfloor m/2\rfloor}^{\ell_t-1}\right)} \bigcup_{n\in\left\{\mathfrak{C}\left(I_k^{\ell_t-1}\right):\, I_n^{\ell_t}\cap I_m^{\ell_t}=\emptyset\right\}} I_n^{\ell_t} \tag{4.20}$$

contains all parent's neighbors children that are not neighbors of the cluster itself.

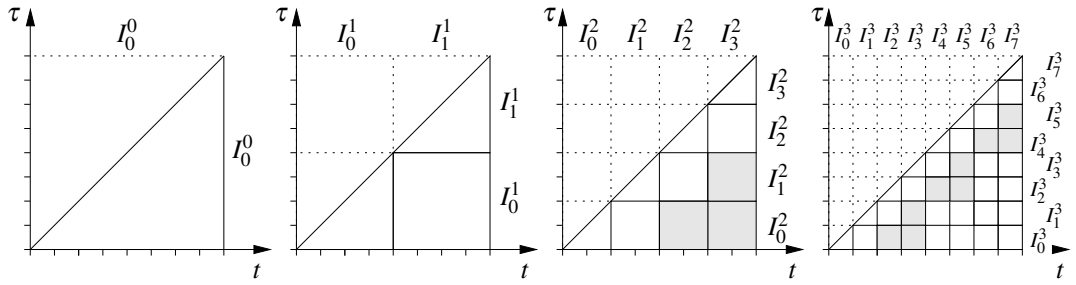

Figure 4.6: Illustration of $\mathfrak{I}(I_m^{\ell_t})$ in gray.

4.3.3 The Causal FMM

Algorithm We use the interaction lists (4.20) to split the discrete bilinear form (4.17) into a near- and farfield. Assuming that $i \in \mathfrak{P}(I_m^{L_t})$ and $m \geq 2$ we may rewrite (4.17)

$$\sum_{j \in \{\mathfrak{P}(I_m^{L_t}) \cup \mathfrak{P}(I_{m-1}^{L_t}) | j \leq i\}} \langle \mathcal{V}\phi_j, \phi_i \rangle q_j^* + \sum_{2 \leq \ell_t \leq L_t} \sum_{I_n^{\ell_t} \in \mathfrak{I}(I_{m^{\ell_t}}^{\ell_t})} \sum_{j \in \mathfrak{P}(I_n^{\ell_t})} \langle \mathcal{V}\phi_j, \phi_i \rangle q_j^* = \langle f, \phi_i \rangle$$

$$\forall i = 0, \ldots N_t - 1 \,, \quad (4.21)$$

where the level ℓ_t parent of $I_m^{L_t}$ has the index $m^{\ell_t} = \left\lfloor m/2^{L_t - \ell_t} \right\rfloor$. The first term on the left hand side of (4.21) is the temporal nearfield containing the singularity, whose contributions are computed directly (cf. Appendix B.1). The second term on the other hand is the farfield or smooth part of the layer potential, where the kernel is replaced by a Lagrange interpolation as described in Section 4.2.1. Thus the approximate farfield contribution of a cluster $I_n^{\ell_t}$ to the i^{th} time step is given by

$$\sum_{j \in \mathfrak{P}(I_n^{\ell_t})} \langle \mathcal{V}\phi_j, \phi_i \rangle q_j^* \approx \sum_{a=0}^{p} \left(\int_{t=ih_t}^{(i+1)h_t} L_a \left(\Phi_{I_{m^{\ell_t}}^{\ell_t}}^{-1}(t) \right) \phi_i(t) \mathrm{d}t \right) \lambda_a^{\ell_t}(I_{m^{\ell_t}}^{\ell_t}) \quad (4.22)$$

with the local expansions

$$\lambda_a^{\ell_t}(I_{m^{\ell_t}}^{\ell_t}) = \sum_{b=0}^{p} V \left(\Phi_{I_m^{\ell_t}}(\omega_a^p) - \Phi_{I_n^{\ell_t}}(\omega_b^p) \right) \mu_b^{\ell_t}(I_n^{\ell_t}) \quad (4.23)$$

and moment expansions

$$\mu_b^{\ell_t}(I_n^{\ell_t}) = \sum_{j \in \mathfrak{P}(I_n^{\ell_t})} \left(\int_{\tau=jh_t}^{(j+1)h_t} L_b \left(\Phi_{I_n^{\ell_t}}^{-1}(\tau) \right) \phi_j(\tau) \mathrm{d}\tau \right) q_j^* \,. \quad (4.24)$$

We call (4.24) Q2M (source to moment), (4.23) M2L (moment to local) and (4.22) L2P (local to potential) translations. If we collect the contributions of all $I_m^{L_t}$'s parents $\{I_{m^{\ell_t}}^{\ell_t}\}_{\ell_t=2}^{L_t}$ interaction lists according to (4.21), we end up with the cFMM approximated farfield. However, the straight forward way of doing that can be improved in two ways.

First, we neither want to compute moments from scratch in all levels nor convert local expansions to potential contributions in all levels. The following interpolation relation between Lagrange polynomials in the parent and child level

$$L_b(\hat{\tau}^{\ell_t}) = L_b\left(\frac{1}{2}\hat{\tau}^{\ell_t+1} \pm \frac{1}{2}\right) = \sum_{a=0}^{p} \mathfrak{q}_{a,b}^{\pm} L_a(\hat{\tau}^{\ell_t+1}) \quad \text{with} \quad \mathfrak{q}_{a,b}^{\pm} = L_b\left(\frac{1}{2}\omega_a^p \pm \frac{1}{2}\right)$$

helps us to avoid this by prolonging finer level moment expansions to coarser levels. This procedure is called upward path and involves M2M (moment to moment) translations

$$\mu_b^{\ell_t}(I_n^{\ell_t}) = \sum_{j \in \mathfrak{C}(I_n^{\ell_t})} \sum_{a=0}^{p} \mathfrak{q}_{a,b}^{\pm} \mu_a^{\ell_t+1}(I_j^{\ell_t+1}) \,. \tag{4.25}$$

In the very same manner, coarser level local expansions can be restricted to finer levels, which is called downward path and involves L2L (local to local) translations

$$\lambda_a^{\ell_t+1}(I_i^{\ell_t+1}) = \sum_{b=0}^{p} \mathfrak{q}_{a,b}^{\pm} \lambda_b^{\ell_t}(I_m^{\ell_t}) \qquad \forall i \in \mathfrak{C}(I_m^{\ell_t}) \,. \tag{4.26}$$

Note that M2M and L2L are the transposed operators of one another, where the directions $(\pm)$ are resolved by the child lists.

Second, the interaction list (4.20) incorporates causality, however, it does not enable forward substitution/elimination of the Töplitz system, yet. In a classical FMM, we would compute all leaf level moment expansions, perform the upward sweep, evaluate all interactions, perform the downward sweep and add the potential contributions of all leaf level local expansions to the directly evaluated nearfield. For a forward elimination, however, we need to be able to compute the whole time history as time progresses. Therefore, we modify the order in which moments are computed, interactions are evaluated and contributions to the potential are calculated to the exact chronological order in which they appear in a forward elimination process (cf. Algorithm 1): In each time step we evaluate moments, interactions and local expansions up to the last level $\ell_t^\diamond$, where the parent $I_{m^{\ell_t}}^{\ell_t}$ of the current leaf level cluster $I_m^{L_t}$ does not change any more. This is sufficient, because everything higher up in the hierarchy does not change and is available from previous steps. The evaluation of the whole ancestry involves the evaluation of one interaction list per level. Since this list is bounded by two, we only need to keep track of two moment expansion vectors in each level at a time. In an attempt to symmetrize the algorithm, we store two local expansions in each level, even though one would be sufficient.

Algorithm 1: The causal fast multipole method

```
for m = 0 to 2^{L_t} do
    %% find ℓ_t^◇, i.e., coarsest level where parents change
    m̄ = m − 1
    for ℓ_t = 2 to L_t − 1 do
        if I^{ℓ_t}_{m ℓ_t} = I^{ℓ_t}_{m̄ ℓ_t} then ℓ_t^◇ = ℓ_t + 1
    end for

    %% compute moments
    m(I^{L_t}_{m−2}) = q2m q*(I^{L_t}_{m−2})

    %% upward path
    for ℓ_t = L_t − 1 to ℓ_t^◇ do
        for j ∈ 𝔠(I^{ℓ_t}_{m ℓ_t − 2}) do
            m(I^{ℓ_t}_{m ℓ_t − 2}) = m(I^{ℓ_t}_{m ℓ_t − 2}) + m2m^± m(I^{ℓ_t+1}_j)
        end for
    end for

    %% interaction phase
    for ℓ_t = L_t to ℓ_t^◇ do
        for n ∈ 𝔍(I^{ℓ_t}_{m ℓ_t}) do
            l(I^{ℓ_t}_{m ℓ_t}) = l(I^{ℓ_t}_{m ℓ_t}) + m2l(d^{ℓ_t}_{m ℓ_t n}) m(I^{ℓ_t}_n)
        end for
    end for

    %% downward path
    for ℓ_t = ℓ_t^◇ to L_t − 1 do
        for i ∈ 𝔠(I^{ℓ_t}_{m ℓ_t}) do
            l(I^{ℓ_t+1}_i) = l(I^{ℓ_t+1}_i) + l2l^± l(I^{ℓ_t}_{m ℓ_t})
        end for
    end for

    %% evaluate potential
    f^{FF}(I^{L_t}_m) = l2p l(I^{L_t}_m)

    %% add nearfield
    f(I^{L_t}_m) = f^{FF}(I^{L_t}_m) + f^{NF}(I^{L_t}_m)
end for
```

Consistency Lemma 4.1 bounds the interpolation error for the above described multilevel structure independently of the temporal level ℓ_t. In what follows we use it to derive a consistency estimate that tells us how to choose the appropriate interpolation order p in order to maintain the convergence rate of the Galerkin scheme [22, 38].

Lemma 4.2. *Let us assume the Galerkin bilinear form $\langle \mathcal{V} q_h^*, v_h \rangle$ as given in* (4.17) *and the approximated bilinear form $\langle \breve{\mathcal{V}} q_h^*, v_h \rangle$, where we replace the kernel of* (4.17) *by a bivariate Lagrange interpolation as described in Lemma 4.1 and evaluated interactions according to Definition 4.4 (cf. Algorithm 1). If we choose the interpolation order to be $p = \mathcal{O}(\log N_t)$ we can guarantee an approximation error of order σ_t*

$$|\langle (\mathcal{V} - \breve{\mathcal{V}}) q_h^*, v_h \rangle_\Upsilon| \leq C h_t^{\sigma_t} \|q_h^*\|_{L_2(\Upsilon)} \|v_h\|_{L_2(\Upsilon)} \qquad \forall q_h^*, v_h \in T_{h_t}^{d_0}(\Upsilon) \, .$$

Proof. Observe that Lemma 4.1 guarantees asymptotic convergence of the multilevel kernel interpolation for the worst cluster interaction described in Definition 4.4. Thus we can use the Cauchy-Schwarz inequality and $(d_{mn}^{\ell_t} - 2) h_t^{\ell_t} > h_t$ due to Definition 4.1 to estimate

$$\begin{aligned}
|\langle (\mathcal{V} - \breve{\mathcal{V}}) q_h^*, v_h \rangle_\Upsilon| &\leq \int_{t=0}^{T} \int_{\tau=0}^{t} \left| (\mathcal{I} - \mathcal{J}_p^2) V(t-\tau) q_h^*(\tau) v_h(t) \right| \mathrm{d}\tau \mathrm{d}t \\
&\leq C \left((d_{mn}^{\ell_t} - 2) h_t^{\ell_t} \right)^{-\frac{1}{2}} \left(\frac{1}{d_{mn}^{\ell_t} - 2} \right)^{p+1} \int_{t=0}^{T} \int_{\tau=0}^{T} |q_h^*(\tau) v_h(t)| \, \mathrm{d}\tau \mathrm{d}t \\
&\leq C h_t^{-\frac{1}{2}} \left(\frac{1}{d_{mn}^{\ell_t} - 2} \right)^{p+1} T \|q_h^*\|_{L_2} \|v_h\|_{L_2} \, ,
\end{aligned}$$

which trivialy holds for the nearfield as well. Finally, claiming $(d_{mn}^{\ell_t} - 2)^{-(p+1)} = \mathcal{O}(h_t^{\sigma_t + \frac{1}{2}})$ we get

$$p = \mathcal{O}\left(\left(\sigma_t + \frac{1}{2} \right) \frac{\log(\frac{1}{h_t})}{\log(d_{mn}^{\ell_t} - 2)} \right) = \mathcal{O}(\log N_t) \, .$$

□

In order to understand how the cFMM algorithm affects the approximation of the discrete bilinear form (4.17), i.e.,

$$\langle \breve{\mathcal{V}} \breve{q}_h^*, v_h \rangle_\Upsilon = \langle f, v_h \rangle_\Upsilon \qquad \forall v_h \in T_{h_t}^{d_0}(\Upsilon) \tag{4.27}$$

we provide the following lemma, which for practical reasons bounds the approximation error in the L_2 norm.

Lemma 4.3. *Let $q^*(\tau) = q^*(\mathbf{y},\tau) \in H^{2,1}_{pw}(\Gamma_S \times \Upsilon)$ be the unique solution of* (4.16) *and $q^*_h \in T^{d_0}_{h_t}(\Upsilon)$ the unique solution of* (4.17) *(cf. Remark 4.3). Further, assume that $\breve{\mathcal{V}}$ is $H^{-\frac{1}{2},-\frac{1}{4}}(\Gamma_S \times \Upsilon)$ elliptic, then the approximate solution $\breve{q}^*_h \in T^{d_0}_{h_t}(\Upsilon)$ of* (4.27) *satisfies*

$$\|q^* - \breve{q}^*_h\|_{L_2(\Gamma_S\times\Upsilon)} \leq Ch_t(\|q^*\|_{H^{2,1}_{pw}(\Gamma_S\times\Upsilon)} + \|q^*\|_{L_2(\Gamma_S\times\Upsilon)}) .$$

Proof. We follow the same strategy as in [38] and apply the triangle inequality together with the inverse inequality (recall that we restricted ourselves to equidistant time discretizations)

$$\begin{aligned}\|q^* - \breve{q}^*_h\|_{L_2(\Gamma_S\times\Upsilon)} &\leq \|q^* - q^*_h\|_{L_2(\Gamma_S\times\Upsilon)} + \|q^*_h - \breve{q}^*_h\|_{L_2(\Gamma_S\times\Upsilon)} \\ &\leq \|q^* - q^*_h\|_{L_2(\Gamma_S\times\Upsilon)} + Ch_t^{-\frac{1}{4}}\|q^*_h - \breve{q}^*_h\|_{H^{-\frac{1}{2},-\frac{1}{4}}(\Gamma_S\times\Upsilon)} .\end{aligned}$$

With the $H^{-\frac{1}{2},-\frac{1}{4}}(\Gamma_S \times \Upsilon)$ ellipticity of $\breve{\mathcal{V}}$ we have due to Galerkin orthogonality

$$\|q^*_h - \breve{q}^*_h\|_{H^{-\frac{1}{2},-\frac{1}{4}}(\Gamma_S\times\Upsilon)} \leq C\|(\mathcal{V} - \breve{\mathcal{V}})q^*_h\|_{H^{\frac{1}{2},\frac{1}{4}}(\Gamma_S\times\Upsilon)}$$

and by duality

$$\|(\mathcal{V} - \breve{\mathcal{V}})q^*_h\|_{H^{\frac{1}{2},\frac{1}{4}}(\Gamma_S\times\Upsilon)} \leq \sup_{0\neq v_h \in T^{d_0}_{h_t}} \frac{\langle (\mathcal{V} - \breve{\mathcal{V}})q^*_h, v_h\rangle_{\Gamma_S\times\Upsilon}}{\|v_h\|_{H^{-\frac{1}{2},-\frac{1}{4}}(\Gamma_S\times\Upsilon)}} .$$

Thus with Lemma 4.2, which also holds if the duality pairing is extended from Υ to $\Gamma_S \times \Upsilon$, the inverse inequality, and the stability of the L_2 projection $\mathcal{Q}^{d_0}_{h_t} : L_2(\Upsilon) \to T^{d_0}_{h_t}(\Upsilon)$ we estimate

$$\begin{aligned}\frac{\langle (\mathcal{V} - \breve{\mathcal{V}})q^*_h, v_h\rangle_{\Gamma_S\times\Upsilon}}{\|v_h\|_{H^{-\frac{1}{2},-\frac{1}{4}}(\Gamma_S\times\Upsilon)}} &\leq Ch_t^{\sigma_t-\frac{1}{4}}\|q^*_h\|_{L_2(\Gamma_S\times\Upsilon)} \\ &\leq Ch_t^{\sigma_t-\frac{1}{4}}\left(\|q^*_h - \mathcal{Q}^{d_0}_{h_t}q^*\|_{L_2(\Gamma_S\times\Upsilon)} + \|\mathcal{Q}^{d_0}_{h_t}q^*\|_{L_2(\Gamma_S\times\Upsilon)}\right) \\ &\leq Ch_t^{\sigma_t-\frac{1}{4}}\left(\hat{C}h_t^{-\frac{1}{4}}\|q^*_h - \mathcal{Q}^{d_0}_{h_t}q^*\|_{H^{-\frac{1}{2},-\frac{1}{4}}(\Gamma_S\times\Upsilon)} + \tilde{C}\|q^*\|_{L_2(\Gamma_S\times\Upsilon)}\right)\end{aligned}$$

and by another application of the triangle inequality and the standard error estimate for the L_2 projection we get

$$\begin{aligned}\|q^*_h - \breve{q}^*_h\|_{H^{-\frac{1}{2},-\frac{1}{4}}(\Gamma_S\times\Upsilon)} &\leq Ch_t^{\sigma_t-\frac{1}{4}}\Bigg(\hat{C}h_t^{-\frac{1}{4}}\Big(\|q^*_h - q^*\|_{H^{-\frac{1}{2},-\frac{1}{4}}(\Gamma_S\times\Upsilon)} \\ &\qquad + \|q^* - \mathcal{Q}^{d_0}_{h_t}q^*\|_{H^{-\frac{1}{2},-\frac{1}{4}}(\Gamma_S\times\Upsilon)}\Big) + \tilde{C}\|q^*\|_{L_2(\Gamma_S\times\Upsilon)}\Bigg) \\ &\leq Ch_t^{\sigma_t-\frac{1}{4}}\left(\hat{C}h_t^{-\frac{1}{4}}\|q^*_h - q^*\|_{H^{-\frac{1}{2},-\frac{1}{4}}(\Gamma_S\times\Upsilon)} + \tilde{C}\|q^*\|_{L_2(\Gamma_S\times\Upsilon)}\right) .\end{aligned}$$

Hence, with Remark 4.3 we conclude that $\sigma_t = 5/4$ is sufficient to maintain the convergence rate of the Galerkin scheme

$$\|q_h^* - \breve{q}_h^*\|_{L_2(\Gamma_S \times \Upsilon)} \leq C h_t \left(\|q^*\|_{H^{2,1}_{pw}(\Gamma_S \times \Upsilon)} + \|q^*\|_{L_2(\Gamma_S \times \Upsilon)} \right) .$$

□

Complexity Due to the equidistant time discretization we have $\dim\left(\mathfrak{P}(I_n^{L_t})\right) = n_t = N_t/2^{L_t}$ time steps in each leaf level cluster. The total number of $2^{L_t+1} - 1$ clusters is $\mathcal{O}(N_t)$ thus the number of arithmetic operations of the presented algorithm comes down to $\mathcal{O}(p^2 N_t)$ and is composed by

- 2^{L_t} Q2M/L2P's at $\mathcal{O}(pn_t)$ each, which results in $\mathcal{O}(pN_t)$ work for the computation of all leaf level moment/local expansions.
- $\mathcal{O}(N_t)$ M2M/L2L's of $\mathcal{O}(p^2)$, resulting in a total cost of $\mathcal{O}(p^2 N_t)$ for all M2M/L2L's.
- $\mathcal{O}(p^2 N_t)$ work for all M2L's, since the number of interactions per cluster is bounded by two and the cost of one M2L is $\mathcal{O}(p^2)$.
- $\mathcal{O}(1)$ work for the nearfield.

Since we only changed the order in which expansions are evaluated, the arithmetic work remains the same as in a classical FMM. However, the amount of memory requirement changes drastically, it amounts in $\mathcal{O}(p^2 \log_2 N_t)$ composed by

- $\mathcal{O}(p^2 \log_2 N_t)$ moment/local expansions, since we only need to keep track of two clusters in each level.
- $\mathcal{O}(1)$ for the expansion coefficients of all Q2M/L2P's and M2M/L2L's, due to the uniform time discretization.
- $\mathcal{O}(p^2 \log_2 N_t)$ coefficients for all M2L's, since the number of M2L's in each level is bounded by two.
- $\mathcal{O}(1)$ memory for the nearfield.

We use matrix notation to describe the algorithm below. Due to the uniform time discretization we only need the following matrices:

- one $\mathbf{q2m} = (\mathbf{l2p})^\top \in \mathbb{R}^{(p+1)\times n_t}$ matrix – (4.24) and (4.22)
- one $\mathbf{m2m}^+ = (\mathbf{l2l}^+)^\top \in \mathbb{R}^{(p+1)\times(p+1)}$ matrix – (4.25) and (4.26)
- one $\mathbf{m2m}^- = (\mathbf{l2l}^-)^\top \in \mathbb{R}^{(p+1)\times(p+1)}$ matrix – (4.25) and (4.26)
- two $\mathbf{m2l}(d^{\ell_t}_{m_t^\ell n}) \in \mathbb{R}^{(p+1)\times(p+1)}$ matrices in each level – (4.23)

Example 4.1. *With this example we want to verify the temporal interpolation error estimate of Lemma 4.1. In order to confirm this pointwise estimate, we choose an arbitrary time interval, e.g.,* $\Upsilon = (0,16)$*, which we discretize by eight time steps of size* $h_t = 2$*. Then we construct a time cluster-tree according to Definition 4.1 with* $n_t = 1$ *time steps per leaf cluster. Thus we end up with a temporal cluster-tree defined by* $L_t = 3$ *and* $h_t^{L_t} = 1$ *with eight temporal leaf level clusters* $\{I_0^{L_t}, I_1^{L_t}, I_2^{L_t} \dots I_7^{L_t}\}$*. Next we set* $t_7 := 14$ *to be the leftmost point of* $I_7^{L_t}$ *and we find that* $I_i^{L_t}$ *for* $i \leq 5$ *are admissible clusters. We choose* $\tau_i = \{8,10,12\}$ *to be the rightmost point of the clusters* $I_3^{L_t}, I_4^{L_t}, I_5^{L_t}$ *(corresponding to* $d = 8,6,4$ *– for simplicity we use* d *instead of* $d_{mn}^{L_t}$*) and evaluate the estimate of Lemma 4.1 for increasing interpolation order* p*.*

	$d=4$	$d=6$	$d=8$
$p=2$	$2.24\ 10^{-2}$	$3.74\ 10^{-3}$	$1.15\ 10^{-3}$
$p=3$	$4.17\ 10^{-3}$	$4.22\ 10^{-4}$	$9.36\ 10^{-5}$
$p=4$	$7.19\ 10^{-4}$	$4.48\ 10^{-5}$	$7.19\ 10^{-6}$
$p=5$	$1.19\ 10^{-4}$	$4.62\ 10^{-6}$	$5.39\ 10^{-7}$
$p=6$	$1.93\ 10^{-5}$	$4.69\ 10^{-7}$	$3.98\ 10^{-8}$
$p=7$	$3.09\ 10^{-6}$	$4.71\ 10^{-8}$	$2.90\ 10^{-9}$
$p=8$	$4.88\ 10^{-7}$	$4.68\ 10^{-9}$	$2.10\ 10^{-10}$
$p=9$	$7.62\ 10^{-8}$	$4.62\ 10^{-10}$	$1.51\ 10^{-11}$
$p=10$	$1.17\ 10^{-8}$	$4.53\ 10^{-11}$	$1.08\ 10^{-12}$

Table 4.1: Interpolation error for $p \backslash d$.

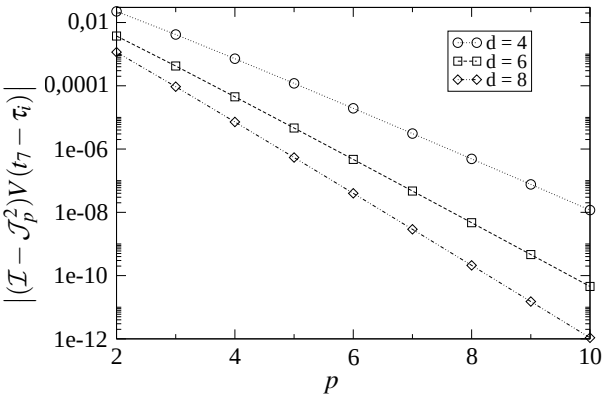

Figure 4.7: Interpolation error vs. order.

In Table 4.1 and Figure 4.7 we present the results, which clearly show the exponential convergence of the interpolation error. Furthermore, we observe that for a larger d *we get faster convergence, which is in perfect agreement with Lemma 4.1.*

Example 4.2. *In agreement with the assumptions at the beginning of this section we set the density* $q^*(\tau) = exp(\tau)$ *to be constant in space and compute the single layer potential on a unit-sphere according to* (4.15)

$$f(t) := \mathcal{V}q^*(t) = \int_0^t V(t-\tau)exp(\tau)\,d\tau = \frac{exp(t)}{4}\left(exp(2)\,erfc\left(\frac{1+t}{\sqrt{t}}\right)\right.$$
$$\left. + 2erf\left(\sqrt{t}\right) - exp(-2)\,erfc\left(\frac{1-t}{\sqrt{t}}\right)\right).$$

In a next step we revert the problem , i.e., we assume $f(t)$ *to be given and solve for the density* $q^*(\tau)$*. However, this cannot be done directly, therefore we solve the discrete problem* (4.17) *for the approximate density* $q_h^*(\tau) \in T_{h_t}^{d_0}(\Upsilon)$ *with* $\Upsilon = (0,T)$ *and* $T = 1$*. For a uniform refinement in time we expect to observe linear order of convergence in the* L_2 *norm (cf. Remark 4.3). Furthermore, in order to verify the consistency of the cFMM approximation* (4.27) *provided by Lemma 4.3, we introduce a temporal cluster tree with* $n_t = 1$*,*

$L_t = 7$, and $h_t^{L_t} = 1/256$ in the coarsest refinement level. We perform a number of uniform temporal refinements where we solve for the cFMM approximated solution $\breve{q}_h^*(\tau) \in T_{h_t}^{d_0}(\Upsilon)$.

	direct		*cFMM*		
	$\|q^* - q_h^*\|_{L_2(\Upsilon)}$	*time* [sec]	p	$\|q^* - \breve{q}_h^*\|_{L_2(\Upsilon)}$	*time* [sec]
$N_t = 128$	$6.21\ 10^{-5}$	$5.03\ 10^{-5}$	*5*	$6.21\ 10^{-5}$	$8.87\ 10^{-4}$
$N_t = 256$	$2.19\ 10^{-5}$	$1.94\ 10^{-4}$	*5*	$2.19\ 10^{-5}$	$1.82\ 10^{-3}$
$N_t = 512$	$7.76\ 10^{-6}$	$5.05\ 10^{-4}$	*6*	$7.76\ 10^{-6}$	$1.77\ 10^{-3}$
$N_t = 1024$	$2.74\ 10^{-6}$	$3.03\ 10^{-3}$	*6*	$2.74\ 10^{-6}$	$3.49\ 10^{-3}$
$N_t = 2048$	$9.69\ 10^{-7}$	$4.92\ 10^{-3}$	*7*	$9.69\ 10^{-7}$	$8.20\ 10^{-3}$
$N_t = 4096$	$3.43\ 10^{-7}$	$1.98\ 10^{-2}$	*7*	$3.43\ 10^{-7}$	$1.68\ 10^{-2}$
$N_t = 8192$	$1.21\ 10^{-7}$	$7.90\ 10^{-2}$	*8*	$1.21\ 10^{-7}$	$3.79\ 10^{-2}$
$N_t = 16384$	$4.28\ 10^{-8}$	$3.17\ 10^{-1}$	*8*	$4.28\ 10^{-8}$	$7.62\ 10^{-2}$
$N_t = 32768$	$1.51\ 10^{-8}$	$1.27\ 10^{0}$	*9*	$1.51\ 10^{-8}$	$1.84\ 10^{-1}$
$N_t = 65536$	$5.36\ 10^{-9}$	$5.08\ 10^{0}$	*9*	$5.36\ 10^{-9}$	$3.68\ 10^{-1}$

Table 4.2: Direct vs. cFMM solution time for the same $L_2(\Upsilon)$ error.

In Table 4.2 we observe that the direct method reproduces the expected convergence rate in the L_2 norm (cf. Remark 4.3) of the initial Dirichlet boundary value problem (4.17)*. Moreover, Lemma 4.3 guarantees that the cFMM approximation of the integral operator maintains the approximation error of the direct method, which is confirmed by the results in Table 4.2, where in each refinement level we have chosen the lowest possible interpolation order p maintaining the error of the direct method. Finally, Table 4.2 reveals the $\mathcal{O}(N_t^2)$ complexity of the standard method* (4.17) *versus the $\mathcal{O}(p^2 N_t)$ complexity of the consistent cFMM approximation* (4.27)*.*

4.4 Thermal Layer Potential at a Fixed Time

In an attempt to isolate the spatial aspect of the pFMM algorithm we assume the thermal single layer potential for a fixed variance $\delta := (t - \tau) > 0$ (with $\alpha \equiv 1$, as mentioned at the beginning of this chapter) and end up with a Gauss transform

$$\mathcal{V}q^*(\mathbf{x}) = \int_\Gamma G(\mathbf{x}-\mathbf{y},\delta)q^*(\mathbf{y})\mathrm{d}s_\mathbf{y} = \frac{1}{(4\pi\delta)^{\frac{3}{2}}}\int_\Gamma \exp\left(-\frac{|\mathbf{x}-\mathbf{y}|^2}{4\delta}\right) q^*(\mathbf{y})\mathrm{d}s_\mathbf{y} = f(\mathbf{x})\,. \quad (4.28)$$

This problem is not only interesting from an explanatory point of view but also from a practical one – as a matter of fact we will encounter it again, when dealing with the efficient nearfield evaluation of thermal layer potentials in Section 4.6. Again we are not

interested in applying the continuous operator (4.28) but its Galerkin discretized bilinear form according to Section 3.1.1

$$\langle \mathcal{V} q_h^*, v_h \rangle_\Gamma = \langle f, v_h \rangle_\Gamma \qquad \forall v_h \in X_{h_x}^{d_{d_x}}(\Gamma) \,, \tag{4.29}$$

which is equivalent to the application of the dense matrix vector product

$$\mathsf{V}\,\mathsf{q}^* = \mathsf{f} \,,$$

with $\mathsf{V}_{k\ell} := \langle \mathcal{V}\varphi_\ell, \varphi_k \rangle$ and $\mathsf{f}_k := \langle f, \varphi_k \rangle$. Throughout this section, we devote ourselves to reduce this otherwise $\mathcal{O}(N_x^2)$ task to almost $\mathcal{O}(N_x)$ by means of the fast Gauss transform [21] with most of the reported details taken from [49, 50].

4.4.1 Truncated Chebyshev Expansion

Based on the hierarchical clustering of Γ described in Section 4.1.2 we interpolate the heat kernel with $\mathbf{x} \in X_u^{\ell_x}$ and $\mathbf{y} \in X_v^{\ell_x}$. Therefore, we introduce local variables $\hat{\mathbf{x}}, \hat{\mathbf{y}} \in [-1,1]^3$

$$\mathbf{x} = \Phi_{X_u^{\ell_x}}(\hat{\mathbf{x}}) = \mathbf{c}_{X_u^{\ell_x}} + \hat{\mathbf{x}} h_x^{\ell_x} \quad \text{and} \quad \mathbf{y} = \Phi_{X_v^{\ell_x}}(\hat{\mathbf{y}}) = \mathbf{c}_{X_v^{\ell_x}} + \hat{\mathbf{y}} h_x^{\ell_x} \,.$$

Hence, we may write the heat kernel in local coordinates

$$G(\mathbf{x}-\mathbf{y},\delta) = G\left(\Phi_{X_u^{\ell_x}}(\hat{\mathbf{x}}) - \Phi_{X_v^{\ell_x}}(\hat{\mathbf{y}}), \delta\right) = G\left(h_x^{\ell_x}(\mathbf{d}_{uv}^{\ell_x} + \hat{\mathbf{x}} - \hat{\mathbf{y}}), \delta\right)$$

with $\mathbf{d}_{uv}^{\ell_x} = (\mathbf{c}_{X_u^{\ell_x}} - \mathbf{c}_{X_v^{\ell_x}})/h_x^{\ell_x}$. Recall that the heat kernel naturally separates into a tensor product of three one-dimensional heat kernels (4.1). Hence, we start by investigating the Chebyshev expansion of the one-dimensional heat kernel with $\mathbf{x} \in X_u^{\ell_x}$ and $\mathbf{y} \in X_v^{\ell_x}$

$$\mathcal{S}_\infty^2 G(x_i - y_i, \delta) = \sum_{k,\ell=0}^{\infty} G_{k,\ell}(\delta)\, T_k\left(\Phi_{X_u^{\ell_x}}^{-1}(x_i)\right) T_\ell\left(\Phi_{X_v^{\ell_x}}^{-1}(y_i)\right) \,, \tag{4.30}$$

where $\mathcal{S}_\infty^2 = \mathcal{S}_{\infty,x} \circ \mathcal{S}_{\infty,y} \equiv \mathcal{S}_{\infty,y} \circ \mathcal{S}_{\infty,x}$ with the coefficients

$$G_{k,\ell}(\delta) = \frac{\gamma_k \gamma_\ell}{\pi^2} \int_{-1}^{1}\int_{-1}^{1} G\left(\Phi_{X_u^{\ell_x}}(\hat{x}) - \Phi_{X_v^{\ell_x}}(\hat{y}), \delta\right) T_k(\hat{x}) T_\ell(\hat{y}) w(\hat{x}) w(\hat{y}) \mathrm{d}\hat{x}\mathrm{d}\hat{y} \,. \tag{4.31}$$

Lemma 4.4. *Assume we truncate the Chebyshev expansion* (4.30) *of the one-dimensional heat kernel with fixed variance* $\delta > 0$ *after* $n := k + \ell > q$ *terms*

$$\mathcal{S}_q^2 G(x_i - y_i, \delta) = \sum_{n=0}^{q} \sum_{k+\ell=n} G_{k,\ell}(\delta)\, T_k\left(\Phi_{X_u^{\ell_x}}^{-1}(x_i)\right) T_\ell\left(\Phi_{X_v^{\ell_x}}^{-1}(y_i)\right) \,,$$

with $\mathbf{x} \in X_u^{\ell_x}$ *and* $\mathbf{y} \in X_v^{\ell_x}$ *in any two clusters* $X_u^{\ell_x}$ *and* $X_v^{\ell_x}$*, where* $h_x^{\ell_x} = \mathcal{O}(\sqrt{\delta})$*. Then we can bound the error by*

$$\left|(\mathcal{I} - \mathcal{S}_q^2)G(x_i - y_i, \delta)\right| \leq C\frac{(q+2)}{\sqrt{\delta}}\left(\frac{1}{a-1}\right)^{q+1},$$

with an arbitrary but fixed $a > 1$*.*

Proof. Since the Chebyshev polynomials are bounded by one, the truncation error of the expansion only depends on the magnitude of the coefficients $G_{k,\ell}(\delta)$. For $a > 1$ and $n = k + \ell$ the following estimate [49, Lemma 1] holds

$$\left|G_{k,\ell}(\delta)\right| \leq \frac{2}{\sqrt{\pi\delta}}\frac{1}{a^n}\exp\left(\frac{(2h_x^{\ell_x})^2}{\delta}\left(a - \frac{1}{a}\right)^2\right),$$

which allows us to estimate

$$\begin{aligned}\left|(\mathcal{I} - \mathcal{S}_q^2)G(x_i - y_i, \delta)\right| &\leq \sum_{n=q+1}^{\infty}\sum_{n=k+\ell}\left|G_{k,\ell}(\delta)\right| \\ &\leq \frac{2}{\sqrt{\pi\delta}}\exp\left(\frac{(2h_x^{\ell_x})^2}{\delta}\left(a - \frac{1}{a}\right)^2\right)\sum_{n=q+1}^{\infty}(n+1)\frac{1}{a^n}.\end{aligned}$$

Estimating the remainder of a geometric series's derivative we further estimate

$$\left|(\mathcal{I} - \mathcal{S}_q^2)G(x_i - y_i, \delta)\right| \leq \frac{2(q+2)}{\sqrt{\pi\delta}}\exp\left(\frac{(2h_x^{\ell_x})^2}{\delta}\left(a - \frac{1}{a}\right)^2\right)\left(\frac{1}{a-1}\right)^{q+1}$$

and, since $a > 1$ is arbitrary but fixed we conclude

$$\left|(\mathcal{I} - \mathcal{S}_q^2)G(x_i - y_i, \delta)\right| \leq C\frac{(q+2)}{\sqrt{\delta}}\left(\frac{1}{a-1}\right)^{q+1}.$$

□

According to Lemma 4.4 we can bound the truncation error for any $\delta > 0$ independently of the spatial variables. We observe that by increasing a one can make the super-exponential decay arbitrarily fast, however, we would like to remark that this comes at the cost of a larger constant C. Further, we note that the estimate only depends on the sum of the indexes rather than their individual value. Thus we only have to retain coefficients from a triangular index set

$$\mathfrak{S}(\mathcal{S}_q^2) = \{k, \ell : 0 \leq k + \ell \leq q\}$$

with about half as many coefficients as we would have in the rectangular index set

$$\mathfrak{S}(\mathcal{J}_q^2) = \{k,\ell : 0 \le k,\ell \le q\}$$

if we had used a tensorial version of the interpolation scheme (4.3). This constant becomes more significant in higher dimensions. Due to the tensor product structure (4.1) the truncated Chebyshev expansion of the three-dimensional Gaussian is given by

$$\mathcal{S}_q^6 G(\mathbf{x}-\mathbf{y},\delta) = \sum_{n=0}^{q} \sum_{|\alpha+\beta|=n} G_{\alpha,\beta}(\delta)\, T_\alpha\left(\Phi_{X_u^{\ell_x}}^{-1}(\mathbf{x})\right) T_\beta\left(\Phi_{X_v^{\ell_x}}^{-1}(\mathbf{y})\right) \tag{4.32}$$

with coefficients

$$G_{\alpha,\beta}(\delta) = G_{\alpha_1,\beta_1}(\delta)\, G_{\alpha_2,\beta_2}(\delta)\, G_{\alpha_3,\beta_3}(\delta)\ . \tag{4.33}$$

Obviously, the cardinality of the index set $\mathfrak{S}(\mathcal{S}_q^6)$ required for the truncated Chebyshev expansion is much less than the cardinality of the index set $\mathfrak{S}(\mathcal{J}_q^6)$ required for the corresponding interpolation approximation, i.e.,

$$\#\mathfrak{S}(\mathcal{S}_q^6) = \begin{pmatrix} q+6 \\ q \end{pmatrix} \ll (q+1)^6 = \#\mathfrak{S}(\mathcal{J}_q^6)\ .$$

Corollary 4.1. *For any $\delta > 0$ and $\mathbf{x} \in X_u^{\ell_x}$ and $\mathbf{y} \in X_v^{\ell_x}$ in any two clusters $X_u^{\ell_x}$ and $X_v^{\ell_x}$ with $h_x^{\ell_x} = \mathcal{O}(\sqrt{\delta})$ we can bound the truncation error of the three-dimensional Chebyshev expansion* (4.32) *after $n := |\alpha+\beta| > q$ terms by*

$$\left|(\mathcal{I}-\mathcal{S}_q^6)G(\mathbf{x}-\mathbf{y},\delta)\right| \le C\frac{(q+1)^6}{\sqrt{\delta^3}}\left(\frac{1}{a-1}\right)^{q+1}\ ,$$

where $a > 1$ is arbitrary but fixed.

Proof. We estimate the three-dimensional Chebyshev expansion coefficients in (4.33) similar to Lemma 4.4

$$\begin{aligned}\left|(\mathcal{I}-\mathcal{S}_q^6)G(\mathbf{x}-\mathbf{y},\delta)\right| &\le \sum_{n=q+1}^{\infty} \sum_{|\alpha+\beta|=n} \left|G_{\alpha,\beta}(\delta)\right| \\ &\le \left(\frac{2}{\sqrt{\pi\delta}}\exp\left(\frac{(2h_x^{\ell_x})^2}{\delta}\left(a-\frac{1}{a}\right)^2\right)\right)^3 \sum_{n=q+1}^{\infty}\begin{pmatrix} n+5 \\ n \end{pmatrix}\frac{1}{a^n}\ .\end{aligned}$$

Estimating the remainder of a geometric series' fifth derivative, taking $h_x^{\ell_x} = \mathcal{O}(\sqrt{\delta})$ into account and an arbitrary but fixed $a > 1$ we get the assertion

$$\left|(\mathcal{I}-\mathcal{S}_q^6)G(\mathbf{x}-\mathbf{y},\delta)\right| \le C\frac{(q+1)^6}{\sqrt{\delta^3}}\left(\frac{1}{a-1}\right)^{q+1}\ .$$

□

After having estimated the truncation error for the Chebyshev expansion of the heat kernel itself, we still need to estimate the truncation error for its derivatives.

Corollary 4.2. *Let us assume $\delta > 0$ and $\mathbf{x} \in X_u^{\ell_x}$ and $\mathbf{y} \in X_v^{\ell_x}$ in any two clusters $X_u^{\ell_x}$ and $X_v^{\ell_x}$ with $h_x^{\ell_x} = \mathcal{O}(\sqrt{\delta})$, then we can bound the truncation error related to the Chebyshev expansion of the heat kernel's gradient. Each component can be estimated by*

$$|(\mathcal{I} - \mathcal{S}_q^6)\frac{\partial}{\partial x_i} G(\mathbf{x}-\mathbf{y},\delta)| \leq C\frac{(q+1)^8}{\sqrt{\delta^3}}\left(\frac{1}{a-1}\right)^{q+1}$$

with an arbitrary but fixed $a > 0$.

Proof. Recall that for $\delta > 0$ the heat kernel is analytic thus we can expand it in a Chebyshev series for any $\mathbf{x} \in X_u^{\ell_x}$ and $\mathbf{y} \in X_v^{\ell_x}$ and we have due to (4.13)

$$\begin{aligned}\mathcal{S}_q^6 \frac{\partial}{\partial x_i} G(\mathbf{x}-\mathbf{y},\delta) &= \frac{\partial}{\partial x_i}\mathcal{S}_q^6 G(\mathbf{x}-\mathbf{y},\delta) \\ &= \sum_{n=0}^{q}\sum_{|\alpha+\beta|=n} G_{\alpha,\beta}(\delta)\frac{\partial}{\partial x_i} T_\alpha\left(\Phi_{X_u^{\ell_x}}^{-1}(\mathbf{x})\right) T_\beta\left(\Phi_{X_v^{\ell_x}}^{-1}(\mathbf{y})\right).\end{aligned}$$

Observe that the gradient of the first kind Chebyshev polynomials (4.14) is not bounded by one any more. However, simple calculus shows that

$$\max_{\hat{x}\in[-1,1]} \frac{\partial}{\partial \hat{x}} T_n(\hat{x}) = nU_{n-1}(\pm 1) = n^2,$$

therefore

$$\left|\frac{\partial}{\partial x_i} T_\alpha\left(\Phi_{X_u^{\ell_x}}^{-1}(\mathbf{x})\right)\right| \leq \frac{\alpha_i^2}{\det(\mathbf{J}_\Phi(\mathbf{x}))} \leq \frac{(q+1)^2}{(h_x^{\ell_x})^3} \leq C\frac{(q+1)^2}{\sqrt{\delta^3}},$$

and the assertion follows from

$$\left|(\mathcal{I}-\mathcal{S}_q^6)\nabla_{\mathbf{x}} G(\mathbf{x}-\mathbf{y},\delta)\right| \leq \sum_{n=q+1}^{\infty}\sum_{|\alpha+\beta|=n} \left|G_{\alpha,\beta}(\delta)\right| \left|\nabla_{\mathbf{x}} T_\alpha\left(\Phi_{X_u^{\ell_x}}^{-1}(\mathbf{x})\right)\right|.$$

□

4.4.2 Spatial Single-Level Structure

Corollaries 4.1 and 4.2 give us a bound for the truncation error of the three-dimensional Chebyshev expansion independent of the spatial variable. Due to the exponential decay of the heat kernel for $|\mathbf{x}-\mathbf{y}| \to \infty$ and the space-time scaling (4.2) we can derive an admissibility criterion that allows to control the approximation error for any fixed variance $\delta > 0$ by taking an almost constant number of cluster interactions in one and only one level into consideration.

Lemma 4.5. *Let us assume $\delta > 0$, then we choose the spatial cluster level ℓ_x according to Definition 4.2 such that $h_x^{\ell_x} = \mathcal{O}(\sqrt{\delta})$. Taking only cluster interactions between two clusters $X_u^{\ell_x}$ and $X_v^{\ell_x}$ into account that are less or equal than*

$$\mathfrak{n}_x = \frac{\sqrt{\delta}}{h_x^{\ell_x}} \left[\log\left(\frac{1}{\varepsilon(4\pi\delta)^{\frac{3}{2}}} \right) \right]^{\frac{1}{2}} - 1$$

clusters apart, we can approximate the discrete Gauss transformation (4.29) *by*

$$\langle \mathcal{V}_B q_h^*, v_h \rangle_\Gamma := \int_\Gamma \int_{\{\mathbf{y}\in\Gamma : \|\mathbf{x}-\mathbf{y}\|_\infty \le 2h_x^{\ell_x}(\mathfrak{n}_x+1)\}} G(\mathbf{x}-\mathbf{y},\delta) q_h^*(\mathbf{y}) ds_{\mathbf{y}} v_h(\mathbf{x}) ds_{\mathbf{x}}$$

leading to a cutoff error

$$|\langle (\mathcal{V}-\mathcal{V}_B) q_h^*, v_h \rangle_\Gamma| \le \frac{\varepsilon}{\sqrt{\delta^3}} |\Gamma| \, \|q_h^*\|_{L_2(\Gamma)} \|v_h\|_{L_2(\Gamma)} \qquad \forall q_h^*, v_h \in X_{h_x}^{d_{d_x}}(\Gamma) \, .$$

Proof. With a separation of $\mathfrak{n}_x$ clusters in the $\|\cdot\|_\infty$ norm we estimate

$$\begin{aligned}
|\langle (\mathcal{V}-\mathcal{V}_B) q_h^*, v_h \rangle_\Gamma| &\le \int_\Gamma \int_{\{\mathbf{y}\in\Gamma : \|\mathbf{x}-\mathbf{y}\|_\infty > 2h_x^{\ell_x}(\mathfrak{n}_x+1)\}} |G(\mathbf{x}-\mathbf{y},\delta) q_h^*(\mathbf{y}) v_h(\mathbf{x})| \, \mathrm{d}s_{\mathbf{y}} \mathrm{d}s_{\mathbf{x}} \\
&\le \max_{\|\mathbf{x}-\mathbf{y}\|_\infty > 2h_x^{\ell_x}(\mathfrak{n}_x+1)} \left| G\left(\frac{\mathbf{x}-\mathbf{y}}{\sqrt{\delta}}, 1 \right) \right| \frac{1}{\sqrt{\delta^3}} \int_\Gamma |q_h^*(\mathbf{y})| \, \mathrm{d}s_{\mathbf{y}} \int_\Gamma |v_h(\mathbf{x})| \mathrm{d}s_{\mathbf{x}} \\
&\le \frac{\varepsilon}{\sqrt{\delta^3}} |\Gamma| \, \|q_h^*\|_{L_2(\Gamma)} \|v_h\|_{L_2(\Gamma)} \, .
\end{aligned}$$

□

Remark 4.4. *Observe that Lemma 4.5 is not sharp in its δ dependence, because it neglects the exponential decay of the heat kernel beyond the truncation radius, but fully accounts for the $\mathcal{O}(1/\sqrt{\delta^3})$ growth of the kernel. Nonetheless, this result is sufficient for our purpose.*

Provided a fixed variance $\delta > 0$, Lemma 4.5 helps us to choose the right spatial cluster half-side length $h_x^{L_x}$ and cutoff parameter $\mathfrak{n}_x$. It constitutes an admissibility criterion, which allows to define the FGT's interaction lists as follows.

Definition 4.5. *Choose L_x such that $2^{-L_x} h_x^0 \ge h_x^{\ell_x} \ge 2^{-(L_x+1)} h_x^0$ with $h_x^{\ell_x} = \mathcal{O}(\sqrt{\delta})$ to ensure that the estimate of Lemma 4.5 still holds. Then the interaction list for the FGT is given by*

$$\mathfrak{I}(X_u^{L_x}) = \bigcup_{X_v^{L_x} : \|\mathbf{d}_{uv}^{L_x}\|_\infty \le 2\mathfrak{n}_x} v \, . \tag{4.34}$$

4.4.3 The Fast Gauss Transform

Algorithm The structure of the fast Gauss transform is very simple. We choose the spatial level L_x according to Lemma 4.5 and the interaction list as proposed in (4.34). Assuming that $k \in \mathfrak{P}(X_u^{L_x})$ we write the discrete bilinear form (4.29) for $\varphi_k(\mathbf{x})$ with $\operatorname{supp}(\varphi_k(\mathbf{x})) \subset X_u^{L_x}$

$$\sum_{X_v^{L_x} \in \mathfrak{I}(X_u^{L_x})} \sum_{\ell \in \mathfrak{P}(X_v^{L_x})} \langle \mathcal{V}\varphi_\ell, \varphi_k \rangle q_\ell^* = \langle f, \varphi_k \rangle \, .$$

Next, we replace the heat kernel by its truncated Chebyshev expansion (4.32), which separates the variables. Thus we get φ_ℓ with $\ell \in \mathfrak{P}(X_v^{L_x})$ contributions to the Galerkin bilinear form tested with φ_k through L2P translations

$$\sum_{\ell \in \mathfrak{P}(X_v^{L_x})} \langle \check{\mathcal{V}}\varphi_\ell, \varphi_k \rangle q_\ell^* = \sum_{|\alpha|=0}^{q} \int_{\operatorname{supp}(\varphi_k)} T_\alpha \left(\Phi_{X_u^{L_x}}^{-1}(\mathbf{x}) \right) \varphi_k(\mathbf{x}) \mathrm{d}s_{\mathbf{x}} \, \lambda_\alpha(X_u^{L_x}) \, , \tag{4.35}$$

local expansions λ_α via M2L translations

$$\lambda_\alpha(X_u^{L_x}) = \sum_{|\beta|=0}^{q-|\alpha|} G_{\alpha,\beta}(\delta) \, \mu_\beta(X_v^{L_x}) \tag{4.36}$$

and moment expansions μ_α via Q2M translations

$$\mu_\beta(X_v^{L_x}) = \sum_{\ell \in \mathfrak{P}(X_v^{L_x})} \int_{\operatorname{supp}(\varphi_\ell)} T_\beta \left(\Phi_{X_v^{L_x}}^{-1}(\mathbf{y}) \right) \varphi_\ell(\mathbf{y}) \mathrm{d}s_{\mathbf{y}} q_\ell^* \, . \tag{4.37}$$

Furthermore, we observe that such a M2L translation (4.36) does not maintain the Gaussian structure of the heat kernel. This becomes evident when writing out the M2L translation in more detail [50], namely

$$\lambda_{\alpha_1,\alpha_2,\alpha_3}(X_u^{L_x}) = \sum_{\beta_1=0}^{q-|\alpha|} G_{\alpha_1,\beta_1}(\delta) \sum_{\beta_2=0}^{q-|\alpha|-\beta_1} G_{\alpha_2,\beta_2}(\delta) \sum_{\beta_3=0}^{q-|\alpha|-\beta_1-\beta_2} G_{\alpha_3,\beta_3}(\delta) \, \mu_{\beta_1,\beta_2,\beta_3}(X_v^{L_x}) \, .$$

Setting $\lambda^{(3)} = \mu(X_v^{L_x})$ and $\lambda^{(0)} = \lambda(X_u^{L_x})$ we have

$$\lambda^{(2)}_{\alpha_1,\alpha_2,\alpha_3,\beta_1,\beta_2} = \sum_{\beta_3=0}^{q-|\alpha|-\beta_1-\beta_2} G_{\alpha_3,\beta_3}(\delta) \, \lambda^{(3)}_{\beta_1,\beta_2,\beta_3}$$

$$\lambda^{(1)}_{\alpha_1,\alpha_2,\alpha_3,\beta_1} = \sum_{\beta_2=0}^{q-|\alpha|-\beta_1} G_{\alpha_2,\beta_2}(\delta) \, \lambda^{(2)}_{\alpha_1,\alpha_2,\alpha_3,\beta_1,\beta_2}$$

$$\lambda^{(0)}_{\alpha_1,\alpha_2,\alpha_3} = \sum_{\beta_1=0}^{q-|\alpha|} G_{\alpha_1,\beta_1}(\delta) \, \lambda^{(1)}_{\alpha_1,\alpha_2,\alpha_3,\beta_1}$$

and a close inspection reveals that from the outer to the inner loop we are dealing with three one-dimensional M2L's whose number of terms are $\#\mathfrak{S}(\mathcal{S}_q^5)$, $\#\mathfrak{S}(\mathcal{S}_q^4)$ and $\#\mathfrak{S}(\mathcal{S}_q^3)$, respectively. Since each sum is bounded by $q+1$ terms, this results in a total cost of $\mathscr{O}(q^6)$. Including more terms in each sum

$$\begin{aligned}
\lambda^{(2)}_{\beta_1,\beta_2,\alpha_3} &= \sum_{\beta_3=0}^{q-\beta_1-\beta_2} G_{\alpha_3,\beta_3}(\delta)\,\lambda^{(3)}_{\beta_1,\beta_2,\beta_3} \\
\lambda^{(1)}_{\beta_1,\alpha_2,\alpha_3} &= \sum_{\beta_2=0}^{q-\beta_1-\alpha_3} G_{\alpha_2,\beta_2}(\delta)\,\lambda^{(2)}_{\beta_1,\beta_2,\alpha_3} \\
\lambda^{(0)}_{\alpha_1,\alpha_2,\alpha_3} &= \sum_{\beta_1=0}^{q-\alpha_2-\alpha_3} G_{\alpha_1,\beta_1}(\delta)\,\lambda^{(1)}_{\beta_1,\alpha_2,\alpha_3}
\end{aligned}$$

leads to each one-dimensional M2L consisting of $\#\mathfrak{S}(\mathcal{S}_q^3)$ terms only. Hence, for a three-dimensional M2L translation of the form

$$\lambda_{\alpha_1,\alpha_2,\alpha_3}(X_u^{L_x}) = \sum_{\beta_1=0}^{q-\alpha_2-\alpha_3} G_{\alpha_1,\beta_1}(\delta) \sum_{\beta_2=0}^{q-\beta_1-\alpha_3} G_{\alpha_2,\beta_2}(\delta) \sum_{\beta_3=0}^{q-\beta_1-\beta_2} G_{\alpha_3,\beta_3}(\delta)\,\mu_{\beta_1,\beta_2,\beta_3}(X_v^{L_x})$$

we have reduced the total cost to $3(q+1)\#\mathfrak{S}(\mathcal{S}_q^3) = \mathscr{O}(q^4)$ arithmetic operations.

Remark 4.5. *If we replace the kernel of* (4.28) *by its normal derivative with respect to* $\mathbf{y}$*, we simply shift the derivative to the moment expansions and end up with modified Q2M translations*

$$\mu_\beta(X_v^{L_x}) = \sum_{\ell\in\mathfrak{P}(X_v^{L_x})_{supp(\varphi_\ell)}} \int \mathbf{n}_\mathbf{y}{}^\top \nabla_\mathbf{y} T_\beta\left(\Phi^{-1}_{X_v^{L_x}}(\mathbf{y})\right)\varphi_\ell(\mathbf{y})ds_\mathbf{y} q_\ell^* \,.$$

The same holds true in case the normal derivative is applied with respect to $\mathbf{x}$*, except that then the L2P translations are affected.*

Remark 4.6. *For implementation purpose we find it sufficient to replace the integrals in* (4.31) *by a* q^{th} *order Gauss-Chebyshev quadrature. This way we compute the one-dimensional expansion coefficients for the M2L translations by*

$$G_{k,\ell}(\delta) \approx \frac{\gamma_k\gamma_\ell}{(q+1)^2}\sum_{m,n=0}^{q} G\left(\Phi_{X_u^{L_x}}(\omega_m^q) - \Phi_{X_v^{L_x}}(\omega_n^q),\delta\right) T_k(\omega_m^q)T_\ell(\omega_n^q)\,.$$

Algorithm 2: The fast Gauss transform

%% compute moments
`for` v `in` $\mathfrak{X}(L_x)$ `do`
    $\mathbf{m}(X_v^{L_x}) = \mathbf{Q2M}(X_v^{L_x})\mathbf{q}^*(X_v^{L_x})$
`end for`

%% interaction phase
`for` u `in` $\mathfrak{X}(L_x)$ `do`
    `for` v `in` $\mathfrak{I}(X_u^{L_x})$ `do`
        $\mathbf{l}(X_u^{L_x}) = \mathbf{l}(X_u^{L_x}) + \mathbf{M2L}(\mathbf{d}_{uv}^{L_x})\mathbf{m}(X_v^{L_x})$
    `end for`
`end for`

%% evaluate potential
`for` u `in` $\mathfrak{X}(L_x)$ `do`
    $\mathbf{f}(X_u^{L_x}) = \mathbf{L2P}(X_u^{L_x})\mathbf{l}(X_u^{L_x})$
`end for`

Consistency Corollaries 4.1 and 4.2 show the exponential convergence of the truncated Chebyshev expansion of the heat kernel, while Lemma 4.5 describes the spatial cutoff error. In the following lemma we use these results to show how the introduction of these approximations affect the behavior of (4.29), i.e.,

$$\langle \breve{\mathcal{V}}_B q_h^*, v_h\rangle_\Gamma = \langle f, v_h\rangle_\Gamma \qquad \forall v_h \in X_{h_x}^{d_{d_x}}(\Gamma)\,. \tag{4.38}$$

Lemma 4.6. *Assume we approximate the discrete Galerkin bilinear form* (4.29) *for* $\delta > 0$ *by* (4.38) *and evaluate interactions according to Definition 4.5 (cf. Algorithm 2). Further, we choose the truncation parameter for the Chebyshev expansion* $q = \mathcal{O}(\log N_x^2)$ *and the spatial cutoff parameter* $\mathfrak{n}_x^2 = \mathcal{O}(\log(N_x^2\delta^{-\frac{3}{2\sigma_x}}))$*, then we can bound the error by*

$$\left|\langle(\mathcal{V} - \breve{\mathcal{V}}_B)q_h^*, v_h\rangle_\Gamma\right| \le C h_x^{\sigma_x} \|q_h^*\|_{L_2(\Gamma)}\|v_h\|_{L_2(\Gamma)} \qquad \forall v_h \in X_{h_x}^{d_{d_x}}(\Gamma)\,.$$

Proof. We estimate

$$\left|\langle(\mathcal{V} - \breve{\mathcal{V}}_B)q_h^*, v_h\rangle_\Gamma\right| \le |\langle(\mathcal{V} - \mathcal{V}_B)q_h^*, v_h\rangle_\Gamma| + \left|\langle(\mathcal{V}_B - \breve{\mathcal{V}}_B)\,, q_h^*, v_h\rangle_\Gamma\right|$$

where we use Lemma 4.5

$$|\langle(\mathcal{V} - \mathcal{V}_B)q_h^*, v_h\rangle_\Gamma| \le \frac{\varepsilon}{\sqrt{\delta^3}}\,|\Gamma|\,\|q_h^*\|_{L_2(\Gamma)}\|v_h\|_{L_2(\Gamma)}$$

with $\mathfrak{n}_x^2 = \mathscr{O}(\log(1/(h_x^{\sigma_x}\sqrt{\delta^3}))) = \mathscr{O}(\log(N_x^2\delta^{-\frac{3}{2\sigma_x}}))$ to get the assertion for the first term. For the second term, on the other hand, we have with Corollary 4.1

$$\begin{aligned}
\left|\langle(\mathcal{V}_B - \breve{\mathcal{V}}_B)q_h^*, v_h\rangle_\Gamma\right| &\leq \int_\Gamma \int_{\{\mathbf{y}\in\Gamma:\|\mathbf{x}-\mathbf{y}\|_\infty \leq 2h_x^{\ell_x}(\mathfrak{n}_x+1)\}} \left|(\mathcal{I} - \mathcal{S}_q^6)G(\mathbf{x}-\mathbf{y},\delta)q_h^*(\mathbf{y})v_h(\mathbf{x})\right| \mathrm{d}s_\mathbf{y}\mathrm{d}s_\mathbf{x} \\
&\leq C\frac{(q+1)^6}{\sqrt{\delta^3}}\left(\frac{1}{a-1}\right)^{q+1} \int_\Gamma\int_\Gamma |q_h^*(\mathbf{y})v_h(\mathbf{x})|\,\mathrm{d}s_\mathbf{y}\mathrm{d}s_\mathbf{x} \\
&\leq C\frac{(q+1)^6}{\sqrt{\delta^3}}\left(\frac{1}{a-1}\right)^{q+1} |\Gamma|\,\|q_h^*\|_{L_2(\Gamma)}\|v_h\|_{L_2(\Gamma)}
\end{aligned}$$

and since $a > 1$ can be chosen arbitrarily, $q = \mathscr{O}(\log N_x^2)$ is sufficient to conclude the proof. □

Complexity Unlike in the causal FMM where we only had a constant number of translation operators due to the uniform time discretization, we need many more translation operators for the FGT since we are dealing with unstructured triangulations Γ. The algorithm requires

- one $\mathbf{Q2M}(X_v^{L_x}) \in \mathbb{R}^{\#\mathfrak{S}(S_q^3)\times\#\mathfrak{P}(X_v^{L_x})}$ matrix and one $\mathbf{L2P}(X_u^{L_x}) \in \mathbb{R}^{\#\mathfrak{P}(X_u^{L_x})\times\#\mathfrak{S}(S_q^3)}$ matrix $\forall v \in \mathfrak{X}(L_x)$ and $\forall u \in \mathfrak{X}(L_x)$, respectively.
- $2(\mathfrak{n}_x+1)+1$ one-dimensional M2Ls $\in \mathbb{R}^{\#\mathfrak{S}(S_q^2)}$ to define all possible $\mathbf{M2L}(\mathbf{d}_{uv}^{L_x})$.

The arithmetic cost of the algorithm becomes $\mathscr{O}(q^4 N_x \mathfrak{n}_x^2)$ due to

- a total cost of Q2M/L2P translations is $\mathscr{O}(q^3 N_x)$.
- a cost for one M2L is $\mathscr{O}(q^4)$, the number of M2L's per cluster is $\mathscr{O}(\mathfrak{n}_x^2)$ and the number of clusters is $\mathscr{O}(N_x)$ which leads to a total cost of $\mathscr{O}(q^4 N_x \mathfrak{n}_x^2)$.

In terms of storage the algorithm requires $\mathscr{O}(q^3 N_x)$ due to

- $\mathscr{O}(q^3 N_x)$ memory for all Q2M/L2P expansion coefficients.
- $\mathscr{O}(q^2 \mathfrak{n}_x^2)$ for all M2L expansion coefficients.

Note that $\mathfrak{n}_x^2 = \mathscr{O}(\log(N_x^2\delta^{-\frac{3}{2\sigma_x}}))$ depends on the order σ_x of the discretization scheme and the temporal variance δ. As a consequence one has to slowly increase the number of interacting clusters in linear direction in order to increase the accuracy. The smaller the variance δ, the more pronounced this effect becomes.

Example 4.3. *With this example we intend to verify the exponential convergence of the truncated heat kernel Chebyshev expansion. Observe that Lemma 4.4 gives a point-wise estimate for $\delta > 0$ and $h_x^{L_x} = \mathcal{O}(\sqrt{\delta})$ independent of the spatial variables $x, y \in \mathbb{R}$, i.e.,*

$$\left|\left(\mathcal{I} - \mathcal{S}_q^2\right) G(x-y,\delta)\right| \leq C \frac{(q+2)}{\sqrt{\delta}} \left(\frac{1}{a-1}\right)^{q+1} .$$

Thus we set $x - y = 0$ and compute the error for $\delta \in \{2^{-i}\}_{i=0}^{4}$ and $h_x^{L_x} = \mathcal{O}(\sqrt{\delta})$. In Table 4.3 and Figure 4.8 we observe the expected exponential decay of the error. Furthermore, keeping the expansion order in Table 4.3 constant we observe the exact $\mathcal{O}(1/\sqrt{\delta})$ behavior as well. Note that this example also serves as a verification of Corollary 4.1 since the expansion of the three-dimensional heat kernel is based on the Gaussian structure of the heat kernel, i.e., the tensor product structure of one-dimensional heat kernels (4.1).

	$\delta = 2^0$	$\delta = 2^{-2}$	$\delta = 2^{-4}$	$\delta = 2^{-6}$	$\delta = 2^{-8}$
$q = 5$	$4.33\ 10^{-2}$	$8.67\ 10^{-2}$	$1.73\ 10^{-1}$	$3.46\ 10^{-1}$	$6.93\ 10^{-1}$
$q = 8$	$9.58\ 10^{-3}$	$1.91\ 10^{-2}$	$3.83\ 10^{-2}$	$7.66\ 10^{-2}$	$1.53\ 10^{-1}$
$q = 11$	$2.83\ 10^{-4}$	$5.67\ 10^{-4}$	$1.13\ 10^{-3}$	$2.26\ 10^{-3}$	$4.53\ 10^{-3}$
$q = 14$	$3.90\ 10^{-5}$	$7.81\ 10^{-5}$	$1.56\ 10^{-4}$	$3.12\ 10^{-4}$	$6.24\ 10^{-4}$
$q = 17$	$5.15\ 10^{-7}$	$1.03\ 10^{-6}$	$2.06\ 10^{-6}$	$4.12\ 10^{-6}$	$8.24\ 10^{-6}$
$q = 20$	$5.06\ 10^{-8}$	$1.01\ 10^{-7}$	$2.02\ 10^{-7}$	$4.04\ 10^{-7}$	$8.09\ 10^{-7}$
$q = 23$	$3.72\ 10^{-10}$	$7.45\ 10^{-10}$	$1.49\ 10^{-9}$	$2.98\ 10^{-9}$	$5.96\ 10^{-9}$

Table 4.3: Chebyshev expansion truncation error – order q vs. variance δ.

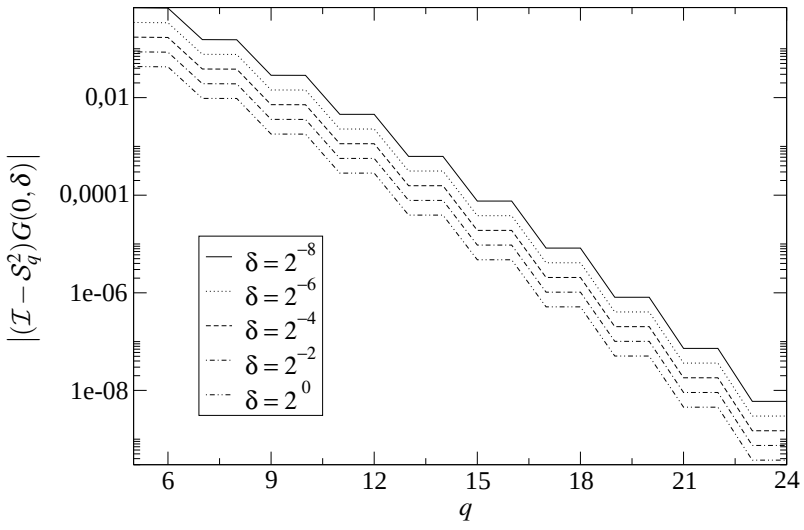

Figure 4.8: Chebyshev expansion truncation error vs. order q.

Example 4.4. *In order to verify the assertion of Lemma 4.5 for $d_{d_x} = d_0$, i.e.,*

$$|\langle(\mathcal{V}-\mathcal{V}_B)q_h^*, v_h\rangle_\Gamma| \leq \varepsilon\,|\Gamma|\,\|q_h^*\|_{L_2(\Gamma)}\|v_h\|_{L_2(\Gamma)} \qquad \forall q_h^*, v_h \in X_{h_x}^{d_0}(\Gamma)\,,$$

we choose Ω to be a unit-cube, split each of its edges into 16 intervals generating a regular grid of 6×16^2 squares, which we split into four equal sized triangles each. Since we are interested in the dependence of the spatial cutoff error on $\mathfrak{n}_x$ and δ we choose $\mathfrak{n}_x \in \{0,1\ldots,6\}$ and $\delta \in \{0.0025, 0.01, 0.04\}$. Due to $h_x^{L_x} = \mathcal{O}(\sqrt{\delta})$ we construct spatial cluster-trees with $L_x \in \{4,3,2\}$ according to Definition 4.2, where we let $\mathbf{x} \in supp\,(\varphi_i) \subset X_u^{L_x}$ and $\mathbf{y} \in supp\,(\varphi_j) \subset X_v^{L_x}$. For simplicity we assume $q_h^* \equiv v_h \equiv 1$, then we get

$$|\langle(\mathcal{V}-\mathcal{V}_B)q_h^*, v_h\rangle_\Gamma| = \left|\sum_i \sum_{j\notin\mathfrak{I}(X_u^{L_x})} \mathsf{V}_{ij}\right| \leq \frac{\varepsilon}{\sqrt{\delta^3}}\,|\Gamma|^2\,, \quad \mathsf{V}_{ij} = \int_{supp(\varphi_i)}\int_{supp(\varphi_j)} G(\mathbf{x}-\mathbf{y},\delta)\,ds_{\mathbf{y}}\,ds_{\mathbf{x}}\,.$$

	$\delta = 1/400$ $L_x = 4$	$\delta = 1/100$ $L_x = 3$	$\delta = 1/25$ $L_x = 2$
$\mathfrak{n}_x = 0$	$3.13\ 10^{1}$	$1.60\ 10^{1}$	$8.03\ 10^{0}$
$\mathfrak{n}_x = 1$	$1.17\ 10^{1}$	$5.53\ 10^{0}$	$2.28\ 10^{0}$
$\mathfrak{n}_x = 2$	$1.88\ 10^{0}$	$7.89\ 10^{-1}$	$2.20\ 10^{-1}$
$\mathfrak{n}_x = 3$	$1.45\ 10^{-1}$	$5.23\ 10^{-2}$	–
$\mathfrak{n}_x = 4$	$5.51\ 10^{-3}$	$1.61\ 10^{-3}$	–
$\mathfrak{n}_x = 5$	$1.01\ 10^{-4}$	$2.18\ 10^{-5}$	–
$\mathfrak{n}_x = 6$	$8.66\ 10^{-7}$	$1.08\ 10^{-7}$	–

Table 4.4: $\left|\langle(\mathcal{V}-\mathcal{V}_B)q_h^*, v_h\rangle\right|$ for $\mathfrak{n}_x$ vs. δ.

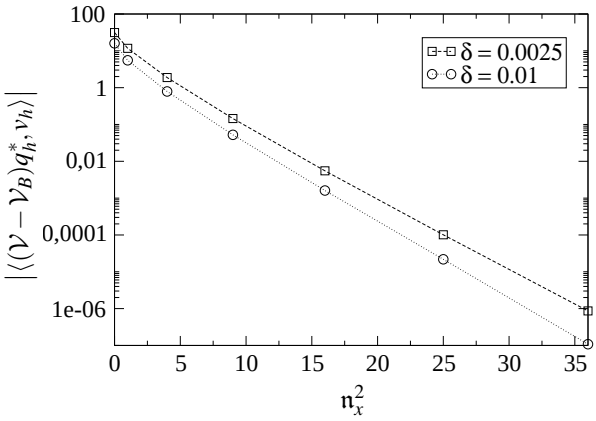

Figure 4.9: Spatial cutoff error vs. $\mathfrak{n}_x^2$.

In Table 4.4 and Figure 4.9 we observe the expected $\mathcal{O}(exp\left(-\mathfrak{n}_x^2\right))$ behavior of the error for a fixed δ. However, we only observe $\mathcal{O}(1/\sqrt{\delta^3})$ for large fixed $\mathfrak{n}_x$, while for smaller $\mathfrak{n}_x$ the results seem to show a more favorable $\mathcal{O}(1/\sqrt{\delta})$ behavior of the error. The reason is given in Remark 4.4, namely the fact that we neglect the exponential decay of the heat kernel beyond the truncation radius. Furthermore, at $L_x = 2$ and $\mathfrak{n}_x = 3$ the truncation radius is larger than the diameter of the domain and, therefore, the truncation error vanishes.

Example 4.5. *After the previous two examples it only remains to verify Lemma 4.6. However, it is quite hard to confirm the assertion, because the matrix entries of $\langle\mathcal{V}_B\varphi_i, \varphi_j\rangle$ are integrated numerically [15], which is very expensive. Instead we try to confirm the intermediate result of Lemma 4.6's proof, i.e., the exponential convergence of*

$$\left|\langle(\mathcal{V}_B-\check{\mathcal{V}}_B)q_h^*, v_h\rangle_\Gamma\right| \leq C\frac{(q+1)^6}{\sqrt{\delta^3}}\left(\frac{1}{a-1}\right)^{q+1}|\Gamma|\,\|q_h^*\|_{L_2(\Gamma)}\|v_h\|_{L_2(\Gamma)} \quad \forall q_h^*, v_h \in X_{h_x}^{d_0}(\Gamma)\,.$$

Again, we choose Ω *to be a unit-cube with the same spatial discretization as in Example 4.4 and set* $q_h^* \equiv v_h \equiv 1$*, while we fix* $\mathfrak{n}_x = 0$*, because it does not appear in the estimate. Furthermore, due to* $q_h^* \equiv 1$ *we can improve the above bound using* $\int_{\mathbf{y}\in\Gamma:\|\mathbf{x}-\mathbf{y}\|\leq 2h_x^{L_x}} ds_{\mathbf{y}} \leq \min\{|\Gamma|, \tilde{C}\delta\}$ *to get*

$$\left|\langle(\mathcal{V}_B - \check{\mathcal{V}}_B)q_h^*, v_h\rangle_\Gamma\right| \leq C\min\{|\Gamma|, \tilde{C}\delta\}\frac{(q+1)^6}{\sqrt{\delta^3}}\left(\frac{1}{a-1}\right)^{q+1}|\Gamma|^{\frac{3}{2}} .$$

	$\delta = 1/400$ $L_x = 3$	$\delta = 1/100$ $L_x = 2$	$\delta = 1/25$ $L_x = 1$
$q = 8$	2.52 10 $^{-3}$	2.12 10 $^{-3}$	1.72 10 $^{-3}$
$q = 10$	1.43 10 $^{-4}$	1.56 10 $^{-4}$	1.45 10 $^{-4}$
$q = 12$	7.81 10 $^{-6}$	9.78 10 $^{-6}$	1.03 10 $^{-5}$
$q = 14$	2.80 10 $^{-7}$	6.12 10 $^{-7}$	6.26 10 $^{-7}$
$q = 16$	1.39 10 $^{-8}$	2.93 10 $^{-8}$	3.32 10 $^{-8}$
$q = 18$	6.98 10^{-10}	1.01 10 $^{-9}$	1.71 10 $^{-9}$
$q = 20$	3.22 10^{-11}	4.49 10^{-11}	8.22 10^{-10}

Table 4.5: FGT approximation error.

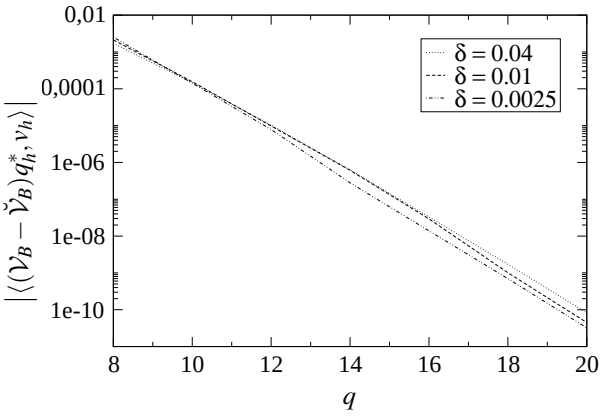

Figure 4.10: FGT approximation error.

The above estimate reveals that we should always obtain exponential convergence in the expansion order as confirmed in Table 4.5 and Figure 4.10. However, observe that we get a more favorable behavior in δ *than the expected* $\mathcal{O}(1/\sqrt{\delta})$*. We observe that with increasing expansion order the error starts to become smaller with decreasing* δ*.*

4.5 Space-Time Dependent Thermal Layer Potentials

In Section 4.3, we have investigated the temporal aspect of thermal layer potentials by itself leading to Volterra integral operators and the cFMM as an algorithm to enforce their efficient application. In an attempt to isolate the spatial aspect of thermal layer potentials in Section 4.4 we came across what is called the Gauss transform with the FGT enabling its fast application. Now we are in the nice position to pick those plums and put them together to form the parabolic FMM [47, 49], an almost optimal algorithm to accelerate the application of arbitrary thermal layer potentials. Let us recall the thermal single layer potential as the model potential we use throughout this section (with $\alpha \equiv 1$, as mentioned at the beginning of this chapter)

$$\mathcal{V}q^*(\mathbf{x},t) = f(\mathbf{x},t) . \tag{4.39}$$

Again we are not dealing with the continuous potential, but with its Galerkin discretized bilinear form according to Section 3.1

$$\langle \mathcal{V} q_h^*, v_h \rangle_{\Gamma\times\Upsilon} = \langle f, v_h \rangle_{\Gamma\times\Upsilon} \qquad \forall v_h \in S_{h_x,h_t}^{d_{d_x},d_{d_t}}(\Gamma\times\Upsilon) \,. \tag{4.40}$$

4.5.1 Lagrange-Chebyshev Kernel Approximation

Based on the hierarchical space-time clustering of Section 4.1, we want to approximate the heat kernel in a space-time cluster-pair with $\mathbf{x} \in X_u^{\ell_x}$, $\mathbf{y} \in X_v^{\ell_x}$, $t \in I_m^{\ell_t}$ and $\tau \in I_n^{\ell_t}$. For this purpose we define local coordinates $\hat{\mathbf{x}}, \hat{\mathbf{y}} \in [-1,1]^3$ and $\hat{t}, \hat{\tau} \in [-1,1]$

$$\begin{aligned} \mathbf{x} &= \mathbf{c}_{X_u^{\ell_x}} + \hat{\mathbf{x}} h_x^{\ell_x} \,, \quad \mathbf{y} = \mathbf{c}_{X_v^{\ell_x}} + \hat{\mathbf{y}} h_x^{\ell_x} \,, \\ t &= c_{I_m^{\ell_t}} + \hat{t} h_t^{\ell_t} \,, \qquad \tau = c_{I_n^{\ell_t}} + \hat{\tau} h_t^{\ell_t} \,. \end{aligned}$$

Now we can write the heat kernel in local coordinates

$$\begin{aligned} G(\mathbf{x}-\mathbf{y}, t-\tau) &= G\left(\Phi_{X_u^{\ell_x}}(\hat{\mathbf{x}}) - \Phi_{X_v^{\ell_x}}(\hat{\mathbf{y}}), \Phi_{I_m^{\ell_t}}(\hat{t}) - \Phi_{I_n^{\ell_t}}(\hat{\tau}) \right) \\ &= G\left(h_x^{\ell_x}(\mathbf{d}_{uv}^{\ell_x} + \hat{\mathbf{x}} - \hat{\mathbf{y}}), h_t^{\ell_t}(d_{mn}^{\ell_t} + \hat{t} - \hat{\tau}) \right) \end{aligned}$$

with

$$\mathbf{d}_{uv}^{\ell_x} = \frac{\mathbf{c}_{X_u^{\ell_x}} - \mathbf{c}_{X_v^{\ell_x}}}{h_x^{\ell_x}} \quad \text{and} \quad d_{mn}^{\ell_t} = \frac{c_{I_m^{\ell_t}} - c_{I_n^{\ell_t}}}{h_t^{\ell_t}} \,.$$

Lagrange interpolation in time. We use Lagrange interpolation for the temporal approximation of the heat kernel, because it conserves its spatial Gaussian structure, which otherwise would be destroyed by a Chebyshev expansion. Hence, we end up with the time interpolated heat kernel

$$\begin{aligned} \mathcal{J}_p^2 G(\mathbf{x}-\mathbf{y}, t-\tau) = \sum_{a,b=0}^{p} & G\left(\mathbf{x}-\mathbf{y}, \Phi_{I_m^{\ell_t}}(\omega_a^p) - \Phi_{I_n^{\ell_t}}(\omega_b^p) \right) \\ & \times L_a\left(\Phi_{I_m^{\ell_t}}^{-1}(t) \right) L_b\left(\Phi_{I_n^{\ell_t}}^{-1}(\tau) \right) \,. \end{aligned} \tag{4.41}$$

By the same argument as used in proof of Lemma 4.1 one can show that the heat kernel satisfies the temporal smoothness condition for $t - \tau > 0$

$$\frac{|D_t^i D_\tau^j G(\mathbf{x}-\mathbf{y}, t-\tau)|}{i!\,j!} \leq \frac{C(i+j)^{\frac{3}{2}}}{|t-\tau|^{i+j+\frac{3}{2}}} \,,$$

which allows to estimate the temporal interpolation error of the heat kernel in the same manner as done in Lemma 4.1

$$|(\mathcal{I} - \mathcal{J}_p^2) G(\mathbf{x}-\mathbf{y}, t-\tau)| \leq C\left((d_{mn}^{\ell_t} - 2) h_t^{\ell_t} \right)^{-\frac{3}{2}} \left(\frac{1}{d_{mn}^{\ell_t} - 2} \right)^{p+1} \,. \tag{4.42}$$

Truncated spatial Chebyshev expansion of the time interpolated heat kernel. For the reasons elaborated in Section 4.4 we do not use the same interpolation scheme in space, but expand the spatial variables of the time interpolated heat kernel (4.41) in a truncated Chebyshev series

$$\mathcal{S}_q^6\mathcal{J}_p^2 G(\mathbf{x}-\mathbf{y},t-\tau) = \sum_{a,b=0}^{p} L_a\left(\Phi_{I_m^{\ell_t}}^{-1}(t)\right) L_b\left(\Phi_{I_n^{\ell_t}}^{-1}(\tau)\right) \times \sum_{|\alpha+\beta|=0}^{q} G_{\alpha,\beta}\left(\Phi_{I_m^{\ell_t}}(\omega_a^p) - \Phi_{I_n^{\ell_t}}(\omega_b^p)\right) T_\alpha\left(\Phi_{X_u^{\ell_x}}^{-1}(\mathbf{x})\right) T_\beta\left(\Phi_{X_v^{\ell_x}}^{-1}(\mathbf{y})\right) . \quad (4.43)$$

Lemma 4.7. *Assume we choose $t \in I_m^{\ell_t}$ and $\tau \in I_n^{\ell_t}$ to be well separated* (4.18) *and $\mathbf{x} \in X_u^{\ell_x}$ and $\mathbf{y} \in X_v^{\ell_x}$ with $\delta = \mathcal{O}(h_t^{\ell_t}) = \mathcal{O}((h_x^{\ell_x})^2)$, then we can bound the error of the Lagrange-Chebyshev approximation* (4.43) *by*

$$\left|(\mathcal{I}-\mathcal{S}_q^6\mathcal{J}_p^2)G(\mathbf{x}-\mathbf{y},t-\tau)\right| \le C\left(\left(\frac{q+1}{h_x^{\ell_x}}\right)^3\left(\frac{1}{d_{mn}^{\ell_t}-2}\right)^{p+1} + \left(\frac{(q+1)^2}{h_x^{\ell_x}}\right)^3\left(\frac{1}{a-1}\right)^{q+1}\right)$$

with an arbitrary but fixed $a > 1$.

Proof. In order to get a handle on the approximation error we write

$$\begin{aligned}\left|(\mathcal{I}-\mathcal{S}_q^6\mathcal{J}_p^2)G(\mathbf{x}-\mathbf{y},t-\tau)\right| &\le \left|((\mathcal{I}-\mathcal{S}_q^6)+\mathcal{S}_q^6(\mathcal{I}-\mathcal{J}_p^2))G(\mathbf{x}-\mathbf{y},t-\tau)\right| \\ &\le \left|(\mathcal{I}-\mathcal{S}_q^6)G(\mathbf{x}-\mathbf{y},t-\tau)\right| \\ &\quad + \left|\mathcal{S}_q^6(\mathcal{I}-\mathcal{J}_p^2)G(\mathbf{x}-\mathbf{y},t-\tau)\right|\end{aligned}$$

and simply estimate the first term by Corollary 4.1 and $h_x^{\ell_x} = \mathcal{O}(\sqrt{\delta})$

$$\left|(\mathcal{I}-\mathcal{S}_q^6)G(\mathbf{x}-\mathbf{y},t-\tau)\right| \le C\left(\frac{(q+1)^2}{h_x^{\ell_x}}\right)\left(\frac{1}{a-1}\right)^{q+1} .$$

For the second term we use

$$\left|\mathcal{S}_q^6(\mathcal{I}-\mathcal{J}_p^2)G(\mathbf{x}-\mathbf{y},t-\tau)\right| \le \|\mathcal{S}_q^6\|_\infty \|(\mathcal{I}-\mathcal{J}_p^2)G(\mathbf{x}-\mathbf{y},t-\tau)\|_\infty ,$$

where we control the interpolation error by (4.42). In order to estimate the operator norm $\|\mathcal{S}_q^6\|_\infty$ we use the following observation. Namely, assuming $f \in L_w^2([-1,1]^6) \cap$

$C^0([-1,1]^6)$ and $f:[-1,1]^6\to\mathbb{R}$ we get

$$\begin{aligned}\left|\mathcal{S}_q^6 f\left(\Phi_\alpha(\hat{\mathbf{x}}),\Phi_\beta(\hat{\mathbf{y}})\right)\right| &= \left|\sum_{|\alpha+\beta|\le q} f_{\alpha,\beta} T_\alpha(\hat{\mathbf{x}}) T_\beta(\hat{\mathbf{y}})\right| \\ &\le \left(\sum_{|\alpha+\beta|\le q}\left|T_\alpha(\hat{\mathbf{x}})T_\beta(\hat{\mathbf{y}})\right|^2\right)^{\frac{1}{2}}\left(\sum_{|\alpha+\beta|\le q}\left|f_{\alpha,\beta}\right|^2\right)^{\frac{1}{2}} \\ &\le C\begin{pmatrix} q+6 \\ q\end{pmatrix}^{\frac{1}{2}}\|f\|_\infty^2,\end{aligned}$$

where the last estimate is due to Remark 4.2. Therefore, we have

$$\|\mathcal{S}_q^6 f\|_\infty \le C(q+1)^3\|f\|_\infty \quad \text{and} \quad \|\mathcal{S}_q^6\|_\infty \le C(q+1)^3$$

and with $h_t^{\ell_t}=\mathcal{O}((h_x^{\ell_x})^2)$ and $d_{mn}^{\ell_t}-2>1$ we arrive at the conclusion

$$\left|\mathcal{S}_q^6(\mathcal{I}-\mathcal{J}_p^2)G(\mathbf{x}-\mathbf{y},t-\tau)\right| \le C\left(\frac{q+1}{h_x^{\ell_x}}\right)^3\left(\frac{1}{d_{mn}^{\ell_t}-2}\right)^{p+1}.$$

□

4.5.2 Space-Time Multi-Level Structure

We start by choosing the number n_t of time steps per leaf cluster, which defines the temporal leaf level L_t according to Definition 4.1. Next, we use Lemma 4.5, where we set $\delta = 2h_t^{L_t}$, to find the spatial leaf level L_x as stated in Definition 4.2. Finally, we assign a spatial level to each temporal level such that the Lagrange-Chebyshev approximation according to Lemma 4.7 is independent of the respective space-time level combination. This is exactly the case when $h_x^{\ell_x}=\mathcal{O}(\sqrt{\delta})$ and $h_t^{\ell_t}=\mathcal{O}(\delta)$, therefore, it turns out that we only have to coarsen the spatial level with every other temporal level.

Not very surprisingly the Lagrange-Chebyshev approximation error estimate in Lemma 4.7 dictates that the temporal interaction list of the parabolic FMM must be the same as for the causal FMM described in Section 4.3.2. Furthermore, it requires the spatial interaction lists to be identical with the FGT's interaction list in Section 4.4.2.

Definition 4.6. *Based on a space-time clustering of $\Gamma\times\Upsilon$ according to Section 4.1 with given spatial- and temporal leaf levels L_x and L_t, we link the spatial level ℓ_x to the temporal level ℓ_t by*

$$\ell_x = max\left(L_x - \left\lfloor\frac{L_t-\ell_t}{2}\right\rfloor, 0\right)$$

and define the space-time interaction lists

$$\mathfrak{I}(X_u^{\ell_x} \times I_m^{\ell_t}) = \mathfrak{I}(X_u^{\ell_x}) \times \mathfrak{I}(I_m^{\ell_t}) \tag{4.44}$$

with $\mathfrak{I}(X_u^{\ell_x})$ *and* $\mathfrak{I}(I_m^{\ell_t})$ *defined in* (4.34) *and* (4.20)*, respectively.*

Remark 4.7. *Observe that the spatial interaction list implies a truncation after* $\mathfrak{n}_x$ *neighboring clusters. Even though in Lemma 4.5 this cutoff is only described for the kernel of the single layer potential, it holds for all other operators in a similar manner as well.*

4.5.3 The Parabolic FMM

Algorithm Assuming that $i \in \mathfrak{P}(I_m^{L_t})$ and $m \geq 2$ and $k \in \mathfrak{P}(X_u^{L_x})$ we use the interaction list (4.44) to split the discrete Galerkin bilinear form (4.40) into a near- and farfield

$$\begin{aligned}\sum_{j \in \{\mathfrak{P}(I_m^{L_t}) \cup \mathfrak{P}(I_{m-1}^{L_t}) | j \leq i\}} \sum_{u \in \mathfrak{X}(L_x)} \sum_{v \in \mathfrak{I}(X_u^{L_x})} \sum_{\ell \in \mathfrak{P}(X_v^{L_x})} \langle \mathcal{V}\phi_j\varphi_\ell, \phi_i\varphi_k\rangle q_{\ell j}^* \\ + \sum_{2 \leq \ell_t \leq L_t} \sum_{n \in \mathfrak{I}(I_{m^{\ell_t}}^{\ell_t})} \sum_{j \in \mathfrak{P}(I_n^{\ell_t})} \sum_{u \in \mathfrak{X}(\ell_x)} \sum_{v \in \mathfrak{I}(X_u^{\ell_x})} \sum_{\ell \in \mathfrak{P}(X_v^{\ell_x})} \langle \mathcal{V}\phi_j\varphi_\ell, \phi_i\varphi_k\rangle q_{\ell j}^* = \langle f, \phi_i\varphi_k\rangle \,. \end{aligned} \tag{4.45}$$

We call the first term on the left hand side the nearfield and evaluate it directly for the time being. The second expression is the farfield, where we replace the kernel by the Lagrange-Chebyshev approximation (4.43). Since the variables of the approximate kernel separate, this allows us to compute an approximate farfield contribution of all sources $\varphi_\ell(\mathbf{y}) \times \phi_j(\tau)$ with $\ell \times j \in \mathfrak{P}(X_v^{\ell_x}) \times \mathfrak{P}(I_n^{\ell_t})$ tested by $\varphi_k(\mathbf{x}) \times \phi_i(t)$ via L2P translation

$$\begin{aligned}\sum_{j \in \mathfrak{P}(I_n^{\ell_t})} \sum_{\ell \in \mathfrak{P}(X_v^{\ell_x})} \langle \check{\mathcal{V}}\phi_j\varphi_\ell, \phi_i\varphi_k\rangle q_{\ell j}^* = \sum_{a=0}^{p} \left(\int_{ih_t}^{(i+1)h_t} L_a\left(\Phi^{-1}_{I_{m^{\ell_t}}^{\ell_t}}(t)\right) \phi_i(t) \mathrm{d}t \right) \\ \times \sum_{|\alpha|=0}^{q} \left(\int_{\mathrm{supp}(\varphi_k)} T_\alpha\left(\Phi^{-1}_{X_u^{\ell_x}}(\mathbf{x})\right) \varphi_k(\mathbf{x}) \mathrm{d}s_{\mathbf{x}} \right) \lambda_{\alpha,a}\left(X_u^{\ell_x} \times I_{m^{\ell_t}}^{\ell_t}\right) \,. \end{aligned} \tag{4.46}$$

Local expansions are computed via M2L translations

$$\lambda_{\alpha,a}\left(X_u^{\ell_x} \times I_{m^{\ell_t}}^{\ell_t}\right) = \sum_{b=0}^{p} \sum_{|\beta|=0}^{q-|\alpha|} G_{\alpha,\beta}\left(\Phi_{I_m^{\ell_t}}(\omega_a^p) - \Phi_{I_n^{\ell_t}}(\omega_b^p)\right) \mu_{\beta,b}\left(X_v^{\ell_x} \times I_n^{\ell_t}\right) \tag{4.47}$$

and moment expansions through Q2M translations

$$\mu_{\beta,b}\left(X_v^{\ell_x}\times I_n^{\ell_t}\right)=\sum_{j\in\mathfrak{P}(I_n^{\ell_t})}\sum_{\ell\in\mathfrak{P}(X_v^{\ell_x})}\left(\int_{jh_t}^{(j+1)h_t}L_b\left(\Phi_{I_n^{\ell_t}}^{-1}(t)\right)\phi_j(\tau)\mathrm{d}\tau\right)$$
$$\times\left(\int_{\mathrm{supp}(\varphi_\ell)}T_\beta\left(\Phi_{X_v^{\ell_x}}^{-1}(\mathbf{y})\right)\varphi_\ell(\mathbf{y})\mathrm{d}s_{\mathbf{y}}\right)q_{\ell j}^*\,. \quad (4.48)$$

Similar to the causal FMM we do not want to compute moment expansions nor evaluate local expansions in all levels directly, as an evaluation of the farfield as presented above would require. Therefore, we introduce M2M translations that allow the computation of space-time moment expansions in coarser space-time combinations from finer levels and vice-versa for local expansions via L2L translations. We observe that there are two kinds of M2M/L2L required. Due to the fact that the spatial level only changes with every other temporal level, we need M2M/L2L translations that shift expansions only between temporal levels, they are identical with the temporal M2M/L2L translation operators (4.25) and (4.26), respectively. In case the spatial level also changes, we have to enrich those translation operators with the capability to shift the moment expansions between spatial levels as well. Since the multi-dimensional Chebyshev expansion is based on a Gaussian structure, we will use the discrete orthogonality of the Chebyshev polynomials to formulate the multi-dimensional translation operators. Due to the cluster extension described in Definition 4.3 we write Chebyshev polynomials in the parent level in terms of the Chebyshev polynomials in the child level

$$T_\ell(\hat{x}^{\ell_x})=T_\ell\left(\frac{\bar{h}_x^{\ell_x+1}}{\bar{h}_x^{\ell_x}}\hat{x}^{\ell_x+1}\pm\left(1-\frac{\bar{h}_x^{\ell_x+1}}{\bar{h}_x^{\ell_x}}\right)\right)=\sum_{k=0}^{\ell}\mathfrak{a}_{k,\ell}^{\ell_x\pm}T_k(\hat{x}^{\ell_x+1})\,,$$

where we have

$$\mathfrak{a}_{k,\ell}^{\pm\ell_x}=\frac{\gamma_k}{\pi}\int_{-1}^{1}T_\ell\left(\frac{\bar{h}_x^{\ell_x+1}}{\bar{h}_x^{\ell_x}}\hat{x}\pm\left(1-\frac{\bar{h}_x^{\ell_x+1}}{\bar{h}_x^{\ell_x}}\right)\right)T_k(\hat{x})w(\hat{x})\mathrm{d}\hat{x}$$
$$=\frac{\gamma_k}{q+1}\sum_{n=0}^{q}T_\ell\left(\frac{\bar{h}_x^{\ell_x+1}}{\bar{h}_x^{\ell_x}}\omega_n^q\pm\left(1-\frac{\bar{h}_x^{\ell_x+1}}{\bar{h}_x^{\ell_x}}\right)\right)T_k(\omega_n^q)$$

due to orthogonality (4.8). The second equality holds since $k\leq\ell\leq q$, which allows to compute the integral exactly by a q^{th} order Gauss Chebyshev quadrature rule. It is easily seen that

$$T_\beta(\hat{\mathbf{x}}^{\ell_x})=\sum_{\alpha\leq\beta}\mathfrak{a}_{\alpha,\beta}^{\pm\ell_x}T_\alpha(\hat{\mathbf{x}}^{\ell_x+1})$$

and hence a space-time M2M translation is given by

$$\mu_{\beta,b}(X_v^{\ell_x} \times I_n^{\ell_t}) = \sum_{j \in \mathfrak{C}(I_n^{\ell_t})} \sum_{\ell \in \mathfrak{C}(X_v^{\ell_x})} \sum_{a=0}^{p} \mathfrak{q}_{a,b}^{\pm} \sum_{\alpha \leq \beta} \mathfrak{a}_{\alpha,\beta}^{\pm \ell_x} \mu_{\alpha,a}(X_\ell^{\ell_x+1} \times I_j^{\ell_t+1}) \tag{4.49}$$

where spatial directions are resolved by the child lists. In order to understand what exactly happens here, we write out the inner most sum in more detail. Thus we write $\mu_\alpha^{(3)} = \mu_{\alpha,a}(X_\ell^{\ell_x+1} \times I_j^{\ell_t+1})$ and $\mu_\beta^{(0)} = \mu_{\beta,b}(X_v^{\ell_x} \times I_n^{\ell_t})$ and neglect the direction $\pm$ and level dependence ℓ_x for sake of clarity. Hence we get

$$\mu_{\beta_1,\beta_2,\beta_3}^{(0)} = \sum_{\alpha_1 \leq \beta_1} \mathfrak{a}_{\alpha_1,\beta_1} \sum_{\alpha_2 \leq \beta_2} \mathfrak{a}_{\alpha_2,\beta_2} \sum_{\alpha_3 \leq \beta_3} \mathfrak{a}_{\alpha_3,\beta_3} \mu_{\alpha_1,\alpha_2,\alpha_3}^{(3)} ,$$

which entangles into three one-dimensional M2M's

$$\begin{aligned}
\mu_{\alpha_1,\alpha_2,\beta_3}^{(2)} &= \sum_{\alpha_3 \leq \beta_3} \mathfrak{a}_{\alpha_3,\beta_3} \mu_{\alpha_1,\alpha_2,\alpha_3}^{(3)} , \\
\mu_{\alpha_1,\beta_2,\beta_3}^{(1)} &= \sum_{\alpha_2 \leq \beta_2} \mathfrak{a}_{\alpha_2,\beta_2} \mu_{\alpha_1,\alpha_2,\beta_3}^{(2)} , \\
\mu_{\beta_1,\beta_2,\beta_3}^{(0)} &= \sum_{\alpha_1 \leq \beta_1} \mathfrak{a}_{\alpha_1,\beta_1} \mu_{\alpha_1,\beta_2,\beta_3}^{(1)}
\end{aligned}$$

adding up to $3(q+1)\#\mathfrak{S}(S_q^3) = \mathscr{O}(q^4)$. Since the number of possible children in space and time is bounded this leads to $\mathscr{O}(p^2q^4)$ for the space-time M2M translation in (4.49). On the other hand, if the spatial level remains the same, M2M translations simplify to

$$\mu_{\beta,b}(X_v^{\ell_x} \times I_n^{\ell_t}) = \sum_{j \in \mathfrak{C}(I_n^{\ell_t})} \sum_{a=0}^{p} \mathfrak{q}_{a,b}^{\pm} \mu_{\alpha,a}(X_v^{\ell_x} \times I_j^{\ell_t+1})$$

with reduced complexity of $\mathscr{O}(p^2q^3)$. In a similar fashion, we can shift local expansions from coarser levels to finer levels all the way down to the leaf level, such that we can restrict potential evaluations to this level only. Full space-time L2L translations of $\mathscr{O}(p^2q^4)$ are given by

$$\lambda_{\alpha,a}(X_k^{\ell_x+1} \times I_i^{\ell_t+1}) = \sum_{b=0}^{p} \mathfrak{q}_{a,b}^{-} \sum_{\beta \leq \alpha} \mathfrak{a}_{\alpha,\beta}^{\ell_x \pm} \lambda_{\beta,b}(X_u^{\ell_x} \times I_m^{\ell_t}) \quad \forall k \in \mathfrak{C}(X_u^{\ell_x}) \quad \forall i \in \mathfrak{C}(I_m^{\ell_t}) , \tag{4.50}$$

which again reduce to $\mathscr{O}(p^2q^3)$ if the spatial level remains the same.

Algorithm 3: The parabolic fast multipole method

```
for m = 0 to 2^{L_t} do
    %% find ℓ_t, i.e., coarsest level where parents change
    for ℓ_t = 2 to L_t − 1 do
        if I^{ℓ_t}_{m^{ℓ_t}} = I^{ℓ_t}_{(m−1)^{ℓ_t}} then ℓ_t = ℓ_t + 1
    end for

    %% compute moments
    for v ∈ 𝔛(L_x) do
        m(X_v^{L_x} × I^{L_t}_{m−2}) = q2m Q2M(X_v^{L_x}) q*(X_v^{L_x} × I^{L_t}_{m−2})
    end for

    %% upward path
    for ℓ_t = L_t − 1 to ℓ_t do
        for j ∈ 𝔈(I^{ℓ_t}_{m^{ℓ_t}−2}) do
            if ((L_t − ℓ_t)/2)%1 = 0
               for v ∈ 𝔛(ℓ_x) and ℓ ∈ 𝔈(X_v^{ℓ_x}) do
                   m(X_v^{ℓ_x} × I^{ℓ_t}_{m^{ℓ_t}−2}) = m(X_v^{ℓ_x} × I^{ℓ_t}_{m^{ℓ_t}−2}) +
                                                        m2m^± M2M^±(ℓ_x) m(X_ℓ^{ℓ_x+1} × I_j^{ℓ_t+1})
               end for
            else
               for v ∈ 𝔛(ℓ_x) do
                   m(X_v^{ℓ_x} × I^{ℓ_t}_{m^{ℓ_t}−2}) = m(X_v^{ℓ_x} × I^{ℓ_t}_{m^{ℓ_t}−2}) + m2m^± m(X_v^{ℓ_x} × I_j^{ℓ_t+1})
               end for
            end if
        end for
    end for

    %% interaction phase
    for ℓ_t = L_t to ℓ_t do
        for n ∈ 𝔍(I^{ℓ_t}_{m^{ℓ_t}}) do
            for u ∈ 𝔛(ℓ_x) and v ∈ 𝔍(X_u^{ℓ_x}) do
                l(X_u^{ℓ_x} × I^{ℓ_t}_{m^{ℓ_t}}) = l(X_u^{ℓ_x} × I^{ℓ_t}_{m^{ℓ_t}}) + m2l(d^{ℓ_t}_{m^{ℓ_t} n}) M2L(d_{uv}^{ℓ_x}) m(X_v^{ℓ_x} × I_n^{ℓ_t})
            end for
        end for
    end for
```

to be continued ...

Algorithm 3: The parabolic fast multipole method

continue ...

```
%% downward path
for ℓ_t = ℓ_t to L_t − 1 do
    for i ∈ 𝔠(I^{ℓ_t}_{m^{ℓ_t}}) do
        if ((L_t − ℓ_t)/2)%1 = 0
            for u ∈ 𝔛(ℓ_x) and k ∈ 𝔠(X_u^{ℓ_x}) do
                l(X_k^{ℓ_x+1} × I_i^{ℓ_t+1}) = l(X_k^{ℓ_x} × I_i^{ℓ_t+1}) + l2l^± L2L^±(ℓ_x) l(X_u^{ℓ_x} × I^{ℓ_t}_{m^{ℓ_t}})
            end for
        else
            for u ∈ 𝔛(ℓ_x) do
                l(X_u^{ℓ_x} × I_i^{ℓ_t+1}) = l(X_u^{ℓ_x} × I_i^{ℓ_t+1}) + l2l^± l(X_u^{ℓ_x} × I^{ℓ_t}_{m^{ℓ_t}})
            end for
        end if
    end for
end for

%% evaluate potential
for u ∈ 𝔛(L_x) do
    f^{FF}(X_u^{L_x} × I_m^{L_t}) = l2p L2P(X_u^{L_x}) l(X_u^{L_x} × I_m^{L_t})
end for

%% add nearfield
for u ∈ 𝔛(L_x) do
    f(X_u^{L_x} × I_m^{L_t}) = f^{FF}(X_u^{L_x} × I_m^{L_t}) + f^{NF}(X_u^{L_x} × I_m^{L_t})
end for
end for
```

Consistency Lemma 4.7 provides exponential convergence of the heat kernel's Lagrange-Chebyshev expansion in space and time. Hence, the same ideas as in Lemma 4.2 and Lemma 4.6 can be used to derive the following consistency estimate for the pFMM approximation of Galerkin discretized boundary integral operators.

Lemma 4.8. *Assume we have the discrete Galerkin bilinear form* $\langle \mathcal{V} q_h^*, v_h \rangle$ *according to* (4.40) *satisfying the space-time scaling condition* (4.2) *with* $h_t = \mathcal{O}(h_x^2)$. *Furthermore, we have the approximated bilinear form* $\langle \check{\mathcal{V}}_B q_h^*, v_h \rangle$, *where we replace the kernel function* $G(\mathbf{x}-\mathbf{y}, t-\tau)$ *by its Lagrange-Chebyshev expansion* (4.43) *and collect interactions according to the Definition 4.6 (cf. Algorithm 3). Choosing* $p = \mathcal{O}(\log N_t)$, $q = \mathcal{O}(\log N_t)$

and $\mathfrak{n}_x^2 = \mathscr{O}(\log N_t)$ *is sufficient to obtain*

$$\left|\left\langle (\mathcal{V}-\breve{\mathcal{V}}_B)q_h^*, v_h\right\rangle_{\Gamma\times\Upsilon}\right| \leq C\left(h_t^{\sigma_t}+h_x^{\sigma_x}\right)\|q_h^*\|_{L_2(\Gamma\times\Upsilon)}\|v_h\|_{L_2(\Gamma\times\Upsilon)} \quad \forall q_h^*, v_h \in S_{h_x,h_t}^{d_{d_x},d_{d_t}}(\Gamma\times\Upsilon)\,.$$

Proof. Similar to the proof of Lemma 4.6 we use the triangle inequality to get

$$\left|\left\langle (\mathcal{V}-\breve{\mathcal{V}}_B)q_h^*, v_h\right\rangle_{\Gamma\times\Upsilon}\right| \leq \left|\left\langle (\mathcal{V}-\mathcal{V}_B)q_h^*, v_h\right\rangle_{\Gamma\times\Upsilon}\right| + \left|\left\langle (\mathcal{V}_B-\breve{\mathcal{V}}_B)q_h^*, v_h\right\rangle_{\Gamma\times\Upsilon}\right|\,,$$

where the spatial truncation error is bounded by

$$\begin{aligned}
\left|\left\langle (\mathcal{V}-\mathcal{V}_B)q_h^*, v_h\right\rangle\right| \leq & \max_{\substack{\|\mathbf{x}-\mathbf{y}\|_\infty \geq 2h_x^{L_x}(\mathfrak{n}_x+1)\\ 2h_t^{L_t}\geq|t-\tau|>0}} G(\mathbf{x}-\mathbf{y},t-\tau)\int_{\tau=0}^{T}\int_{\Gamma} q_h^*(\mathbf{y},\tau)\mathrm{d}s_{\mathbf{y}}\mathrm{d}\tau \int_{t=0}^{T}\int_{\Gamma} v_h(\mathbf{x},t)\mathrm{d}s_{\mathbf{x}}\mathrm{d}t \\
& + \max_{\substack{\|\mathbf{x}-\mathbf{y}\|_\infty \geq 2h_x^{\ell_x}(\mathfrak{n}_x+1)\\ |t-\tau|\geq 2h_t^{\ell_t}}} G(\mathbf{x}-\mathbf{y},t-\tau)\int_{\tau=0}^{T}\int_{\Gamma} q_h^*(\mathbf{y},\tau)\mathrm{d}s_{\mathbf{y}}\mathrm{d}\tau \int_{t=0}^{T}\int_{\Gamma} v_h(\mathbf{x},t)\mathrm{d}s_{\mathbf{x}}\mathrm{d}t \\
& \leq \max_{\substack{\|\mathbf{x}-\mathbf{y}\|_\infty \geq 2h_x^{\ell_x}(\mathfrak{n}_x+1)\\ |t-\tau|\geq 2h_t^{\ell_t}}} G(\mathbf{x}-\mathbf{y},t-\tau) 2T\left|\Gamma\right|\|q_h^*\|_{L_2(\Gamma\times\Upsilon)}\|v_h\|_{L_2(\Gamma\times\Upsilon)}
\end{aligned}$$

and we see that due to $h_t^{\ell_t} = \mathscr{O}((h_x^{\ell_x})^2)$ and $h_t \leq h_t^{\ell_t}$ it suffices to have $\mathfrak{n}_x^2 = \mathscr{O}(\log N_t)$ in order to guarantee

$$\max_{\substack{\|\mathbf{x}-\mathbf{y}\|_\infty \geq 2h_x^{\ell_x}(\mathfrak{n}_x+1)\\ |t-\tau|\geq 2h_t^{\ell_t}}} G(\mathbf{x}-\mathbf{y},t-\tau) \leq C_1 h_t^{-\frac{3}{2}}\exp\left(-C_2(\mathfrak{n}_x+1)^2\right) \leq h_t^{\sigma_t}\,.$$

Next we use Lemma 4.7 to estimate the remaining term, i.e.,

$$\begin{aligned}
\left|\left\langle (\mathcal{V}_B-\breve{\mathcal{V}}_B)q_h^*, v_h\right\rangle\right| &= \int_{t=0}^{T}\int_{\Gamma}\int_{\tau=0}^{t}\int_{\Gamma}\left(\mathcal{I}-\mathcal{J}_p^2\mathcal{S}_q^6\right)G(\mathbf{x}-\mathbf{y},t-\tau)q_h^*(\mathbf{y},\tau)\mathrm{d}s_{\mathbf{y}}\mathrm{d}\tau v_h(\mathbf{x},t)\mathrm{d}s_{\mathbf{x}}\mathrm{d}t \\
&\leq C\left(\left(\frac{q+1}{h_x^{\ell_x}}\right)^3\left(\frac{1}{d_{mn}^{\ell_t}-2}\right)^{p+1} + \left(\frac{(q+1)^2}{h_x^{\ell_x}}\right)^3\left(\frac{1}{a-1}\right)^{q+1}\right)\times \\
&\qquad T\left|\Gamma\right|\|q_h^*\|_{L_2(\Gamma\times\Upsilon)}\|v_h\|_{L_2(\Gamma\times\Upsilon)}
\end{aligned}$$

and with $h_t^{\ell_t} = \mathscr{O}((h_x^{\ell_x})^2)$, $h_t = \mathscr{O}(h_x^2)$, $h_x \leq h_x^{\ell_x}$ and $h_t \leq h_t^{\ell_t}$ we observe that $p = \mathscr{O}(\log N_t)$ and $q = \mathscr{O}(\log N_x^2) = \mathscr{O}(\log N_t)$ are sufficient to get

$$\left(\left(\frac{q+1}{h_x^{\ell_x}}\right)^3\left(\frac{1}{d_{mn}^{\ell_t}-2}\right)^{p+1} + \left(\frac{(q+1)^2}{h_x^{\ell_x}}\right)^3\left(\frac{1}{a-1}\right)^{q+1}\right) \leq C(h_x^{\sigma_x}+h_t^{\sigma_t})\,,$$

which concludes the proof. □

Lemma 4.9. *Lemma 4.8 can be used to show how to obtain a consistent pFMM approximation of all initial boundary value problems as long as* $p, q, \mathfrak{n}_x^2 = \mathscr{O}(\log N_t)$.

1. *Satisfying the assumptions of Lemma 3.1 together with the discrete ellipticity of* $\breve{\mathcal{V}}$, *the pFMM approximated solution* $\breve{\breve{q}}_h^* \in S_{h_x,h_t}^{d_0,d_0}(\Gamma \times \Upsilon)$ *of* (3.17) *fulfills*

$$\|q^* - \breve{\breve{q}}_h^*\|_{L_2(\Gamma\times\Upsilon)} \leq C(h_x + h_t^{\frac{1}{2}}) \left(\|q^*\|_{H^{2,1}_{pw}(\Gamma\times\Upsilon)} + \|g_D\|_{H^{2,1}(\Gamma\times\Upsilon)} + \|q^*\|_{L_2(\Gamma\times\Upsilon)} \right) .$$

2. *Satisfying the assumptions of Lemma 3.2 together with the discrete ellipticity of* $\breve{\mathcal{D}}$, *the pFMM approximated solution* $\breve{\breve{u}}_h \in S_{h_x,h_t}^{c_1,d_0}(\Gamma \times \Upsilon)$ *of* (3.21) *suffices*

$$\|u - \breve{\breve{u}}_h\|_{L_2(\Gamma\times\Upsilon)} \leq C(h_x^2 + h_t) \left(\|u\|_{H^{2,1}(\Gamma\times\Upsilon)} + \|g_N^*\|_{H^{1,\frac{1}{2}}_{pw}(\Gamma\times\Upsilon)} + \|u\|_{L_2(\Gamma\times\Upsilon)} \right) .$$

3. *Satisfying the assumptions of Lemma 3.4 together with the discrete ellipticity of* $\breve{\mathcal{V}}$ *and* $\breve{\mathcal{D}}$, *the solution* $\breve{\breve{u}}_h \in S_{h_x,h_t}^{c_1,d_0}(\Gamma \times \Upsilon)$ *of* (3.28) *satisfies*

$$\|u - \breve{\breve{u}}_h\|_{L_2(\Gamma\times\Upsilon)} \leq C(h_x^2 + h_t) \Big(\|u\|_{H^{2,1}(\Gamma\times\Upsilon)} + \|\mathcal{S}u\|_{H^{1,\frac{1}{2}}_{pw}(\Gamma\times\Upsilon)} + \|g_R^*\|_{H^{1,\frac{1}{2}}_{pw}(\Gamma\times\Upsilon)} + \|u\|_{L_2(\Gamma\times\Upsilon)} \Big) .$$

4. *Satisfying the assumptions of Lemma 3.5 together with the discrete ellipticity of* $\breve{\mathcal{V}}$ *and* $\breve{\mathcal{D}}$, *the solution* $\breve{\breve{u}}_h \in S_{h_x,h_t}^{c_1,d_0}(\Gamma \times \Upsilon)$ (3.32) *is controlled by*

$$\|u - \breve{\breve{u}}_h\|_{L_2(\Gamma\times\Upsilon)} \leq C(h_x^2 + h_t) \Big(\|u\|_{H^{2,1}(\Gamma\times\Upsilon)} + \|\mathcal{S}u\|_{H^{1,\frac{1}{2}}_{pw}(\Gamma\times\Upsilon)} + \|g_{NR}^*\|_{H^{1,\frac{1}{2}}_{pw}(\Gamma\times\Upsilon)} + \|\mathcal{S}\tilde{g}_D\|_{H^{1,\frac{1}{2}}_{pw}(\Gamma\times\Upsilon)} + \|\tilde{g}_D\|_{H^{2,1}(\Gamma\times\Upsilon)} + \|u\|_{L_2(\Gamma\times\Upsilon)} \Big) .$$

Proof. The proof follows along the lines of Lemma 4.3. □

Complexity Due to fact that we do a FGT at every interpolation-point combination in time, the arithmetic complexity results in $\mathscr{O}(p^2q^4N_tN_x\mathfrak{n}_x^2)$ composed by

- $\mathscr{O}(pN_t)$ times $\mathscr{O}(q^3N_x)$ for all Q2M/L2P translations.
- $\mathscr{O}(p^2N_t)$ times $\mathscr{O}(q^4N_x)$ for all M2M/L2L translations.
- $\mathscr{O}(p^2N_t)$ times $\mathscr{O}(q^4N_x\mathfrak{n}_x^2)$ M2L translations.

- $\mathcal{O}(N_x)$ work for the nearfield.

The storage requirement $\mathcal{O}(p^2q^3N_x\log_2 N_t)$ on the other side results from

- $\mathcal{O}(p^2\log_2 N_t)$ times $\mathcal{O}(q^3N_x)$ moment/local expansions.
- $\mathcal{O}(1)$ for all Q2M/L2P and M2M/L2L translation coefficients due to the uniform space-time clustering.
- $\mathcal{O}(p^2\log_2 N_t)$ times $\mathcal{O}(q^2\mathfrak{n}_x)$ for all M2L translation coefficients.
- $\mathcal{O}(N_x)$ memory for the nearfield.

In the description of the algorithm below the FGT translations are performed inside the cFMM loops. Except of the spatial $\mathbf{M2M}^{\pm}(\ell_x)$ and $\mathbf{L2L}^{\pm}(\ell_x)$ translations defined in (4.49) and (4.50) all matrices are defined in the previous sections.

Example 4.6. *We let $\hat{t}=-1$, $\hat{\tau}=1$ with $t=\Phi_{I_m^{\ell_t}}(\hat{t})\in I_m^{\ell_t}$, $\tau=\Phi_{I_n^{\ell_t}}(\hat{\tau})\in I_n^{\ell_t}$ with $d_{mn}^{\ell_t}=4$, to obtain the worst possible and admissible temporal point. Further, we choose $\hat{\mathbf{x}},\hat{\mathbf{y}}=\mathbf{0}$ and $\mathbf{x}=\Phi_{X_u^{\ell_x}}(\hat{\mathbf{x}})\in X_u^{\ell_x}$, $\mathbf{y}=\Phi_{X_v^{\ell_x}}(\hat{\mathbf{y}})\in X_v^{\ell_x}$ with $\mathbf{d}_{uv}^{\ell_x}=\mathbf{0}$ to obtain the worst possible and admissible spatial point. In this setting, we choose $h_t^{\ell_t}=0.5$ and $h_x^{\ell_x}=2$ to investigate the estimate of Lemma 4.7*

$$\left|(\mathcal{I}-\mathcal{S}_q^6\mathcal{J}_p^2)G(\mathbf{x}-\mathbf{y},t-\tau)\right| \leq C\left(\left(\frac{q+1}{h_x^{\ell_x}}\right)^3\left(\frac{1}{d_{mn}^{\ell_t}-2}\right)^{p+1} + \left(\frac{(q+1)^2}{h_x^{\ell_x}}\right)^3\left(\frac{1}{a-1}\right)^{q+1}\right)$$

for varying temporal interpolation order p and spatial expansion truncation parameter q.

	$p=3$	$p=4$	$p=5$	$p=6$	$p=7$	$p=8$	$p=9$
$q=5$	$8.40\,10^{-3}$	$8.31\,10^{-3}$	$8.31\,10^{-3}$	$8.31\,10^{-3}$	$8.31\,10^{-3}$	$8.31\,10^{-3}$	$8.31\,10^{-3}$
$q=7$	$3.93\,10^{-3}$	$3.62\,10^{-3}$	$3.58\,10^{-3}$	$3.58\,10^{-3}$	$3.58\,10^{-3}$	$3.58\,10^{-3}$	$3.58\,10^{-3}$
$q=9$	$1.82\,10^{-3}$	$1.32\,10^{-3}$	$1.23\,10^{-3}$	$1.22\,10^{-3}$	$1.22\,10^{-3}$	$1.22\,10^{-3}$	$1.22\,10^{-3}$
$q=11$	$1.09\,10^{-3}$	$4.76\,10^{-4}$	$3.63\,10^{-4}$	$3.44\,10^{-4}$	$3.41\,10^{-4}$	$3.40\,10^{-4}$	$3.40\,10^{-4}$
$q=13$	$8.94\,10^{-4}$	$2.35\,10^{-4}$	$1.08\,10^{-4}$	$8.49\,10^{-5}$	$8.08\,10^{-5}$	$8.01\,10^{-5}$	$8.00\,10^{-5}$
$q=15$	$8.50\,10^{-4}$	$1.78\,10^{-4}$	$4.65\,10^{-5}$	$2.17\,10^{-5}$	$1.71\,10^{-5}$	$1.63\,10^{-5}$	$1.62\,10^{-5}$
$q=17$	$8.41\,10^{-4}$	$1.67\,10^{-4}$	$3.38\,10^{-5}$	$8.57\,10^{-6}$	$3.89\,10^{-6}$	$3.03\,10^{-6}$	$2.88\,10^{-6}$
$q=19$	$8.40\,10^{-4}$	$1.65\,10^{-4}$	$3.16\,10^{-5}$	$6.22\,10^{-6}$	$1.50\,10^{-6}$	$6.37\,10^{-7}$	$4.80\,10^{-7}$
$q=21$	$8.40\,10^{-4}$	$1.65\,10^{-4}$	$3.13\,10^{-5}$	$5.85\,10^{-6}$	$1.12\,10^{-6}$	$2.56\,10^{-7}$	$9.76\,10^{-8}$

Table 4.6: Lagrange-Chebyshev expansion truncation error $\left|(\mathcal{I}-\mathcal{S}_q^6\mathcal{J}_p^2)G(\mathbf{0},1)\right|$.

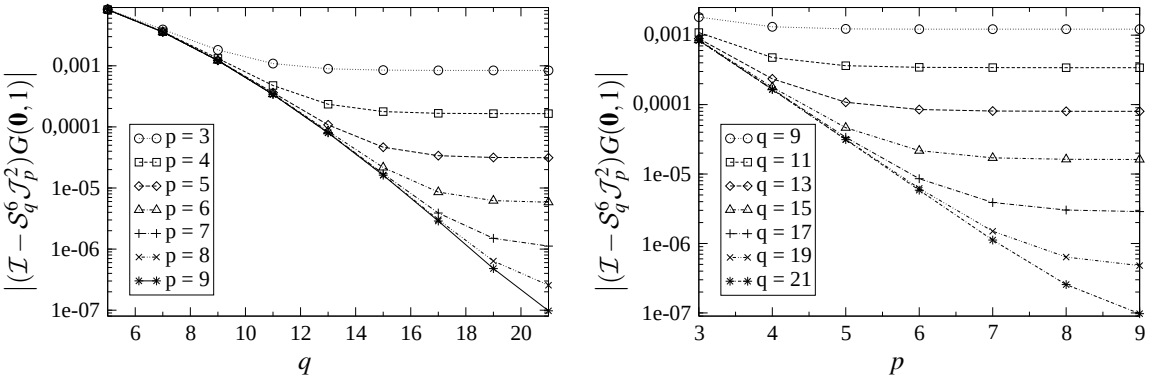

(a) Super-exponential convergence in space.

(b) Exponential convergence in time.

Figure 4.11: Lagrange-Chebyshev expansion truncation error $\left|(\mathcal{I}-\mathcal{S}_q^6\mathcal{J}_p^2)G(\mathbf{0},1)\right|$.

In Table 4.6 we clearly observe the expected behavior stated by the estimate above, namely exponential convergence in time and super-exponential convergence in space, which is even more evident from Figure 4.11.

The verification of Lemma 4.8 and Lemma 4.9 is postponed to Chapter 5.

4.6 Acceleration of the Temporal Nearfield

We observe that even though the complexity estimate of the pFMM suggests optimality of the nearfield, there is space for improvement. First of all there are time steps in the nearfield where the kernel is not singular (that is always the case if $n_t > 1$). Second, we notice that the complexity estimate for the nearfield only holds as long as $h_x = \mathcal{O}(h_t^a)$ with $a \leq \frac{1}{2}$, however in many practical applications this might not be the case. Just imagine a problem, where the spatial resolution of the domain needs to be much higher than the temporal one. The same holds for problems, where the spatial cutoff does not become effective, yet. We address this drawback by the techniques presented in [34], i.e., since the temporal well separation condition is not satisfied any more, we have to give up the interpolation in time. However, we observe that the singularity of the heat kernel (2.9) is only limited to the diagonal $t = \tau$ as depicted in Figure 4.12, thus we can still apply fast techniques in space.

In a naive way we would just use the explicit kernels expressions of Section 3.1.4 to evaluate the whole nearfield directly. However, since these kernels are time integrated versions of the heat kernel, they still exhibit exponential decay for $\mathbf{x}-\mathbf{y} \to \infty$. Moreover, for $d > 1$ they are infinitely smooth as stated in Section 3.1.4 and, therefore, one could accelerate them by some modified FGT algorithm. Although this strategy sounds promising, the downside of such an approach would be that these time integrated kernels have lost the

Gaussian structure (4.1) of the heat kernel, with the consequence that an efficient form of the translation operators as in Section 4.4.3 is not possible anymore. Thus we resort to a different approach, namely we apply a composite quadrature adapted to the temporal structure, which leaves the structure of the heat kernel unchanged, and use the FGT to accelerate spatial interactions at each Gauss point.

In Section 4.6.1, we provide the appropriate lemmas to control the error, which stems from the Gauss-Legendre quadrature presented in Section 4.6.2. We start with the acceleration of all time steps where the kernel is regular, then we proceed with those where the kernel is singular (cf. Figure 4.12). In order for this idea to succeed, we split these time steps into smaller and smaller parts and accelerate the ones that are far enough away from the singularity. Due to the space-time scaling (4.2) of the heat kernel this temporal localization leads to a spatial localization of the required direct evaluations and thus to an optimal algorithm.

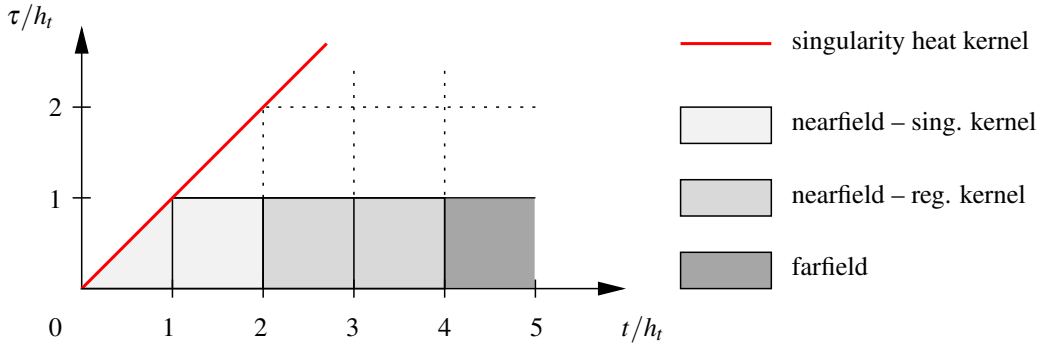

Figure 4.12: Temporal midfield splitting for $n_t = 2$.

4.6.1 Gauss Legendre Quadrature

Estimates of the error of the Gauss-Legendre quadrature applied to functions with analytic extension into the complex plane have been derived in [9]. Unfortunately, the results there assume that either the quadrature order or the region of analyticity are sufficiently large and are thus not directly applicable when these values are specified, as needed in this work. However, the methodology can be modified to derive similar results which are more suitable for the following discussion.

For a function $f : [-1,1] \to \mathbb{R}$, which has an analytic extension into the complex plane, the error E_g of the Gauss-Legendre rule

$$\int_{-1}^{1} f(\xi)\mathrm{d}\xi = \sum_{j=0}^{g-1} f(\xi_j) w_j + E_g(f)$$

can be expressed in terms of an integral over a simply closed contour γ that encloses the interval $[-1,1]$ and is contained in a region of the complex plane where f is analytic

$$E_g(f) = \frac{1}{\pi i}\int_\gamma \frac{Q_g(z)}{P_g(z)} f(z)\mathrm{d}z \tag{4.51}$$

with the Legendre function of the second kind

$$Q_g(z) = \frac{1}{2}\int_{-1}^{1} \frac{P_g(\xi)}{z-\xi}\mathrm{d}\xi\ , \qquad z \notin [-1,1].$$

Because of the properties of the Legendre polynomials P_g [14, Section 12.4] it is convenient to let the contour γ be the ellipse ϵ_ρ, which is the image of the circle of radius ρ in the complex plane under the transformation $z = 1/2(\zeta + 1/\zeta)$, i.e.,

$$\epsilon_\rho = \left\{ \tfrac{1}{2}\left(\zeta + \tfrac{1}{\zeta}\right) : |\zeta| = \rho \right\}\ . \tag{4.52}$$

Lemma 4.10. *Let $f(z)$ be analytic in a domain that contains the ellipse ϵ_ρ in* (4.52) *for some $\rho > \sqrt{2}$, then the error of the Gauss-Legendre quadrature can be bounded by*

$$\left|E_g(f)\right| \le C_0\sqrt{g}\frac{\rho^2}{\rho^2-2}M(\rho)\rho^{-2g}.$$

where $M(\rho) = \max|f(z)|$ on ϵ_ρ and $C_0 = \frac{3\sqrt{\pi}}{2} exp\left(\frac{1}{6}\right) = 3.1408\ldots$.

Proof. It is well known that for $z \in \epsilon_\rho$ (4.52) the Legendre polynomials have the representation [14, Lemma 12.4.1]

$$P_g(z) = \sum_{j=0}^{g} a_{g-j}a_j\zeta^{g-2j} \quad \text{with} \quad a_j = \frac{(2j)!}{(j!)^2 4^j} \tag{4.53}$$

and $a_{g-j}a_j \le a_g$ [14, eq. (12.4.5)]. Thus we have

$$P_g(z) = a_g\zeta^g\left(1 + \sum_{j=1}^{g}\frac{a_{g-j}a_j}{a_g}\zeta^{-2j}\right)$$

and with $\rho > \sqrt{2}$

$$\left|P_g(z)\right| \ge a_g\rho^g\left(1 - \sum_{j=1}^{g}\rho^{-2j}\right) \ge a_g\rho^g\frac{\rho^2-2}{\rho^2-1}\ .$$

An estimate for the Legendre functions of the second kind is given in [9, eq. (15)]

$$\left|Q_g(z)\right| \leq \frac{2\rho}{\rho^2-1}\rho^{-g}\,, \qquad z \in \epsilon_\rho\,.$$

From the contour integral formula (4.51) it follows with the length $\ell(\epsilon_\rho)$ of ϵ_ρ that

$$\left|E_g(f)\right| \leq \frac{\ell(\epsilon_\rho)}{\pi}\frac{2}{a_g}\frac{\rho}{\rho^2-2}M(\rho)\rho^{-2g} = C_g^\rho\sqrt{g}\frac{\rho^2}{\rho^2-2}M(\rho)\rho^{-2g}\,,$$

where the factor

$$C_g^\rho = \frac{\ell(\epsilon_\rho)}{\pi\rho}\frac{2}{\sqrt{g}a_g}$$

is uniformly bounded in g and ρ. This is easily seen when using Stirling's formula [1] to estimate a_g defined in (4.53)

$$\frac{1}{\sqrt{\pi g}}e^{-\frac{1}{6g}} \leq a_g \leq \frac{1}{\sqrt{\pi g}}e^{\frac{1}{24g}}\,, \qquad g \geq 1\,,$$

from where the upper bound $C_0 = \frac{3\sqrt{\pi}}{2}\exp\left(\frac{1}{6}\right)$ is derived by elementary arguments. □

Lemma 4.11. *Let $d \geq 3$, $g \geq 1$ and $\sigma(\xi) = a + b\xi$ be a linear function with coefficients $|a| \leq 1$ and $|b| \leq 1$. Then for $f(\xi) = G(\mathbf{r}, d+\xi)\sigma(\xi)$ the estimate*

$$\left|E_g(f)\right| \leq C_1 g^2 d\left(d+\sqrt{d^2-1}\right)^{-2g}$$

holds, where $C_1 = \frac{192}{7}C_0$ with $C_0 = \frac{3\sqrt{\pi}}{2}exp\left(\frac{1}{6}\right)$.

Proof. Since $f(\xi)$ has a singularity at $\xi = -d$ we must choose $\rho \in (\sqrt{2}, d+\sqrt{d^2-1})$ for the extension into the complex plane according to Lemma 4.10. To obtain a tight error bound we must minimize $M(\rho)\rho^{-2g}$. We observe that for $z \in \epsilon_\rho$

$$\left|\frac{1}{(d+z)^{\frac{3}{2}}}\right|\exp\left(-\frac{|\mathbf{r}|^2}{d+z}\right) \leq \left(d - \frac{1}{2}\left(\rho+\frac{1}{\rho}\right)\right)^{-\frac{3}{2}}$$

holds for any $\mathbf{r}$. Therefore, it is sufficient to minimize $(d-1/2(\rho+1/\rho))^{-\frac{3}{2}}\rho^{-2g}$ and simple calculus shows that the optimal ρ is given by $\rho^*(\vartheta)$

$$\rho^*(\vartheta) = \frac{d+\sqrt{d^2-1+\vartheta^2}}{1+\vartheta} \quad \text{with} \quad \vartheta := \tfrac{3}{4g} \in \left[0, \tfrac{3}{4}\right] \subset [0,1]\,.$$

It is easy to see that the function $\rho^*(\vartheta)$ is monotonically decreasing for positive ϑ, hence $\rho^*(\vartheta)$ is in the aforementioned interval of ρ. Moreover, $\rho^*(\vartheta)$ is concave up, thus we have

$$\rho^*(\vartheta) \geq \left(d+\sqrt{d^2-1}\right)(1-\vartheta)\,,$$

where the right hand side is the linearization of $\rho^*(\vartheta)$ at $\vartheta = 0$, which gives us the estimate

$$(\rho^*(\vartheta))^{-2g} \leq \left(d+\sqrt{d^2-1}\right)^{-2g}\left(1-\frac{3}{4g}\right)^{-2g} \leq 16\left(d+\sqrt{d^2-1}\right)^{-2g}, \quad g \geq 1\,. \tag{4.54}$$

Since $d(t) := 1/2(t+1/t)$ for $t > 1$ and $\rho^*(\vartheta)$ are concave up, it follows that the composition $d(\rho^*(\vartheta))$ is concave up as well. Thus we have the estimate

$$d(\rho^*(\vartheta)) \leq d(0) + (d(1)-d(0))\,\vartheta = d - \frac{\vartheta}{2}\left(d-\frac{1}{d}\right),$$

which implies that

$$(d-d(\rho^*(\vartheta)))^{-\frac{3}{2}} \leq \vartheta^{-\frac{3}{2}}\left(\frac{1}{2}\left(d-\frac{1}{d}\right)\right)^{-\frac{3}{2}} = g^{\frac{3}{2}}\left(\frac{3}{8}\left(d-\frac{1}{d}\right)\right)^{-\frac{3}{2}} \leq g^{\frac{3}{2}}, \qquad d \geq 3\,. \tag{4.55}$$

Furthermore, we have $\rho^*(\vartheta) > \rho^*(1) = d$ with the estimate

$$\frac{(\rho^*(\vartheta))^2}{(\rho^*(\vartheta))^2-2} \leq \frac{d^2}{d^2-2} \leq \frac{9}{7}, \qquad d \geq 3 \tag{4.56}$$

and for $z \in \epsilon_\rho$, $|a| \leq 1$ and $|b| \leq 1$ we also have

$$\begin{aligned} |\sigma(z)| &= |a+bz| \leq 1+|z| \leq 1+\frac{1}{2}\left(\rho^*(\vartheta)+\frac{1}{\rho^*(\vartheta)}\right) = 1+d^*(\vartheta) \\ &\leq 1+d^*(0) = 1+d = \left(1+\frac{1}{d}\right)d \leq \frac{4d}{3}, \qquad d \geq 3\,. \end{aligned} \tag{4.57}$$

Finally, the assertion follows from Lemma 4.10, (4.54), (4.55), (4.56) and (4.57). □

4.6.2 Temporal Nearfield Splitting

Since the heat kernel only depends on the difference $t-\tau = (d+\hat{t}-\hat{\tau})h_t$, we define

$$\xi = 2(\hat{t}-\hat{\tau}) \quad \text{and} \quad \eta = 2(\hat{t}-\hat{\tau}-1)$$

for the transformation of (3.9), which yields

$$V_d(\mathbf{r}) = \begin{cases} \sqrt{\frac{h_t}{8}}\int_{-1}^{1}\int_{-(1-\xi)}^{(1-\xi)} G\left(\mathbf{r}\sqrt{\frac{2}{h_t}}, 2d+1+\xi\right)\,\mathrm{d}\eta\mathrm{d}\xi & d=0 \\ \sqrt{\frac{h_t}{8}}\int_{-1}^{1}\int_{-(1+\xi)}^{(1+\xi)} G\left(\mathbf{r}\sqrt{\frac{2}{h_t}}, 2d-1+\xi\right)\,\mathrm{d}\eta\mathrm{d}\xi & \\ \quad +\sqrt{\frac{h_t}{8}}\int_{-1}^{1}\int_{-(1-\xi)}^{(1-\xi)} G\left(\mathbf{r}\sqrt{\frac{2}{h_t}}, 2d+1+\xi\right)\,\mathrm{d}\eta\mathrm{d}\xi & d \geq 1 \end{cases}.$$

After such a rotation we can perform the inner integration explicitly

$$V_d(\mathbf{r}) = \begin{cases} V_d^+(\mathbf{r}) & d = 0 \\ V_d^-(\mathbf{r}) + V_d^+(\mathbf{r}) & d \geq 1 \end{cases} \tag{4.58}$$

with

$$V_d^\pm(\mathbf{r}) = \sqrt{2h_t} \int_{-1}^{1} G\left(\boldsymbol{r}(\mathbf{r}), \mathfrak{d}^\pm(d) + \xi\right) \sigma^\pm(\xi)\, \mathrm{d}\xi \tag{4.59}$$

and the definitions

$$\boldsymbol{r}(\mathbf{r}) := \mathbf{r}\sqrt{\frac{2}{h_t}}\,, \qquad \sigma^\pm(\xi) := \frac{1 \mp \xi}{2}\,, \quad \text{and} \quad \mathfrak{d}^\pm(d) := 2d \pm 1\,.$$

For $\mathfrak{d}^\pm(d) \geq 3$ the kernel in (4.59) is $C^\infty(\mathbb{R}^3 \times [-1,1])$, hence we can apply a Gauss-Legendre quadrature rule of order g

$$V_d^\pm(\mathbf{r}) = \sqrt{2h_t} \left\{ \sum_{i=0}^{g-1} G\left(\boldsymbol{r}(\mathbf{r}), \mathfrak{d}^\pm(d) + \xi_i\right) \sigma^\pm(\xi_i) w_i + E_g^\pm\left(\boldsymbol{r}(\mathbf{r}), \mathfrak{d}^\pm(d)\right) \right\}, \tag{4.60}$$

where $\{\xi_i\}_{i=0}^{g-1}$ and $\{w_i\}_{i=0}^{g-1}$ are the Gauss-Legendre quadrature points and weights, respectively, and the quadrature error $E_g^\pm$ is bounded by Lemma 4.11. Furthermore, this approach directly translates to $K_d^\pm(\mathbf{r})$, ${K'}_d^\pm(\mathbf{r})$ and $D_d^\pm(\mathbf{r})$ by simply exchanging the kernel.

For $\mathfrak{d}^\pm(d) < 3$ the integrands are singular and a composite quadrature rule must be applied. To this end, we introduce a new parameter $0 < \mu < 1$ and consider the following dyadic splitting of the interval

$$[-1,1] = \bigcup_{m=0}^{M} I_m$$

where

$$I_M = [-1, 2\mu^M - 1] \quad \text{and} \quad I_m = \left[2\mu^{m+1} - 1, 2\mu^m - 1\right] \qquad \forall m = 0, \ldots M-1\,.$$

The kernel $V_d^\pm(\mathbf{r})$ with $\mathfrak{d}^\pm(d) = 1$ can now be written as a sum of the kernels

$$V_{0,m}^+(\mathbf{r}),\, V_{1,m}^-(\mathbf{r}) := \sqrt{2h_t} \int_{I_m} G\left(\mathbf{r}\sqrt{\tfrac{2}{h_t}}, 1 + \xi\right) \sigma^+(\xi)\, \mathrm{d}\xi \qquad \forall m = 0, \ldots M\,.$$

The factor M is selected such that the kernels $V_{0,M}^+(\mathbf{r})$ and $V_{1,M}^-(\mathbf{r})$ are sufficiently local in space and, hence, can be evaluated directly with $O(N_x)$ cost, while the integrands of the remaining kernels $V_{0,m}^+(\mathbf{r})$ and $V_{1,m}^-(\mathbf{r})$ for $m < M$ are smooth and approximated by a

Gauss-Legendre quadrature rule similar to (4.60). Transforming I_m to the standard interval leads to

$$V_{0,m}^{+}(\mathbf{r}),\, V_{1,m}^{-}(\mathbf{r}) = \frac{\sqrt{2h_t}}{\sqrt{\mu^m - \mu^{m+1}}} \int_{-1}^{1} G(\boldsymbol{r}_m(\mathbf{r}), \mathfrak{d}_\mu^{\pm} + \xi)\sigma_m^{\pm}(\xi)\, \mathrm{d}\xi \tag{4.61}$$
$$= \frac{\sqrt{2h_t}}{\sqrt{\mu^m - \mu^{m+1}}} \left\{ \sum_{j=0}^{g-1} G(\boldsymbol{r}_m(\mathbf{r}), \mathfrak{d}_\mu^{\pm} + \xi_j)\sigma_m^{\pm}(\xi_j) w_j + E_{g,m}^{\pm}(\boldsymbol{r}_m(\mathbf{r}), \mathfrak{d}_\mu^{\pm}) \right\}$$

with

$$\boldsymbol{r}_m(\mathbf{r}) := \mathbf{r}\sqrt{\frac{2}{h_t(\mu^m - \mu^{m+1})}}\,, \qquad \mathfrak{d}_\mu^{\pm} := \frac{1+\mu}{1-\mu}\,,$$

and

$$\sigma_m^{+}(\xi) := 1 - \left(\frac{\mu^m + \mu^{m+1}}{2} + \frac{\mu^m - \mu^{m+1}}{2}\xi \right),$$
$$\sigma_m^{-}(\xi) := \frac{\mu^m + \mu^{m+1}}{2} + \frac{\mu^m - \mu^{m+1}}{2}\xi\,.$$

We choose $\mu = 1/2$, which leads to $\mathfrak{d}_\mu^{\pm} = 3$ in order to reproduce the same error as for $\mathfrak{d}^{\pm}(d) = 3$. Thus, adding all contributions due to the dyadic splitting

$$\sum_{m=0}^{M-1} \left(\mu^m - \mu^{m+1}\right)^{-\frac{1}{2}} \left| E_{g,m}^{\pm}(\boldsymbol{r}_m(\mathbf{r}), \mathfrak{d}_\mu^{\pm}) \right| \leq C g^2 \mathfrak{d}_\mu^{\pm} \left(\mathfrak{d}_\mu^{\pm} + \sqrt{\mathfrak{d}_\mu^{\pm 2} - 1} \right)^{-2g} \tag{4.62}$$

it turns out that the quadrature error for the singular time steps remains bounded in M and exponentially decaying in the quadrature order due to Lemma 4.11. Last but not least, the operators $V_{1,M}^{\pm}(\mathbf{r})$ still need to be evaluated directly. Hence, in order to limit their complexity to $\mathscr{O}(N_x)$, only contributions in a neighborhood of radius of $\mathscr{O}(h_x)$ should be considered. Since the heat kernel decays in space like $\mathscr{O}(\sqrt{\mu^M h_t})$ this leads to

$$M = \mathscr{O}\left(\log_\mu \left(\frac{h_x^2}{h_t} \right) \right). \tag{4.63}$$

Remark 4.8. *Observe that for $K_{0,m}^{+}(\mathbf{r})$, $K_{1,m}^{-}(\mathbf{r})$, $K'^{+}_{0,m}(\mathbf{r})$, $K'^{-}_{1,m}(\mathbf{r})$, $D_{0,m}^{+}(\mathbf{r})$, and $D_{1,m}^{-}(\mathbf{r})$ the same strategy applies, however, the explicit expressions for $V_{0,M}^{+}(\mathbf{r})$, $V_{1,M}^{-}(\mathbf{r})$, $K_{0,M}^{+}(\mathbf{r})$, $K_{1,M}^{-}(\mathbf{r})$, $K'^{+}_{0,M}(\mathbf{r})$, $K'^{-}_{1,M}(\mathbf{r})$, $D_{0,M}^{+}(\mathbf{r})$, and $D_{1,M}^{-}(\mathbf{r})$ must be computed separately and are listed in Appendix B.2. Observe that the hyper-singular bilinear form exhibits the form of* (3.8)*, where $V_{0,M}^{+}(\mathbf{r})$ and $V_{1,M}^{-}(\mathbf{r})$ can be recycled.*

4.6.3 Spatial Levels for the FGT

From the previous discussion it follows that the kernel $V_d(\mathbf{r})$ can be approximated by some composite Gauss-Legendre quadrature rule. We summarize

$$V_d(\mathbf{r}) \approx \begin{cases} \sum_{j=0}^{g-1} G\left(\boldsymbol{r}(\mathbf{r}), \mathfrak{d}^-(d)+\xi_j\right) \mathfrak{w}_j^- & \\ \qquad + \sum_{j=0}^{g-1} G\left(\boldsymbol{r}(\mathbf{r}), \mathfrak{d}^+(d)+\xi_j\right) \mathfrak{w}_j^+ & d \geq 2 \\ V_{1,M}^-(\mathbf{r}) + \sum_{m=0}^{M-1} \sum_{j=0}^{g-1} G\left(\boldsymbol{r}_m(\mathbf{r}), \mathfrak{d}_\mu^\pm + \xi_j\right) \mathfrak{w}_{j,m}^- & \\ \qquad + \sum_{j=0}^{g-1} G\left(\boldsymbol{r}(\mathbf{r}), 3+\xi_j\right) \mathfrak{w}_j & d = 1 \\ V_{0,M}^+(\mathbf{r}) + \sum_{m=0}^{M-1} \sum_{j=0}^{g-1} G\left(\boldsymbol{r}_m(\mathbf{r}), \mathfrak{d}_\mu^\pm + \xi_j\right) \mathfrak{w}_{j,m}^+ & d = 0 \end{cases}, \tag{4.64}$$

where $\xi_j \in [-1,1]$ are the Gauss points, while $\mathfrak{w}_j^\pm$ and $\mathfrak{w}_{j,m}^\pm$ combine the Gauss weights w_j with the functions $\sigma^\pm(\xi_j)$ and $\sigma_m^\pm(\xi_j)$ and the pre-factors in (4.60) and (4.61), respectively. The layer operators with singular kernels $V_{0,M}^+(\mathbf{r})$ and $V_{1,M}^-(\mathbf{r})$ are local and evaluated directly, while the kernels $G(\boldsymbol{r}(\mathbf{r}), \mathfrak{d}^\pm(d)+\xi_j)$ and $G(\boldsymbol{r}_m(\mathbf{r}), \mathfrak{d}_\mu^\pm + \xi_j)$ are Gaussians and evaluated via FGT. Since the temporal proximity of interactions in these cases is closer than in the temporal farfield, they have to be computed in finer spatial levels. Therefore, we introduce uniform refinements above level L_x by simply adding more levels $L_x^\circ > L_x$ to the spatial cluster-tree of Section 4.1.2 and choose the appropriate level for the FGT such that the truncation error of exponential function's argument is less or equal to the corresponding value for the temporal farfield

$$\frac{|x-y|^2}{\delta} \geq \frac{1}{2} \frac{\left(2h_x^{L_x}(\mathfrak{n}_x+1)\right)^2}{4h_t^{L_t}(d+2)},$$

where the factor $1/2$ is due to Definition 4.6 and the fact that the spatial level only changes with every other temporal level. Thus, with $h_t^{L_t} = n_t h_t/2$ due to Definition 4.1, $d \in \{4,6\}$ for the farfield due to (4.18), and Definition 4.2 we get

$$L_x^\circ \leq L_x + \log_4\left(\frac{32 n_t h_t}{\delta}\right). \tag{4.65}$$

By setting

$$\delta = \begin{cases} 4h_t(d+1) & \mathfrak{d}^\pm(d) \geq 3 \\ 4h_t\mu^m & \mathfrak{d}^\pm(d) < 3 \end{cases}$$

as an upper bound in (4.65) for all quadrature nodes we finally have

$$L_x^\circ = \begin{cases} L_x + \left\lfloor \log_4\left(\frac{8n_t}{d+1}\right)\right\rfloor & \mathfrak{d}^\pm(d) \geq 3 \\ L_x + \left\lfloor \log_4\left(\frac{8n_t}{\mu^m}\right)\right\rfloor & \mathfrak{d}^\pm(d) < 3 \end{cases}. \tag{4.66}$$

Consistency In order to get a similar consistency estimate as with Lemma 4.8 we provide the following lemma, which can be incorporated into Lemma 4.9 to obtain consistent pFMM approximations of variational Galerkin initial boundary value problems.

Lemma 4.12. *Assume that we replace the temporal nearfield of $\mathcal{V}$, i.e., the first term in* (4.45) *by a composite quadrature rule ($\mathcal{V} \to \hat{\mathcal{V}}$) according to* (4.64) *and perform the resulting Gauss transformations by a sum of FGT's ($\hat{\mathcal{V}} \to \dot{\mathcal{V}}_B$). If we chose their spatial Levels L_x° according to* (4.66)*, the dyadic splitting parameter M in agreement with* (4.63)*, the quadrature order $g = \mathcal{O}(\log N_t)$ and the Chebyshev expansion truncation parameter $q = \mathcal{O}(\log N_x^2)$, then we obtain*

$$\left|\left\langle (\mathcal{V} - \dot{\mathcal{V}}_B) q_h^*, w_h \right\rangle_{\Gamma\times\Upsilon}\right| \leq C \left(h_t^{\sigma_t} + h_x^{\sigma_x}\right) \|q_h^*\|_{L_2(\Gamma\times\Upsilon)} \|w_h\|_{L_2(\Gamma\times\Upsilon)}$$

and the error due to the nearfield acceleration can be controlled in analogy to the farfield error in Lemma 4.8.

Proof. With the triangle inequality we have

$$\begin{aligned}\left|\left\langle (\mathcal{V} - \dot{\mathcal{V}}_B) q_h^*, w_h \right\rangle_{\Gamma\times\Upsilon}\right| \leq \left|\left\langle (\mathcal{V} - \hat{\mathcal{V}}) q_h^*, w_h \right\rangle_{\Gamma\times\Upsilon}\right| + \left|\left\langle (\hat{\mathcal{V}} - \hat{\mathcal{V}}_B) q_h^*, w_h \right\rangle_{\Gamma\times\Upsilon}\right| \\ + \left|\left\langle (\hat{\mathcal{V}}_B - \dot{\mathcal{V}}_B) q_h^*, w_h \right\rangle_{\Gamma\times\Upsilon}\right|\end{aligned}$$

and by Lemma 4.11, Cauchy-Schwarz, and $g = \mathcal{O}(\log N_t)$ we get

$$\begin{aligned}\left|\left\langle (\mathcal{V} - \hat{\mathcal{V}}) q_h^*, w_h \right\rangle_{\Gamma\times\Upsilon}\right| &\leq C g^2 d \left(d + \sqrt{d^2-1}\right)^{-2g} |T|\,|\Gamma|\,\|q_h^*\|_{L_2(\Gamma\times\Upsilon)} \|w_h\|_{L_2(\Gamma\times\Upsilon)} \\ &\leq C h_t^{\sigma_t} \|q_h^*\|_{L_2(\Gamma\times\Upsilon)} \|w_h\|_{L_2(\Gamma\times\Upsilon)} \,.\end{aligned}$$

Choosing $L_x^\circ \geq L_x$ according to (4.66) we can control the spatial cutoff error, i.e., the second term with the same $\mathfrak{n}_x$ as for the farfield. Finally, since we have a maximum of gM FGT's we use Cauchy-Schwarz and $q = \mathcal{O}(\log N_x^2)$ to conclude the proof similar to Lemma 4.6

$$\begin{aligned}\left|\left\langle (\hat{\mathcal{V}}_B - \dot{\mathcal{V}}_B) q_h^*, w_h \right\rangle_{\Gamma\times\Upsilon}\right| &\leq C g M \frac{(q+6)^6}{\sqrt{\delta^3}} \left(\frac{1}{a-1}\right)^{q+1} |T|\,|\Gamma|\,\|q_h^*\|_{L_2(\Gamma\times\Upsilon)} \|w_h\|_{L_2(\Gamma\times\Upsilon)} \\ &\leq C h_x^{\sigma_x} \|q_h^*\|_{L_2(\Gamma\times\Upsilon)} \|w_h\|_{L_2(\Gamma\times\Upsilon)} \,.\end{aligned}$$

□

Observe that the computational complexity is reduced to $\mathcal{O}(N_x)$ for the direct evaluations and gM times the complexity of an FGT. Since both, g and M, depend only logarithmically on the number of unknowns, this is a nearly optimal reduction of computational cost. Note that the verification of this estimate and Lemma 4.12 is postponed to Chapter 5.

Example 4.7. *With this example we want to numerically confirm the behavior of the quadrature error for* $\mathfrak{d}^{\pm}(d) \geq 3$*. According to Lemma 4.11 it is exponentially decaying, which is nicely confirmed by the semi-logarithmic plots in Figure 4.13.*

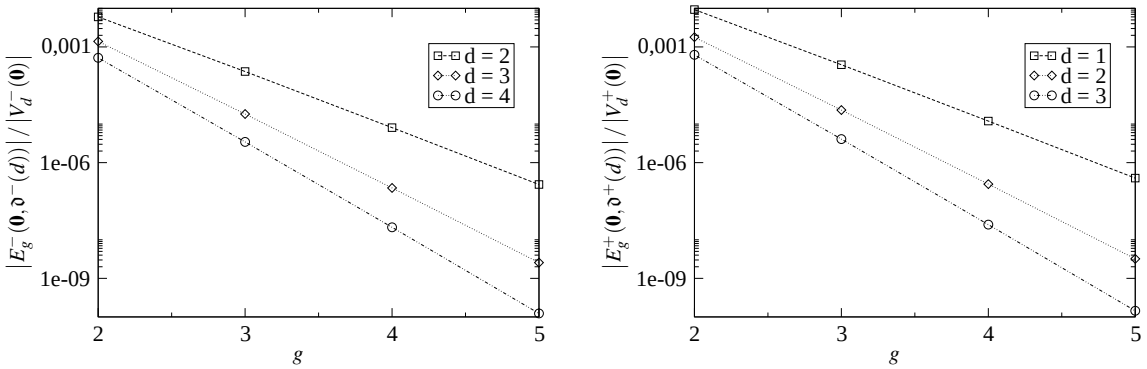

(a) $\left|E_g^-(\mathbf{0},\mathfrak{d}^-(d))\right| / \left|V_d^-(\mathbf{0})\right|$ vs. g (b) $\left|E_g^+(\mathbf{0},\mathfrak{d}^+(d))\right| / \left|V_d^+(\mathbf{0})\right|$ vs. g

Figure 4.13: Quadrature error at $\boldsymbol{r}(\mathbf{r}) = \mathbf{0}$ vs. quadrature order g.

Example 4.8. *In contrast to the previous example we want to confirm the quadrature error for* $\mathfrak{d}^{\pm}(d) < 3$ *which results in* $\mathfrak{d}_{\mu}^{\pm} = 3$*. Thus in Table 4.7 we present the relative quadrature error*

$$\sqrt{2h_t}\sum_{m=0}^{M-1}\left(\mu^m - \mu^{m+1}\right)^{-\frac{1}{2}}\left|E_{g,m}^{\pm}(\boldsymbol{r}_m(\mathbf{r}),\mathfrak{d}_{\mu}^{\pm})\right| / \left|V_1^{\pm}(\boldsymbol{r}_m(\mathbf{r}),\mathfrak{d}_{\mu}^{\pm})\right|$$

and observe that it is still exponentially decaying in the quadrature order g and bounded in M as predicted by (4.62)*.*

	$M=1$	$M=4$	$M=7$	$M=10$	$M=13$
$g=2$	9.70×10^{-5}	2.48×10^{-4}	3.02×10^{-4}	3.21×10^{-4}	3.27×10^{-4}
$g=3$	2.42×10^{-6}	6.21×10^{-6}	7.55×10^{-6}	8.02×10^{-6}	8.19×10^{-6}
$g=4$	6.31×10^{-8}	1.61×10^{-7}	1.96×10^{-7}	2.08×10^{-7}	2.13×10^{-7}
$g=5$	1.68×10^{-9}	4.31×10^{-9}	5.24×10^{-9}	5.57×10^{-9}	5.69×10^{-9}

Table 4.7: Relative quadrature error at $\boldsymbol{r}_m(\mathbf{r}) = \mathbf{0}$ vs. order g and M.

5 NUMERICAL EXAMPLES

5.1 Benchmark Tests

In this section, we continue Examples 3.1 through 3.4 by means of pFMM accelerated layer potentials, which serves as a verification of Lemma 4.8 and Lemma 4.9. Thus we solve the homogeneous initial boundary value problems described in Section 2.4 for $\Omega = (-0.5,0.5)^3$ and $t \in \Upsilon = (0,0.5)$. In all cases, we choose the boundary data corresponding to a heat point source $g_D(\mathbf{x},t) = G(\mathbf{x}-\mathbf{x}_0,t)$, $g_N^*(\mathbf{x},t) = \alpha\partial_{\mathbf{n}_\mathbf{x}} G(\mathbf{x}-\mathbf{x}_0,t)$, and $g_R^*(\mathbf{x},t) = \alpha\partial_{\mathbf{n}_\mathbf{x}} G(\mathbf{x}-\mathbf{x}_0,t) + \kappa^*(\mathbf{x})G(\mathbf{x}-\mathbf{x}_0,t)$ located at $\mathbf{x}_0 := (1.5,1.5,1.5)^\top$ with $\alpha, \kappa^* = 1$.

In all examples of this section we have chosen the parameters $p, q, \mathfrak{n}_x, g, M$ such that the convergence rates of the Galerkin scheme derived in Section 3.2 according to Lemmas 4.8, 4.9, and 4.12 are preserved. We would like to remark that a choice of $\mathfrak{n}_x = 2$ was sufficient for all computations below (due to discretization and clustering parameters). Furthermore, we would like to emphasize that we have chosen $g = 5$ for all composite quadrature rules in the parabolic nearfield, which seems to be justified by the results.

Since all systems are elliptic, the related Galerkin discretized matrices (sub matrices of the block Töplitz system) turn out to be symmetric and positive definite. Therefore, we use a conjugate gradient (CG) solver with a block diagonal preconditioner in each time step (based on the explicitly computed information of the first time step).

Finally, for sake of readability we write $\mathcal{V}$ instead of $\dot{\mathring{\mathcal{V}}}$ and q_h^* instead of $\dot{\mathring{q}}_h^*$, i.e., we omit all accents from operator approximations in Chapter 4.

5.1.1 Initial Dirichlet BVP

In our first example we present some further refinement levels to Example 3.1. We solve the pFMM approximated variational form related to the initial Dirichlet boundary value problem (3.17), i.e., find $\bar{q}_h^* \in S_{h_x,h_t}^{d_0,d_0}(\Gamma\times\Upsilon)$ such that

$$\langle \mathcal{V}\bar{q}_h^*, w_h\rangle_{\Gamma\times\Upsilon} = \left\langle \left(\tfrac{\mathcal{I}}{2} + \mathcal{K}\right)\bar{g}_D, w_h\right\rangle_{\Gamma\times\Upsilon} \qquad \forall w_h \in S_{h_x,h_t}^{d_0,d_0}(\Gamma\times\Upsilon)$$

with the perturbed right hand side $\bar{g}_D = \mathcal{Q}_{h_t}^{d_0}\mathcal{Q}_{h_x}^{c_1} g_D \in S_{h_x,h_t}^{c_1,d_0}(\Gamma\times\Upsilon)$. Instead of presenting results for $h_t = \mathcal{O}(h_x^a)$ with arbitrary $a \geq 0$ we focus on two special cases.

In Table 5.1, Figure 5.1, and Figure 5.2 we present some further results for $h_t = \mathcal{O}(h_x^2)$. Despite previous arguments regarding the awkwardness of $\bar{q}_h \in S^{d_0,d_0}_{h_x,h_t}(\Gamma \times \Upsilon)$ in combination with $h_t = \mathcal{O}(h_x^2)$ they show the optimality of our scheme with respect to the total number of unknowns $N_x N_t$. Observe that in order to maintain the $\mathcal{O}(\sqrt{h_t})$ behavior of the Galerkin scheme we only have to increase the temporal interpolation order p and the Chebyshev expansion truncation order q very slowly as predicted by Lemma 4.9. Finally, we observe that the block diagonal preconditioner seems to work well, as the number of iterations is independent of the refinement level.

$N_x N_t$	L_x/L_t	q/p	$\|q^* - \bar{q}_h^*\|_{L_2}/\|q^*\|_{L_2}$	$\#^{\mathbf{V}_0}_{CG}$	cpu[sec]	mem[GB]
12,288	0/5	22/3	$1.23\ 10^{-1}$	6	$4.68\ 10^{1}$	$5.90\ 10^{-2}$
196,608	1/7	24/4	$6.07\ 10^{-2}$	6	$1.87\ 10^{2}$	$2.15\ 10^{-1}$
3,145,728	2/9	26/5	$3.01\ 10^{-2}$	6	$3.35\ 10^{3}$	$1.08\ 10^{0}$
50,331,648	3/11	28/6	$1.50\ 10^{-2}$	6	$1.05\ 10^{5}$	$6.10\ 10^{0}$

Table 5.1: Dirichlet IBVP with uniform space-time refinement – $h_t = \mathcal{O}(h_x^2)$.

$N_x N_t$	L_x°/L_t	q/p	M	$\|q^* - \bar{q}_h^*\|_{L_2}/\|q^*\|_{L_2}$	$\#^{\mathbf{V}_0}_{CG}$	cpu[sec]	mem[GB]
12,288	0/5	22/3	0	$1.23\ 10^{-1}$	6	$4.68\ 10^{1}$	$5.90\ 10^{-2}$
49,152	1/5	24/3	2	$6.35\ 10^{-2}$	8	$1.78\ 10^{2}$	$2.88\ 10^{-1}$
196,608	2/5	26/3	4	$3.63\ 10^{-2}$	11	$9.34\ 10^{2}$	$1.74\ 10^{0}$
786,432	3/5	28/3	6	$2.54\ 10^{-2}$	17	$5.85\ 10^{3}$	$1.05\ 10^{1}$

Table 5.2: Dirichlet IBVP with uniform space refinement – $h_t = \mathcal{O}(h_x^0)$.

Finally, in Table 5.2, Figure 5.1, and Figure 5.2 we present more details for a purely spatial refinement, i.e., $h_t = \mathcal{O}(h_x^0)$. A naive application of the pFMM algorithm for such a scheme leads to non optimal complexity due to the quadratic nearfield growth. The simple explanation for this behavior is that the spatial truncation is linked to the temporal discretization. Since in this case we have a fixed temporal discretization, the number of spatial interactions grows like $\mathcal{O}(N_x^2)$. The composite quadrature rule described in Section 4.6 resolves this problem by localizing spatial contributions (M is the dyadic splitting parameter), which in combination with the FGT leads to an optimal nearfield evaluation. One may wonder why the number of iterations in this case grows compared to the previously described optimal refinement scheme, where only a constant number of iterations was required. The simple reason for this behavior is that the dyadic splitting reduces the information contained in the block-diagonal preconditioner, which is why it does not work properly any more. Furthermore, observe that the dyadic splitting parameter M grows like $\mathcal{O}(logN_x)$ (4.63) which adds further complexity.

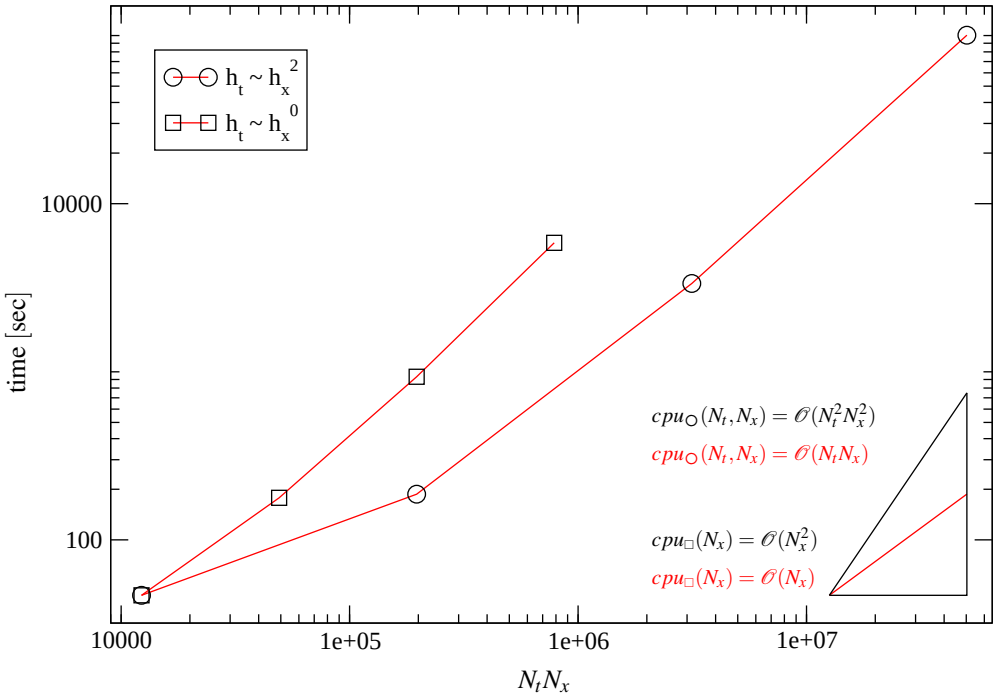

Figure 5.1: Dirichlet IBVP – computational complexity of the pFMM.

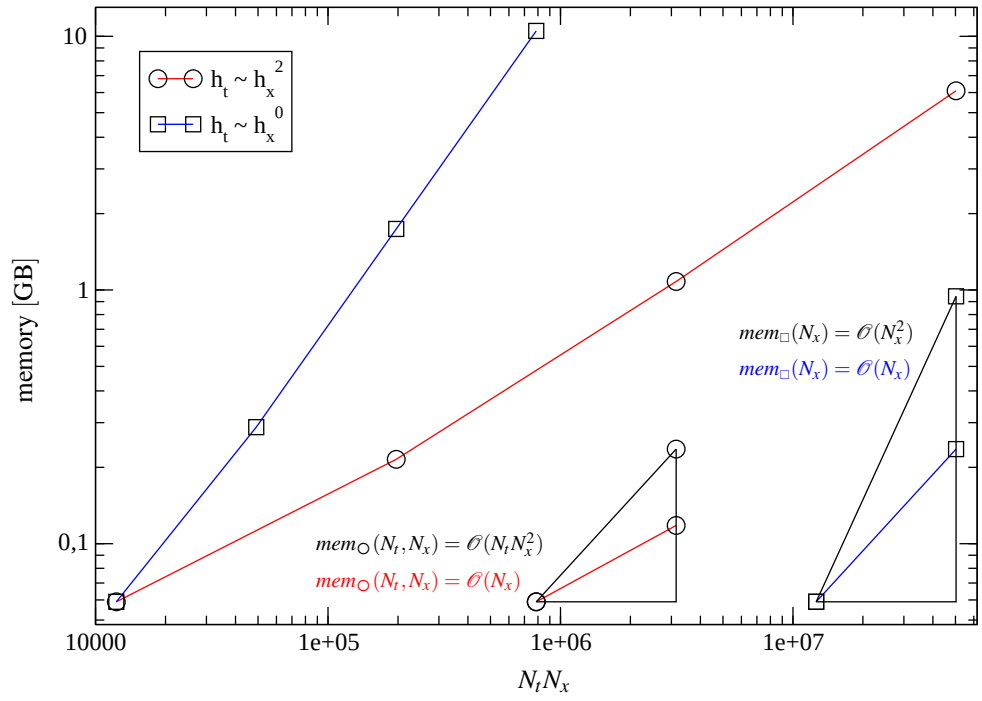

Figure 5.2: Dirichlet IBVP – memory consumption of the pFMM.

Comparing the second row of Table 5.1 with the finest discretization of Example 3.1 reveals that even at this coarse discretization level, the pFMM performs already much better then the standard formulation, i.e., 187 sec vs. 4270 sec and 0.22 GB vs. 3.5 GB. Extrapolating these numbers due to the quadratic complexity of the standard method would lead to almost 9 years of computation time for the last refinement level in Table 5.1, assuming we had 7.2 TB of memory.

5.1.2 Initial Neumann BVP

We solve the pFMM approximated variational form related to the initial Neumann boundary value problem (3.21), i.e., find $\bar{u}_h \in S^{c_1,d_0}_{h_x,h_t}(\Gamma \times \Upsilon)$ such that

$$\langle \mathcal{D}\bar{u}_h, v_h \rangle_{\Gamma\times\Upsilon} = \left\langle \left(\tfrac{\mathcal{I}}{2} - \mathcal{K}'\right) \bar{g}^*_N, v_h \right\rangle_{\Gamma\times\Upsilon} \qquad \forall v_h \in S^{c_1,d_0}_{h_x,h_t}(\Gamma \times \Upsilon)$$

with the perturbed right hand side $\bar{g}^*_N = \mathcal{Q}^{d_0}_{h_t}\mathcal{Q}^{d_0}_{h_x} g^*_N \in S^{d_0,d_0}_{h_x,h_t}(\Gamma \times \Upsilon)$. Observe that the following results are due to some further refinements of Example 3.2 focusing on the two strategies $h_t = \mathscr{O}(h_x^a)$ with $a = 2$ and $a = 0$, respectively.

In Table 5.3, Figure 5.3, and Figure 5.4 we present more results including computation time and memory requirement for a $h_t = \mathscr{O}(h_x^2)$ refinement. Table 5.3 reveals that the temporal interpolation order p and the spatial Chebyshev expansion truncation parameter q only have to be increased very slowly to maintain the optimal $\mathscr{O}(h_t)$ behavior of the space-time Galerkin scheme as predicted by Lemma 4.9. Furthermore, Table 5.3, Figure 5.3, and Figure 5.4 show that this choice still maintains almost optimal complexity in terms of computation time and memory consumption. In order to show that this is not just the case for $h_t = \mathscr{O}(h_x^a)$ with $a = 2$ but also for $a < 2$ we present more details for $a = 0$ in Table 5.4, Figure 5.3, and Figure 5.4. Observe that the dyadic splitting of the nearfield according to Section 4.6 leads to optimal complexity just like for the initial Dirichlet boundary value problem before. We note that the number of CG iterations increases for the same reason as in the previous example, which is why the computational complexity of the pFMM for the $h_t = \mathscr{O}(h_x^0)$ refinement is somewhat less obvious.

$N_x N_t$	L_x/L_t	q/p	$\|u-\bar{u}_h\|_{L_2}/\|u\|_{L_2}$	$\#^{\mathbf{D}_0}_{CG}$	cpu[sec]	mem[GB]
6,208	0/5	23/3	$2.74\ 10^{-2}$	5	$1.05\ 10^{2}$	$4.95\ 10^{-2}$
98,560	1/7	26/4	$6.65\ 10^{-3}$	5	$3.61\ 10^{2}$	$2.14\ 10^{-1}$
1,573,888	2/9	29/5	$1.67\ 10^{-3}$	5	$4.82\ 10^{3}$	$1.09\ 10^{0}$
25,169,920	3/11	32/6	$4.18\ 10^{-4}$	5	$1.44\ 10^{5}$	$7.20\ 10^{0}$

Table 5.3: Neumann IBVP with uniform space-time refinement – $h_t = \mathscr{O}(h_x^2)$.

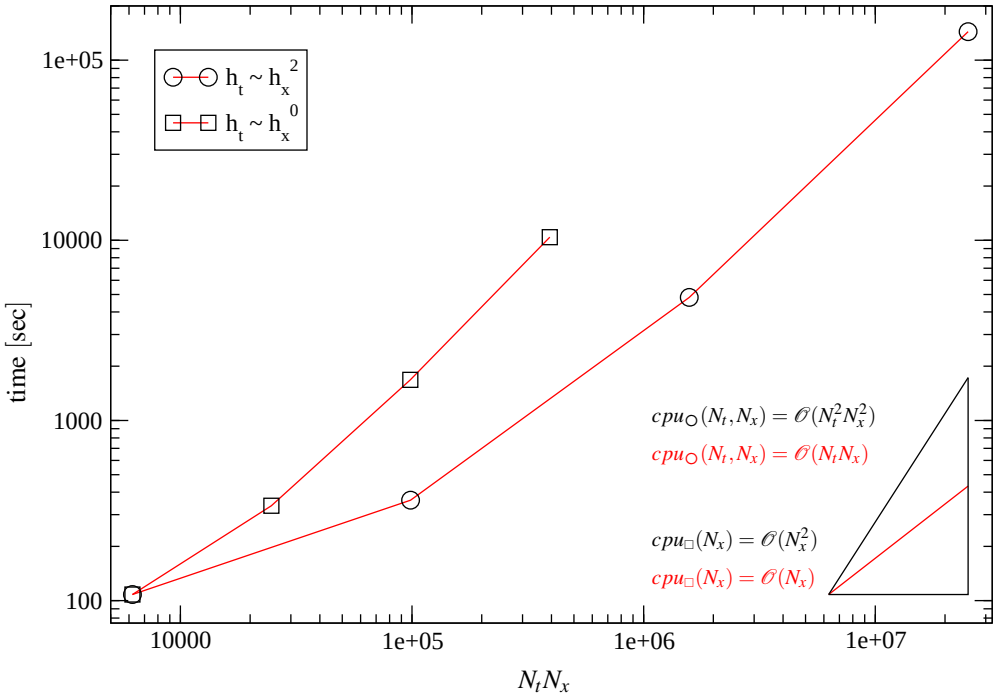

Figure 5.3: Neumann IBVP – computational complexity of the pFMM.

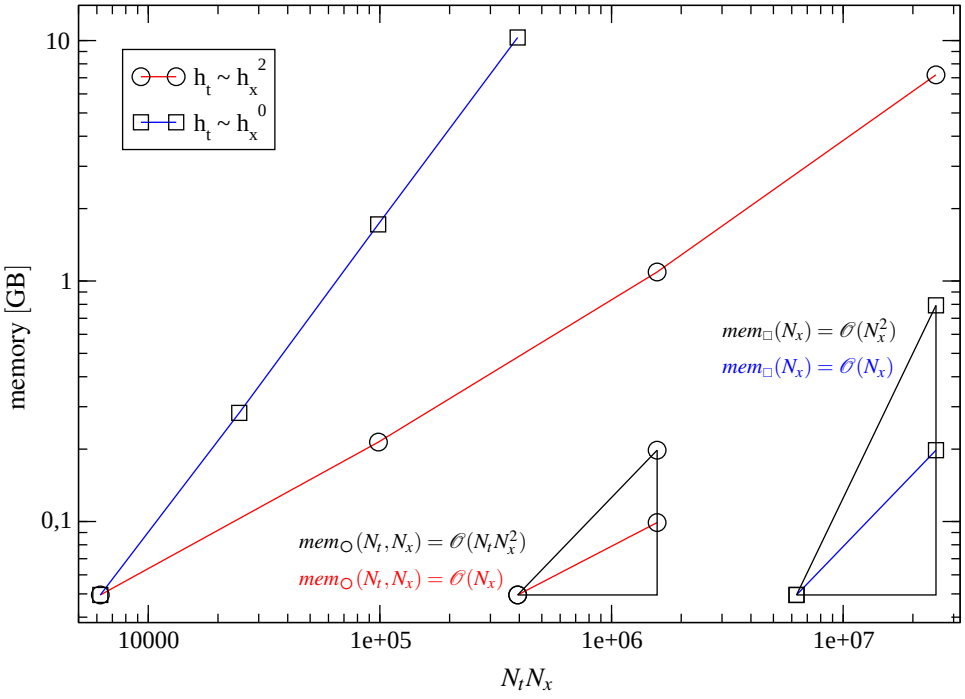

Figure 5.4: Neumann IBVP – memory consumption of the pFMM.

N_xN_t	L_x°/L_t	q/p	M	$\|u-\bar{u}_h\|_{L_2}/\|u\|_{L_2}$	$\#_{CG}^{\mathbf{D}_0}$	cpu[sec]	mem[GB]
6,208	0/5	23/3	0	2.74 10^{-2}	5	1.05 10^2	4.95 10^{-2}
24,704	1/5	26/3	2	2.21 10^{-2}	6	3.36 10^2	2.83 10^{-1}
98,368	2/5	29/3	4	2.19 10^{-2}	9	1.68 10^3	1.92 10^0
393,280	3/5	32/3	6	2.19 10^{-2}	14	1.04 10^4	1.24 10^1

Table 5.4: Neumann IBVP with uniform space refinement – $h_t = \mathcal{O}(h_x^0)$.

Comparing the second row of Table 5.3 with the finest discretization of Example 3.2 shows again that even at this coarse discretization level, the pFMM performs much better then the standard formulation, i.e., 361 sec vs. 6510 sec and 0.21 GB vs. 1.8 GB. Extrapolating these numbers due to the quadratic complexity of the standard method would lead to more than 13 years of computation time for the finest level in Table 5.3, assuming we had 3.7 TB of memory.

5.1.3 Initial Robin BVP

We solve the pFMM approximated variational form related to the initial Robin boundary value problem (3.28), i.e., find $\bar{u}_h \in S_{h_x,h_t}^{c_1,d_0}(\Gamma \times \Upsilon)$ such that

$$\left\langle (\bar{\mathcal{S}} + \kappa^*)\bar{u}_h, v_h \right\rangle_{\Gamma\times\Upsilon} = \langle g_R^*, v_h \rangle_{\Gamma\times\Upsilon} \qquad \forall v_h \in S_{h_x,h_t}^{c_1,d_0}(\Gamma \times \Upsilon)$$

with the perturbed right hand side $\bar{g}_R^* = \mathcal{Q}_{h_t}^{d_0}\mathcal{Q}_{h_x}^{d_0} g_R^* \in S_{h_x,h_t}^{d_0,d_0}(\Gamma \times \Upsilon)$ and the pFMM version of the symmetric approximation of the Steklov-Poincaré operator in Lemma 3.3. In the following, we present some further refinement levels to Example 3.3 focusing on the two strategies $h_t = \mathcal{O}(h_x^a)$ with $a = 2$ and $a = 0$, respectively, just like in the previous two sections. However, observe that due to the symmetric approximation of the Steklov Poincaré operator we need to solve the initial Dirichlet boundary value problem (3.26) in each iteration, thus the two iteration numbers in Table 5.5 and Table 5.6.

N_xN_t	L_x/L_t	q/p	$\|u-\bar{u}_h\|_{L_2}/\|u\|_{L_2}$	$\#_{CG}^{\mathbf{V}_0}/\#_{CG}^{\mathbf{D}_0}$	cpu[sec]	mem[GB]
6,208	0/5	23/3	2.19 10^{-2}	10/9	1.47 10^2	8.83 10^{-2}
98,560	1/7	26/4	5.46 10^{-3}	10/9	5.08 10^2	3.55 10^{-1}
1,573,888	2/9	29/5	1.36 10^{-3}	10/9	8.45 10^3	2.00 10^0
25,169,920	3/11	32/6	3.41 10^{-4}	10/9	2.69 10^5	1.23 10^1

Table 5.5: Robin IBVP with uniform space-time refinement – $h_t = \mathcal{O}(h_x^2)$.

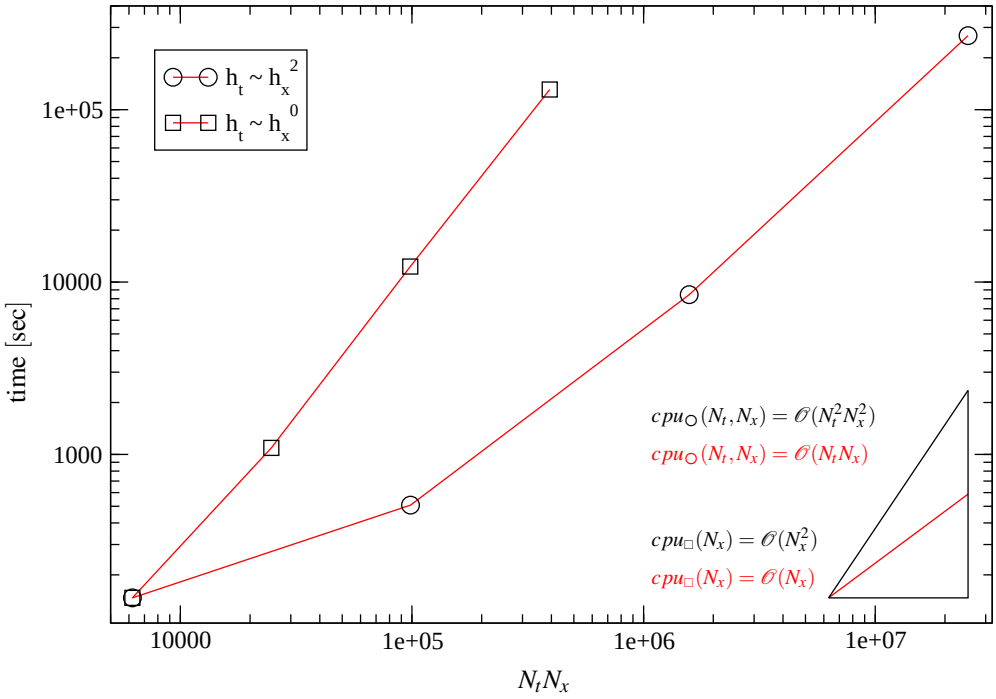

Figure 5.5: Robin IBVP – computational complexity of the pFMM.

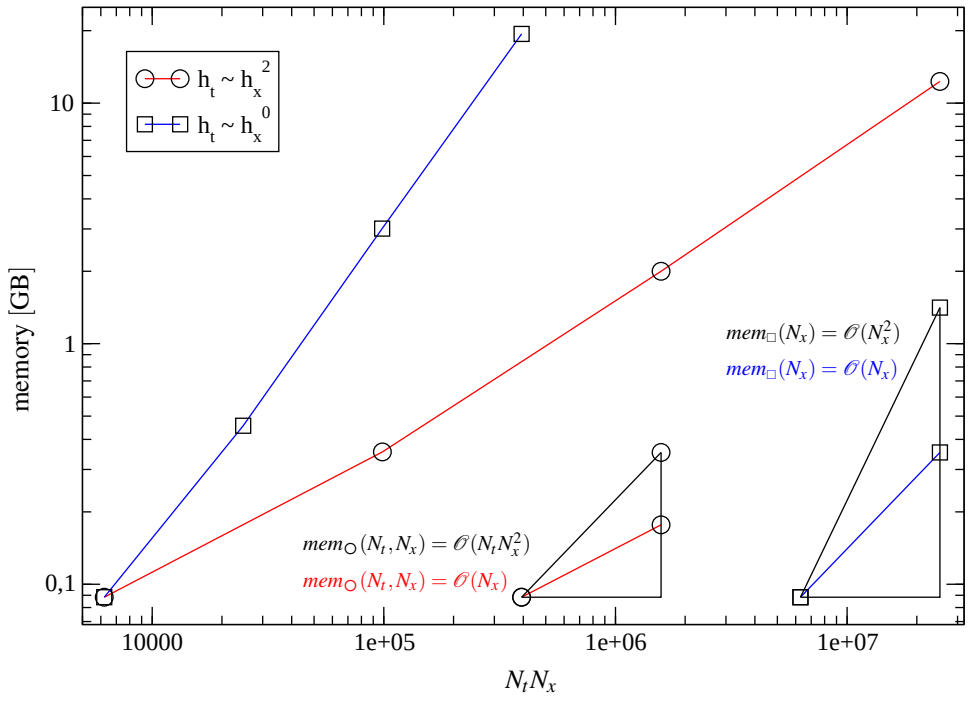

Figure 5.6: Robin IBVP – memory consumption of the pFMM.

N_xN_t	L_x°/L_t	q/p	M	$\|u-\bar{u}_h\|_{L_2}/\|u\|_{L_2}$	$\#_{CG}^{\mathbf{V}_0}/\#_{CG}^{\mathbf{D}_0}$	cpu[sec]	mem[GB]
6,208	0/5	23/3	0	$2.19\ 10^{-2}$	10/9	$1.47\ 10^{2}$	$8.83\ 10^{-2}$
24,704	1/5	26/3	2	$2.11\ 10^{-2}$	10/9	$1.09\ 10^{3}$	$4.56\ 10^{-1}$
98,368	2/5	29/3	4	$2.10\ 10^{-2}$	12/11	$1.23\ 10^{4}$	$3.01\ 10^{0}$
393,280	3/5	32/3	6	$2.10\ 10^{-2}$	17/15	$1.31\ 10^{5}$	$1.94\ 10^{1}$

Table 5.6: Robin IBVP with uniform space refinement – $h_t = \mathscr{O}(h_x^0)$.

In Table 5.5, Figure 5.5, and Figure 5.6 we present more details on a $h_t = \mathscr{O}(h_x^2)$ refinement scheme. They reveal that only a slight increase of the Lagrange interpolation order p and Chebyshev expansion truncation order q is required to maintain the optimal order of convergence at almost optimal complexity as stated by Lemma 4.9. After the previous two examples it seems needless to mention that the presented method remains optimal also for $h_t = \mathscr{O}(h_x^0)$, nonetheless, for completeness sake the confirmation can be found in Table 5.6 and Figure 5.6. However, observe that both iteration numbers – $\#_{CG}^{\mathbf{V}_0}$ and $\#_{CG}^{\mathbf{D}_0}$ – grow for the same reason as in the previous two examples. Unfortunately though, because of the nested solution scheme, the consequence is more severe then in those previous examples as can be seen in Table 5.6 and Figure 5.5.

Nonetheless, if we compare the second row of Table 5.5 and Table 5.6 with the finest discretization of Example 3.3, we see that even at this coarse discretization level, the pFMM performs much better then the standard formulation. An extrapolation with the standard formulation's complexity would lead to more than 17 years and 11 TB for the finest level of Table 5.5 and 24 days and 1.4 TB for the finest level of Table 5.6, which, despite the issue with the growing iteration numbers within the nested solution scheme, is much more than the actual cost of the pFMM version reported in Table 5.5 and Table 5.6.

5.1.4 Initial Dirichlet-Neumann-Robin BVP

Finally, in our last benchmark problem we solve the pFMM approximated variational form of the mixed initial Dirichlet-Neumann-Robin boundary value problem (3.32), i.e., find $\bar{\tilde{u}}_h \in S_{h_x,h_t}^{c_1,d_0}(\Gamma_{NR}\times\Upsilon) := S_{h_x,h_t}^{c_1,d_0}(\Gamma\times\Upsilon)\cap\widetilde{H}^{\frac{1}{2},\frac{1}{4}}(\Gamma_{NR}\times\Upsilon)$ such that

$$\left\langle(\bar{\mathcal{S}}+\kappa^*)\bar{\tilde{u}}_h, v_h\right\rangle_{\Gamma\times\Upsilon} = \left\langle\bar{g}_{NR}^* - (\bar{\mathcal{S}}+\kappa^*)\bar{\tilde{g}}_D, v_h\right\rangle_{\Gamma\times\Upsilon} \qquad \forall v_h \in S_{h_x,h_t}^{c_1,d_0}(\Gamma_{NR}\times\Upsilon)$$

with the perturbed right hand side $\bar{g}_{NR}^* = \mathcal{Q}_{h_x}^{d_0}\mathcal{Q}_{h_t}^{d_0} g_{NR}^* \in S_{h_x,h_t}^{d_0,d_0}(\Gamma_{NR}\times\Upsilon) := S_{h_x,h_t}^{d_0,d_0}(\Gamma\times\Upsilon)\cap H^{-\frac{1}{2},-\frac{1}{4}}(\Gamma_{NR}\times\Upsilon)$ and $\bar{\tilde{g}}_D = \mathcal{Q}_{h_x}^{c_1}\mathcal{Q}_{h_t}^{d_0}\tilde{g}_D \in S_{h_x,h_t}^{c_1,d_0}(\Gamma\times\Upsilon)$ and the pFMM version of the symmetric approximation of the Steklov-Poincaré operator in Lemma 3.3. In the following, we present some further refinement levels to Example 3.4 focusing again on the two refinement strategies $h_t = \mathscr{O}(h_x^a)$ with $a = 2$ and $a = 0$, respectively.

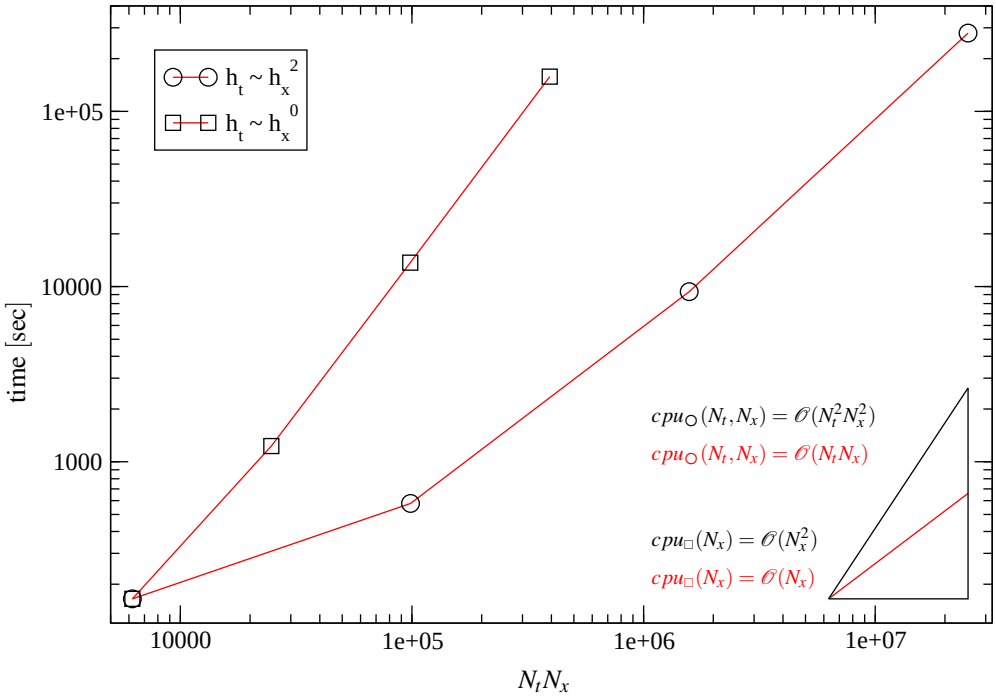

Figure 5.7: Mixed IBVP – computational complexity of the pFMM.

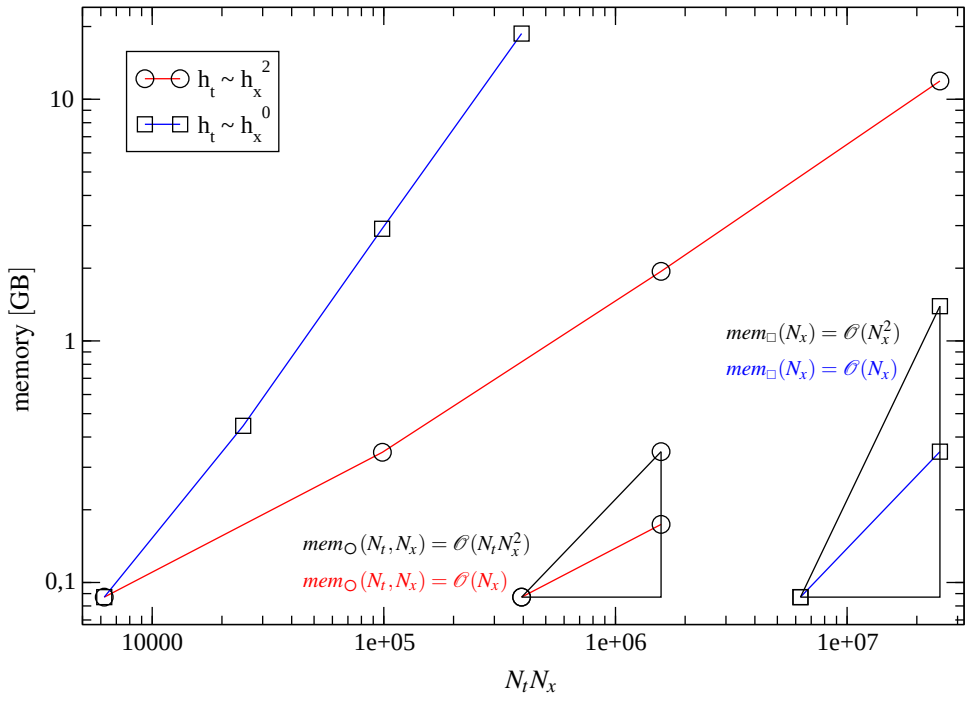

Figure 5.8: Mixed IBVP – memory consumption of the pFMM.

To avoid confusion, we recap the definitions of the respective boundaries, i.e., in Example 3.4 we had $\Omega = (-0.5,0.5)^3$ with $\Gamma_D = (-0.5,0.5) \times -0.5 \times (-0.5,0.5)$, $\Gamma_N = (-0.5,0.5) \times 0.5 \times (-0.5,0.5)$, and $\overline{\Gamma}_R = \Gamma \setminus (\overline{\Gamma}_N \cup \overline{\Gamma}_D)$.

$N_x N_t$	L_x/L_t	q/p	$\|u-\bar{u}_h\|_{L_2}/\|u\|_{L_2}$	$\#^{\mathbf{V}_0}_{CG}/\#^{\mathbf{D}_0}_{CG}$	cpu[sec]	mem[GB]
6,208	0/5	23/3	$2.19\ 10^{-2}$	10/9	$1.65\ 10^{2}$	$8.70\ 10^{-2}$
98,560	1/7	26/4	$5.45\ 10^{-2}$	10/9	$5.78\ 10^{2}$	$3.46\ 10^{-1}$
1,573,888	2/9	29/5	$1.36\ 10^{-3}$	10/9	$9.35\ 10^{3}$	$1.94\ 10^{0}$
25,169,920	3/11	32/6	$3.41\ 10^{-4}$	10/9	$2.80\ 10^{5}$	$1.19\ 10^{1}$

Table 5.7: Mixed IBVP with uniform space-time refinement – $h_t = \mathcal{O}(h_x^2)$.

$N_x N_t$	L_x°/L_t	q/p	M	$\|u-\bar{u}_h\|_{L_2}/\|u\|_{L_2}$	$\#^{\mathbf{V}_0}_{CG}/\#^{\mathbf{D}_0}_{CG}$	cpu[sec]	mem[GB]
6,208	0/5	23/3	0	$2.19\ 10^{-2}$	10/9	$1.65\ 10^{2}$	$8.70\ 10^{-2}$
24,704	1/5	26/3	2	$2.11\ 10^{-2}$	10/9	$1.23\ 10^{3}$	$4.45\ 10^{-1}$
98,368	2/5	29/3	4	$2.10\ 10^{-2}$	13/12	$1.37\ 10^{4}$	$2.91\ 10^{0}$
393,280	3/5	32/3	6	$2.10\ 10^{-2}$	18/17	$1.58\ 10^{5}$	$1.87\ 10^{1}$

Table 5.8: Mixed IBVP with uniform space refinement – $h_t = \mathcal{O}(h_x^0)$.

In Table 5.7, Table 5.8, Figure 5.7, and Figure 5.8 we find the confirmation that our method remains optimal in the number of unknowns for this initial boundary value problem as well, regardless the refinement scheme. Again, note optimality is not so obvious in terms of computational complexity for the $h_t = \mathcal{O}(h_x^0)$ because the number of inner and outer iterations increases which heavily affects the complexity due to the nested solution scheme.

Nonetheless, if we compare the second row of Table 5.7 and Table 5.8 with the finest discretization of Example 3.4, we observe that even at such a coarse discretization, the pFMM performs much better then the standard formulation. An extrapolation of Example 3.4's results would lead to more than 14 years and 8.4 TB for the finest level of Table 5.7 and still 21 days and about 1 TB for the finest level of Table 5.8, which, despite the issue with the growing iteration numbers within the nested solution scheme, is much more than the actual cost of the pFMM version reported in Table 5.7 and Table 5.8.

Remark 5.1. *If, instead of using the dyadic splitting strategy for the case $h_t = \mathcal{O}(h_x^0)$, we had kept $M = 0$ in all spatial refinement levels of the $h_t = \mathcal{O}(h_x^0)$ refinement strategy, we would have gotten a bounded number of iterations (at a quadratic complexity in N_x). The explanation lies in the preconditioner, which due to the dyadic splitting becomes more and more localized as M increases. This observation suggests to use a different preconditioning strategy, namely, instead of using a block diagonal preconditioner based on the localized nearfield one should use information from the whole first time step.*

5.2 Industrial Applications

5.2.1 The Press Hardening Process

Process description Press hardening (form hardening, hot forming) is a sheet metal forming process for the production of high-strength structural parts, mainly used in the automotive industry [51]. This process basically consists of the following steps shown in Figure 5.9: Waiting for the hot blank, closing of the binder and upper tool, fast forming, and rapid cooling of the blank in the closed and cooled tool.

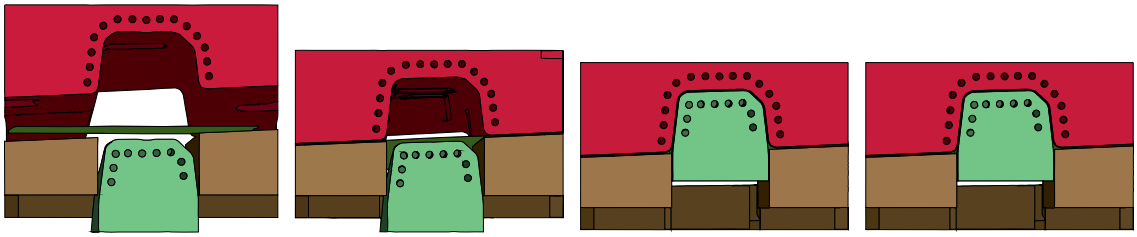

(a) Waiting. (b) Closing. (c) Forming. (d) Cooling.

Figure 5.9: Schematic press hardening process.

Press hardened components have two major advantages over cold formed ones. First, due to the fact that the hardening process takes place in the closed tool, the allotropic transformation of the micro-structure happens after the forming process, which reduces residual stresses and spring-back effects within the finished part. Second, the layout of the cooling channels allows to steer the local cooling rate of the tool and, hence, of the metal sheet. Since the mechanical properties of the formed components strongly depend on the cooling rate (e.g. a cooling rate of $27\,{}^{\circ\mathrm{C}}/_{\mathrm{sec}}$ is required to obtain a martensitic micro-structure for the widely used boron alloyed press hardening steel 22MnB5), it turns out that the press hardening process can be used to produce lightweight structural parts with distinct material properties in different regions.

Up until now it was common practice to neglect the hot forming tools within the overall simulation in the sense that they were only regarded as rigid bodies with constant temperature. Weiss [51] proposed to overcome this crude approximation by an isolated simulation of the press hardening tools without considering the overall thermal-mechanically coupled process. His approach enables the design engineer to simulate and adapt the cooling performance of the tools within the design phase. As already mentioned earlier, the material properties of the final component depends on the cooling rate, which is linked to the temperature difference between the part and the tools. Hence, the design relevant thermal quantity is the surface temperature of the hot forming tools. This observation together with the fact that these tools and the cooling channel geometry can be almost arbitrarily com-

plicated suggests to use a direct Boundary Element Method for their thermal simulation.

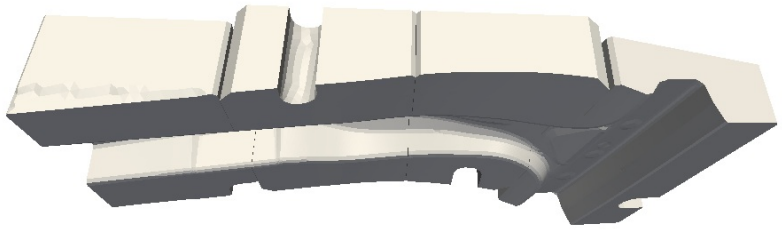

(a) Upper tool.

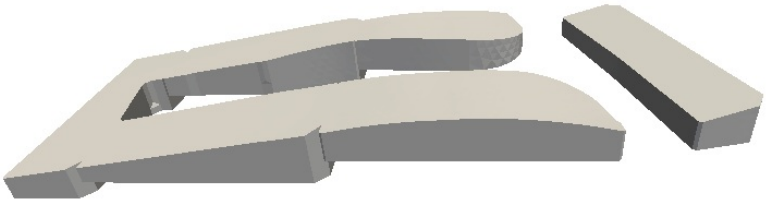

(b) Binder.

(c) Lower tool.

Figure 5.10: Arrangement of the press hardening tools for the simulated b-pillar.

Thermal model The aim of Weiss' model [51] is to predict the quasi-static surface temperature distribution of press hardening tools based on an energy balance. Within this model, this is the surface temperature distribution, averaged over one production cycle of the series production, i.e., after the start-up phase. Beside this information, it is important to know the closing surface temperature distribution of the tools, which is the temperature at the beginning of the forming step.

At the base of the tools, i.e., where they are connected to the hydraulic press, it is sufficient to assume a constant temperature, while for the mantle and cooling channels the heat transfer coefficient (convective or Robin-type boundary condition) is easily determined. However, for the active surface the situation is more involved. Assuming that the total energy E_c[J] to be withdrawn from the blank during one process cycle is absorbed by the tools, leads to the mean surface heat flux

$$q_m = \frac{E_c}{AT_c} ,$$

with the surface measure $A[\mathrm{m}^2]$ of the blank and the cycle duration T_c[sec]. However, simply prescribing this averaged heat flux as a Neumann-type boundary condition is to rough of an approximation for the real process. With the argument that cooler areas of the tool withdraw more energy from the blank than hotter ones, Weiss [51] aims to use a Robin-type boundary condition

$$q(\mathbf{x},t) = -\kappa(u(\mathbf{x},t) - u_\infty(\mathbf{x})) ,$$

which links the heat flux to the temperature difference rather than prescribing a constant surface heat flux. However, since the heat transfer coefficient $\kappa[\mathrm{W}/^\circ\mathrm{Cm}^2]$ is not known, a fictitious $\kappa_f[\mathrm{W}/^\circ\mathrm{Cm}^2]$ is introduced

$$q_m = -\kappa_f(u_t - u_b) ,$$

with the mean temperature of the blank $u_b[^\circ\mathrm{C}]$ before the forming step, the mean quasi-static temperature of the tool $u_t[^\circ\mathrm{C}]$, and the mean surface heat flux $q_m[\mathrm{W}/\mathrm{m}^2]$ know from above. While the assumption for $u_b[^\circ\mathrm{C}]$ is an arbitrary choice, the assumption for $u_t[^\circ\mathrm{C}]$ needs to be verified after the real simulation and, if necessary, corrected (cf. [51, Chapter 6]). Finally, since the material properties of the tool do not vary significantly throughout the working temperature range, we assume a constant heat conduction coefficient $\lambda = 25\,\mathrm{W}/\mathrm{m}^\circ\mathrm{C}$, specific heat capacity $c_p = 450\,\mathrm{J}/\mathrm{kg}^\circ\mathrm{C}$, and density $\varrho = 7647\,\mathrm{kg}/\mathrm{m}^3$.

Figure 5.10 depicts the general arrangement of the press hardening tools for a b-pillar, which consist of three parts, the upper tool, the lower tool and the binder. For the upper tool, the boundary conditions are given in Table 5.9, which are simply mirrored onto the lower tool as well. However, since the binder has neither a base area nor channels, these two types of boundary do not appear for this part of the assembly.

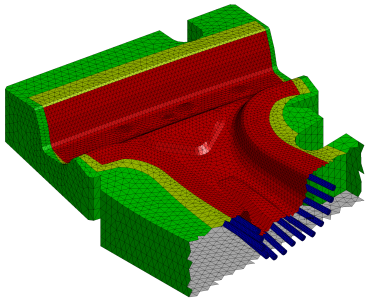

	$g_D^a/g_D^b\,[^\circ\mathrm{C}]$	$\kappa_{(f)}^a/\kappa^b[\mathrm{W}/^\circ\mathrm{Cm}^2]$	$u_\infty^a/u_\infty^b\,[^\circ\mathrm{C}]$
gray	23/23	-	-
green	-	10/10	23/23
blue	-	1100/1100	23/23
red	-	47/10	850/23

Table 5.9: BC's for heating (a) and cooling (b).

Thus, together with the boundary conditions for the heating (a) and cooling (b) process given in Table 5.9 and an initial temperature of $u_0 = 23\,^\circ\mathrm{C}$, the initial boundary value problem is given by

$$\begin{aligned}
\frac{\partial u(\tilde{\mathbf{x}},t)}{\partial t} &= \frac{\lambda}{\varrho c_p}\Delta u(\tilde{\mathbf{x}},t) && (\tilde{\mathbf{x}},t) \in (\Omega \times \Upsilon)\,,\\
u(\tilde{\mathbf{x}},0) &= u_0 && \tilde{\mathbf{x}} \in \Omega\,,\\
u(\mathbf{x},t) &= \begin{cases} g_D^a & t \le 15T_c \\ g_D^b & t > 15T_c \end{cases} && (\mathbf{x},t) \in (\Gamma_D \times \Upsilon)\,,\\
q(\mathbf{x},t) &= \begin{cases} -\kappa^a_{(f)}(u(\mathbf{x},t) - u^a_\infty(\mathbf{x})) & t \le 15T_c \\ -\kappa^b(u(\mathbf{x},t) - u^b_\infty(\mathbf{x})) & t > 15T_c \end{cases} && (\mathbf{x},t) \in (\Gamma_R \times \Upsilon)\,.
\end{aligned}$$

Observe that the quasi-static working temperature of the tool will be reached after approximately 15 cycles of $T_c = 59.4\,\mathrm{sec}$ and the closing temperature after yet another $t_c = 43.8\,\mathrm{sec}$. Furthermore, it is important to note that the initial condition is constant throughout the whole domain. Therefore, this initial boundary value problem can trivially be transformed into a homogeneous one and the boundary integral formulation given in Section 2.4.4 is used as an equivalent description to find the surface temperature distribution $u(\mathbf{x},t)$ with $(\mathbf{x},t) \in (\Gamma \times \Upsilon)$ and $\Gamma := \overline{\Gamma}_D \cup \overline{\Gamma}_R$ (the Robin type boundary condition needs to be scaled according to Remark 2.4).

Due to the approximation of the Steklov-Poincaré operator (Lemma 3.3), the number of spatial unknowns in the system amounts to the combined number of all triangles plus the number of nodes on the Robin boundary. For the upper tool this yields $N_x = 142,754 + 64,112 = 206,866$, for the lower tool $N_x = 94,518 + 43,374 = 137,892$, and for the binder $N_x = 6,892 + 3,450 = 10,342$. The total time of $T = 15T_c + t_c = 891 + 43.8 = 943.8\,\mathrm{sec}$ is split into $N_t = 128$ time steps. Thus, the total number of unknowns for the upper tool results in $N_x N_t = 26,478,848$, for the lower tool in $N_x N_t = 17,650,176$, and for the binder in $N_x N_t = 1,323,776$. Keeping in mind the initial temperature of $23\,^\circ\mathrm{C}$ in Figures 5.11 – 5.13 we present screen shots of the quasi-static working temperature after 15 cycles along with the closing temperature of the upper tool, the lower tool, and the binder, respectively. In these plots hotter regions are colored in red, while colder regions are colored in blue. Obviously, the tools heat up throughout the production process as they withdraw the energy form the hot blanks. We observe that in regions, where the cooling channels are further away from the surface, the temperature is higher than in regions, where the channels are closer to the surface. Finally, the closing temperature is obtained by switching the boundary condition of the active surface after 15 cycles to the same parameters as for the mantle, i.e., a free surface in contact with the surrounding atmosphere, and letting the tools cool for $43.8\,\mathrm{sec}$.

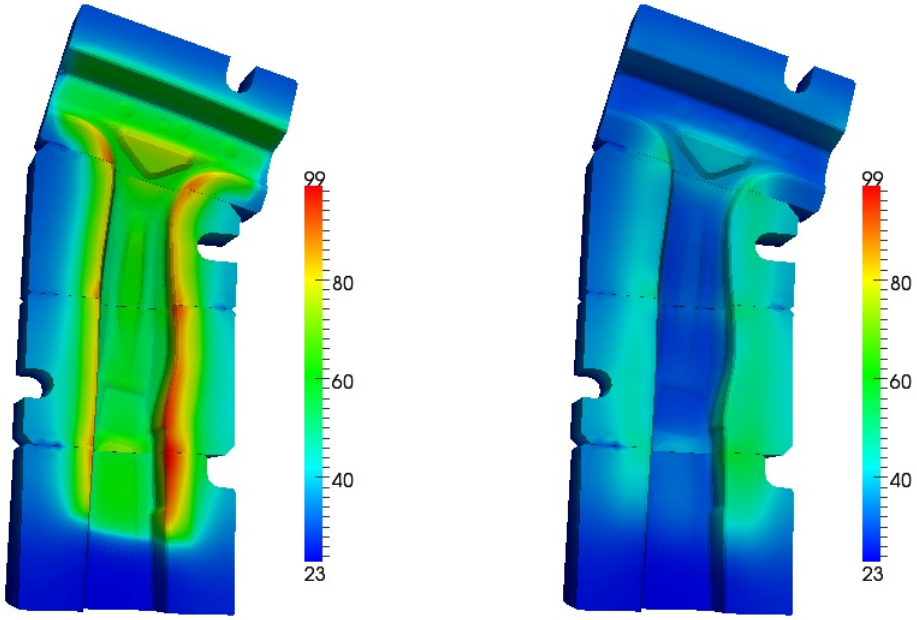

(a) Quasi-Static working temperature [°C]. (b) Closing temperature [°C].

Figure 5.11: Surface temperature of the upper tool.

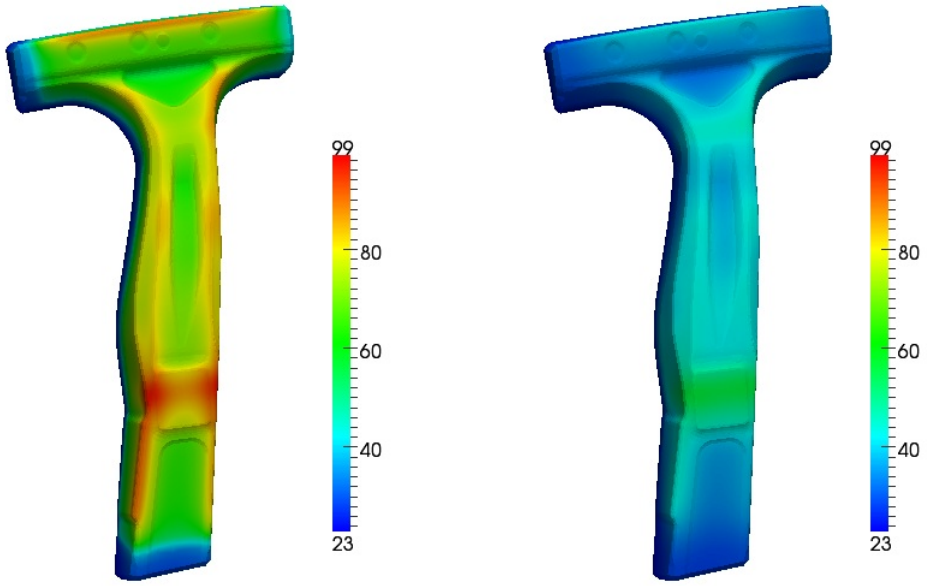

(a) Quasi-Static working temperature [°C]. (b) Closing temperature [°C].

Figure 5.12: Surface temperature of the lower tool.

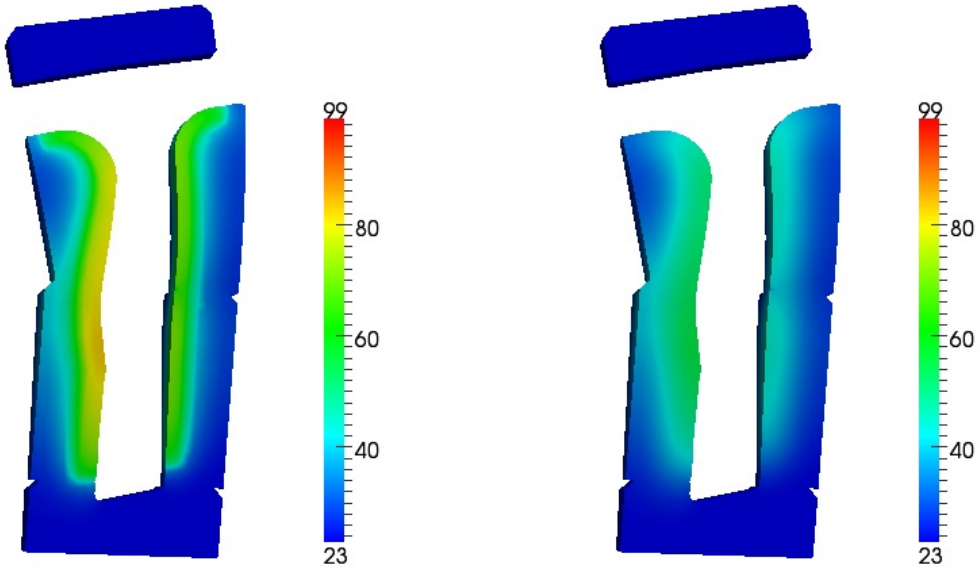

(a) Quasi-Static working temperature [°C]. (b) Closing temperature [°C].

Figure 5.13: Surface temperature of the binder.

At first sight the results visualized in Figures 5.11 – 5.13 seem plausible, however, we would like to have a more sound verification. In contrast to the benchmark problems of the previous section, there is no analytic solution to this problem though. Therefore, we resort to a comparison with in situ temperature measurements. In Figure 5.14, we show the location of three thermo-elements placed at significant positions within the upper tool. The thermo-element T1 and T3 are located close to the active surface inside the cooling channels, where we expect a rather strong temperature oscillation, while T2 is placed outside the cooling channels in a region, where we expect this effect to be less pronounced. Using the representation formula (2.8) we compute the temperature at these three points and compare the result with the measurement data in Figures 5.15 – 5.17. In all three plots, we observe that not only the quasi-static temperature after 15 cycles matches quite accurately with the mean working temperature, but also the simulated closing temperature is within an acceptable range to the lowest temperature measured in a production cycle ($\pm 10\,°C$ accuracy is acceptable for the design engineers in this case). Additionally, we observe that the region inside the cooling channels reacts much faster than the region behind the cooling channels, i.e., the quasi-static working temperature in the region inside the cooling channels (T1, T3) is reached much faster then outside (T2), this is what one would intuitively expect as well. Further, it is important to note that the misalignment of the cooling phase between simulation and real process is irrelevant. The choice of taking 15 cycles as the end of the start-up phase is motivated by experience and any other time in its neighborhood could be taken as start point for the cooling phase.

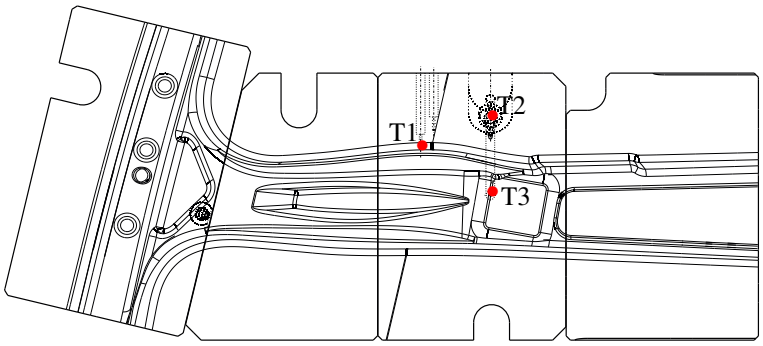

(a) Top view of the upper tool with the position of T1 – T3.

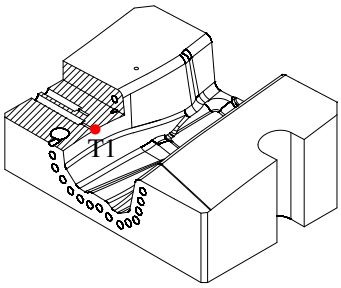

(b) Position of T1.

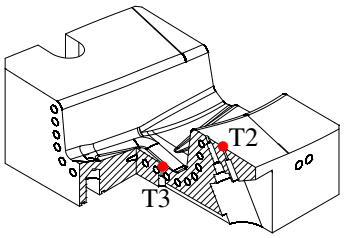

(c) Position of T2 and T3.

Figure 5.14: Position of all thermo-elements T1–T3 in the upper tool [51].

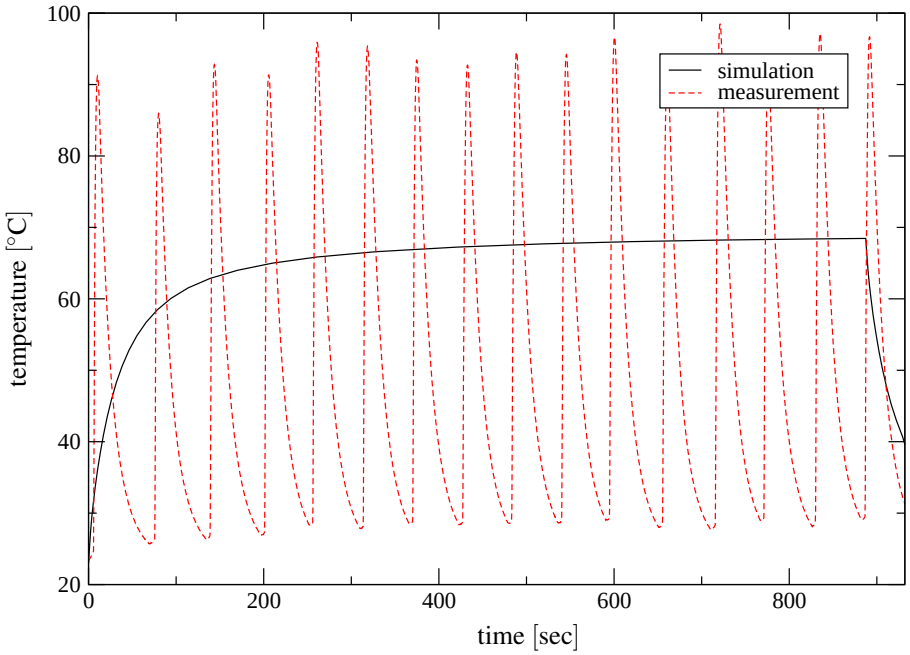

Figure 5.15: Surface temperature T1 – simulation vs. measurement [51].

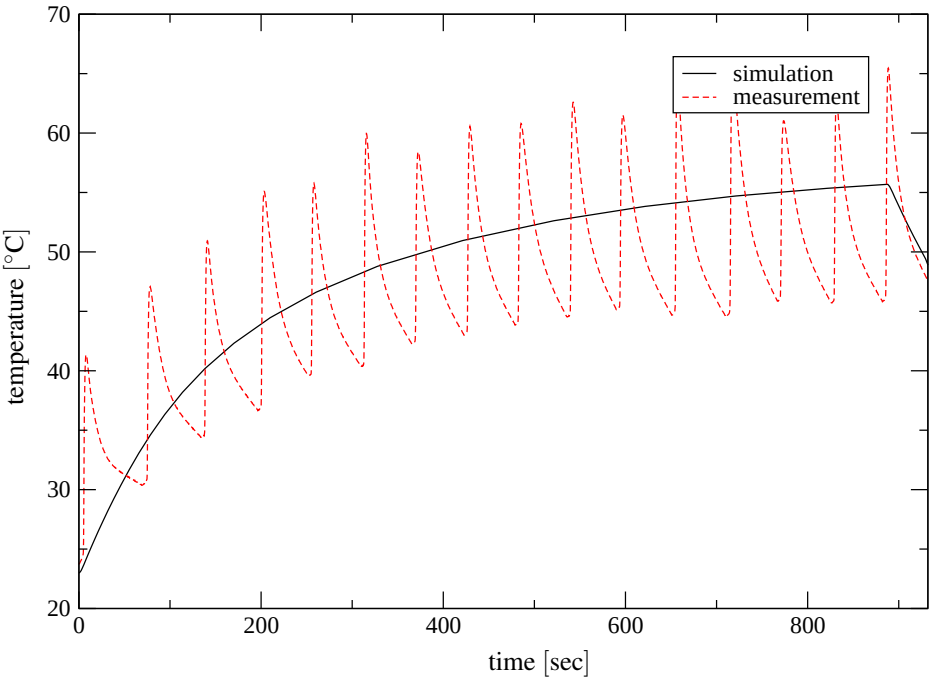

Figure 5.16: Surface temperature T2 – simulation vs. measurement [51].

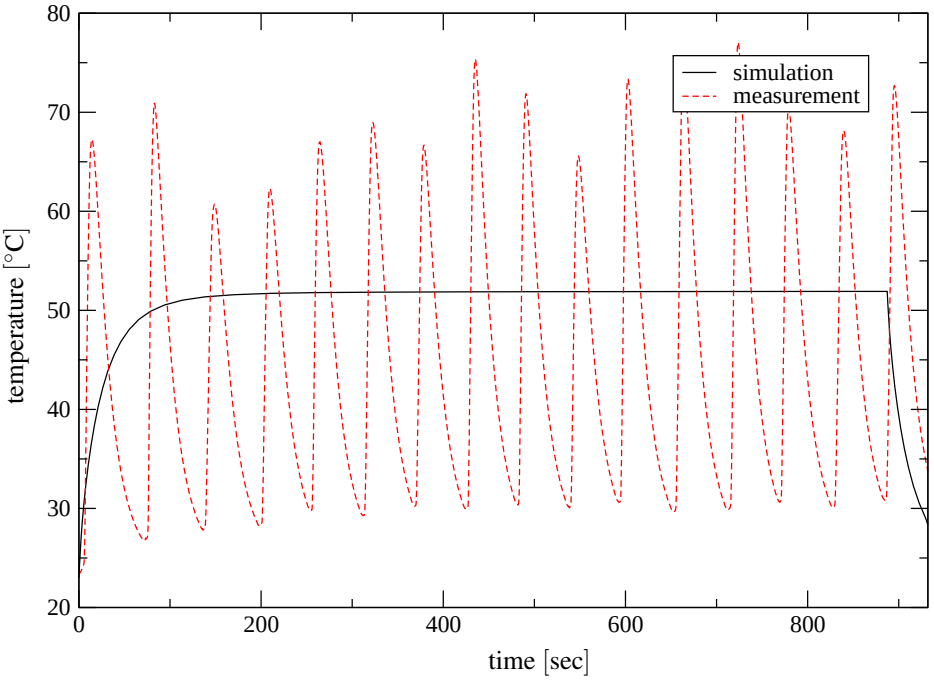

Figure 5.17: Surface temperature T3 – simulation vs. measurement [51].

6 CONCLUSION

With the intention to numerically simulate large scale heat conduction problems in Lipschitz domains we have presented a Galerkin boundary element method for pure and mixed initial boundary value problems of the heat equation with homogeneous initial condition. Our motivation to work with a boundary element method is given by the knowledge that an optimal formulation, i.e., optimal in the number of unknowns $N_x N_t = \mathcal{O}(h_x^{-2} h_t^{-1})$, will at some point always rule out other popular numerical methods (FEM, FDM, FVM), which are based on a volume discretization with the implication of $N_x N_t = \mathcal{O}(h_x^{-3} h_t^{-1})$.

Based on the framework of boundary integral operators of the heat equation, we have given a symmetric formulation for pure Dirichlet, Neumann, and Robin-type initial boundary value problems. Moreover, we have also given a symmetric formulation of a general mixed initial boundary value problem with a combination of all previously mentioned boundary conditions. Due to the ellipticity and boundedness of the single layer and hyper-singular operator in their energy norms and the boundedness of the double layer and adjoint double layer operator, these formulations are uniquely solvable and stable due to the Lemma of Lax-Milgram. Furthermore, with Cea's Lemma we get uniqueness, stability, and quasi-optimality of the approximate solution in the energy norm. Using conforming subspaces, e.g., piecewise polynomial tensor product spaces, we directly obtain error estimates in the energy norm through the approximation property of those finite-dimensional spaces. For practical sake we use the well known regularity results of the thermal layer operators to derive estimates in the L_2 norm and confirm them in a series of benchmark problems. We do that not only for the case of $h_t = \mathcal{O}(h_x^a)$ with $a = 2$, but also for $a \to 0$ and $a \to \infty$.

Since standard boundary element methods yield dense linear system of dimension $N_x N_t$ we end up with $\mathcal{O}(h_x^{-4} h_t^{-2})$ complexity for the solution and $\mathcal{O}(h_x^{-4} h_t^{-1})$ in terms of storage, which is due to the equidistant time discretization. To remedy this setback of the boundary element method, we introduce the parabolic fast multipole method to approximate the application of the linear system at a cost of almost $\mathcal{O}(h_x^{-2} h_t^{-1})$ and a memory requirement of $\mathcal{O}(h_x^{-2})$. These estimates hold for the parabolic farfield, however, not necessarily for the nearfield. We observe that the complexity of the nearfield amounts to $\mathcal{O}(h_x^{-2} h_t^{-1})$ for $h_t = \mathcal{O}(h_x^a)$ with $a \geq 2$. For $0 < a < 2$ the cost grows faster because the number of spatial unknowns grows faster than the spatial truncation decreases, especially for $a \to 0$ this leads to an explosion of the computational complexity and storage requirement. We resolved this inconvenience by a dyadic subdivision of the parabolic nearfield and application of a composite quadrature rule in time. We combined this quadrature rule with FGTs in space in those intervals, where the heat kernel is regular enough. With this strategy we link

the spatial truncation of the heat kernel to the temporal localization of the singularity and thus limit the direct evaluations to $\mathcal{O}(h_x^{-2}h_t^{-1})$ with $h_t = \mathcal{O}(h_x^a)$ and $0 < a < 2$. For the FGTs we simply extend the spatial cluster structure of the parabolic FMM to higher levels from where we choose the FGT level via the space-time scaling of the heat kernel once again. The confirmation that this algorithm is optimal indeed, is given in all benchmark problems by the investigation of a purely spatial refinement scheme, which corresponds to $h_t = \mathcal{O}(h_x^a)$ with $a \to 0$.

Finally, our method was used by Weiss [51] to perform the thermal simulation of press hardening tools, where its applicability to industrial problems of large scale is shown. We presented some results from an experimental setup as a part of Weiss' PhD thesis [51], where a kind of quasi-static start-up phase of the cyclic press hardening process with the cooling phase of one cycle at the end was simulated. These results, namely the quasi-static working temperature of the tools and the temperature at the end of the cooling phase, i.e., just before a new blank is formed, are the crucial results required by the engineers. After a satisfactory experimental validation of these results at some points inside the tools presented in [51] and summarized in Section 5.2, a real process at *WEBA GmbH* was simulated and validated with some further in-situ measurements. Unfortunately, these results are confidential and can therefore not be presented in this work, however, they were pleasing enough for *WEBA GmbH* to use our algorithm for the simulation of further press hardening tools.

A ANISOTROPIC SOBOLEV SPACES

We recite some important properties of anisotropic Sobolev spaces [28, 29] as they play a crucial role in the whole numerical analysis framework [11, 37].

Definition A.1. *For real $r,s \geq 0$ the anisotropic Sobolev space*

$$H^{r,s}(\mathbb{R}^3 \times \mathbb{R}) := L_2\left(\mathbb{R}; H^r(\mathbb{R}^3)\right) \cap H^s\left(\mathbb{R}; L_2(\mathbb{R}^3)\right)$$

is associated with the norm

$$\|u\|^2_{H^{r,s}(\mathbb{R}^3\times\mathbb{R})} := \int\limits_{\mathbb{R}} \int\limits_{\mathbb{R}^3} \left[(1+|\xi|^2)^r + (1+|\tau|^2)^s\right] |\mathcal{F}u(\xi,\tau)|^2 \, d\xi \, d\tau \,,$$

where $\mathcal{F}u(\xi,\tau)$ denotes the Fourier transform in space and time and for real $r,s<0$ we have by duality

$$H^{r,s}(\mathbb{R}^3 \times \mathbb{R}) := \left[H^{-r,-s}(\mathbb{R}^3 \times \mathbb{R})\right]' \,.$$

Definition A.2. *For an open domain Ω with Lipschitz boundary Γ and the time interval $\Upsilon := (0,T)$ with $\mathbb{R} \ni T > 0$ the space $H^{r,s}(\Gamma \times \Upsilon)$ with $\mathbb{R} \ni r,s \geq 0$ and $|r| \leq 1$ is obtained by restriction [11] and equipped with the quotient norm, while $H^{r,s}(\Gamma \times \Upsilon)$ for $\mathbb{R} \ni r,s < 0$ is defined by duality.*

Definition A.3. *Assume $\Gamma_i \subset \Gamma$ to be an open boundary part, then for $\mathbb{R} \ni r,s \geq 0$ and $|r| \leq 1$ we define the subspace*

$$\widetilde{H}^{r,s}(\Gamma_i \times \Upsilon) := \left\{ v = \tilde{v}_{|(\Gamma_i \times \Upsilon)} : \tilde{v} \in H^{r,s}(\Gamma \times \Upsilon),\ supp_{\mathbf{x}}(\tilde{v}) \subset \Gamma_i \right\} \subset H^{r,s}(\Gamma \times \Upsilon) \,,$$

while for $\mathbb{R} \ni r,s < 0$ and $|r| \leq 1$ we need

$$H^{r,s}(\Gamma_i \times \Upsilon) := \left[\widetilde{H}^{-r,-s}(\Gamma_i \times \Upsilon)\right]' \,.$$

Definition A.4. *Assume $\Gamma = \bigcup_{j=1}^{J} \overline{\Gamma}_j$ with Γ_j smooth, $\Gamma_i \cap \Gamma_j = \emptyset$ for $i \neq j$, and $r,s \geq 0$, then we define*

$$H^{r,s}_{pw}(\Gamma \times \Upsilon) := L_2(\Upsilon; H^r_{pw}(\Gamma)) \cap H^s(\Upsilon; L_2(\Gamma)) \,,$$

equipped with the norm

$$\|v\|_{H^{r,s}_{pw}(\Gamma\times\Upsilon)} := \sum_{j=1}^{J} \left(\|v_{|\Gamma_j}\|_{H^{r,s}(\Gamma_j\times\Upsilon)^2} \right)^{\frac{1}{2}} \,.$$

B ANALYTIC EXPRESSIONS OF FUNDAMENTAL SOLUTIONS

B.1 Analytic Expressions for the cFMM

For the temporal nearfield of the cFMM in Section 4.3 we perform the time integration in (4.17) analytically. Since we used a piecewise constant time discretization we have

$$\mathsf{V}_{ij} = \mathsf{V}_{i-j} = \mathsf{V}_d = \begin{cases} \sqrt{\frac{h_t}{\alpha^3}} \int_0^1 \int_0^t V(t-\tau)\mathrm{d}\tau\mathrm{d}t & d = 0 \\ \sqrt{\frac{h_t}{\alpha^3}} \int_0^1 \int_0^1 V(d+t-\tau)\mathrm{d}\tau\mathrm{d}t & d \geq 1 \end{cases},$$

which results in

$$\mathsf{V}_d = \sqrt{\frac{h_t}{\alpha^3}} \left[V^{(-2)}(d+1) - 2V^{(-2)}(d) + V^{(-2)}(d-1) \right],$$

with

$$V^{(-2)}(\mathfrak{d}) = \begin{cases} 0 & \mathfrak{d} \leq 0 \\ \sqrt{\frac{4\mathfrak{d}}{9\pi}} \left[\mathfrak{d} + \left(\sqrt{\frac{\pi}{\mathfrak{d}}} + \frac{3}{2}\sqrt{\pi\mathfrak{d}} \right) \operatorname{erfc}\left(\frac{1}{\sqrt{\mathfrak{d}}} \right) - (\mathfrak{d}+1)\exp\left(-\frac{1}{\mathfrak{d}} \right) \right] & \mathfrak{d} > 0 \end{cases}.$$

B.2 Analytic Expressions for the pFMM

Within the acceleration of the temporal nearfield in Section 4.6 we perform the time integration for $V^+_{0,M}(\mathbf{r})$, $V^-_{1,M}(\mathbf{r})$, $K^+_{0,M}(\mathbf{r})$, $K^-_{1,M}(\mathbf{r})$, $K'^+_{0,M}(\mathbf{r})$, $K'^-_{1,M}(\mathbf{r})$, $D^+_{0,M}(\mathbf{r})$, and $D^-_{1,M}(\mathbf{r})$ analytically. Since we used a piecewise constant time discretization we have

$$V^+_{0,M}(\mathbf{r}) = \frac{-1}{8\pi\alpha^2} \left[\sqrt{\frac{4\alpha h_t \mu^M}{\pi}} \exp\left(-\frac{|\mathbf{r}|^2}{4\alpha h_t \mu^M} \right) - \operatorname{erfc}\left(\frac{|\mathbf{r}|}{\sqrt{4\alpha h_t \mu^M}} \right) \left(\frac{2\alpha h_t}{|\mathbf{r}|} + |\mathbf{r}| \right) \right]$$

$$V^-_{1,M}(\mathbf{r}) = \frac{1}{8\pi\alpha^2} \left[\sqrt{\frac{4\alpha h_t \mu^M}{\pi}} \exp\left(-\frac{|\mathbf{r}|^2}{4\alpha h_t \mu^M} \right) - \operatorname{erfc}\left(\frac{|\mathbf{r}|}{\sqrt{4\alpha h_t \mu^M}} \right) |\mathbf{r}| \right]$$

$$K^{+}_{0,M}(\mathbf{r}) = -\frac{\mathbf{r}^{\top}\mathbf{n}_{\mathbf{y}}}{8\pi\alpha}\left[\operatorname{erfc}\left(\frac{|\mathbf{r}|}{\sqrt{4\alpha h_t \mu^M}}\right)\left(\frac{2\alpha h_t}{|\mathbf{r}|^2}-1\right)+\frac{1}{|\mathbf{r}|}\sqrt{\frac{4\alpha h_t}{\pi\mu^M}}\exp\left(-\frac{|\mathbf{r}|^2}{4\alpha h_t \mu^M}\right)\right]$$

$$K^{-}_{1,M}(\mathbf{r}) = -\frac{\mathbf{r}^{\top}\mathbf{n}_{\mathbf{y}}}{8\pi\alpha}\left[\operatorname{erfc}\left(\frac{|\mathbf{r}|}{\sqrt{4\alpha h_t \mu^M}}\right)\right]$$

$$K'^{+}_{0,M}(\mathbf{r}) = \frac{\mathbf{r}^{\top}\mathbf{n}_{\mathbf{x}}}{8\pi\alpha}\left[\operatorname{erfc}\left(\frac{|\mathbf{r}|}{\sqrt{4\alpha h_t \mu^M}}\right)\left(\frac{2\alpha h_t}{|\mathbf{r}|^2}-1\right)+\frac{1}{|\mathbf{r}|}\sqrt{\frac{4\alpha h_t}{\pi\mu^M}}\exp\left(-\frac{|\mathbf{r}|^2}{4\alpha h_t \mu^M}\right)\right]$$

$$K'^{-}_{1,M}(\mathbf{r}) = \frac{\mathbf{r}^{\top}\mathbf{n}_{\mathbf{x}}}{8\pi\alpha}\left[\operatorname{erfc}\left(\frac{|\mathbf{r}|}{\sqrt{4\alpha h_t \mu^M}}\right)\right]$$

$$D^{+}_{0,M}(\mathbf{r}) = \frac{\mathbf{n}_{\mathbf{x}}{}^{\top}\mathbf{n}_{\mathbf{y}}}{4\pi\,|\mathbf{r}|}\left[\operatorname{erfc}\left(\frac{|\mathbf{r}|}{\sqrt{4\alpha h_t \mu^M}}\right)+\frac{1-\mu^M}{\mu^M}\sqrt{\frac{1}{4\pi\alpha h_t \mu^M}}\exp\left(-\frac{|\mathbf{r}|^2}{4\alpha h_t \mu^M}\right)\right]$$

$$D^{-}_{1,M}(\mathbf{r}) = \frac{\mathbf{n}_{\mathbf{x}}{}^{\top}\mathbf{n}_{\mathbf{y}}}{4\pi}\left[\sqrt{\frac{1}{4\pi\alpha h_t \mu^M}}\exp\left(-\frac{|\mathbf{r}|^2}{4\alpha h_t \mu^M}\right)-\frac{1}{|\mathbf{r}|}\operatorname{erfc}\left(\frac{|\mathbf{r}|}{\sqrt{4\alpha h_t \mu^M}}\right)\right]$$

REFERENCES

[1] M. Abramowitz and I. A. Segun, editors. *Handbook of Mathematical Functions*. U.S. Govt. Print. Off., 1964.

[2] R. A. Adams and J. F. Fournier. *Sobolev Spaces*. Elsevier, 2003.

[3] Paul Åkerström. *Modelling and Simulation of Hot Stamping*. PhD thesis, Luleå Tekniska Universitet, 2006.

[4] D. Arnold and P. J. Noon. Coercivity of the Single Layer Heat Potential. *J. Comput. Math.*, 7:100–104, 1989.

[5] H. D. Baehr and K. Stephan. *Heat and Mass Transfer*. Springer, 2006.

[6] K. J. Bathe. *Finite Element Procedures*. Prentice-Hall, 1996.

[7] S. C. Brenner and L. R. Scott. *The Mathematical Theory of Finite Element Methods*. Springer, 2008.

[8] R. M. Brown. The Method of Layer Potentials for the Heat Equation in Lipschitz Cylinders. *Amer. J. Math.*, 111(2):339–379, 1989.

[9] M. M. Chawla and M. K. Jain. Error Estimates for Gauss Quadrature Formulas for Analytic Functions. *Math. Comp.*, 11(101):82–90, 1968.

[10] H. Cheng, L. Greengard, and V. Rokhlin. A Fast Adaptive Multipole Algorithm in Three Dimensions. *J. Comput. Phys.*, 155:468–498, 1999.

[11] M. Costabel. Boundary Integral Operators for the Heat Equation. *Integr. Eq. Oper. Theory*, 13(4):498–552, 1990.

[12] M. Costabel. Time-Dependent Problems with the Boundary Integral Equation Method. *Encycl. Comp. Mech.*, 2004.

[13] J. Crank and P. Nicolson. A Practical Method for Numerical Evaluation of Solutions of Partial Differential Equations of the Heat-Conduction Type. *Proc. Camb. Phil. Soc.*, 43:207–226, 1947.

[14] P. J. Davis. *Interpolation and Approximation*. Blaisdell, 1963.

[15] S. Erichsen and S. A. Sauter. Efficient Automatic Quadrature in 3-d Galerkin BEM. *Comput. Methods Appl. Mech. Eng.*, 157:215–224, 1998.

[16] N. R. Eyres, D. R. Hartree, J. Ingham, R. Jackson, R. J. Sarjant, and J. B. Wagstaff. The Calculation of Variable Heat Flow in Solids. *Philosophical Transactions of the Royal Society of London. Series A, Mathematical and Physical Sciences*, 240(813): 1–57, 1946.

[17] L. Greengard and P. Lin. Spectral Approximation of the Free-Space Heat Kernel. *Appl. Comput. Harmon. Anal.*, 9:83–97, 1999.

[18] L. Greengard and V. Rokhlin. A Fast Algorithm for Particle Simulations. *J. Comput. Phys.*, 73:325–348, 1987.

[19] L. Greengard and V. Rokhlin. A New Version of the Fast Multipole Method for the Laplace Equation in Three Dimensions. *Acta Mech.*, 6:229–269, 1997.

[20] L. Greengard and J. Strain. A Fast Algorithm for the Evaluation of Heat Potentials. *Comm. Pure Appl. Math.*, 43:949–963, 1990.

[21] L. Greengard and J. Strain. The Fast Gauss Transfrom. *SIAM J. Sci. Comput.*, 12: 79–94, 1991.

[22] K. Griebermann. Multilevel Approximation of Boundary Integral Operators. *Computing*, 67:183–207, 2001.

[23] W. Hackbusch and Z. P. Nowak. On the Fast Matrix Multiplication in the Boundary Element Method by Panel Clustering. *Numer. Math.*, 54:463–491, 1989.

[24] F. P. Incropera and D. P. DeWitt. *Fundamentals of Heat and Mass Transfer*. John Wiley & Sons, 2002.

[25] O. D. Kellog. *Foundations of Potential Theory*. Springer, 1929.

[26] L. Kielhorn. *A Time-Domain Symmetric Galerkin BEM for Viscoelastodynamics*, volume 5 of *Computation in Engineering and Science*. Verlag der Technischen Universtiät Graz, 2009.

[27] J. R. Li and L. Greengard. High Order Accurate Methods for the Evaluation of Layer Heat Potentials. *SIAM J. Sci. Comput.*, 31:3847–3860, 2009.

[28] J. L. Lions and E. Magnes. *Non-Homogeneous Boundary Value Problems and Applications*, volume 1. Springer, Berlin, 1972.

[29] J. L. Lions and E. Magnes. *Non-Homogeneous Boundary Value Problems and Applications*, volume 2. Springer, Berlin, 1972.

[30] Y. J. Liu and N. Nishimura. The Fast Multipole Boundary Element Method for Potential Problems: A Tutorial. *Eng. Anal. Bound. Elem.*, 30:371–381, 2006.

[31] Ch. Lubich and R. Schneider. Time Discretization of Parabolic Boundary Integral Equations. *Numer. Math.*, 63:455–481, 1992.

[32] M. Merklein and J. Lechler. Investigation of the Thermo-Mechanical Properties of Hot Stamping Steels. *J. Mat. Tech.*, 177(1):452–455, 2006.

[33] M. Messner, M. Messner, F. Rammerstorfer, P. Urthaler, Th. Traub, and B. Kager. Hyperbolic and Elliptic Numerical Analysis C++ BEM Library. http://www.mech.tugraz.at/HyENA, 2013.

[34] M. Messner, J. Tausch, and M. Schanz. Fast Galerkin Method for Parabolic Space-Time Boundary Integral Equations. *J. Comput. Phys.*, 258:15–30, 2014.

[35] T. N. Narasimhan. Fourier's Heat Conduction Equation: History, Influence, and Connections. *Rev. Geophys.*, 37(1):151–172, 1999.

[36] N. Nishimura, K. Yoshida, and S. Kobayashi. A Fast Multipole Boundary Integral Equation Method for Crack Problems in 3D. *Eng. Anal. Bound. Elem.*, 23:97–105, 1999.

[37] P. J. Noon. *The Single Layer Heat Potential and Galerkin Boundary Element Methods for the Heat Equation*. PhD thesis, University of Maryland, 1988.

[38] G. Of, O. Steinbach, and W. L. Wendland. Applications of a Fast Multipole Galerkin Boundary Element Method in Linear Elastostatics. *Comp. Vis. Science*, 8:201–209, 2005.

[39] S. Oh and T. N. Altan. *Metal Forming and the Finite-Element Method*. Oxford University Press, 1989.

[40] W. Pogorzelski, A. Kacner, J. Schorr-Con, and Z. S. Olesiak. *Integral Equations and their Applications*, volume 1. Pergamon Press Oxford, 1966.

[41] F. J. Rizzo and D. J. Shippy. A Method of Solution for Certain Problems of Transient Heat Conduction. *AIAA J.*, 8(11):2004–2009, 1970.

[42] J. Rodrigues and P. Martins. Coupled Thermo-Mechanical Analysis of Metal-Forming Processes Through a Combined Finite Element–Boundary Element Approach. *Int. J. Num. Meth. Eng.*, 42(4):631–645, 1998.

[43] S. Sauter and C. Schwab. *Randelementmethoden: Analyse, Numerik und Implementierung Schneller Algorithmen*. Teubner, 2004.

[44] O. Steinbach. *Numerical Approximation Methods for Elliptic Boundary Value Problems*. Springer, 2008.

[45] J. Strain. Fast Adaptive Methods for the Free-Space Heat Equation. *SIAM J. Sci. Comput.*, 15:185–206, 1994.

[46] G. Strang and G. J. Fix. *An Analysis of the Finite Element Method*. Prentice-Hall, 1973.

[47] J. Tausch. A fast method for solving the heat equation by layer potentials. *J. Comput. Phys.*, 224:956–969, 2007.

[48] J. Tausch. Nyström Discretization of Parabolic Boundary Integral Equations. *Appl. Numer. Math.*, 59(11):2843–2856, 2009.

[49] J. Tausch. Fast Nyström Methods for Parabolic Boundary Integral Equations. In U. Langer, M. Schanz, O. Steinbach, and W. L. Wendland, editors, *Fast Boundary Element Methods in Engineering and Industrial Applications*, volume 63 of *Lecture Notes in Applied and Computational Mechanics*, pages 185–219. Springer, 2011.

[50] J. Tausch and A. Weckiewicz. Multidimensional Fast Gauss Transforms by Chebyshev Expansions. *SIAM J. Sci. Comput.*, 31:3547–3565, 2009.

[51] W. Weiss. *Thermische Auslegung von Werkzeugen für Presshärteprozesse*. PhD thesis, Graz University of Technology, 2013.

[52] E. L. Wilson and R. E. Nickell. Application of the Finite Element Method to Heat Conduction Analysis. *Nucl. Eng. Des.*, 4(3):276–286, 1966.

Monographic Series TU Graz

Computation in Engineering and Science

Vol. 1 Steffen Alvermann

Effective Viscoelastic Behaviour of Cellular Auxetic Materials
2008
ISBN 978-3-902465-92-4

Vol. 2 Sendy Fransiscus Tantono

The Mechanical Behaviour of a Soilbag under Vertical Compression
2008
ISBN 978-3-902465-97-9

Vol. 3 Thomas Rüberg

Non-conforming FEM/BEM Coupling in Time Domain
2008
ISBN 978-3-902465-98-6

Vol. 4 Dimitrios E. Kiousis

Biomechanical and Computational Modeling of Atherosclerotic Arteries
2008
ISBN 978-3-85125-023-7

Vol. 5 Lars Kielhorn

A Time-Domain Symmetric Galerkin BEM for Viscoelastodynamics
2009
ISBN 978-3-85125-042-8

Vol. 6 Gerhard Unger

Analysis of Boundary Element Methods for Laplacian Eigenvalue Problems
2009
ISBN 978-3-85125-081-7

Monographic Series TU Graz

Computation in Engineering and Science

Vol. 7 Gerhard Sommer

Mechanical Properties of Healthy and Diseased Human Arteries
2010
ISBN 978-3-85125-111-1

Vol. 8 Mathias Nenning

Infinite Elements for Elasto- and Poroelastodynamics
2010
ISBN 978-3-85125-130-2

Vol. 9 Thanh Xuan Phan

Boundary Element Methods for Boundary Control Problems
2011
ISBN 978-3-85125-149-4

Vol. 10 Loris Nagler

Simulation of Sound Transmission through Poroelastic Plate-like Structures
2011
ISBN 978-3-85125-153-1

Vol. 11 Markus Windisch

Boundary Element Tearing and Interconnecting Methods for Acoustic and Electromagnetic Scattering
2011
ISBN: 978-3-85125-152-4

Monographic Series TU Graz

Computation in Engineering and Science

Vol. 12 Christian Walchshofer

Analysis of the Dynamics at the Base of a Lifted Strongly Buoyant Jet Flame Using Direct Numerical Simulation
2011
ISBN 978-3-85125-185-2

Vol. 13 Matthias Messner

Fast Boundary Element Methods in Acoustics
2012
ISBN 978-3-85125-202-6

Vol. 14 Peter Urthaler

Analysis of Boundary Element Methods for Wave Propagation in Porous Media
2012
ISBN 978-3-85125-216-3

Vol. 15 Peng Li

Boundary Element Method for Wave Propagation in Partially Saturated Poroelastic Continua
2012
ISBN 978-3-85125-236-1

Vol. 16 Andreas J. Schriefl

Quantification of Collagen Fiber Morphologies in Human Arterial Walls
2012
ISBN 978-3-85125-238-5

Vol. 17 Thomas S. E. Eriksson

Cardiovascular Mechanics
2013
ISBN 978-3-85125-277-4

Monographic Series TU Graz

Computation in Engineering and Science

Vol. 18 Jianhua Tong

Biomechanics of Abdominal Aortic Aneurysms
2013
ISBN 978-3-85125-279-8

Vol. 19 Jonathan Rohleder

Titchmarsh–Weyl Theory and Inverse Problems for Elliptic Differential Operators
2013
ISBN 978-3-85125-283-5

Vol. 20 Martin Neumüller

Space-Time Methods
2013
ISBN 978-3-85125-290-3

Vol. 21 Michael J. Unterberger

Microstructurally-Motivated Constitutive Modeling of Cross-Linked Filamentous Actin Networks
2013
ISBN 978-3-85125-303-0

Vol. 22 Vladimir Lotoreichik

Singular Values and Trace Formulae for Resolvent Power Differences of Self-Adjoint Elliptic Operators
2013
ISBN 978-3-85125-304-7

Vol. 23 Michael Meßner

A Fast Multipole Galerkin Boundary Element Method for the Transient Heat Equation
2014
ISBN 978-3-85125-350-4